U.PORTO

INSTITUTO DE CIÊNCIAS BIOMÉDICAS ABEL SALAZAR
UNIVERSIDADE DO PORTO

FC

universidade de aveiro
theoria poiesis praxis

MODELLING THE BIOGEOCHEMICAL DYNAMICS OF THE IBERIAN UPWELLING SYSTEM

ROSA REBOREDA BOUZA

Tese de doutoramento em Ciências do Mar e do Ambiente

2013

ROSA REBOREDA BOUZA

MODELLING THE BIOGEOCHEMICAL DYNAMICS OF THE IBERIAN UPWELLING SYSTEM

Tese de Candidatura ao grau de Doutor em Ciências do Mar e do Ambiente.
Especialidade em Oceanografia e Ecossistemas Marinhos.
Programa Doutoral da Universidade do Porto (Instituto de Ciências Biomédicas de Abel Salazar e Faculdade de Ciências) e da Universidade de Aveiro.

Orientador: Doutor Jesus Dubert.
Categoria: Professor Auxiliar.
Afiliação: Centro de Estudos do Ambiente e do Mar (CESAM) e Departamento de Física da Universidade de Aveiro.

Co-orientador: Doutor Henrique Queiroga.
Categoria: Professor Auxiliar com Agregação.
Afiliação: Centro de Estudos do Ambiente e do Mar (CESAM) e Departamento de Biologia da Universidade de Aveiro.

Á miña familia e á memoria da avoa Eudosia

Agradecimentos

Ao meu orientador, Prof. Jesus Dubert, e co-orientador, Prof. Henrique Queiroga, por me terem colocado este desafio nas mãos e por me terem transmitido a confiança que necessitava para o levar a bom fim. Agradeço o seu apoio e o respeito pelo meu trabalho, deixando-me margem para desenvolver as minhas próprias ideias. Aos dois muito obrigado por me terem facilitado sempre tudo o que esteve na sua mão.

À Doutora Rita Nolasco, pela sua paciência e disponibilidade constantes para as dúvidas e dificuldades técnicas com o ROMS. O meu trabalho não teria sido possível sem a sua contribuição na parte hidrodinâmica do modelo.

À Doutora Carmen G. Castro e ao Doutor Xosé A. Álvarez-Salgado, do IIM-CSIC de Vigo, *graciñas* por todos os conhecimentos que me transmitiram sobre os processos biogeoquímicos na margem Ibérica, sempre com a melhor simpatia e disponibilidade. Obrigado também por terem facilitado os dados do projecto DYBAGA para apoiar a validação do modelo.

A todos os colegas que fazem ou fizeram parte do Grupo de Modelação do Oceano ao longo destes quatro anos, pois todos eles nalgum momento me ajudaram. Em particular, ao meu colega e amigo Nuno G. Cordeiro, pelo seu infinito apoio com o Matlab® e com os cálculos estatísticos. Um obrigado especial para a Ana Pires e a Fabiola Amorim, que para alem de colegas são grandes amigas que muito me têm apoiado neste percurso nem sempre fácil. O meu agradecimento também ao Martinho por toda a ajuda nos meus inicios com o ROMS e com Linux, pois foi com ele que aprendi a impor respeito a um computador (é só chama-lo a ele!). Obrigada pelas saudáveis doses de sarcasmo e sentido do humor.

A todas as pessoas do laboratório, os do oceano e os da atmosfera, pelo convívio diário, as conversas, os almoços, os lanches ...

Aos meus colegas da primeira edição do Programa Doutoral em Ciências do Mar e do Ambiente, pela camaradagem e amizade que mantiveram ao longo destes quase 5 anos.

A todos os meus amigos, os que estão perto e os que estão longe, especialmente aos que têm acompanhado mais esta etapa final, dando-me ánimo, preocupando-se por mim,

ou simplesmente arrastando-me de vez em quando para longe da minha secretária: Obrigada Ana (Sousa), obrigada Nayara, *gracias* Sergio e Maruxa (e Roque!), obrigado Israel, *eskerrik asko* Lidia ...

Finalmente, o meu agradecemento máis importante, á miña familia, por ter sido fonte constante de apoio e comprensión nesta etapa, como en todas. Aos meus pais, Domingos e Pilar, por térenme apoiado sempre nos meus estudios, o que me permitiu chegar até aquí. Ao meu irmán, Mingos, por terme contaxiado desde cedo o gusto pola ciencia. E á miña cuñada, Ana, por transmitirme o seu ánimo como unha irmá. O esforzo investido neste traballo é dedicado a vós.

Este trabalho foi possível graças ao financiamento da Fundação para a Ciência e a Tecnologia (FCT), mediante a bolsa de doutoramento que me foi atribuida (SFRH/BD/33388/2008). O trabalho desenvolveu-se como parte do projecto RAIA (Observatorio oceánico del margen Ibérico, POCTEP-FEDER, 0520_RAIA_CO_1_E). Os resultados contribuiram parcialmente para os objectivos do projecto HAB-SPOT (Harmful Algal Bloom dynamics - Shelf Processes of Transport and retention Offshore Aveiro, PTDC/MAR/100348/2008).

Resumo

As interações físico-biológicas que ocorrem na margem Ibérica Atlântica sustentam um ecossistema muito produtivo, caracterizado por uma biodiversidade marinha elevada e importantes recursos piscatórios e marisqueiros. Este facto deve-se principalmente ao efeito fertilizante da ressurgência costeira forçada pelo vento, principalmente entre a Primavera e o Verão, mas também a outras interações sazonais, interanuais e de curto prazo que influenciam a dinâmica do ecossistema. O objectivo deste trabalho foi o estudo dos padrões espacio-temporais do ecossistema planctônico sobre a plataforma e região oceância adjacente, recorrendo à modelção físico-biogeoquímica de alta resolução. Para este fim acoplaram-se à base hidrodinámica duma configuração regional do modelo Regional Ocean Modeling System (ROMS) três modulos biogeoquimicos de diferêntes níveis de complexidade, do tipo NPZD (Nutrientes-Fitoplâncton-Zooplâncton-Detritos). Os resultados das simulações numéricas foram validados por comparação com dados de deteção remota obtidos do SeaWiFS ou de uma interpolação óptima dos dados de SeaWiFS, MODIS e MERIS (clorofila) e do AVHRR (SST), e com observações *in situ* de dados termohalinos e biogeoquimicos. O modelo reproduziu de modo satisfatório a variabilidade espacio-temporal observada, embora tenham sido detectadas algumas limitações. O modelo foi posteriormente aplicado ao estudo da influência das condições fisicas na variabilidade sazonal, interanual e de curto prazo das propriedades biogeoquimicas (biomassa de fitoplâncton/clorofila e zooplâncton, detritos, nutrientes e oxigénio). Na região oceânicia da área de estudo as variações sazonais na clorofila e na concentração de oxigénio foram acompanhadas por variações sazonais na profundidade da camada de mistura. Os padrões sazonais de clorofila e oxigénio verificados no oceano aberto foram também encontrados, de modo geral, na plataforma continental. No entanto, na plataforma observou-se maior variabilidade consequência dos períodos de ressurgência, da dinâmica da vertente (corrente para o Polo) e da dinâmica das plumas dos rios. A oceanografia regional influenciou os padrões espacio-temporais de concentração de oxigénio e biomassa planctônica, sobrepondo-se às variações sazonais e interanuais nos forçamentos atmosféricos. Esta influência deveu-se essencialmente à interação

entre duas massas de água centrais de origem subpolar e subtropical com diferentes características termohalinas e biogeoquimicas.

Abstract

The physical-biological interactions in the Atlantic Iberian margin underlie a very productive ecosystem characterized by a rich marine biodiversity and important fish and shellfish resources. This is mainly driven by the fertilizing effect of the wind-driven coastal upwelling throughout spring and summer, although other seasonal, interannual, and event-scale interactions are known to influence the ecosystem dynamics. The aim of this thesis was to study the spatio-temporal patterns of the plankton ecosystem over the shelf and the adjacent oceanic region, taking advantage of a high-resolution physical-biogeochemical ocean model. To this end, the hydrodynamic base of a regional configuration of the Regional Ocean Modeling System (ROMS) was coupled to three biogeochemical modules of different complexity levels, all of them NPZD-type (Nutrients-Phytoplankton-Zooplankton-Detritus). Model outputs were validated by comparison with remotely sensed data obtained from SeaWiFS or from an optimal interpolation of SeaWiFS, MODIS and MERIS data (chlorophyll) and from AVHRR (SST), and with *in situ* observations of thermohaline and biogeochemical data. The spatio-temporal variability observed was satisfactorily reproduced by the model, albeit some limitations that were also detected. The model was subsequently applied to study the influence of the physical conditions in the seasonal, interannual, and short-term variability of the biogeochemical properties (chlorophyll/phytoplankton and zooplankton biomass, detritus, nutrients, and oxygen). Over the oceanic part of the area of study the seasonal changes in the chlorophyll and oxygen concentration were parallel to the seasonal changes in the mixed layer depth. The seasonal patterns of chlorophyll and oxygen found offshore generally occurred also in the shelf region, but over the shelf more variability was introduced by the upwelling events, the slope dynamics (poleward flow) and the dynamics of the river plumes. Overlapped to the seasonal and interannual changes in atmospheric forcings, the regional oceanography influenced the spatio-temporal patterns of oxygen concentration and plankton biomass. This influence was mainly due to the interplay between two branches of central waters with subpolar and subtropical origin with differing thermohaline and biogeochemical characteristics.

Contents

List of Tables

List of Figures

Chapter 1

Introduction

1.1 Thesis outline

This thesis is organized in seven chapters that constitute a compilation of four independent original research papers in different stages of publication process. Chapter 1 is a general introduction to the thesis. Chapter 2 is a description of the ocean model setup used for all the simulations conducted to obtain the modeling results presented. A *Model setup* section is also included in each of the following chapters, with the specific configurations used for each work, as they constitute standing alone documents. Therefore, the reader is invited to chose only one of them for reference, either Chapter 2 or the *Model setup* section of each chapter, to avoid repetitiveness. Chapters 3 to 6 are written in the form of scientific papers and present the main research undertaken within the frame of this thesis. Chapter 3 has been submitted to the Journal of Marine Systems, and presents a general characterization of the spatio-temporal patterns of the planktonic production in the Iberian margin based on a $NChlPZD$ biogechemical model. Chapter 4 has been published in co-authorship (as second author) in PlosOne (Marta-Almeida et al., 2012) and it describes the operational implementation of the biogeochemical model regional configuration developed in Chapter 3 to an on-line information server. My contribution to the paper included analyzing the biogeochemical model results, writing the results involving chlorophyll analyses as well as the main text of the introduction, and contributing to conceive and design the model configurations. Chapter 5 has been submitted to Progress in Oceanography and is currently in revision by the authors. It provides a characterization of the seasonal oxygen cycle in the region based on a $NChlPZD + O_2$ biogeochemical model. Chapter 6 has been submitted to the Journal of Sea Research within the frame of a special issue about the Atlantic Iberian Margin. This chapter analyses

the interannual and seasonal variability of chlorophyll for a simulation of the period 2001-2010, based on a $N_2ChlPZD_2$ biogeochemical model. Finally, Chapter 7 presents an overview and outlook of the thesis .

Additional information on the biogeochemical model and the physical model is given in Appendix A and Appendix B, respectively.

1.2 General

Marine Biogeochemistry studies the distribution of chemical elements in seawater and the processes that control it. Understanding what controls the mean concentrations as well as the spatial and temporal variability of elements that are influenced by biological processes is a major concern. This involves studying transport processes such as advection and diffusion of chemicals as well as sinks and sources such as biological uptake and mineralization (Sarmiento and Gruber, 2006). Particularly relevant are the cycles of carbon (C), nitrogen (N), and oxygen (O_2).

Phytoplankton production is the base of most marine trophic webs and thus its variability affects the dynamics of the whole ecosystem, including some economically important fisheries. Phytoplankton depends on the temperature and the availability of nutrients (mainly nitrate and ammonium) and light for growth. These are highly variable factors related with the hydrodynamics and with seasonal changes (Mann and Lazier, 2006).

The western Iberian margin is the northern limit of the NW African upwelling region (Wooster et al., 1976; Fiuza et al., 1982; Barton et al., 1998), split from the northwestern African shelf by the Strait of Gibraltar and the Mediterranean outflow, being the only coastal upwelling region in Europe. Its major characteristics are comparable to other Eastern Boundary Current Systems (Benguela, Humbolt and California), presenting a general meridional alignment of the coastline and predominant equatorward wind direction during a substantial part of the year (April to September), which forces an offshore Ekman transport in the upper layer and an alongshore equatorward jet (Peliz et al., 2002; Relvas et al., 2007). This supplies cold and nitrate rich subsurface water (Eastern North Atlantic Central Water) (Fraga, 1981; Relvas et al., 2007) increasing phytoplankton biomass in the upper water column along the coast, particularly from Cape Fisterra (NW Spain) to Cape São Vicente (SW Portugal), making this region a very productive ecosystem governed by morphological-physical-biological interactions. Seasonal and interannual variations defining the cycle of primary and secondary production are thus the result of the

coupling between the physical, geochemical and biological fields, in which the short-term variability associated to mesoscale physical features such as eddies, filaments and river buoyant plumes are a major forcing factor (e.g. Castro et al., 2000; Álvarez-Salgado et al., 2007). Observational studies have monitored the biogeochemical processes in the region verifying their large temporal and spatial variability (e.g. Álvarez-Salgado et al., 1997, 2002). However, observational studies alone do not allow a complete study of the entire system due to sampling limitations in spatial and time coverage. As a result, the existing knowledge of elemental cycles and budgets that control the ecosystem functioning is not enough to understand the spatio-temporal variability, the processes involved, and to predict responses of the ecosystem to perturbations.

Three-dimensional (3D) coupled physical-biogeochemical ocean models have been developed over the last two decades as essential research tools in synergy with observations (Doney, 1999; Doney et al., 2001). They are built as simplified representations of processes and compartments of the system in the form of a set of mathematical equations that are solved computationally, taking advantage of the high improvements achieved in computational power nowadays. Ocean biogeochemical models derive mainly from the model of Fasham et al. (1990), which include plankton populations as broadly defined trophic compartments (phytoplankton, zooplankton, detritus) and track the flow of nitrogen, as a limiting element, among the compartments. The complexity and applications of ocean biogeochemical models developed afterwards are diverse (Doney, 1999). For scientific purposes, they provide a tool for large scale and mesoscale characterization, hypothesis testing, and prediction. Besides, they can be used as decision making tools for managers and easy visualizing tools for the general public and policy makers. Some 3D coupled physical-biogeochemical models have allowed to successfully resolve limited domains at eddy-resolving resolution, which is particularly relevant for the study of biogeochemical dynamics in coastal upwelling systems (Gruber et al., 2006, and references therein). That is the case of the Regional Ocean Modeling System (ROMS) (Shchepetkin and McWilliams, 2005), applied in this thesis to address for the first time the coupling of ocean physics and plankton ecosystem in the western Iberian margin.

1.3 Motivation and objectives

After my first academic year in the Marine and Environmental Sciences Doctoral Program, attending multidisciplinary classes at the CIIMAR-University of Porto, I faced the decision to choose an interesting PhD topic that would be appealing for my preferences. In an advisory meeting, where Professor Henrique Queiroga was present, I expressed my

interest for some topics related to ocean biogeochemical research. He suggested to contact Professor Jesus Dubert, from the University of Aveiro, who had introduced us to the world of Physical Oceanography in his classes. For some time Professor J. Dubert had been looking for someone who would take the challenge to start the biogeochemical modeling of the Iberian upwelling system, as a step forward in the hydrodynamic modeling work developed by his research group. A multidisciplinary background in marine sciences and not fearing scary differential equations and computers seemed to be advantageous. I was graduated in Marine Sciences, I was not really aware of what ocean modeling was about to fear it, so I found the challenge motivating and decided to take it.

ROMS has been broadly used to model the hydrodynamics of the Atlantic Iberian margin about the last decade (Peliz et al., 2003; Marta-Almeida et al., 2006; Peliz et al., 2007a; Otero et al., 2008; Peliz et al., 2009; Nolasco et al., 2013), contributing to the understanding of the regional circulation and providing a good hydrodynamic base to move forward into coupled hydrodynamic-biogeochemical modeling. Taking this step would be useful to study the physical-biological interactions of the system and help to understand their influence on the seasonal evolution, and the variability and distribution of biogeochemical properties, as seen for other coastal upwelling systems such as California (Moisan and Hofmann, 1996; Gruber et al., 2006; Powell et al., 2006), Humboldt (Echevin et al., 2008), and Benguela (Koné et al., 2005; Machu et al., 2005). Also, there was an increasing demand for operational information and forecast of biogeochemial properties, for monitoring and management purposes.

The literature review showed that, although some efforts had been carried out for applying biogeochemical models to the region, they had been local applications to coastal embayments (Barciela et al., 1999; Torres et al., 2006; Torres-López et al., 2005; Rodrigues et al., 2009) or a particular coastal region (Slagstad and Wassmann, 2001; Lopes et al., 2009), usually for an specific oceanographic period. An early attempt by Penas and Varela (1986) tried to model primary production in the Galician shelf, although it was not formulated in quantitative terms. Barciela et al. (1999) applied a box model with a specified upwelling flux to study the primary production in a Galician Ria. Most of subsequent studies used reduced order hydrodynamic models, such as the 1D approach used in Torres-López et al. (2005) and Torres et al. (2006) for another Galician Ria. Slagstad and Wassmann (2001) applied the first 3D coupled hydrodynamic-biogeochemical model at eddy-resolving resolution, applied to study carbon export along the northwestern Iberian margin during an upwelling period. They obtained some satisfactory results, although with a time-lag of 1-2 weeks from the observations. More recently, the phytoplankton dynamics of a coastal zone centered in Aveiro, during upwelling conditions, was studied

using a 3D physical-ecological model (Lopes et al., 2009), although some inconsistencies were revealed during model validation. To sum up, the biogeochemical modeling of the Iberian margin was far from been at the same stage as it was for the other main coastal upwelling regions, and there was much work ahead to reach a similar point.

The aim of this thesis was to implement a high resolution 3D physical-biogeochemical ocean numerical model to the Iberian margin that could reasonably reproduce the spatio-temporal patterns of the plankton ecosystem over the shelf and the adjacent oceanic region. Thus, starting from the hydrodynamic configuration of ROMS for the Iberian margin previously developed by the research group, three biogeochemical modules of slightly different complexity available for ROMS were coupled to the high resolution circulation model. They were tuned to reproduce some of the existing observations of the plankton ecosystem and biogeochemistry over the region. Biogeochemical model results were validated by comparison with remotely sensed chlorophyll, biogeochemical proprieties from the World Ocean Atlas (nitrate, oxygen), and some in situ observations. This was made in close collaboration with the Oceanology Group of the Instituto de Investigacións Mariñas de Vigo-CSIC (Spain), due to their broad experience in biogeochemical observational studies and their availability of data collected over the northwestern Iberian shelf. The collaboration took place within the frame of the RAIA (2009-2011) and RAIAco projects (2012-2013) (Observatorio Oceanográfico da Marxe Ibérica; www.marnaraia.com).

A specific objective was to study the influence of the physical conditions in the seasonal, interannual and short-term variability of the biogeochemical propierties (phytoplankton and zooplankton biomass, detritus, nutrients, and oxygen). For that, once validated, biogeochemical model results were applied to make a 3D characterization of the seasonality of the plankton ecosystem, with a focus on chlorophyll (Chapter 3 and Chapter 4 for the operational implementation) and oxygen concentration (Chapter 5), exploring the physical, geochemical and biological coupling. Finally, an interannual modeling study of chlorophyll variability over the decade 2001-2010 was addressed in Chapter 6. Overall, this research aimed to provide a better understanding of the present situation as a mandatory first step to move forward into exploring future trends in the biogeochemical dynamics of the ecosystem.

Chapter 2

Ocean model description

The seasonal dynamics of the Iberian System (IS) was simulated with a high resolution nested configuration of the Regional Ocean Modeling System (ROMS) (Shchepetkin and McWilliams, 2005; Haidvogel et al., 2008) using AGRIF (Adaptive Grid Refinement In Fortran) nesting[1] (Penven et al., 2006). ROMS is a three-dimensional (3D) ocean circulation model with free-surface, vertical terrain-following coordinates (sigma-coordinates), and horizontal orthogonal curvilinear coordinates, designed to resolve regional problems, such as coastal areas and regional seas at the mesoscale. ROMS solves the incompressible primitive equations based on the Boussinesq and hydrostatic approximations, and is coupled with advection/diffusion schemes for potential temperature and salinity as well as a nonlinear equation of state. The advection scheme involves the split of advection and diffusion, in order to reduce spurious diapycnal mixing in sigma-coordinate models (Marchesiello et al., 2009). Vertical mixing consists in the KPP (K-profile parameterization) scheme (Large et al., 1994), which has special relevance for biogeochemistry simulations as it allows an appropriate exchange of properties between the mixed layer and the thermocline.

ROMS is coupled to a biogeochemical model that calculates the source and sink terms for the biological and chemical components. The biogeochemical model is a nitrogen based NPZD-type model (Nutrients-Phytoplankton-Zooplankton-Detritus). Three options of this model are configurable by the user in ROMS, with increasing number of biological and chemical components. The variables solved by ROMS are potential temperature and salinity, surface elevation, barotropic and baroclinic horizontal velocity components, vertical velocity, and the state variables of the biogeochemical model.

[1] ROMS-AGRIF version 2.1

A high-resolution configuration for the western Iberian margin using two offline nested domains was implemented. The biogeochemical-ecosystem dynamics of the IS was studied running the following simulations:

1. A climatological simulation (9 years): $NChlPZD$ model, including O_2.
2. A simulation of the period May 2001-April 2002: $NChlPZD$ model, including O_2.
3. An interannual simulation 2001-2010: $N_2ChlPZD_2$ model.

In the next sections the configuration of the hydrodynamic model and the biogeochemical models used in this work are described. The hydrodynamic configuration is the same used in Nolasco et al. (2013) and Marta-Almeida et al. (2012), who validated the hydrodynamic model to characterize the seasonal ocean dynamics of the IS. Similar configurations of the model have been successfully applied to study the hydrodynamics of the region (Peliz et al., 2007a; Oliveira et al., 2009; Peliz et al., 2009).

2.1 Hydrodynamic model

2.1.1 Model domains

The range of scales to be solved, from the large-scale to the mesoscale, was handled using a two-domain approach, as shown in Figure 3.1. A large-scale first domain (FD) was run independently (offline) in order to provide initial and boundary conditions to our second domain (SD).

The FD had 1/10° ($\sim$9 km) horizontal resolution and 30 vertical sigma levels, in order to resolve the large-scale circulation features, such as the Azores Current, and its interaction with the Atlantic margin of the Iberian Peninsula. The stretching factors were θ_s=7 and θ_b=0, to guarantee a good near-surface resolution over the entire domain. The bathymetry was based on ETOPO1 (Amante and Eakins, 2009), with corrections near the slope and a smoothing filter to fulfill the r=Δh/2h criteria (Haidvogel and Beckmann, 1999), r$<$0.2.

Open boundary conditions (section 2.1.2) were introduced as in Marchesiello et al. (2001), with inflow (outflow) nudging timescales of 1 (360) days for tracers and 10 (360) days for momentum respectively. Sponge layers were applied along the edges with a band of 120 km, with a lateral viscosity coefficient ranging from 600 m^2/s at the boundary to zero

at the interior. Explicit viscosity and diffusivity was null, and a linear drag formulation with coefficient r = 3×10^{-4} m s^{-1} was applied at the bottom.

The high-resolution nested domain, or second domain (SD) (Fig. 3.1), covers the target region of study. It included the coastal and adjacent oceanic region from the Gulf of Cádiz to northwest Iberia (Galicia) (34.5° N to 45.5° N and 5.5° W to 12.5° W; $\sim$1200$\times$600 km). The horizontal resolution was 1/27° ($\sim$3 km) and 60 vertical sigma levels in order to properly resolve the Mediterranean undercurrent (MU), which circulation is known to influence the surface transport of chemical and biological properties (Serra et al., 2010). θ_s=4 and θ_b=0 are used to enhance near-surface resolution. The bathymetry by Sibuet et al. (2004) was used, which had a resolution of $\sim$1 km and was smoothed in order to fulfill the same r-factor criteria (r-factor less than 0.2) of the large-scale domain.

Similarly to the large-scale simulation, a nudging sponge layer was introduced in the SD. Open boundary conditions were the same as for the FD configuration, however the sponge layers were applied to a band of 40 km, with a lateral viscosity coefficient ranging from 200 m^2 s^{-1} at the boundary to zero at the interior. A quadratic drag coefficient of 5×10^{-3} was used.

2.1.2 Boundary and initial conditions

2.1.2.1 Climatological simulation

A climatological surface forcing (see below) was applied in the surface boundary condition of both domains in order to study the mean ecological-biogeochemical situation and seasonal evolution of the IS, i.e., without considering the interannual variability. The $NChlPZD$ biogeochemical model was used (section 2.2.1).

The FD was initialized with temperature and salinity climatologies from Conkright et al. (2002), which also provided the open boundary conditions. The surface was forced with monthly climatological wind stress and fluxes of heat and freshwater from the Comprehensive Ocean-Atmosphere dataset (COADS; da Silva et al., 1994). Initial velocities were zero and monthly geostrophic velocities (referenced to 1200 m) and Ekman velocities were calculated from the climatology and applied along the lateral boundaries.The Mediterranean outflow was introduced as a nudging condition as described in Peliz et al. (2007a).This configuration (FD) was run for 15 years, and it was validated by a comparison of mean eddy kinetic energy maps with AVISO altimetry data, with a methodology similar to that described by Peliz et al. (2007a).

The forcing for the high-resolution (SD) configuration was the same used for the FD, i.e., COADS climatology. The initialization (1st January) and the boundary conditions were obtained using year 5 from FD, with average values of the physical variables stored every 3 days. The exchange of Atlantic and Mediterranean waters at the Strait of Gibraltar was explicitly represented in the high resolution domain by the imposition of vertical profiles of temperature, salinity and zonal velocity at the 5 grid points at the Strait, similarly to Peliz et al. (2007a). This condition was designed to setup a transport of 0.8 Sv leaving the domain through the surface layer, and 0.7 Sv entering the domain through the bottom layer. A vertical profile of nitrate was additionally imposed, based in the nitrate climatology for the Mediterranean provided by the University of Liège (http://gher-diva.phys.ulg.ac.be), which avoided negative values at the Strait. The process of entrainment of Atlantic Central Waters with the MU was also parameterized by increasing the viscosity and diffusivity coefficients in a region where the MW is strongly mixed with the overlying Atlantic waters, until the MW vein forms along the northern slope of the Gulf of Cadiz.

The freshwater continental runoff from the main rivers of the region (identified in Figure 3.1) was included with monthly climatological discharge values: For the Portuguese rivers, climatological values were provided by Instituto Nacional da Água (INAG); the climatological discharge of the Galician rivers was obtained from Río-Barja and Rodríguez-Lestegás (1992).

The nested (SD) domain was run for 6 years, having reached a stable equilibrium solution in the 3rd year, until the Mediterranean water was in equilibrium and adjusted along the western and northern Iberian margin. The month of January of the 7th year run was chosen to initialize the biogeochemical models described in section 2.2.1 and section 2.2.2, which ran for 9 more years. Both configurations converge in 1-2 years as observed by the time evolution of the biogeochemical variables. Therefore, we let 3 years of spin up, and model results presented are seasonal/monthly/annual averages over 6 years (4th to 9th climatological years).

2.1.2.2 Interannual simulation 2001-2010

A simulation of the period 2001–2010 was performed using the same two-nested domains configuration, with the aim to study the interannual variability of the ecosystem-biogeochemical characteristics of the IS. The $N_2ChlPZD_2$ biogeochemical model was used (section 2.2.3). An indepented simulation of the period January 2001 - April 2002 was run for the $NChlPZD + O_2$ biogeochemical model (section 2.2.2).

A climatological run of five years of the FD was used as the initial state to run a realistic simulation of the hydrodynamic model for the period 2001-2010 for this domain. The surface forcing was extracted from NCEP 2 reanalysis for air-sea fluxes (Kanamitsu et al., 2002), provided by the NOAA, and QuikSCAT surface wind reanalysis (2001–2008) at $0.5° \times 0.5°$ spatial resolution provided by CERSAT. For 2009 and 2010, ASCAT surface wind reanalysis ($0.25° \times 0.25°$ spatial resolution) was used, also provided by CERSAT, since QuikSCAT mission stopped towards the end of 2009.

The year 2001 was initialized from 1st January for the SD, using initial conditions from the climatological run of the coupled hydrodyanamic-biogeochemical model (9th year). The boundary conditions were provided by the simulation of 2001–2010 for the FD, and the same surface forcing was applied. The biogeochemical boundary conditions were climatological, as will be described in section 2.2.

The continental runoff from the main rivers of the region was included, either as monthly climatological discharge values, as described before or, when available, as realistic discharges for 2001–2010 provided by INAG (available for the three main rivers: Minho, Douro, and Tagus, Figure 3.1).

2.2 Biogeochemical model

Two biogeochemical models have been used to simulate the base trophic levels and biogeochemical components of the Iberian System: A $NChlPZD$ model (optional Oxygen) (sections 2.2.1 and 2.2.2) and a $N_2ChlPZD_2$ model (section 2.2.3). Both models derive from the ecosystem model of Fasham et al. (1990), although introducing considerable modifications described in Gruber et al. (2006). Thus, the remineralization process was introduced using implicit parameterizations, allowing the elimination of the bacteria pool as a variable. Dissolved organic nitrogen (DON) and detrital organic nitrogen were replaced with one pool of detritus ($NChlPZD$ model) or two pools of detritus ($N_2ChlPZD_2$ model), i.e., a fast sinking pool (large detritus) and a slow sinking pool (small detritus), the latter mimicking DON and fine, slow-sinking particles. Sinking is modelled explicitly, which allows lateral advection of the variables even in the aphotic zone. A variable chlorophyll:carbon ratio was also introduced. Most of the changes described aimed to simplify the model and reduce the number of parameters, while keeping or improving the skill of the model (Gruber et al., 2006). The models used here are a subsequent addaptation from the biological model of ROMS developed by Gruber et al. (2006) at UCLA, to be introduced in the AGRIF version of ROMS (Koné et al., 2005).

The 3D time evolution of the concentration of any of the biogeochemical variables (B_i) is influenced by diffusion, horizontal advection, vertical mixing and the biogeochemical processes that act as sink or source for the variable:

$$\frac{\partial B_i}{\partial t} = \nabla \cdot K \nabla B_i - u \cdot \nabla_h B_i - (w + w_{sink}) \frac{\partial B_i}{\partial z} + SMS(B_i) \tag{2.1}$$

where K is the eddy kinematic diffusivity tensor, u is the horizontal velocity, w and w_{sink} are the vertical velocity and the vertical sinking rate of the biogeochemical variable (all particulated variables, except zooplankon), respectively. The biogeochemical processes included in the source minus sink (SMS) term are specific for each variable, and will be described in detail in the next sections.

2.2.1 $NChlPZD$ model

The biogeochemical $NChlPZD$ model consists of a 4-component nitrogen based ecosystem model, computing 5 state variables: nitrate (NO_3), phytoplankton ($Phyt$), zooplankton (Zoo) and detritus (Det), all expressed in mmol N m^{-3} (Fig. 2.1). Additionally, chlorophyll-a (mg m^{-3}) is derived from phytoplankton concentration using a variable chlorophyll:carbon ratio, θ (mg chlorophyll-a (mg C)$^{-1}$), that is a function of light and nutrients availability, and a C:N ratio of 6.625 (mmol C (mmol N)$^{-1}$), i.e., a Redfield ratio. The variable θ describes the proportion of photosynthetically fixed carbon that is used for chlorophyll-a biosynthesis considering the model of Geider et al. (1997). Its implementation in the ocean model is described in Gruber et al. (2006) and reproduced in the appendix (A.1).

The biogeochemical processes included in SMS for each variable (Eq. 2.1) represent the conceptual description that follows. Phytoplankton uptakes nitrate (NO_3) at a rate that is dependent on the instantaneous nitrate concentration and light intensity (PAR: photosynthetically available radiation), and further constrained by temperature (T). The nutrient (NO_3) limitation of the growth rate, $\mu(NO_3)$, is calculated by a Michaelis-Menten function

$$\mu(NO_3) = \frac{NO_3}{K_{NO3} + NO_3} \tag{2.2}$$

where K_{NO3} is the half-saturation constant for nitrate uptake by phytoplankton. T and PAR limitation of the phytoplankton growth rate, $\mu(T, PAR)$, follows the equations of Smith (1936) (Eq. 2.3) and Eppley (1972) (Eq. 2.4) modified to include θ.

$$\mu(PAR, T) = \frac{\mu(T) \cdot \alpha \cdot PAR \cdot \theta}{\sqrt{\mu(T)^2 + (\alpha \cdot PAR \cdot \theta)^2}} \tag{2.3}$$

$$\mu(T) = ln2 \cdot 0.851 \cdot (1.066)^T \tag{2.4}$$

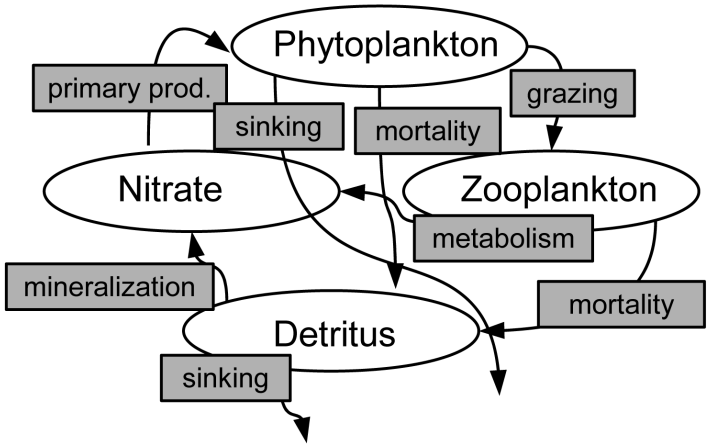

Figure 2.1: Diagram of the $NChlPZD$ model. Model state variables (nitrate, phytoplankton, zooplankton and detritus) are represented in terms of nitrogen concentration.

Parameter		Value	Unit
K_w	Light attenuation in seawater	0.04	m^{-1}
k_{chla}	Light attenuation by chlorophyll	0.024	$(m^2\,mg\ Chla)^{-1}$
α	Initial slope of the P-I curve	1	mg C (mg ChlaW m^{-2} d)$^{-1}$
θ	Maximum cellular chlorophyll:C ratio	0.03	mg Chla(mg C)$^{-1}$
K_{NO3}	Half-saturation for phytoplankton NO_3 uptake	1.5	mmol N m^{-3}
K_P	Zooplankton half-saturation constant for ingestion	1	mmol N m^{-3}
g_{max}	Maximum zooplankton growth rate	0.9	d^{-1}
β	Zooplankton assimilation coefficient	0.75	n.d.
m_{PD}	Phytoplankton mortality rate	0.03	d^{-1}
m_{ZD}	Zooplankton mortality rate	0.1	d^{-1}
t_{Zmetab}	Zooplankton specific excretion rate	0.1	d^{-1}
t_{Dremin}	Detrital mineralization to NO_3 rate	0.05	d^{-1}
w_P	Sinking velocity for phytoplankton	0.5	m d^{-1}
w_D	Sinking velocity for detritus	5	m d^{-1}

Table 2.1: Parameter values of the $NChlPZD$ model.

The inclusion of θ tried to represent the expected increase in photosynthesis when phytoplankton cells allocate a higher percentage of their structure to the photosynthetic apparatus (higher θ), which seems to occur in nearly nutrient-replete regions such as the upwelling zone or in the proximity of the sub-surface chlorophyll maximum (Gruber et al., 2006). PAR refers to in situ PAR, and α is the initial slope of the growth versus light relationship. PAR at the surface, PAR_0, is calculated as 43% of the incident radiation and attenuated with depth as it is absorbed by water and chlorophyll,

$$PAR = PAR_0 \cdot exp\ (k_w + k_{chla}\ Chl)\Delta z \tag{2.5}$$

where k_w and k_{chla} are attenuation coefficients for pure water and chlorophyll and Δz is the depth step. PAR is given in W m^{-2}. The total phytoplankton growth rate is written as

$$\mu = \mu(PAR, T) \cdot \mu(NO_3) \tag{2.6}$$

Phytoplankton dies at a constant linear rate (m_{PD}) been automatically incorporated to the detritus pool. Zooplankton growth relies on its grazing on phytoplankton, which rate depends on prey (phytoplankton) concentration, through a Michaelis-Menten function,

$$g = g_{max}\ \frac{Phyt}{K_P + Phyt} \tag{2.7}$$

and on zooplankton assimilation efficiency (β). A constant excretion rate ($t_{Z_{metab}}$) is attributed to zooplankton, providing a source of nutrients to the nitrate pool. Zooplankton incorporates to the detritus pool at a constant linear mortality rate (m_{ZD}). Mineralization of detritus is formulated as direct transformation to nitrate at a constant nitrification rate ($t_{D_{remin}}$). Model parameters values for the sink/source terms selected to represent our region of study are listed in Table 2.1. These parameters aimed at representing the eutrophic coastal ecosystem dominated by diatoms, what necessarily implied reducing the ability of the model to represent correctly the oligotrophic offshore environment, as only one phytoplankton functional group was included.

The set of SMS equations for each of the biogeochemical variables is:

$$SMS(NO_3) = -\mu(PAR, T) \cdot \mu(NO_3) \cdot Phyt + t_{D_{remin}}\ Det + t_{Z_{metab}}\ Zoo \tag{2.8}$$

$$SMS(Phyt) = \mu(PAR, T) \cdot \mu(NO_3) \cdot Phyt - m_{PD}\ Phyt - g_{max}\ Zoo\ \frac{Phyt}{K_P + Phyt} \tag{2.9}$$

$$SMS(Zoo) = \beta\ g_{max}\ Zoo\ \frac{Phyt}{K_P + Phyt} - m_{ZD}\ Zoo - t_{Z_{metab}}\ Zoo \tag{2.10}$$

$$SMS(Det) = m_{PD}\ Phyt + m_{ZD}\ Zoo + (1-\beta)\ g_{max}\ Zoo\ \frac{Phyt}{K_P + Phyt} - t_{D_{remin}}\ Det \tag{2.11}$$

$$SMS(\theta) = \mu(PAR, T) \cdot \mu(NO_3) \cdot \left(\frac{\mu(T) \cdot \mu(NO_3) \cdot \theta_{max}}{\sqrt{\mu(T)^2 + (\alpha\ PAR\ \theta)^2}} - \theta \right) \tag{2.12}$$

The concentration of nitrate and chlorophyll-a for the model initial and boundary conditions were supplied by the climatological data sets World Ocean Atlas 2009 (Garcia et al., 2010b) and SeaWiFS, respectively. For nitrate, seasonal (for depths down to 500 m) and annual (depths below 500 m) climatologies were used. For chlorophyll-a, the seasonal climatology of surface concentrations from SeaWiFs data was used. Seasonal vertical profiles were created from these surface concentrations using the algorithm of Morel and Berthon (1989). The initial and boundary values of phytoplankton and zooplankton were derived from chlorophyll-a ($Phyt = 0.5 \cdot Chl$; $Zoo = 0.2 \cdot Chl$), as in Gruber et al. (2006). Detritus was not available from climatological datasets, so it was introduced constant (initial and boundary conditions) with the value 0.02 mmol N m^{-3}. Boundary conditions were supplied seasonally. The riverine inputs of nitrate and chlorophyll were used constant along the year (Table 4.1).

2.2.2 $NChlPZD + O_2$ model

Biogeochemical simulations of the oxygen (O_2) cycle were performed with a $NPZD + O_2$ model (Nitrate-Phytoplankton-Zooplankton-Detritus + Oxygen) coupled to ROMS. The NPZD model was a simple 4-components nitrogen based biogeochemical model computing the mentioned state variables in mmol N m^{-3}, as described in section 2.2.1. O_2 concentration (expressed in mmol O_2 m^{-3}) was computed in the model so that it was influenced by other biogeochemical variables, but O_2 did not have an effect on them, as will be detailed below (Fig. 2.2). The biogeochemical processes affecting O_2 concentration and included in the SMS term (equation 2.1) are indicated in Figure 2.2, and the parameters used to represent them are listed in Table 2.2. The parameters affecting the NPZD part of the model take the same values previously indicated in section 2.2.1. Next, the O_2 sinks ands sources in the model are described in more detail. A detailed description of the sink and sources for the other biogeochemical variables was already presented in section 2.2.1

Oxygen is produced by photosynthesis during phytoplankton growth, so its production rate can be calculated from nitrate uptake using a Redfieldian $r_{O_2:NO_3}$ stoichiometric ratio. Zooplankton metabolism consumes O_2, and this is estimated from the excretion of nutrients to the environment. Bacterial mineralization of detritus to nutrients also consumes O_2. Since the model only has one nutrient compartment, nitrate, the mineralization process was simplified to a direct oxidation from detritus to nitrate and the O_2 consumed was computed using again the $r_{O_2:NO_3}$ ratio. The sediment compartment was not included in the model, so the detritus reaching the seafloor was simply incorporated to the bottom layer of the model in the water column, where it mineralized to nitrate at the specified

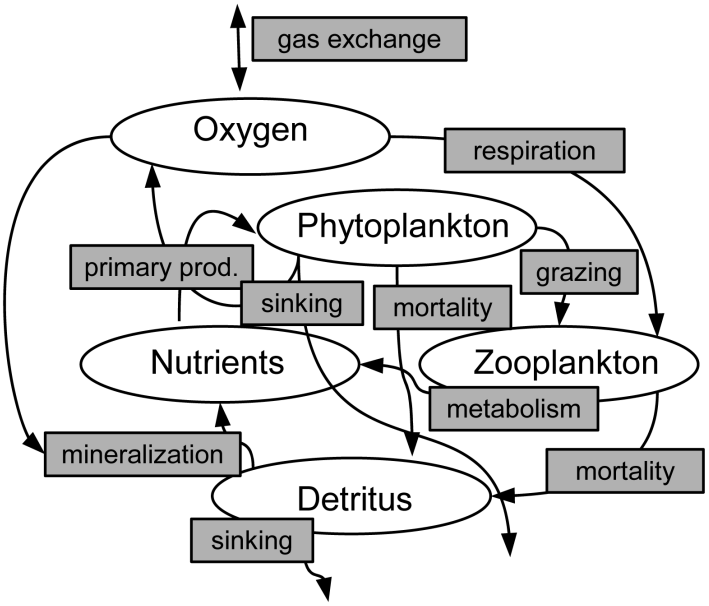

Figure 2.2: Diagram of the $NPZD + O_2$ model. Model state variables (nitrate, phytoplankton, zooplankton and detritus) are represented in terms of nitrogen concentration.

Parameter		Value	Unit
K_w	Light attenuation in seawater	0.04	m^{-1}
K_{chla}	Light attenuation by chlorophyll	0.024	$(m^2\,mg\ Chla)^{-1}$
α	Initial slope of the P-I curve	1	mg C (mg ChlaW m^{-2} d)$^{-1}$
$r_{C:NPhyt}$	C:N ratio for phytoplankton	6.625	mol C(mol N)$^{-1}$
$r_{O2:Nmetab}$	O_2:N ratio for zooplankton metabolism	6.625	mol O_2(mol N)$^{-1}$
$r_{O2:NO3}$	O_2:N ratio for photosynthesis/mineralization	8.625	mol O_2(mol N)$^{-1}$
θ_{max}	Maximum cellular chlorophyll:C ratio	0.03	mg Chla(mg C)$^{-1}$
K_{NO3}	Half-saturation for phytoplankton NO_3 uptake	1.5	mmol N m^{-3}
K_P	Zooplankton half-saturation constant for ingestion	1	mmol N m^{-3}
g_{max}	Maximum zooplankton growth rate	0.9	d^{-1}
β	Zooplankton assimilation coefficient	0.75	n.d.
m_{PD}	Phytoplankton mortality rate	0.03	d^{-1}
m_{ZD}	Zooplankton mortality rate	0.1	d^{-1}
t_{Zmetab}	Zooplankton specific excretion rate	0.1	d^{-1}
t_{Dremin}	Detrital mineralization to NO_3 rate	0.05	d^{-1}
w_P	Sinking velocity for phytoplankton	0.5	m d^{-1}
w_D	Sinking velocity for detritus	5	m d^{-1}

Table 2.2: Parameter values of the $NPZD + O_2$ model.

mineralization rate. This representation of detritus mineralization near the bottom was in agreement with the findings of (Arístegui et al., 2009), showing that in the Iberian shelf most organic matter reaching the bottom during the upwelling period was oxidized in the nepheloid layer and not in the sediment. Gas exchange with the atmosphere at the ocean surface was introduced in the top cells of the model. Thus, the O_2 SMS term takes the form:

$$SMS(O_2) = \mu(PAR,T) \cdot \mu(NO_3) \cdot Phyt \cdot r_{O_2:NO_3} - t_{Z_{metab}}\, Zoo \cdot r_{O_2:N_{metab}} - t_{D_{remin}}\, Det \cdot r_{O_2:NO_3} + Q_{ge}\,(O_2sat - O_2) \quad (2.13)$$

where the first term in the right hand side of the equation accounts for O_2 production by photosynthesis (phytoplankton growth). Phytoplankton growth rate (μ) is limited by light (photosynthetically available radiation: PAR), temperature (T) and nutrients (N) using the equations $\mu(PAR,T)$ and $\mu(N)$ described in section 2.2.1, with $\mu(PAR,T)$ modified as in Gruber et al. (2006) to include a variable chlorophyll:C ratio (θ).

The second term in Equation 2.13 accounts for O_2 consumption by zooplankton respiration (basal metabolism), estimated from the excretion of nutrients to the environment, with $t_{Z_{metab}}$ the zooplankton specific excretion rate (Table 2.2). The third term of the equation formulates detritus mineralization as an O_2 sink, with $t_{D_{remin}}$ the detrital mineralization to nitrate rate (Table 2.2). The stoichiometric ratios for photosynthesis/ mineralization ($r_{O_2:NO_3}$) and zooplankton respiration ($r_{O_2:N_{metab}}$) convert Nitrogen concentration to O_2 concentration (Table 2.2).

The last term in Equation 2.13 represents the exchange of O_2 with the atmosphere at the sea surface. This flux can be either to the ocean (source) or from the ocean to the atmosphere (sink), depending on whether the surface layer is under-saturated or over-saturated in O_2. It is calculated after the biogeochemical reactions were calculated. The gas exchange rate of O_2 is calculated as:

$$Q_{ge} = \frac{K_v}{\Delta z} \quad (2.14)$$

where Δz is the height of the top cell and K_v is the gas transfer coefficient calculated as:

$$K_v = 0.31 \cdot u^2 \cdot \sqrt{\frac{660}{Sc}} \quad (2.15)$$

with u the wind speed and Sc the Schmidt number calculated after Wanninkhof (1992). The saturation concentration of oxygen (O_2sat) is calculated in a separated subroutine.

Initial and boundary conditions for O_2 and nitrate were supplied from climatological data of the World Ocean Atlas (WOA) 2009 (Garcia et al., 2010a,b). Seasonal (for depths

down to 500 m) and annual (depths below 500 m) climatologies were used. Initial and boundary chlorophyll-a concentrations were attributed from SeaWiFS seasonal climatology. Seasonal vertical profiles were created from these surface concentrations using the algorithm of Morel and Berthon (1989). Phytoplankton and zooplankton initial and boundary data where derived from chlorophyll-a ($Phyt = 0.5 \cdot Chl$; $Zoo = 0.2 \cdot Chl$) (Gruber et al., 2006). Initial and boundary values of detritus concentrations were introduced as constant (0.02 mmol N m^{-3}). Boundary conditions for all the biogeochemical variables were supplied seasonally (15th February for Winter, 15th May for Spring, 15th August for Summer, and 15th November for Autumn). Constant river inputs of nitrate and chlorophyll were used along the year (Table 4.1; Marta-Almeida et al., 2012)). Also, a constant river input of oxygen was used (125 mmol O_2 m^{-3}), based on data from Ferreira et al. (2003).

2.2.3 $N_2ChlPZD_2$ model

The biogeochemical $N_2ChlPZD_2$ model consists of a 6-component nitrogen based ecosystem model, computing 7 state variables: nitrate (NO_3), ammonium (NH_4), phytoplankton ($Phyt$), zooplankton (Zoo), large detritus ($LDet$), and small detritus ($SDet$), all expressed in mmol N m^{-3} (Fig. 2.3). Additionally, chlorophyll-a (mg m^{-3}) is derived from phytoplankton concentration using a variable chlorophyll:carbon ratio, θ (mg chlorophyll-a (mg C)$^{-1}$) and a C:N ratio of 6.625 (mmol C (mmol N)$^{-1}$), i.e., a Redfield ratio. As it was explained in section 2.2.1, the variable θ describes the proportion of photosynthetically fixed carbon that is used for chlorophyll-a biosynthesis considering the model of Geider et al. (1997) (see appendix A.1).

The biogeochemical processes included in SMS for each variable (Eq. 2.1) are similar to those previously described for the $NChlPZD$ model, except for including nitrogen limitation of phytoplankton growth by two nutrients, nitrate and ammonium, and including two pools of detritus, large detritus (fast sinking) and small detritus (slow sinking). Nitrate and ammonium are the most important sources of nitrogen for phytoplankton in the ocean, the first one is supplied from the thermocline (new production) and the second one coming from recycling of organic matter (regenerated production) (Dugdale and Goering, 1967; Sarmiento and Gruber, 2006). Therefore, the inclusion of ammonium in the model allows for a more realistic representation of remineralization processes. The introduction of a small detritus pool mimicks DON and fine slow-sinking particles, with this two-size approach allowing for a reasonable reproduction of observed particle dynamics in terms of organic matter export out of the upper ocean (Jackson, 2001; Gruber et al., 2006).

Phytoplankton growth rates are thus controlled by nitrate and ammonium concen-

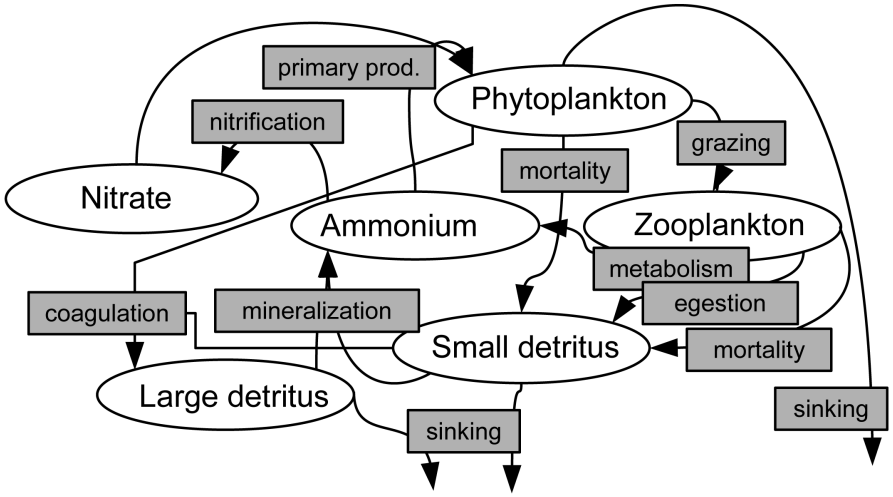

Figure 2.3: Diagram of the N_2PZD_2 model. Model state variables (nitrate, ammonium, phytoplankton, zooplankton, small detritus and large detritus) are represented in terms of nitrogen concentration.

Parameter		Value	Unit
K_w	Light attenuation in seawater	0.04	m^{-1}
K_{chla}	Light attenuation by chlorophyll	0.024	$(m^2\,mg\,Chla)^{-1}$
α	Initial slope of the P-I curve	1	mg C (mg ChlaW m^{-2} d)$^{-1}$
θ_{max}	Maximum cellular chlorophyll:C ratio	0.03	mg Chla(mg C)$^{-1}$
K_{NO3}	Half-saturation for phytoplankton NO_3 uptake	0.9	mmol N m^{-3}
K_{NH4}	Half-saturation for phyoplankton NH_4 uptake	0.5	mmol N m^{-3}
K_P	Zooplankton half-saturation constant for ingestion	1	mmol N m^{-3}
g_{max}	Maximum zooplankton growth rate	0.6	d^{-1}
β	Zooplankton assimilation coefficient	0.75	n.d.
m_{PD}	Phytoplankton mortality rate to small detritus	0.072	d^{-1}
m_{ZD}	Zooplankton mortality rate to small detritus	0.025	d^{-1}
t_{Zmetab}	Zooplankton specific excretion rate	0.1	d^{-1}
$t_{SDremin}$	Small detritus mineralization to NH_4 rate	0.03	d^{-1}
$t_{LDremin}$	Large detritus mineralization to NH_4 rate	0.01	d^{-1}
$t_{NH4nitr}$	NH_4 nitrification rate	0.05	d^{-1}
S_{agg}	Specific aggregation rate (Phyt + SDet)	0.005	(mmol N d)$^{-1}$
w_P	Sinking velocity for phytoplankton	0.5	m d^{-1}
w_{LD}	Sinking velocity for large detritus	10	m d^{-1}
w_{SD}	Sinking velocity for small detritus	1	m d^{-1}

Table 2.3: Parameter values of the $N_2ChlPZD_2$ model.

tration, light (PAR), and temperature. The light dependent, temperature limited growth rate, $\mu(T, PAR)$, is the same as in equation 2.3 (Smith, 1936), with $\mu(T)$ as in equation 2.4 (Eppley, 1972). The exponential decrease of PAR with depth is calculated following equation 2.5. Taking into account that ammonium is taken up preferencially over nitrate (Dugdale and Goering, 1967), phytoplankton growth rates $\mu(NO_3)$ and $\mu(NH_4)$ are formulated using a Michaelis-Menten equation where NH_4 is preferred to NO_3 for phytoplankton uptake (Parker, 1993):

$$\mu(NH_4) = \frac{NH_4}{K_{NH_4} + NH_4} \tag{2.16}$$

$$\mu(NO_3) = \frac{NO_3}{K_{NO_3} + NO_3} \cdot \frac{K_{NH_4}}{K_{NH_4} + NH_4} \tag{2.17}$$

The final nutrient limited growth rate is thus an additive function weighted towards ammonium:

$$\mu(NO_3, NH_4) = \frac{NO_3}{K_{NO_3} + NO_3} \cdot \frac{K_{NH_4}}{K_{NH_4} + NH_4} + \frac{NH_4}{K_{NH_4} + NH_4} \tag{2.18}$$

where K_{NO_3} and K_{NH_4} are the half-saturation constants for nitrate and ammonium uptake, respectively. Phytoplankton dies at a constant linear rate (m_{PD}) been automatically incorporated to the small detritus pool, a formulation similar to the model of Gruber et al. (2006) and references therein. Zooplankton growth relies on its grazing on phytoplankton, which rate depends on prey (phytoplankton) concentration, through a Michaelis-Menten function (Eq. 2.7) and on zooplankton assimilation efficiency (β). The fraction of organic nitrogen that is consumed by zooplankton but not assimilated ($(1-\beta)\ g_{max}\ Zoo\ \frac{Phyt}{K_P+Phyt}$), i.e., egestion as fecal pellets, is incorporated to the small detritus pool. A constant excretion rate ($t_{Z_{metab}}$) is attributed to zooplankton, providing a source of nutrients to the ammonium pool. Zooplankton incorporates to the small detritus pool at a constant linear mortality rate (m_{ZD}). Large detritus (fast sinking) particles are formed by coagulation of phytoplankton with small detritus (slow sinking) particles. The particle coagulation is formulated assuming that the probability of particles making contact and coagulating is proportional to the concentration of particles ($S_{agg} \cdot (Phyt + SDet)^2$), with S_{agg} the specific aggregation rate (Stolzenbach and Elimelech, 1994; Gruber et al., 2006). Coagulation is therefore a sink for phytoplankton cells, an approach that is motivated by the observation that diatom blooms are often terminated by massive coagulation events (e.g. Alldredge and Gotschalk, 1989). Mineralization of large and small detritus is formulated as transformation into ammonium at constant ammonification rates, $t_{LD_{remin}}$ and $t_{SD_{remin}}$, respectively. Nitrification, i.e. the conversion of ammonium to nitrate, is represented using a constant nitrification rate $t_{NH4_{nitr}}$, the process being limited to the night period ($PAR = 0$) to account for photoinhibition of the nitrifying bacteria. Model parameters values for the sink/source terms selected to represent our region of study with this model

are listed in Table 2.3. As stated for the $NChlPZD$ model, these parameters aimed at representing the eutrophic coastal ecosystem dominated by diatoms, what necessarily implied reducing the ability of the model to represent correctly the oligotrophic offshore environment, as only one phytoplankton functional group was included.

The set of SMS equations for each of the biogeochemical variables is:

$$SMS(NO_3) = -\mu(PAR,T)\cdot\mu(NO_3)\cdot Phyt + t_{NH4_{nitr}}\ NH_4 \tag{2.19}$$

$$\begin{aligned} SMS(NH_4) = &-\mu(PAR,T)\cdot\mu(NH_4)\cdot Phyt - t_{NH4_{nitr}}\ NH_4 + t_{Z_{metab}}\ Zoo \\ &+ t_{SD_{remin}}\ SDet + t_{LD_{remin}}\ LDet \end{aligned} \tag{2.20}$$

$$\begin{aligned} SMS(Phyt) = &\mu(PAR,T)\cdot\mu(NO_3,NH_4)\cdot Phyt - m_{PD}\ Phyt \\ &- g_{max}\ Zoo\ \frac{Phyt}{K_P + Phyt} \end{aligned} \tag{2.21}$$

$$SMS(Zoo) = \beta\ g_{max}\ Zoo\ \frac{Phyt}{K_P + Phyt} - m_{ZD}\ Zoo - t_{Z_{metab}}\ Zoo \tag{2.22}$$

$$\begin{aligned} SMS(SDet) = &m_{PD}\ Phyt + m_{ZD}\ Zoo + (1-\beta)\ g_{max}\ Zoo\ \frac{Phyt}{K_P + Phyt} \\ &- t_{SD_{remin}}\ SDet - S_{agg}\ SDet\cdot(Phyt + SDet) \end{aligned} \tag{2.23}$$

$$SMS(LDet) = -t_{LD_{remin}}\ LDet + Sagg\cdot(Phyt + SDet)^2 \tag{2.24}$$

$$SMS(\theta) = \mu(PAR,T)\cdot\mu(NO_3,NH_4)\cdot\left(\frac{\mu(T)\cdot\mu(NO_3,NH_4)\cdot\theta_{max}}{\sqrt{\mu(T)^2 + (\alpha\ PAR\ \theta)^2}} - \theta\right) \tag{2.25}$$

The concentration of nitrate, phytoplankton (and chlorophyll-a), and zooplankton for the model initial conditions (January) were obtained from the 9th year climatological simulation of the $NChlPZD$ biogeochemical model (section 2.2.1). Boundary conditions for nitrate and chlorophyll were supplied by the climatological data sets World Ocean Atlas 2009 (Garcia et al., 2010b) and SeaWiFS, respectively. For nitrate, seasonal (for depths down to 500 m) and annual (depths below 500 m) climatologies were used. For chlorophyll-a, the seasonal climatology of surface concentrations from SeaWiFs data was used. Seasonal vertical profiles were created from these surface concentrations using the algorithm of Morel and Berthon (1989). Boundary conditions were supplied seasonally. Ammonium, small detritus, and large detritus initial and boundary conditions were not available from climatological data sets, so they were introduced as constant analytical values: 0.1 mmol N m^{-3} (ammonium) and 0.02 mmol N m^{-3} (both detritus sizes). The riverine inputs of nitrate and chlorophyll were used constant along the year (Table 4.1).

Chapter 3

Seasonal cycle of plankton production in the Iberian margin based on a high resolution ocean model

Rosa Reboreda, Rita Nolasco, Carmen G. Castro, Xosé A. Álvarez-Salgado, Nuno G. F. Cordeiro, Henrique Queiroga, Jesus Dubert.

3.1 Abstract

A $NChlPZD$ biogeochemical model was coupled to a physical high resolution configuration of the 3D Regional Ocean Modeling System (ROMS), to simulate the seasonal variability of plankton in the Iberian margin. Monthly mean conditions from COADS were applied to force the model at the surface. The $NChlPZD$ model simulated the time and space evolution of nitrate, phytoplankton/chlorophyll-a, zooplankton and detritus. Model results were compared to remotely sensed sea surface temperature from AVHRR, mixed layer depth from ARGO floats, and sea surface chlorophyll-a from both SeaWiFS climatology and optimal interpolation of SeaWiFS, MODIS, and MERIS. The model was able to reasonably reproduce the seasonal cycle of phytoplankton biomass in the Iberian Atlantic margin and the adjacent oceanic region. It allowed to make a general characterization of the spatio-temporal patterns of phytoplankton and zooplankton biomass, as well as detritus and nitrate distribution. However, some shortcomings in the model were detected,

as the anticipation and overestimation of the offshore spring phytoplankton bloom, and the overestimation of upwelling-related coastal maxima of chlorophyll-a in the northwestern shelf. The latter was probably a consequence of an intensified upwelling in the model due to the use of climatological winds. On the other hand, winter chlorophyll-a decrease simulated by the model over the shelf agreed with in situ samplings reported in the literature, contrasting with the high chlorophyll-a estimations of satellite data. This evidenced that care should be taken when validating model results in the Iberian coastal region using satellite chlorophyll-a products, particularly in winter.

3.2 Introduction

Phytoplankton biomass in the Iberian shelf reaches maxima in summer because of the fertilizing effect of the wind-driven coastal upwelling (Wooster et al., 1976; Fiuza et al., 1982; Barton et al., 1998) (Fig. 3.1). This physical-biological interaction makes the Iberian margin a very productive ecosystem, characterized by a rich marine biodiversity and important fishing and shellfish resources (Tenore et al., 1995; Figueiras et al., 2002; Santos et al., 2005).

The upwelling season is driven by dominant northerly winds from April to September (Wooster et al., 1976), which cause an offshore Ekman transport of surface sea water and the upwelling of cold and nutrient rich subsurface Eastern North Atlantic Central Water (ENACW) (Fraga, 1981; Peliz et al., 2002; Relvas et al., 2007). Although nutrient levels of subsurface ENACW are 1/2 - 1/3 of those in other upwelling systems, the gross primary production for the upwelling season ($\sim$2.5 g C m^{-2} day^{-1}, Álvarez-Salgado et al., 2010; Arístegui et al., 2006) is similar to other coastal upwelling regions. This fact is usually attributed to an efficient recycling (mineralization) of organic matter under periodic (1-3 weeks) wind stress-relaxation cycles (Arístegui et al., 2009; Álvarez-Salgado et al., 1993). The autumn (October-November) brings a shift to southerly winds, which favors downwelling conditions over the shelf (Álvarez-Salgado et al., 2003), coinciding with the onset of a warm and saline poleward current over the slope, the Iberian Poleward Current (IPC) (Haynes and Barton, 1990). This shift is usually coincident with a phytoplankton autumn bloom in the coast (Bode et al., 1996; Casas et al., 1997; Castro et al., 1997; Álvarez-Salgado et al., 2003). Upwelling pulses are still observed during winter which, along with water column haline stratification and nutrient supply from continental runoff, may keep chlorophyll-a concentration high (Ribeiro et al., 2005). In the adjacent oceanic region (Fig. 3.1) the seasonal cycle is characterized by low offshore phytoplankton biomass in summer (June-September), when nutrient depletion by strong thermal stratification

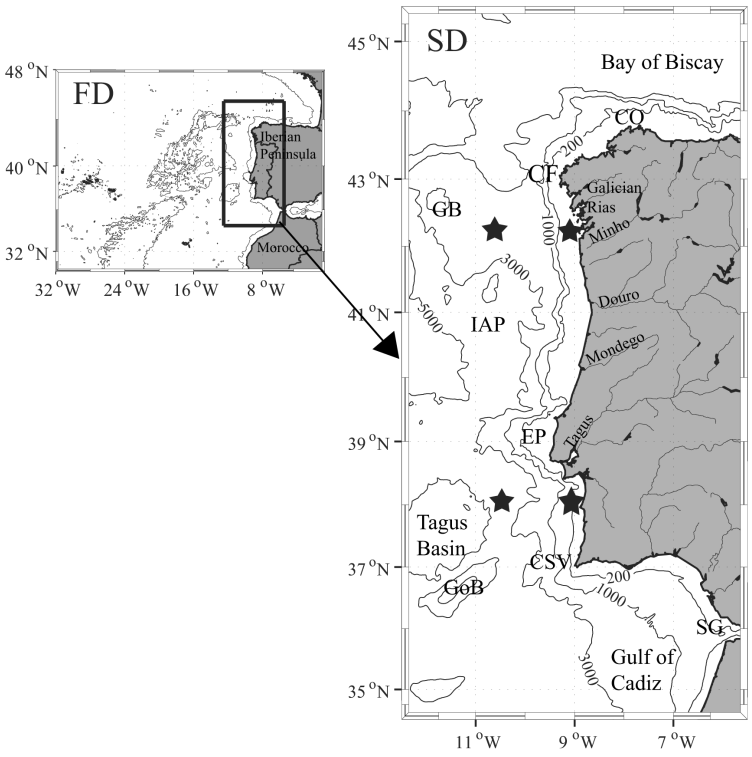

Figure 3.1: Region of study and model domains: the first domain (FD), comprising the Iberian Peninsula, the north of Africa (Morocco) and the Azores Islands; and the second domain (SD), comprising the Iberian margin. Main bathymetrics and topographic features are shown: Strait of Gibraltar (SG), Cape St Vicente (CSV), Gorringe Bank (GoB), Estremadura Promontory (EP), Iberian Abyssal Plain (IAP), Galicia Bank (GB), Cape Finisterre (CF) and Cape Ortegal (CO). The stars show the locations of model-satellite time series comparisons in section 3.5.2.

occurs, and by a conspicuous spring bloom, as part of the North Atlantic spring bloom (Longhurst, 1998).

In the western Iberian margin, the event-scale variability associated to mesoscale phenomena such as fronts, eddies, filaments, and river buoyant plumes are a major factor influencing the variability of the ecosystem through a tight morphological-physical-biological coupling (e.g. Castro et al., 2000; Queiroga et al., 2007; Santos et al., 2007; Cravo et al., 2010). For example, the shelf-ocean exchange of biogenic materials is thought to be strongly influenced by such mesoscale events, the off-shelf export being favored through filaments developed during the spring-summer upwelling (Álvarez-Salgado et al., 2001, 2007; Cravo et al., 2010) in opposition to *in situ* mineralization favored by autumn-winter termohaline fronts developed under downwelling conditions/ slope poleward flow (Álvarez-Salgado et al., 2003). Differences in the shelf width and the presence of topographical structures, such as capes, promontories and submarine

canyons are related to spatial differences in the mesoscale activity (Relvas et al., 2007), which is thought to have effects on the spatial differences in the ecosystem along the Iberian margin (Cunha, 2002).

The temporal and spatial variability of biological production in the Iberian margin has been sampled over the last decades, with field studies (e.g. Bode et al., 1996; Casas et al., 1997; Moita, 2001; Castro et al., 2006; Silva et al., 2009); satellite ocean color images (Sousa and Bricaud, 1992; Oliveira et al., 1994; Peliz and Fiuza, 1999; Álvarez et al., 2012a) or frequently a combination of both (e.g. Álvarez-Salgado et al., 2002, 2003; Joint et al., 2002; Ribeiro et al., 2005). These studies have contributed to our understanding of the planktonic ecosystem and biogeochemical functioning and variability in the Iberian margin. However, most of them are local or subregional studies and/or present a limited time coverage, due to the inherent diffulties of oceanographic sampling. Also, a division between the studies focusing on the NW Iberian margin and on the Portuguese margin is evident from a literature review, despite the common regional oceanography, so a joint view of the Iberian plankton ecosystem functioning and variability is usually lacking. In this respect ocean modeling can contribute to improve the current knowledge of the Iberian plankton ecosystem, complementing the spatial and temporal constraints of observations. Coupled physical-biogeochemical ocean models are useful to study the physical-biological interactions and help to understand their influence on the seasonal evolution and the variability and distribution of biogeochemical properties, as seen for other coastal upwelling systems such as California (Moisan and Hofmann, 1996; Gruber et al., 2006; Powell et al., 2006), Humboldt (Echevin et al., 2008), and Benguela (Koné et al., 2005; Machu et al., 2005). Although some previous ocean biogeochemical modeling studies exist for the Atlantic Iberian margin, they are either local applications to coastal embayments (Torres et al., 2006; Torres-López et al., 2005; Rodrigues et al., 2009) or modeling studies limited to a small coastal region and/or for a specific oceanographyc period (Slagstad and Wassmann, 2001; Lopes et al., 2009). On the other hand, the study of the regional hydrodynamics off western Iberia has benefited from high resolution three-dimensional (3D) modeling studies over the last years (Peliz et al., 2003; Marta-Almeida et al., 2006; Peliz et al., 2007a, 2009; Nolasco et al., 2013), giving a good base to move forward to coupled hydrodynamic-biogeochemical modeling studies in the Iberian margin.

The aim of this work was to couple a high resolution regional configuration of the three-dimensional (3D) Regional Ocean Modeling System (ROMS) to a NPZD (Nitrate-Phytoplankton-Zooplankton-Detritus) biogeochemical model, to simulate the seasonal evolution of the Iberian margin plankton ecosystem. Special attention is given to phytoplankton pigment (chlorophyll-a) distribution, as a proxy of phytoplankton biomass and primary

production. The regional configuration of the coupled hydrodynamical-biogeochemical model was forced with climatological conditions over 9 years. The following sections describe the model setup, data sets used for model validation, present the validation of model results, and show a general characterization of the spatio-temporal patterns of the plankton ecosystem in western Iberia.

3.3 Model setup

3.3.1 Hydrodynamic model

A climatological simulation was run for a high resolution regional configuration of the Regional Ocean Modeling System (ROMS) (Shchepetkin and McWilliams, 2005; Haidvogel et al., 2008; Penven et al., 2006) for the Iberian margin. ROMS is a three dimensional (3D) ocean circulation model with free-surface, vertical terrain-following coordinates (sigma-coordinates), and horizontal orthogonal curvilinear coordinates. The range of scales to be solved, from the large-scale to the mesoscale, was handled using a two-domain approach, as shown in Figure 3.1. A large-scale first domain (FD) was run independently (offline) in order to provide initial and boundary conditions to our second domain (SD). The first domain (FD) included the northeast Atlantic region between 30° N - 48° N and 0.8° E - 32° W, and had 1/10° ($\sim$9 km) horizontal resolution and 30 vertical s-levels, in order to resolve the large-scale circulation features. The high-resolution nested domain, or second domain (SD), included the western Iberian region from the Gulf of Cádiz to northwest Iberia (Galicia) (34.5° N - 45.5° N and 5.5° W - 12.5° W; $\sim$1200 x 600 km) (Fig. 3.1) and had horizontal resolution of 1/27° ($\sim$3 km) and 60 vertical s-levels in order to properly resolve the Mediterranean undercurrent, which circulation is known to influence the surface transport of chemical and biological properties (Serra et al., 2010). A more detailed description of this climatological regional configuration of ROMS can be found in Nolasco et al. (2013).

The FD was initialized with temperature and salinity climatologies from Conkright et al. (2002), which also provided the open boundary conditions. The surface was forced with monthly climatological wind stress and fluxes of heat and freshwater from the Comprehensive Ocean-Atmosphere dataset (COADS; da Silva et al., 1994). Initial velocities were zero and monthly geostrophic velocities (referenced to 1200 m) and Ekman velocities were calculated from the climatology and applied along the lateral boundaries.The Mediterranean outflow was introduced as a nudging condition as described in Peliz et al. (2007a). The forcing for the high-resolution (SD) configuration was the same used for the

FD, i.e., COADS climatology. The initialization (1st January) and the boundary conditions of the physical boundaries were obtained using year 5 from FD. The exchange of Atlantic and Mediterranean waters at the Strait of Gibraltar was explicitly represented in the high resolution domain by the imposition of vertical profiles of temperature, salinity and zonal velocity at the 5 grid points at the Strait, similarly to (Peliz et al., 2007a). A vertical profile of nitrate was additionally imposed, based in the nitrate climatology for the Mediterranean provided by the University of Liège (http://gher-diva.phys.ulg.ac.be).

The freshwater continental runoff from the main rivers of the region (identified in Figure 3.1) was included with monthly climatological discharge values: For the Portuguese rivers, climatological values were provided by Instituto Nacional da Água (INAG); the climatological discharge of the Galician rivers was obtained from Río-Barja and Rodríguez-Lestegás (1992).

The nested (SD) domain was run for 6 years, having reached a stable equilibrium solution in the 3rd year, until the Mediterranean water was in equilibrium and adjusted along the western and northern Iberian margin. The month of January of the 7th year run was chosen to initialize the biogeochemical model, which ran for 9 more years.

3.3.2 Biogeochemical model

A biogeochemical $NChlPZD$ model was run coupled to the hydrodynamic model to simulate the base trophic levels and biogeochemical components of the system. The biogeochemical model consisted of a 4-component nitrogen based ecosystem model, computing 5 state variables: nitrate (NO_3), phytoplankton ($Phyt$), zooplankton (Zoo) and detritus (Det), all expressed in mmol N m^{-3} (Fig. 2.1). Additionally, chlorophyll-a (mg m^{-3}) is derived from phytoplankton concentration using a variable chlorophyll:carbon ratio, θ (mg chlorophyll-a (mg C)$^{-1}$), that is a function of light and nutrients availability, and a C:N ratio of 6.625 (mmol C (mmol N)$^{-1}$), i.e., a Redfield ratio. The variable θ describes the proportion of photosynthetically fixed carbon that is used for chlorophyll-a biosynthesis considering the model of Geider et al. (1997). Its implementation in the ocean model is described in Gruber et al. (2006).

The 3D time evolution of the concentration of any of the biogeochemical variables (B_i) is influenced by diffusion, horizontal advection, vertical mixing and the biogeochemical processes that act as sink or source for the variable:

$$\frac{\partial B_i}{\partial t} = \nabla \cdot K \nabla B_i - u \cdot \nabla_h B_i - (w + w_{sink}) \frac{\partial B_i}{\partial z} + SMS(B_i) \qquad (3.1)$$

where K is the eddy kinematic diffusivity tensor, u is the horizontal velocity, w and w_{sink}

are the vertical velocity and the vertical sinking rate of the biogeochemical variable (all particulated variables, except zooplankon), respectively. The biogeochemical processes included in the source minus sink (SMS) term are specific for each variable.

The set of SMS equations for each of the biogeochemical variables is:

$$SMS(NO_3) = -\mu(PAR,T)\cdot\mu(NO_3)\cdot Phyt + t_{D_{remin}}\ Det + t_{Z_{metab}}\ Zoo \tag{3.2}$$

$$SMS(Phyt) = \mu(PAR,T)\cdot\mu(NO_3)\cdot Phyt - m_{PD}\ Phyt - g_{max}\ Zoo\ \frac{Phyt}{K_P + Phyt} \tag{3.3}$$

$$SMS(Zoo) = \beta\ g_{max}\ Zoo\ \frac{Phyt}{K_P + Phyt} - m_{ZD}\ Zoo - t_{Z_{metab}}\ Zoo \tag{3.4}$$

$$SMS(Det) = m_{PD}\ Phyt + m_{ZD}\ Zoo + (1-\beta)\ g_{max}\ Zoo\ \frac{Phyt}{K_P + Phyt} - t_{D_{remin}}\ Det \tag{3.5}$$

$$SMS(\theta) = \mu(PAR,T)\cdot\mu(NO_3)\cdot\left(\frac{\mu(T)\cdot\mu(NO_3)\cdot\theta_{max}}{\sqrt{\mu(T)^2 + (\alpha\ PAR\ \theta)^2}} - \theta\right) \tag{3.6}$$

The biogeochemical processes included in the SMS terms represent the conceptual description that follows. Phytoplankton uptakes nitrate (NO_3) at a rate that is dependent on the instantaneous nitrate concentration and light intensity (PAR: photosynthetically available radiation), and further constrained by temperature (T). The nutrient (NO_3) limitation of the growth rate, $\mu(NO_3)$, is calculated by a Michaelis-Menten function

$$\mu(NO_3) = \frac{NO_3}{K_{NO3} + NO_3} \tag{3.7}$$

where K_{NO3} is the half-saturation constant for nitrate uptake by phytoplankton. T and PAR limitation of the phytoplankton growth rate, $\mu(PAR,T)$, follows the equations of Smith (1936) (Eq. 3.8) and Eppley (1972) (Eq. 3.9) modified to include θ.

$$\mu(PAR,T) = \frac{\mu(T)\cdot\alpha\cdot PAR\cdot\theta}{\sqrt{\mu(T)^2 + (\alpha\cdot PAR\cdot\theta)^2}} \tag{3.8}$$

$$\mu(T) = ln2\cdot 0.851\cdot(1.066)^T \tag{3.9}$$

The inclusion of θ tried to represent the expected increase in photosynthesis when phytoplankton cells allocate a higher percentage of their structure to the photosynthetic apparatus (higher θ), which seems to occur in nearly nutrient-replete regions such as the upwelling zone or in the proximity of the sub-surface chlorophyll maximum (Gruber et al., 2006). PAR refers to in situ PAR, and α is the initial slope of the growth versus light relationship. PAR at the surface, PAR_0, is calculated as 43% of the incident radiation and attenuated with depth as it is absorbed by water and chlorophyll-a,

$$PAR = PAR_0\cdot exp\ (k_w + k_{chla}\ Chl)\Delta z \tag{3.10}$$

where k_w and k_{chla} are attenuation coefficients for pure water and chlorophyll-a and Δz is the depth step. PAR is given in W m^{-2}. The total phytoplankton growth rate is written as

$$\mu = \mu(PAR, T) \cdot \mu(NO_3) \tag{3.11}$$

Phytoplankton dies at a constant linear rate (m_{PD}) been automatically incorporated to the detritus pool. Zooplankton growth relies on its grazing on phytoplankton, which rate depends on prey (phytoplankton) concentration, through a Michaelis-Menten function,

$$g = g_{max} \frac{Phyt}{K_P + Phyt} \tag{3.12}$$

and on zooplankton assimilation efficiency (β). A constant excretion rate ($t_{Z_{metab}}$) is attributed to zooplankton, providing a source of nutrients to the nitrate pool. Zooplankton incorporates to the detritus pool at a constant linear mortality rate (m_{ZD}). Mineralization of detritus is formulated as direct transformation to nitrate at a constant nitrification rate ($t_{D_{remin}}$). Model parameters values for the sink/source terms selected to represent our region of study are listed in Table 2.1. These parameters aimed at representing the eutrophic coastal ecosystem dominated by diatoms, what necessarily implied reducing the ability of the model to represent correctly the oligotrophic offshore environment, as only one phytoplankton functional group was included.

The concentration of nitrate and chlorophyll-a for the model initial and boundary conditions were supplied by the climatological data sets World Ocean Atlas 2009 (Garcia et al., 2010b) and SeaWiFS, respectively. For nitrate, seasonal (for depths down to 500 m) and annual (depths below 500 m) climatologies were used. For chlorophyll-a, the seasonal climatology of surface concentrations from SeaWiFs data was used. Seasonal vertical profiles were created from these surface concentrations using the algorithm of Morel and Berthon (1989). The initial and boundary values of phytoplankton and zooplankton were derived from chlorophyll-a ($Phyt = 0.5 \cdot Chl$; $Zoo = 0.2 \cdot Chl$), as in Gruber et al. (2006). Detritus was not available from climatological datasets, so it was introduced constant (initial and boundary conditions) with the value 0.02 mmol N m^{-3}. Boundary conditions were supplied seasonally. The riverine inputs of nitrate and chlorophyll were used constant along the year (Table 4.1; Marta-Almeida et al., 2012).

3.4 Data sets for model evaluation

Model outputs presented are monthly and annual averages over 6 years (4th to 9th climatological years). Model results were evaluated by comparison with climatological databases. Sea surface temperature (SST) was compared with data from the Advanced

Very High Resolution Radiometer (AVHRR) of the National Oceanic and Atmospheric Administration (NOAA). The data were extracted from the EUMETSAT Ocean & Sea Ice Satellite Application Facility (OSI-SAF) (www.osi-saf.org) and were made available by CERSAT (IFREMER, France). The product has a horizontal resolution of about 2 km, and corresponds to the SST average over the years 2002 to 2008 of the night satellite sweep. Annual and monthly surface chlorphyll-a was compared with the corresponding SeaWiFS climatology. The climatology, averaged over the period 1997-2004, was generated by the NASA Goddard Space Flight Center (http://oceancolor.gsfc.nasa.gov). The horizontal resolution is 9 km. In addition, chlorophyll-a daily time series for the period 2001-2010 obtained by optimal interpolation of SeaWiFS/MERIS/MODIS ocean color data and made available by CERSAT-IFREMER (1.1 km horizontal resolution), were used for statistical quantitative comparisons with model results.

Mixed layer depth (MLD) was calculated from model temperature profiles, following Lorbacher et al. (2006) criteria, and averaged over the model domain along one climatological year. The resulting MLD time series was compared to a monthly climatology (2002-2010) constructed using ARGO floats profiles within the region (Holte et al., 2010).

3.5 Results and Discussion

The reliability of the model to reproduce the physical and biogeochemical characteristics of the Iberian system was assessed. Firstly, a general assessment of the hydrodynamic model is presented, by comparing the SST annual average of model results with satellite (AVHRR) observations (section 3.5.1). The modeled seasonal evolution of the MLD over the domain was next compared to a MLD climatology from Argo floats in the region. A detailed validation of the hydrography, seasonal circulation, vertical structure of the flow and meridional transport of this ROMS climatological configuration for the Iberian margin has been carried out by Nolasco et al. (2013). A general evaluation of the biogeochemical model to reproduce the spatio-temporal distribution of phytoplankton biomass was carried out by comparing the modeled annual and monthly means of surface chlorophyll-a concentration ([Chl]) with the corresponding means from the SeaWiFS climatology (section 3.5.2). Additionally, a quantitative analysis was performed calculating statistical indices (bias, rms and skill) to compare monthly/daily modeled surface [Chl] time series averaged over the domain and at four specific locations with the corresponding monthly/ daily time series from an optimal interpolation of merging SeaWiFS/MODIS/MERIS data. In order to make a general characterization of the spatial patterns of the biomass and and nutrient pools in the Iberian margin, surface annual means of zooplankton, detritus

and nitrate were presented and discussed (section 3.5.3). Finally, the seasonal vertical distribution of chlorophyll, nitrate and detritus along the Iberian margin was analyzed through cross-shelf monthly means at three selected zonal sections (section 3.5.4).

3.5.1 Hydrodynamic model evaluation

The conspicuous meridional gradient of SST in the region was well represented in the model (Figure 3.2). The SST annual mean of model and AVHRR climatological values agreed reasonably well, presenting a bias lower than 1°C for most part of the domain (white regions in Figure 3.2 (c)). However, there was a band of coastal water noticeably colder in the model than in the AVHRR climatology (typical bias of -1 to -2 °C). This band was restricted to the inner shelf in the NW coast and the central Estremadura promontory, whereas to the north and south of this promontory the band occupied the entire shelf (Figure 3.2 (c)). This bias resulted from an overestimation of the upwelling intensity during the summer (not shown). Note that climatological winds (COADS) do not account for the

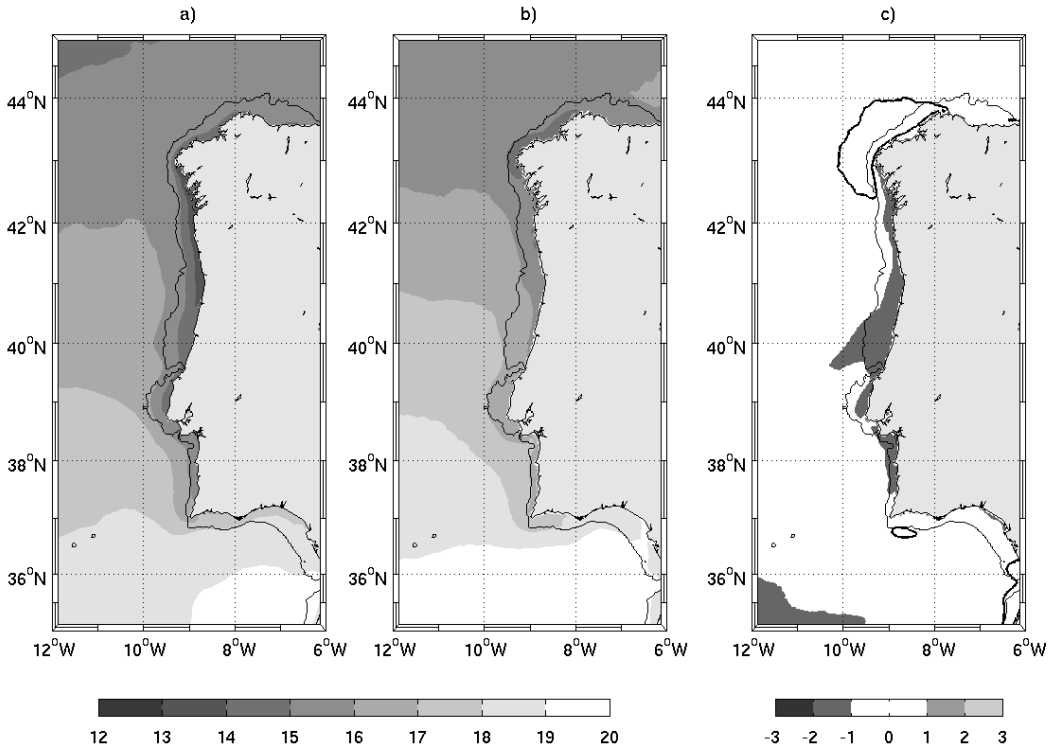

Figure 3.2: Annual mean SST from ROMS model (a), from AVHRR climatology (b) and difference between them (model-AVHRR) (c). The 200 m isobath is shown.

drop-off of the wind stress in the neighborhood of the coast (Veitch et al., 2010, and references therein), and thus the upwelling is overestimated. Also, COADS data lack the synoptic variability that characterizes the Iberian upwelling, with typical intermittent upwelling/relaxation events of 1-3 weeks (Álvarez-Salgado et al., 1993; Arístegui et al., 2009). On the other hand, Dufois et al. (2012b) have alerted for a warm bias in satellite observations nearshore in eastern boundary upwelling systems. A colder region in the model was also observed in the SW, close to the boundary of the domain (Figure 3.2 (c)). On the contrary, in the NW region around cape Finisterre the modeled SST was overestimated. It seemed that the the strong upwelling center usually found there, was not entirely reproduced by the model. According to Torres et al. (2003), the wind field in the NW Iberian Peninsula is very heterogeneous and has a number of dominant patterns that are responsible for the typical distributions of upwelling/downwelling off the Galician coast, namely the formation of filaments. Thus, due to the particular structure of the real wind field, the climatological winds cannot properly reproduce the offshore extension of upwelling observed off Galicia.

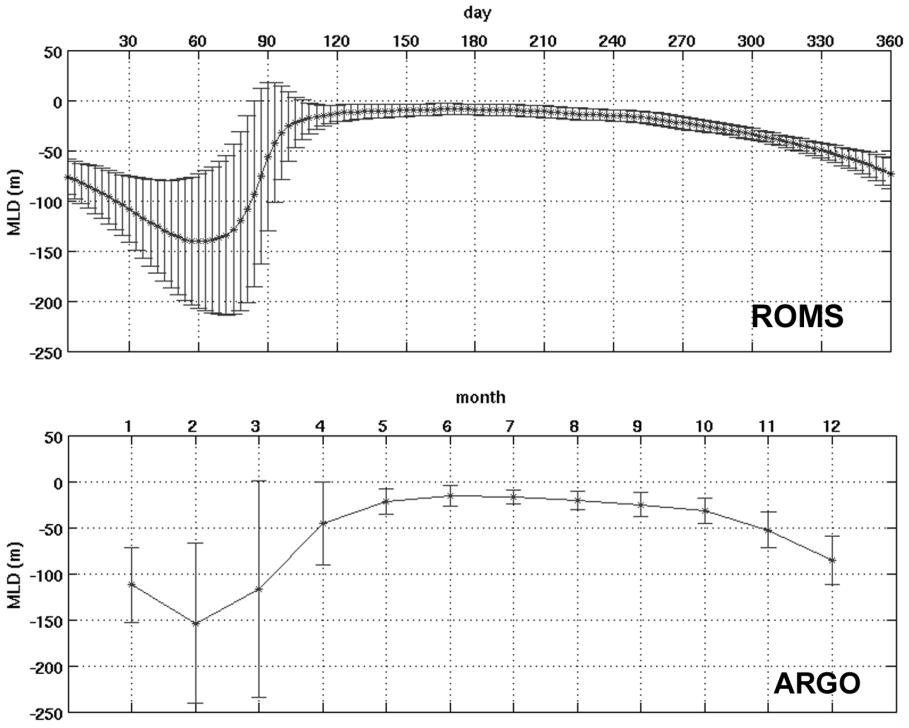

Figure 3.3: Mixed layer depth (m) annual cycle in the Iberian margin (SD model domain) obtained from ROMS temperature profiles for the 6th climatological year (3 days averages; mean $\pm$ sd) (upper panel) compared with a monthly (mean $\pm$ sd) climatology (2002-2010) from Argo floats selecting profiles available for the same area (lower panel).

The modeled seasonal evolution of MLD over the domain could satisfactorily repro-

duce the climatological seasonal evolution obtained from ARGO floats profiles (Fig. 3.3). The mixed layer depth was maximum in February (domain average ∼150 m), corresponding to the winter vertical mixing in the region, and shoaling in the subsequent spring months to less than 50 m. The summer was characterized by a remarkable stratification of the water column from May to September and then the MLD started deepening again in autumn. The similar standard deviations between both series also indicated the reproduction of a similar variability of the MLD in the model and in ARGO observations. On the other hand, the February standard deviation showed that the domain-averaged winter vertical mixing in the model was somehow shallower than observed.

3.5.2 Evaluation of annual and seasonal [Chl] at the sea surface

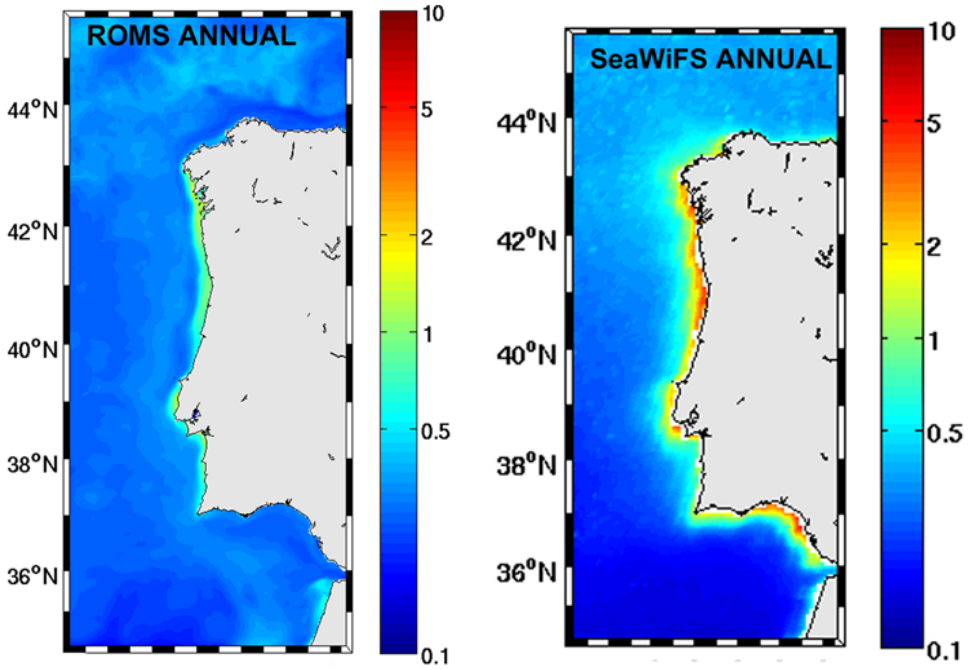

Figure 3.4: Annual mean of modeled surface [Chl] (mg m^{-3}) (left) compared with SeaWiFS annual mean climatology (right). Model result corresponded to 6 years average, and the SeaWiFS annual climatology was averaged over the period 1997-2004. Note different spatial resolution in model and satellite fields.

The modeled annual [Chl] in the offshore region of the domain showed similar values to the SeaWiFS climatology, i.e., generally lower than 0.5 mg m^{-3} (Fig. 3.4). Nevertheless, in the southern part of the domain, modeled annual [Chl] was slightly higher than the [Chl] from SeaWiFS. The SeaWiFS climatology suggested that to the south of about 37° N [Chl] tended to be lower than in the rest of the region, whereas this was not evident in model results, except for the southernmost limit of the domain. [Chl] was highest over

the western shelf, where model values ($\sim$1 mg m^{-3}) were lower than satellite-derived values ($\sim$2 mg m^{-3}). Even though some underestimation could occur in model results, an overestimation of SeaWiFS [Chl] in the Iberian coastal region is also likely, as this effect has been reported for the coastal zone when using SeaWiFS data, originated by errors in the algorithm estimations of [Chl] (Le Fouest et al., 2006). Higher [Chl] occurred in the northwestern shelf than in the southwestern shelf, south of the Estremadura promontory, for the SeaWiFS data, whereas this difference was not evident in the model. Over the northern and southern shelves (east of Cape Finisterre and Gulf of Cadiz, respectively), modeled [Chl] was noticeably low, contrasting with satellite values. These low values were unexpected for the shelf, suggesting an underestimation of modeled [Chl] in these areas. The underestimations were probably related to the limitations of the climatological wind forcing (COADS) to reproduce the synoptic wind variability mentioned in section 3.5.1. The averaged wind probably lacked the occurrence of winds with significant zonal component which induce upwelling events in the northern and southern shelf (García Lafuente and Ruiz, 2007; Ospina-Alvarez et al., 2010), in contrast to the dominant northeasterlies that induce upwelling in the N-S oriented western shelf. Nevertheless, in the case of the Galician coast, a general north to south increase in [Chl] has been reported (Bode et al., 1996; Álvarez et al., 2012a). It has been attributed to the parallel increase in nutrients mineralization to the south, which is thought to be a consequence of coastal morphology, namely the presence of the Rias Baixas, four large coastal embayments in the southwest Galician coast which export organic matter to the adjacent shelf (Fraga, 1981; Álvarez-Salgado et al., 1993, 1997; Prego et al., 1999).

Figure 3.5 presents a comparison of monthly means of modeled surface [Chl] with the corresponding monthly means for the SeaWiFS climatology, for selected months that aim to represent the seasonal evolution of [Chl]: January (winter), April (spring), July (summer), and October (autumn). The modeled [Chl] in January was similar to that of the SeaWiFS climatology, with moderate offshore values ($\sim$0.5 mg m^{-3}), but as pointed out for the annual mean, modeled [Chl] over the shelf was noticeably lower than in the satellite data. An overestimation of [Chl] in the SeaWiFS data for the coastal zone was likely, as already discussed, specially considering the expected higher amount of suspended matter from increased continental runoff in winter, interfering with the remotely sensed [Chl] estimations. Nonetheless, it is possible that the use of climatological rivers in the model, i.e., monthly averaged discharges and constant nutrients (nitrate) concentrations, was not able to reproduce the input of nutrients and stratification conditions that is thought to contribute to some events of [Chl] increase in the Western Iberia Buoyant Plume (WIBP) (Ribeiro et al., 2005). In addition, the lack of synoptic winds already mentioned could not account for the episodic upwelling events known to occur in winter (Ribeiro et al.,

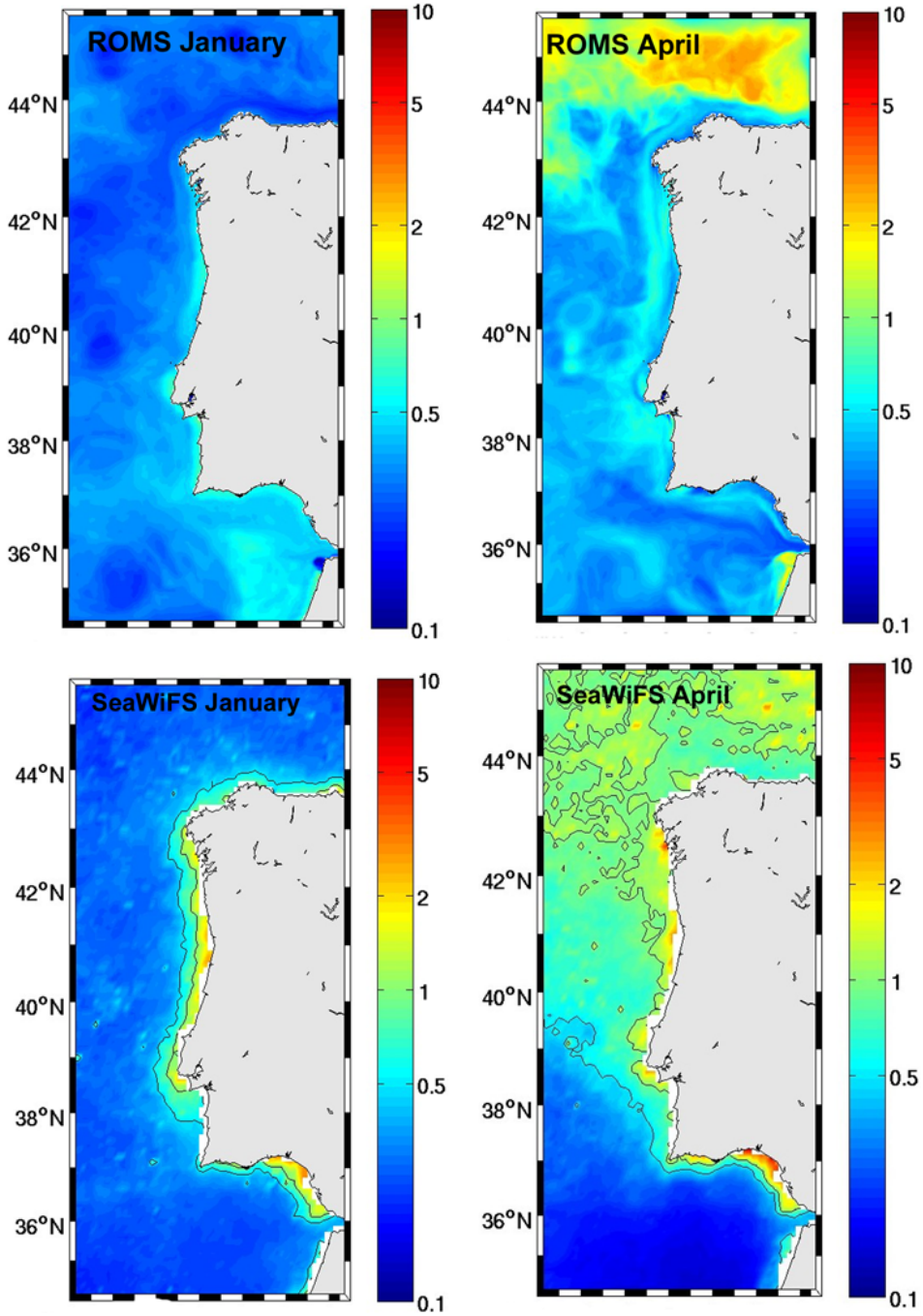

Figure 3.5: Monthly mean (January [winter]; April [spring]; July [summer]; October [Autumn]) of modeled surface [Chl] (mg m^{-3}) compared with SeaWiFS monthly mean climatology. Model results corresponded to 6 years averages, and the SeaWiFS monthly climatology was averaged over the period 1997-2004. Lines of 1 mg m^{-3} and 2 mg m^{-3} are shown. Note different spatial resolution in model and satellite fields. (Continued).

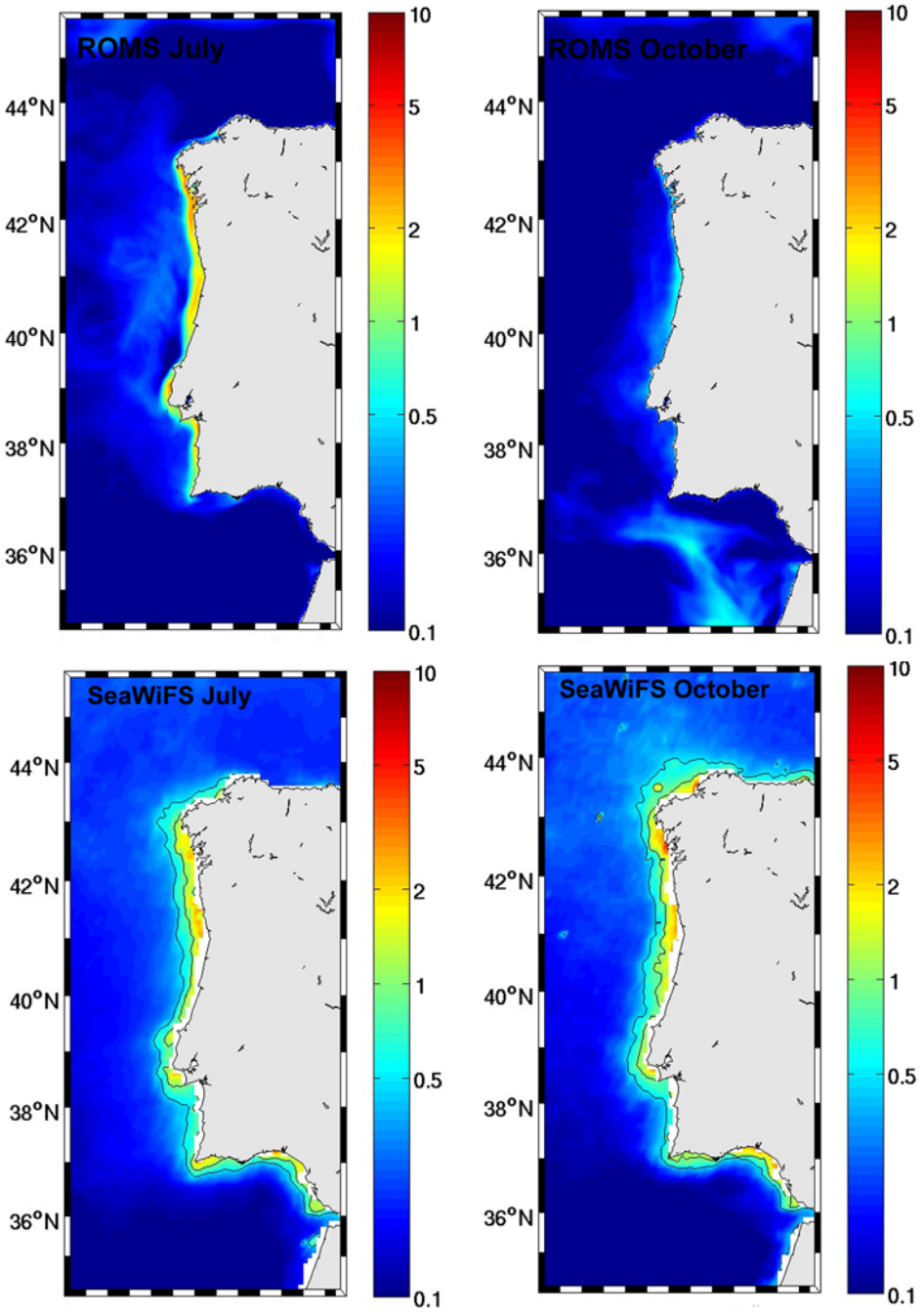

Figure 3.5: Continued.

2005; Álvarez et al., 2012b). These limitations of the COADS wind forcing to model [Chl] variability were also pointed out by Gruber et al. (2006) for the California upwelling region. The high surface [Chl] of April, corresponding to the spring phytoplankton bloom over the North Atlantic, was reproduced by the model (Fig. 3.5). The bloom was characterized by a marked latitudinal gradient, with [Chl] decreasing from N-S. [Chl] in the northern part of the domain (north of 42-43° N) generally exceeded 2 mg m^{-3} in the SeaWiFS climatology, whereas this value was higher in model results for this area. On the contrary, modeled [Chl] seemed to be lower than in the satellite climatlogy between ∼40-42° N. Also for April, modeled [Chl] over the shelf was lower than in the SeaWiFS climatology. In July the surface [Chl] distribution was characterized by high values (>2 mg m^{-3}) over the shelf, as a result of the summer dominant upwelling conditions, and low offshore values resulting from thermal stratification of the water column (Fig. 3.5). These patterns were captured by the model, although the offshore [Chl] was considerably lower than observed in the satellite climatology, except in the vicinities of the shelf, where the cross-shelf exchange was probably the reason for the increased [Chl]. As for the shelf, the modeled [Chl] was similar to that observed in the SeaWiFS climatology (>2 mg m^{-3}), showing that the model could appropriately reproduce the increase in phytoplankton biomass due to the upwelling of cold and nitrate rich subsurface ENACW driven by the prevailing northerly winds and the associated offshore Ekman transport (Fraga, 1981; Peliz et al., 2002; Relvas et al., 2007). The [Chl] over the shelf seemed to be higher in the North, off the Galician Rias Baixas and the northwestern Portuguese shelf, than in the southwestern Portuguese shelf, both in the model and SeaWiFS images. These differences have also been observed in data obtained during the CICLOS cruises, that seasonally sampled the Portuguese shelf during 1985-1986 (Moita, 2001; Cunha, 2002). They were mainly attributed to the wider extension of the northern shelf compared to the southern shelf and the possible differences in the upwelling dynamics associated. Also, high mineralization rates have been found for these areas of the northwestern shelf, increasing the potential primary production (Álvarez-Salgado et al., 1997). In October, low [Chl] over the shelf was obtained from model outputs, whereas SeaWiFS [Chl] over the shelf was about the same found in July. October-November represent a transition in the ecosystem from the summer dominant upwelling situation to the autumn dominant downwelling situation (Castro et al., 1997; Álvarez-Salgado et al., 2003), driven by a shift in the wind regime from northerlies to southerlies. It also coincides with the onset of the relatively warm and saline IPC over the slope (Haynes and Barton, 1990). This shift is usually coincident with a phytoplankton autumn bloom in the coast (Bode et al., 1996; Casas et al., 1997; Castro et al., 1997; Álvarez-Salgado et al., 2003). However this coastal bloom was not evident from model outputs. The offshore [Chl] in the model remained low, contrasting with the

higher values in the SeaWiFS climatology, which showed a slight increase in [Chl] in the NW offshore region. Also in October, there was an anomalous entry of high [Chl] from the southern boundary of the model domain, caused by a local intensification of the nitrate concentration through that boundary (not shown) as a result of the local circulation. The seasonal evolution of [Chl] just described seemed to be related with the seasonal variation of the MLD described in section 3.5.1 (Fig. 3.3). During summer, high SST induced the devopment of a shallow MLD, which seemed to correspond to low [Chl] offshore, due to nutrients depletion (Figure 3.5, July). The autumn-winter deepening of the MLD seemed to supply new nutrient to allow phytoplankton growth offshore (Figure 3.5, January). The spring bloom coincided with the steep shoaling of the MLD (Figure 3.5, April).

The contrasting seasonal evolution of [Chl] over the shelf between the SeaWiFS climatology, which showed high [Chl] for every season, and the model results, which indicated noticeable changes in [Chl] along the year, rose the question of whether the satellite data were overestimating or the model results were underestimating [Chl] values over the shelf. Comparisons with in situ observations were limited by the scarcity of data series with enough time and space distribution along the western Iberian shelf. Still, comparisons with surface [Chl] data provided by the referred CICLOS cruises over the western and southern Portuguese shelf (CICLOS I, August 1985; CICLOS II, November 1985; CICLOS III, January 1986; CICLOS IV, March 1986) revealed a similar seasonal evolution of [Chl] to that reproduced by the model. Highest [Chl] was found in August (summer) ($\sim$1-3 mg m^{-3}), moderate [Chl] occurred in November and March (autumn-spring) ($\sim$0.5-1 mg m^{-3}), whereas the lowest surface [Chl] was found in January (winter) ($\sim$0.5 mg m^{-3}) (Moita, 2001). For the northwestern Iberian shelf off Galicia, Álvarez-Salgado et al. (2003) showed some [Chl] data from several cruises carried out in the region during the 80s-90s at different times of the year. Low surface [Chl] was observed during January 1998 (winter, CD110b cruise), comparable to model results, and they drew attention to a in situ value of 0.85 mg m^{-3} contrasting with the 2.2 mg m^{-3} SeaWiFS estimate at the same location (albeit 6 days later). On the contrary, high [Chl] was detected during late winter 1984 (February-March, GALICIA VII cruise) in the same region, but coinciding with a period of upwelling favorable winds (Álvarez-Salgado et al., 2003). High surface [Chl] ($>$3 mg m^{-3}) was also observed during June-July 1998 (Bg9815c cruise) under a typical summer upwelling situation, comparing well with both model and SeaWiFS data. The autumn [Chl] values of September 1991 (GALICIA XII cruise) and November-December 1993 (MORENA II cruise) were considerably high ($>$1 mg m^{-3}), contrasting with the low modeled [Chl] of October. The late spring cruise of May 1993 (MORENA I) found unexpected low [Chl] values for this time of the year, because of the dominant downwelling conditions, and thus it did not compare well with neither the model or the

SeaWiFS climatology. These comparisons supported that care should be taken when evaluating the model performance over the shelf based only on SeaWiFS estimations, as previously pointed out.

For a quantitative comparison, model error relative to satellite surface [Chl] estimations from merging SeaWiFS, MODIS, and MERIS data was calculated using the *bias*, *rms* and *skill* reliability indices. They are commonly used for ocean-ecosystem models validation (Allen et al., 2007; Stow et al., 2009; Warner et al., 2005), and are next defined. The statistics were calculated (1) in a domain averaged monthly basis comparison, for a general assessment (Fig. 3.6), and (2) in a quasi-daily basis (3 days mean) at four selected locations within the domain (Fig. 3.1), aiming to assess the shelf-ocean and North-South differences in model performance in the short-term (Figs 3.7 and 3.8). It should be outlined that model validation must take into account the combination of model and observational uncertainties, as well as the balance between precision and trend, and therefore several error statistics must be considered (Allen et al., 2007; Stow et al., 2009). The *bias* gives an estimation of whether the model is systematically overestimating or underestimating the observations, being the model result as better as the bias is closest to zero:

$$Bias = \frac{\sum_{n=1}^{n}(M_n - D_n)}{\sum_{n=1}^{n} D_n} \tag{3.13}$$

where M is the model estimation, D the data, and n is the nth comparison of total grid points. The *rms* is the *root mean squared error* of n model-data comparisons (total grid points):

$$rms = \sqrt{\frac{\sum_{n=1}^{n}(M_n - D_n)^2}{n}} \tag{3.14}$$

The closer the rms to zero the better the fit between the model and observations. Finally, the *skill* is a quantitative agreement between the model and observations where M_n is compared with a time mean $\overline{D}$:

$$Skill = 1 - \frac{\sum |M_n - D_n|^2}{\sum (|M_n - \overline{D}| + |D_n - \overline{D}|)^2} \tag{3.15}$$

Perfect agreement between model results and observations would yield a skill of one, and complete disagreement would correspond to zero model skill.

Figure 3.6 showed that the model reasonably reproduced the seasonal trend of surface [Chl] over the domain, although with an anticipation of 1 month in the maximum of the spring bloom (March instead of April). The model also tended to overestimate [Chl] during the spring bloom compared to the satellite observations, however the negative bias obtained indicated that for most part of the year the model actually tended to slightly underestimate the [Chl]. The low rms and high skill indicated an overall good performance

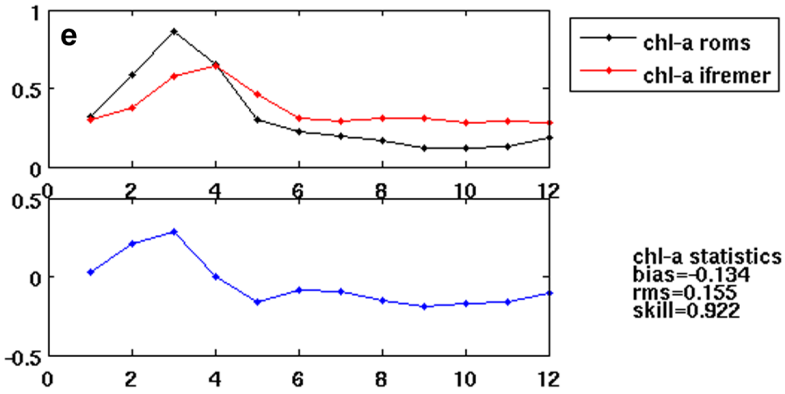

Figure 3.6: Comparison of model surface [Chl] (mg m^{-3}) time series averaged over the domain with the corresponding domain averaged satellite time series from the IFREMER (2001-2010 average). The time series correspond to monthly averages (over 6 climatological years for the model and over 2001-2010 for satellite data). Satellite data were filtered for concentration values higher than 5 mg m^{-3}. Difference between the model and satellite time series shown in blue. Also shown the error statistics of model-satellite comparisons: bias, rms, and skill.

of the model when considering monthly averages over the domain. The model error was higher when considering quasi-daily time series for particular locations within the domain (Figs. 3.7 and 3.8). That was expected given the exigent nature of such a like-with-like comparison focused on precision (Allen et al., 2007). The model trend for the offshore locations (Fig. 3.7) captured that of the satellite, although in the model the spring phytoplankton bloom was anticipated and [Chl] overestimated, as detected for the domain averaged time series. This overestimation was noticeably higher at the SW-offshore location (Fig. 3.7b) than at the NW-offshore location (Fig. 3.7a). This was reflected in the model bias, which was negative for the NW-offshore location, as in the domain analysis, whereas it was positive for the SW-location. Note that the positive bias was mainly caused by the difference in spring, as for the rest of the year the model matched well the satellite observations. It should also be highlighted that in spite of the higher spring overestimation in the SW-offshore location, peak model values (1.5 mg m^{-3} in the north vs. $<$1 mg m^{-3} in the south) indicated that a latitudinal gradient, with decreasing [Chl] values to the south, was still reproduced. The rms was similar between both locations, likely because the main differences occurred for the same period, whereas the skill was better for the NW-offhshore location. Regarding the shelf locations (Fig. 3.8), the summer increase in modeled [Chl] associated to the upwelling period was the most prominent feature at the NW-shelf location (Fig. 3.8a) whereas this effect was not detected at the SW-shelf location (Fig. 3.8b). It should be noted, however, that even though both locations were at the same longitude (9° W) they were at different distances from the coast, i.e. at different water depths ($\sim$50 m NW-shelf location and $\sim$100 m SW-shelf location), and that

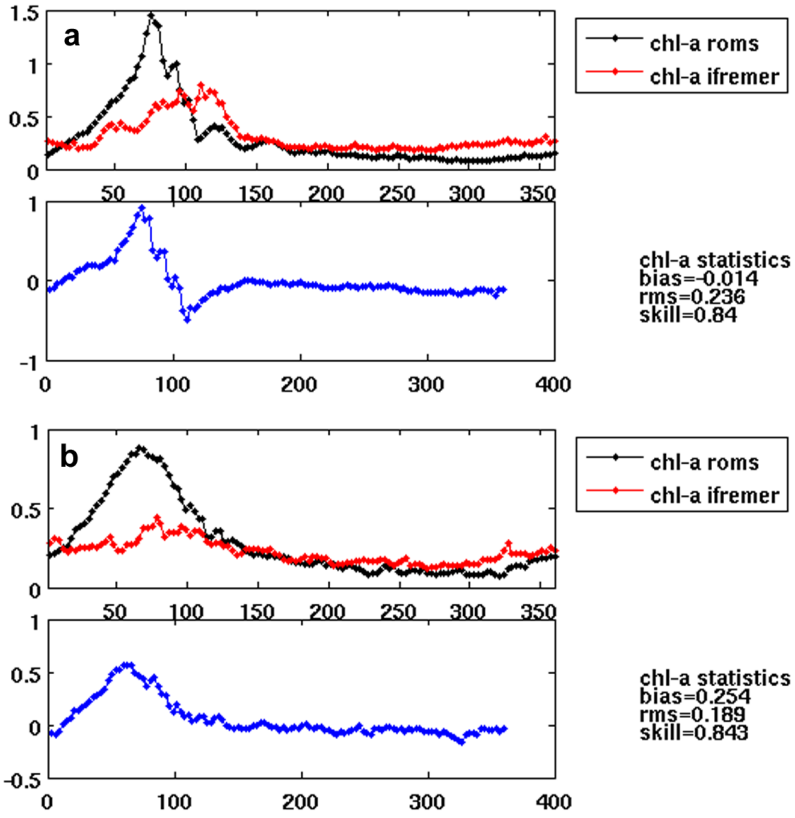

Figure 3.7: Comparison of modeled surface [Chl] (mg m^{-3}) time series at two offshore locations with the corresponding satellite time series from the IFREMER (2001-2010 average). The time series correspond to 3 days averages (over 6 climatological years for the model and over 2001-2010 for satellite data) in a square of 0.1° × 0.1° centered at the locations indicated: a) 42° N 10.5° W (NW-offshore); b) 38° N 10.5° W (SW-offshore); Satellite data were filtered for concentration values higher than 5 mg m^{-3}. Difference between the model and satellite time series shown in blue. Also shown the error statistics of model-satellite comparisons: bias, rms, and skill.

[Chl] increased near the coast. Thus, higher [Chl] was expected in the northern location independent of other latitudinal factors. The modeled summer increase in the NW-shelf location contrasted with the rather constant [Chl] from satellite estimations, as discussed in Fig. 3.5. Nevertheless, the model bias was negative at that location, as for the rest of the year the model underestimated [Chl]. Given the described differences between the model and satellite time series, a high rms and a low skill was obtained for the NW-shelf location. These errors should be taken with caution, bearing in mind the concerns discussed about the low variability of [Chl] over the shelf for satellite estimations. The apparent overestimation of modeled [Chl] in summer at this NW-shelf location may be related to an intensified upwelling due to the use of climatological winds, as discussed in section 3.5.1, and reflected in lower modeled SST than observed over this shelf region (Fig. 3.2). As for the SW-shelf location (Fig. 3.8b), modeled and satellite estimations of

[Chl] were closer, without a clear signal of the upwelling period, although with a trend for model underestimation reflected in the negative model bias. As a consequence, the rms and skill were noticeably better than in the NW-shelf location.

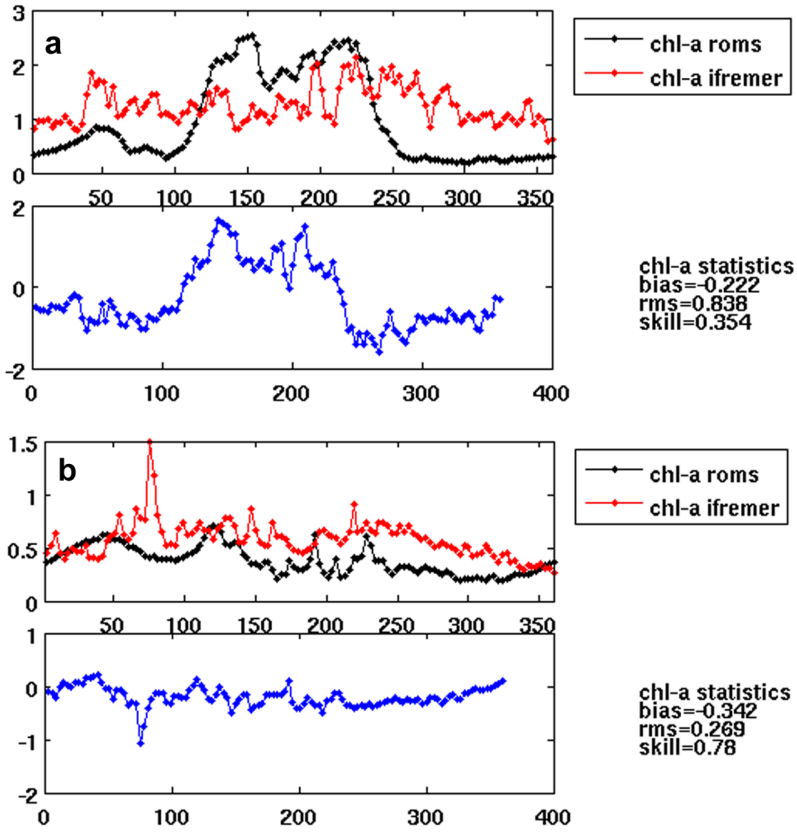

Figure 3.8: As for Fig. 3.7 but for time series at two locations in the shelf: a) 42° N 9° W (NW-shelf); and b) 38° N 9° W (SW-shelf).

3.5.3 Mean Zoo, Det and NO_3 standing stocks at the sea surface

The surface annual mean of zooplankton, detritus, and nitrate obtained from model outputs for the western Iberia ecosystem are presented in Fig. 3.9. As expected, the zooplankton distribution resembled that of chlorophyll, as a consequence of zooplankton concentrating in the areas of highest phytoplankton biomass for grazing. Higher zooplankton biomass was reproduced over the western shelf, and progressively decreased offshore. The northwestern shelf, north of Cape Roca, showed higher zooplankton biomass than the southwestern shelf, as described also for chlorophyll (Fig. 3.4). This model result was in agreement with the findings of Cunha (2002) from the CICLOS cruises, who concluded that conditions for primary and secondary marine production in the western Iberian shelf

were better off the northern coast than off the southern coast. In the northwestern shelf off the vicinity of the river Douro estuary, the model climatology showed higher zooplankton biomass in the outer shelf than in the inner shelf (Fig. 3.9). This was consistent with observations in this area showing that thermohaline fronts are preferential areas for zooplankton concentration, also separating different zooplankton communities (Queiroga et al., 2005). The southern (Gulf of Cadiz) and particularly the northern (Cantabrian) shelves presented low zooplankton biomass, which was likely a consequence of what was already discussed for chlorophyll, i.e., the limitations of the climatological wind forcing for this part of the coast with a different orientation.

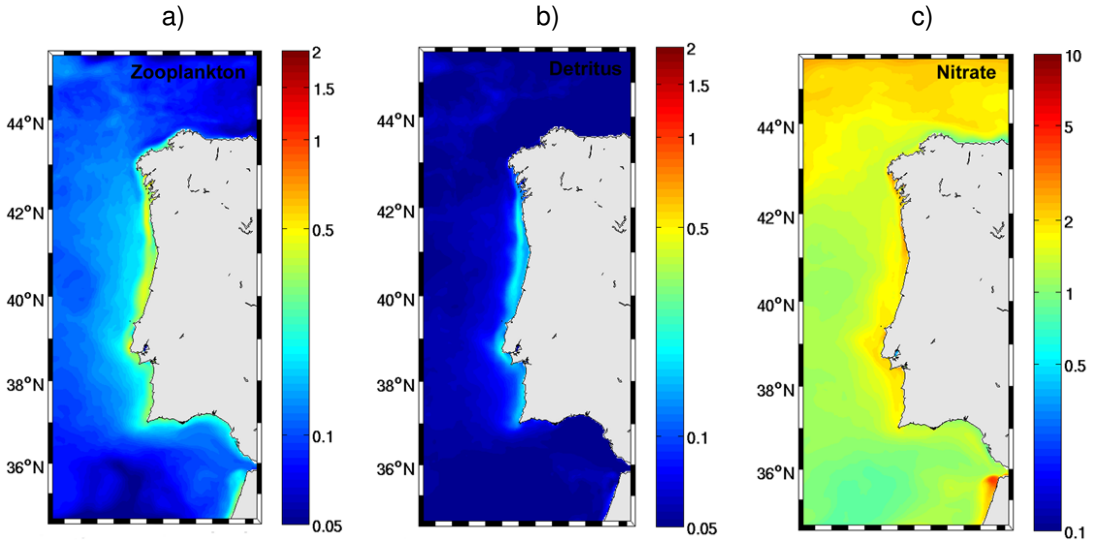

Figure 3.9: Modeled sea surface annual mean of zooplankton (a), detritus (b), and nitrate (c) in the western Iberia ecosystem. All variables in mmol N m^{-3}.

The detritus distribution was similar to that of chlorophyll as well (Fig. 3.9b), although with a more pronounced onshore-offshore decrease than phytoplankton or zooplankton biomass. This was due to the different sinking velocities (Table 2.1), as the detritus sinking velocity was one order of magnitude higher than the phytoplankton sinking velocity (no sinking velocity attributed to zooplankton). As a result, the detritus was less susceptible to surface offshore transport. As described for phytoplankton and zooplankton biomass, surface detritus concentration was higher over the northwestern shelf than over the southwestern shelf.

The nitrate distribution (Fig. 3.9c) was characterized by a latitudinal and onshore-offshore gradient. The latitudinal gradient of nitrate was a manifestation of the regional hydrography characterized by the presence of two subsurface branches of ENACW: a water branch of subpolar origin (ENACWp) to the North, with higher nitrate concentration, and a water branch of subtropical origin (ENACWt) and lower nitrate concentration to the South

(Fiuza, 1984; Rios et al., 1992; Perez et al., 1993; Fiuza et al., 1998), which the model was able to reproduce. Another relevant feature known to cause the nitrate latitudinal gradient was the shallower winter vertical mixing in the south ($\sim$100 m) compared to the north ($\sim$300 m), resulting in a general northward increase in the nitrate concentration (Perez et al., 2005). In addition, the model reproduced a marked onshore-offshore gradient of nitrate as a consequence of the upwelling of subsurface ENACW along the shelf mainly during the spring-summer upwelling favorable wind conditions.

3.5.4 Seasonal vertical distribution of Chl, NO_3 and Det along the western Iberian shelf

Differences in the vertical seasonal distribution of chlorophyll-a, nitrate and detritus along the western Iberian shelf were explored plotting three cross-shelf monthly averages from model results at 42° N, 40° N, and 38° N (Figs. 3.10, 3.11, and 3.12). Monthly averages of the thermohaline properties were also plotted with chlorophyll (Fig. 3.10). Each of the four months plotted aimed to represent a particular season (January-Winter, April-Spring, July-Summer, October-Autumn). The latitudes for the cross-shelf sections were selected to represent the spatial differences in the shelf characteristics along the western Iberian margin. The 42° N section represented the northern shelf off the Galician coast, with an irregular coastline due to the presence of four coastal embayments, the Rias Baixas, and medium shelf width. The wide shelf between the river Minho mouth and Cape Roca (Fig. 3.1) was represented in the section at 40° N, whereas the southern narrow shelf between Cape Roca and Cape São Vicente was represented in the 38° N section. Both areas present a regular coastline with meridional orientation. In addition, a main difference between them was the higher continental runoff to the northern shelf than to the southern shelf.

In the three sections the evolution of [Chl] along the year was similar to that described in section 3.5.2, i.e., a progressive increase from winter (January) to spring (April), when the maximum of the spring bloom occurred, and a summer (July) coastal maximum associated to the prevailing upwelling conditions, as evidenced by the upward blending of the isotherms near the coast (Fig. 3.10). Offshore, surface [Chl] was low during summer and autumn (October) due to surface nitrate depletion caused by strong thermal stratification (Figs. 3.10 and 3.11). Nevertheless, a subsurface [Chl] maximum developed at about the base of the thermocline, at $\sim$50 m. The [Chl] at the subsurface maximum and particularly at the surface coastal maximum noticeably decreased from North to South, supporting the idea that conditions for primary production are more favorable in the wide

northwestern shelf than in the narrow southwestern shelf (Cunha, 2002). Subsurface upwelled water was colder, less saline and showed a higher nitrate concentration in the northwestern shelf than in the southwestern shelf (Figs. 3.10 and 3.11). This illustrated the prevalence of ENACWp in the northern shelf, and of ENACWt in the southern shelf. Also, as the residence time of upwelled water in the narrow southern shelf was lower, i.e., the nitrate rich water was more rapidly washed-out, it was less available for in situ phytoplankton growth. Nonetheless, [Chl] was higher in the 42° N section than in the 40° N section, in spite of the narrower shelf width, which suggested a higher influence of the characteristics of the upwelled water than of the shelf width.

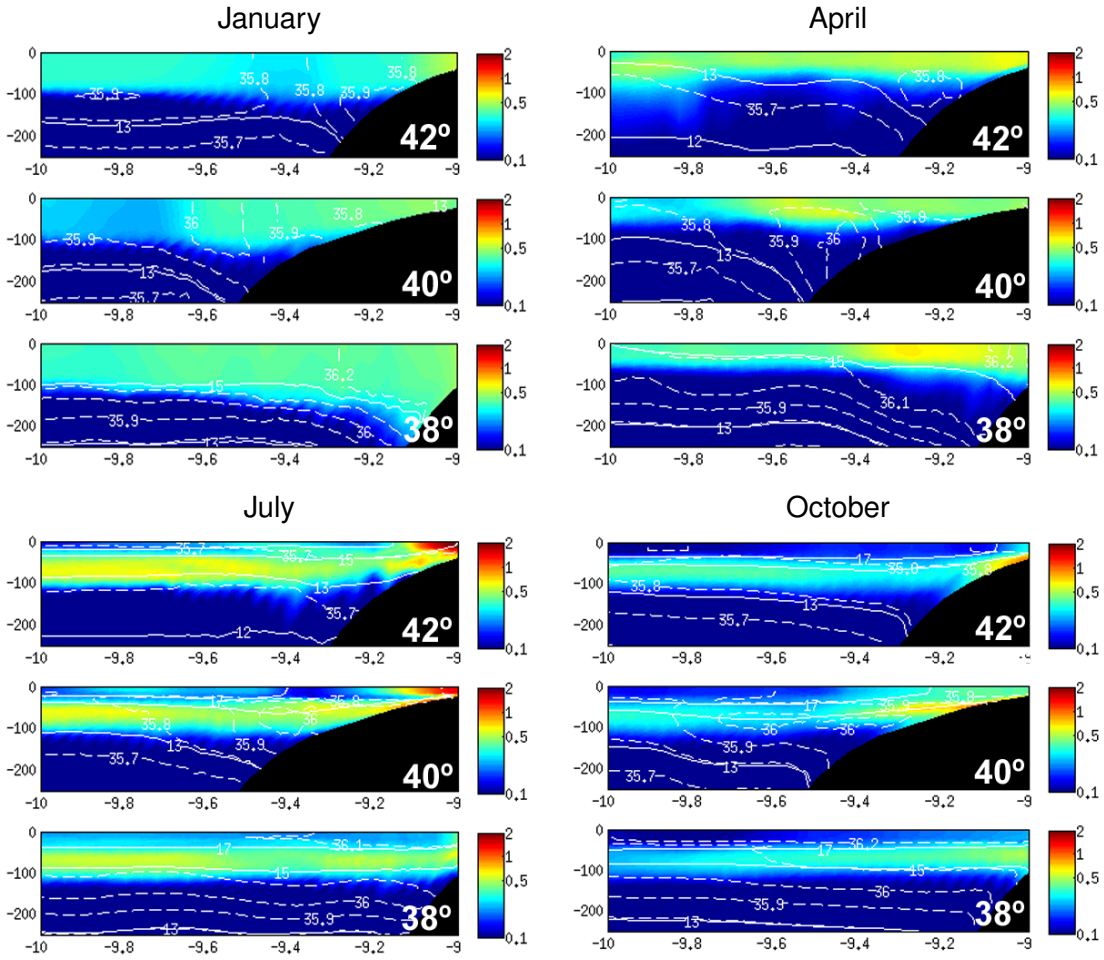

Figure 3.10: Cross-shelf vertical sections of modeled chlorophyll (mg m $^{-3}$, color scale), temperature (solid line, depicted every 2℃), and salinity (dashed line, depicted every 0.1 psu) monthly means (January-winter; April-Spring; July-Summer; October-Autumn) across 3 locations in the western Iberian margin: 42° N, 40° N, and 38° N.

The detritus distribution was similar to the chlorophyll distribution, with the highest concentrations offshore during the spring bloom and a coastal and subsurface maximum

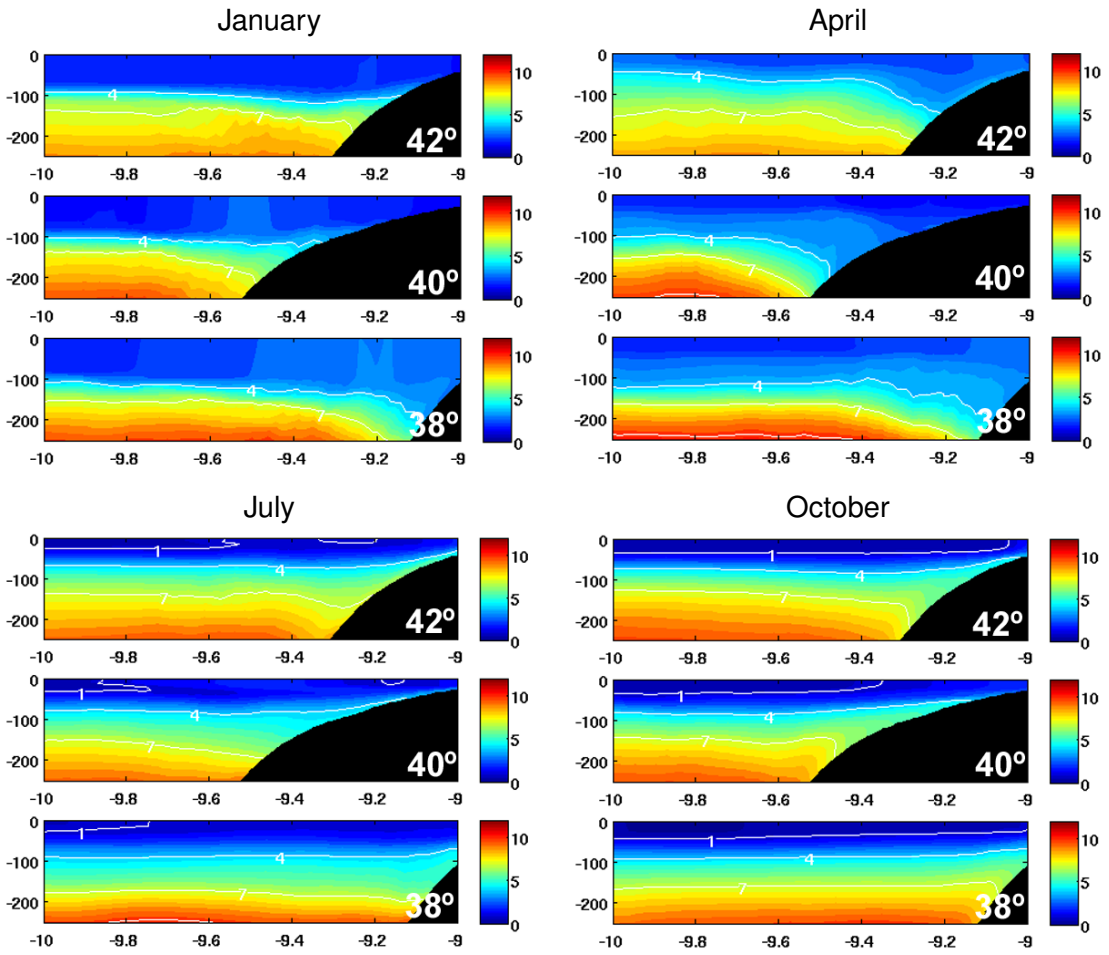

Figure 3.11: Cross-shelf vertical sections of modeled nitrate (mmol N m^{-3}, color scale and solid contour line) across 3 locations in the western Iberian margin: 42° N, 40° N, and 38° N.

during the summer upwelling (Fig. 3.12). The shelf width differences seemed to strongly influence the detritus concentration and fate, as the highest detritus concentration occurred over the wider shelf, at 40° N, and the lowest detritus concentration was that over the narrower shelf at 38° N. In the narrow southwestern shelf the subsurface maximum of detritus reached farther offshore, indicating that organic matter export was favored in opposition to accumulation. Cunha (2002) proposed that over the western Iberian shelf phytogenic material is advected from the north into the south under northern winds and that part of this material sinks in the south increasing benthic production due to higher bottom detritus concentration, contrasting with the higher pelagic production in the north. However, model results did not show higher detritus concentration reaching the shelf bottom in the south that would support this hypothesis. The northern shelves receive a higher freshwater input (climatological river outflow was used in the model), which seemed to have an effect on the winter chlorophyll cross-shelf distribution (Fig. 3.10). The low

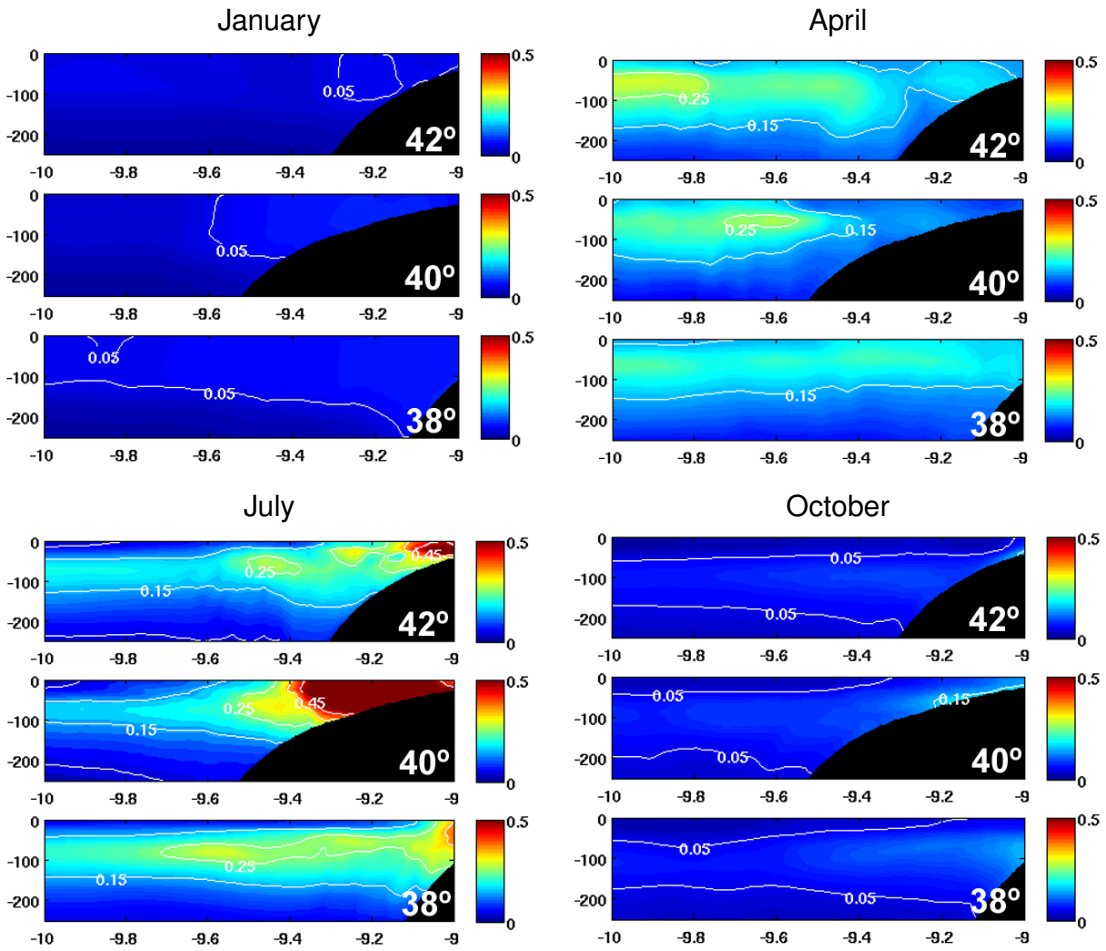

Figure 3.12: Cross-shelf vertical sections of modeled detritus (mmol N m^{-3}, color scale and solid contour line) across 3 locations in the western Iberian margin: 42° N, 40° N, and 38° N.

salinity over the shelf at 42° N and 40° N (<35.8) in January showed the influence of the rivers discharge, with the presence of the WIBP (Peliz et al., 2002) delimiting an area of higher [Chl] over the shelf (∼0.5 mg m^{-3}) where stratification favored phytoplankton growth (Ribeiro et al., 2005). Maximum salinity cores showed the presence of the IPC in October and January in the vicinities of the shelf, although no evident effect on [Chl] could be detected from model results.

3.6 Summary and Conclusions

The coupled hydrodynamic-biogeochemical model was able to reasonably reproduce the climatological seasonal cycle of phytoplankton biomass in the Iberian Atlantic margin and the adjacent oceanic region. It allowed to make a general characterization of the

spatio-temporal patterns of phytoplankton biomass (chlorophyll-a), as well as a general characterization of zooplankton, detritus and nitrate distributions. These model results were discussed together with remotely sensed data and in situ observational data from the literature, giving for the first time a joint picture of the plankton ecosystem variability in western Iberia, limited so far for the difficulties of long time and space oceanographic samplings. The implementation of the ocean-biogoechemical model to the Iberian margin is also an important contribution for potential research applications and forecast of ocean biogeochemical properties. Still, during the evaluation process some differences with the remotely sensed climatologies were detected, which should be taken into account. Namely, the anticipation and overestimation of the offshore spring phytoplankton bloom, and the overestimation of upwelling-related coastal maxima in the northwestern shelf, apparently due to the intensified upwelling in the model. On the other hand, the rather constant [Chl] over the shelf retrieved from satellite estimations contrasted not only with the marked seasonality of modeled [Chl], which showed a considerable decrease in winter, but also with in situ samplings reported in the literature showing a similar seasonal trend. This evidenced that care should be taken when validating model results in the Iberian coastal region using satellite [Chl] products, as there seemed to be an overestimation in remotely sensed [Chl] values, particularly in winter.

The seasonality of chlorophyll-a obtained from model results showed a progressive increase from winter to spring, when the offshore maximum of the spring phytoplankton bloom occurred. This was followed by a coastal [Chl] maximum in summer associated to the dominant upwelling conditions, driven by northerly winds, together with an offshore subsurface [Chl] maximum located at around the base of the thermocline ($\sim$50 m) that remained in autumn, but with lower [Chl] values. The offshore seasonal cycle of phytoplankton biomass seemed to follow the seasonal evolution of the averaged MLD over the region. Over the western shelf, the climatological model results confirmed the north-to-south decrease in [Chl] during the summer upwelling period, showing that it was parallel to a general decrease in the nitrate concentration and an increase in temperature and salinity of the upwelled water. This was the result of the regional hydrography, with the transition from the influence of ENACWp in the north to the influence of ENACWt in the south. Similarly, zooplankton biomass and detritus were higher in the north than in the south, supporting that in the Iberian western shelf there was a trend for better conditions for primary and secondary production in the north than in the south. Differences in shelf width along the Iberian margin had an important influence on the organic matter concentration and fate, the subsurface offshore export of detritus being favored in the narrow southern shelf, whereas detritus concentration was highest over the central wide shelf.

Chapter 4

Towards operational modelling and forecasting of the Iberian shelves ecosystem

Martinho Marta-Almeida, Rosa Reboreda, Carlos Rocha, Jesus Dubert, Rita Nolasco, Nuno Cordeiro, Tiago Luna, Alfredo Rocha, João D. Lencart e Silva, Henrique Queiroga, Álvaro Peliz, Manuel Ruiz-Villareal

4.1 Abstract

There is a growing interest on physical and biogeochemical oceanic hindcasts and forecasts from a wide range of users and businesses. In this contribution we present an operational biogeochemical forecast system for the Portuguese and Galician oceanographic regions, where atmospheric, hydrodynamic and biogeochemical variables are integrated. The ocean model ROMS, with a horizontal resolution of 3 km, is forced by the atmospheric model WRF and includes a Nutrients-Phytoplankton-Zooplankton-Detritus biogeochemical module (NPZD). In addition to oceanographic variables, the system predicts the concentration of nitrate, phytoplankton, zooplankton and detritus (mmol N m^{-3}). Model results are compared against radar currents and remote sensed SST and chlorophyll. Quantitative skill assessment during a summer upwelling period shows that our modelling system adequately represents the surface circulation over the shelf including the observed spatial variability and trends of temperature and chlorophyll concentration. Additionally, the skill assessment also shows some deficiencies like the overestimation of upwelling

circulation and consequently, of the duration and intensity of the phytoplankton blooms. These and other departures from the observations are discussed, their origins identified and future improvements suggested.The forecast system is the first of its kind in the region and provides free online distribution of model input and output, as well as comparisons of model results with satellite imagery for qualitative operational assessment of model skill.

4.2 Introduction

Providing operational oceanographic data on biological and chemical variables has become an issue of concern over the last years. The demand for this kind of information arises from a range of fields and applications such as scientific research on marine ecosystems, monitoring of seawater quality and decision-making support for marine and coastal management. A recent questionnaire conducted by ICES-WGOOFE (International Council for the Exploration of the Sea, Working Group on Operational Oceanographic Products for Fisheries and Environment) showed that temperature, currents, salinity, chlorophyll standing stock and primary production were the most requested products among ocean sciences scientific community, who scored several biological parameters in the top 10 rankings of products on demand (Berx et al., 2011). There is a well known increasing interest in combined physical, chemical and biological operational products, including near-real time and forecast, which are currently possible due to facilitated access to computational resources, development of numerical solutions and improvement of modelling algorithms and performance.

The marine policies implemented in many countries to protect the sea from increasing environmental pressures has urged the need for monitoring systems of seawater quality. In the European Union, the Water Framework Directive and the Marine Strategy Framework Directive launched in 2000 and 2008, commit the member states to the evaluation and monitoring of the ecological status of their river basins/coastal waters and marine waters, respectively (e.g. Borja, 2005; Borja et al., 2010). The setting up of the European Earth Monitoring Programme GMES (Global Monitoring for Environment and Security) by the European Commission, which includes an important ocean component and aims to be fully operational by 2014, highlights the interest on reliable and up-to-date marine environmental information (Brachet, 2004).

Biogeochemical models constitute a valuable tool for operational oceanography when coupled with circulation models. They can complement the time and space limitation of observations and offer the possibility to help explain processes and variability. The

simplest version of these models are the NPZD (Nutrients-Phytoplankton-Zooplankton-Detritus) models. They can give information on concentration of the biological state variables over time, and have strong potentialities for analysis and prediction. Nevertheless, modelling the ocean biogeochemical properties has a number of difficulties that make it a challenging task. The parameters used in biogeochemical models are often not well constrained in the literature and finding an appropriate set of parameters through trial runs is seldom straightforward. In addition, independently of the level of complexity of a biogeochemical model, it is still a great simplification of the reality.

The strong dependency of biology on hydrodynamics requires an ocean circulation model able to reproduce adequately the main features and variability in the modelling domain, at both seasonal and event time scales. In regional coastal domains, sufficiently high resolution is required to resolve the shelf mesoscale eddy processes, which depends upon high performance computational facilities.

Operational modelling products of ocean biogeochemical variables are rarely provided by online operational systems, presumable because of the difficulties mentioned above. In the western Iberia, an early experience of chlorophyll forecast in 1998 in the Gulf of Cadiz is referred in Pinardi and Woods (2002), Chap 11. The GMES ocean data server MyOcean (http://www.myocean.eu) provides modeled biogeochemical data for the European northwest shelf since April 2011, including the northernmost part of the Iberian maritime region. The model used has been implemented operationally over the last years in the seas around the UK and Ireland (Siddorn et al., 2007). The Project EasyCO (model products in several European maritime regions, including the western Iberia) foresees to distribute biogeochemical data, although this type of information is currently available only for the western French coast. Other regions in Europe with operational modelling products for biology are the Baltic Sea, developed by the Baltic ocean community (Neumann, 2000), and the Mediterranean Sea, developed by the Istituto Nazionale di Oceanografia e di Geofisica Sperimentale, OGS, in collaboration with other Italian Institutions (INGV, CINECA and GOS-ISAC-CNR) (Lazzari et al., 2010; Teruzzi et al., 2011). Both available through MyOcean.

In this contribution we present an operational biogeochemical forecast system implemented for the Atlantic Iberian shelf ecosystem: Portuguese and Galician shelf and slope and nearby oceanic regions. This product is the first of its kind in the region and provides free online access to all ocean state and biogeochemical simulated variables. The hydrodynamic forecast system is working since 1st November 2008 and the biogeochemical module is available operationally since 10th June 2011.

The next section describes the ocean model setup, the atmospheric model providing surface data for the ocean model, the biogeochemical model and the operational system setup. Then, results are presented and compared with observations. In the last section we present the summary and outlook of upcoming improvements.

4.3 Modelling setup

4.3.1 Ocean model

The numerical model implemented is the Regional Ocean Modelling System, ROMS (Shchepetkin and McWilliams, 2005; Penven et al., 2006; Haidvogel et al., 2008). ROMS is a free-surface terrain-following primitive equation hydrostatic model with Boussinesq approximations and configurable for realistic applications. ROMS has been used in a variety of time and space scales, from very small regions, like harbours, to the coastal, large and global scale.

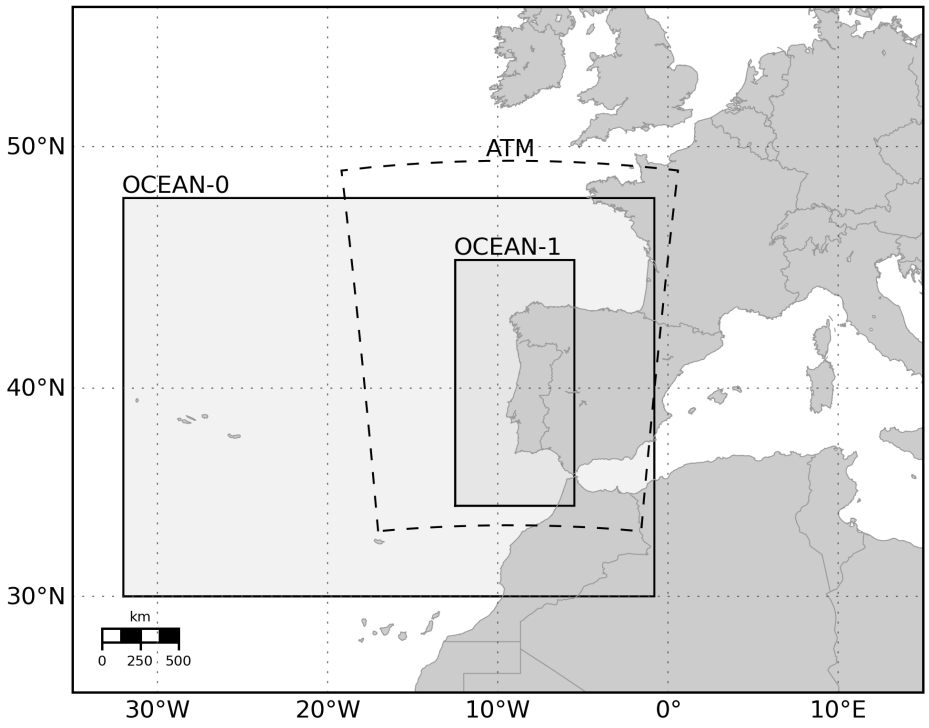

Figure 4.1: Study region with nested grids configurations of the atmospheric model (ATM) and ocean model (OCEAN-0 and target domain OCEAN-1).

The model configuration in use has been successfully applied in the western Iberian region during roughly the last ten years, to many different studies, like dispersion of larvae (Marta-Almeida et al., 2006, 2008; Peliz et al., 2007b), river plumes (Silva et al., 2007; Otero et al., 2008, 2009, 2011) and pollution transport (Ruiz-Villarreal et al., 2006; Sotillo et al., 2008). The Gibraltar exchange flow and the large scale circulation associated with the Azores Current are included in the modelling configuration and were based on Peliz et al. (2007a, 2009).

The ocean model uses two different domains, illustrated in Figure 4.1 as OCEAN-0 and OCEAN-1. The large domain, OCEAN-0, has horizontal resolution of 1/10°, able to resolve the large scale circulation features, and vertical resolution of 30 s-levels with enhanced surface and bottom resolution. The simulations of OCEAN-0 started from rest with temperature and salinity climatologies from Levitus and Boyer (1994) and Levitus et al. (1994), used to initialise and constrain the open boundaries of this domain. The surface was forced with fluxes from the Atlas of Surface Marine Data (da Silva et al., 1994). Monthly geostrophic velocities (referenced to 1200 m) and Ekman velocities were calculated from the climatologies and applied along the lateral boundaries. The Mediterranean inflow/outflow and spreading was parametrised following Peliz et al. (2007a). This configuration ran for several years until a stable kinetic solution was attained by year five. The monthly mean of this last year is considered a good resolution climatology and thus used to provide initial and boundary data to the high resolution configuration OCEAN-1.

The target domain OCEAN-1 (Figures 4.1 and 4.2) has a horizontal resolution of about 3 km extending from Gibraltar to North Galicia ($\sim$1200 km). The domain width is about 600 km. In the vertical 60 s-levels are used with increased near bottom resolution, in order to deal with the Mediterranean exchange (parametrised in the same way as in OCEAN-0). This model was initialised at 1st November 2008 and forced with realistic high resolution surface fluxes from a local solution of the atmospheric model WRF (described in the next section).

The main riverine fresh water inputs from Portugal and Galicia were included in both domains as monthly climatologies. All rivers used are indicated in Figure 4.2 together with the corresponding percentage of freshwater input in the model domain. The river discharges were obtained from the Portuguese Water Institute (INAG, http://www.inag.pt) and from estimations presented in Otero et al. (2010). A fixed value of 12℃ was used for river temperatures.

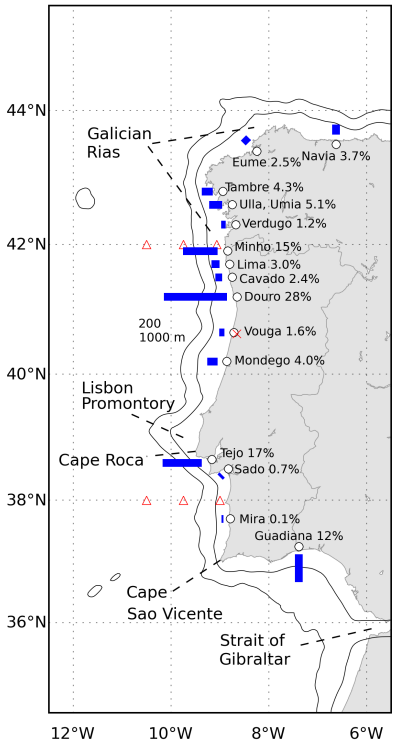

Figure 4.2: Operational ocean model domain with the location of geographical features and landmarks referenced through the text. The model grid covers the Portuguese and Galician coasts. The main riverine sources of the model are indicated together with the corresponding percentages of fresh water inputs (rivers were introduced as monthly climatologies). The three triangles at the latitudes 42° N and 38° N indicate the locations of surface currents (42° only), temperature and chlorophyll comparisons, between model and observations, done in this work. The cross near the Vouga river mouth is the location of wind comparison.

4.3.2 Atmospheric model

The model, which provides surface forcing data to the ocean domain OCEAN-1 (Figure 4.2), is an operational implementation of the Weather Research and Forecasting Advance Research model (WRF-ARW) version 3.2.1 (Skamarock et al., 2008). The WRF model is driven by GFS forecasts (NOAA, 2003) with an horizontal resolution of 0.5° $\times$ 0.5°, and vertical domain extending from a surface pressure of 1000 hPa to 0.27 hPa, discretized in 64 vertical unequally-spaced levels (15 levels are located below 800 hPa and 24 levels above 100 hPa).

The atmospheric forecasts are performed daily by the Group of Meteorology and

Climatology of Aveiro University (CliM@UA, http://climetua.fis.ua.pt) and encompass the Portuguese mainland, Madeira and Azores archipelagos. The oceanic operational system uses the weather forecasts for Portuguese mainland domain with spatial resolution of 25 km (Figure 4.1).

The atmospheric model in use by CliM@UA was configured after a set of numerical experiments described by Ferreira (2007). Model outputs were tested against observations and the best combination of model parameterizations was found for the region.

4.3.3 Biological Model

The biogeochemical model contains a 4-component nitrogen based ecosystem NPZD model (based on Fasham et al. (1990)), computing 4 state variables: nutrients (nitrate), phytoplankton, zooplankton and detritus, all expressed in mmol N m^{-3}. Chlorophyll a (mg m-3) is derived from phytoplankton concentration using a variable chlorophyll:C ratio (θ) that is a function of light and nutrients availability, and a C:N ratio of 6.625 (mmol C/ mmol N), i.e., a Redfield ratio. The equation for θ describes the proportion of photosynthetically fixed carbon that is used for chlorophyll a biosynthesis considering the model of Geider et al. (1997), which implementation in the ocean model is described in Gruber et al. (2006). The 3D time evolution of the concentration of any of the biogeochemical variables (B_i) follows the general equation:

$$\frac{\partial B_i}{\partial t} = \nabla \cdot K \nabla B_i - u \cdot \nabla_h B_i - (w + w_{sink}) \frac{\partial B_i}{\partial z} + SMS(B_i) \tag{4.1}$$

where the terms in the right hand side account for diffusion, horizontal advection, vertical mixing and source minus sink (SMS) biological processes, respectively. K is the eddy kinematic diffusivity tensor, u is the horizontal velocity of the fluid, w and w_sink are the vertical velocity of the fluid and the vertical sinking rate of the biogeochemical tracer, respectively, with the exception of zooplankton and nitrate, to which no sinking rate is attributed.

The biogeochemical processes included in SMS are specific for each variable and represent the following conceptual description: phytoplankton uptakes nitrate at a rate that is dependent on the instantaneous nitrate concentration, temperature and light intensity/PAR (photosynthetically available radiation). PAR at the surface is calculated as 43% of the incident radiation and attenuated with depth as it is absorbed by water and chlorophyll. Phytoplankton dies at a constant linear rate, been automatically incorporated to the detritus pool. Zooplankton growth relies on its grazing on phytoplankton, which rate

depends on prey concentration, and its assimilation efficiency. A constant excretion rate is attributed to zooplankton, providing a source of nutrients to the nitrate pool. Zooplankton incorporates to the detritus pool at a constant linear mortality rate. Mineralization of detritus is formulated as direct transformation to nitrate at a constant nitrification rate. Model parameters for the sink/source terms selected to represent our region of study are listed in Table 2.1. A detailed description of the biogeochemical model equations, including sink-source terms, can be found in Koné et al. (2005).

River	Nitrate (mmol m^{-3})	Chlorophyll (mg m^{-3})
Navia	0.1	0.1
Eume	6.4	0.1
Tambre	23.2	0.1
Ulla, Ulmia	13.3	0.1
Verdugo	4.4	0.1
Minho	34.7	2.0
Lima	11.8	2.4
Cavado	33.2	0.9
Douro	88.5	5.4
Vouga	44.4	0.1
Mondego	2.3	5.0
Tejo	21.0	8.5
Sado	21.3	9.6
Mira	10.6	0.9
Guadiana	5.2	0.1

Table 4.1: River inputs of nitrate and clorophyll.

The concentration of nitrate and chlorophyll a for the model initial and boundary conditions were supplied by the climatological data sets World Ocean Atlas 2005 (Garcia et al., 2006) and SeaWiFS, respectively. The initial and boundary data of phytoplankton and zooplankton were derived from chlorophyll a. Detritus were introduced constant with the value 0.02 mmol N m^{-3}. Boundary conditions were supplied seasonally. The riverine inputs of nitrate and chlorophyll were used constant along the year and were obtained from Ferreira et al. (2003) and from the European Environment Agency (http:// www.eea.europa.eu). The values used are listed in Table 4.1.

The biological model runs as a module integrated in the ocean model. It became operational at 10th June 2011.

4.3.4 Operational system

The ocean and biological modelling system was implemented operationally with OOFε (Operational Ocean Forecast Python Engine, Marta-Almeida et al., 2011b). OOFε is a comprehensive set of tools, written in the Python programming language, which creates

and operates the model input/output and controls all the required tasks for the operationality of the ocean model. The operational engine executes daily analysis and forecast (currently three days), whose cycles are repeated continuously in a robust and fully automated manner. The operational engine also includes a visualisation module able to produce many types of slices and plots from the ocean model inputs/outputs. Some graphical outputs of the current implementation can be seen at the homepage of the forecast system, http://neptuno.fis.ua.pt/oof[1]. Among the several outputs are horizontal slices at several depths of temperature, salinity and chlorophyll, as well as forcing wind, sea surface height, currents, etc. For a quick comparison to observational data sets, the web site also shows satellite observations, namely sea surface temperature from O& SI-SAF (Ocean & Sea Ice Satellite Application Facility, www.osi-saf.org) and from OSTIA (Operational Sea Surface Temperature and Sea Ice Analysis, http://ghrsst-pp.metoffice.com), and high resolution chlorophyll processed and distributed by IFREMER (http://cersat.ifremer.fr/science/ocean color).

The full model data sets are freely available through the Python OPenDAP server Pydap (http://pydap.org). OPeNDAP is an efficient protocol for allowing the remote access of data sets (e.g. Cornillon et al., 2009; Signell et al., 2008). Data usually available as a set of different individual large data files is made available in an efficient and consistent way by OPeNDAP servers.

The system implemented with OOFε has been successfully operating the ROMS model in other locations, like the Brazilian region (Marta-Almeida et al., 2011a) and the Northern Gulf of Mexico (Zhang et al., 2012).

4.4 Results

The results presented give an overview of model ability to reproduce the hydrodynamic (surface currents and surface temperature) and chlorophyll fields for the four months following the operational implementation of the biogeochemical model (10th June 2011 to 10th October 2011). These preliminary results are thus addressed as a general reliability assessment rather than a thorough validation, which would need more comparisons with observations and for a longer time period. The period studied corresponds to summer and early autumn, which is characterised in the western Iberian coastal region by recurrent

[1]This site is no longer available. Currently the results of the ocean operational system are provided in collaboration with the Group of Meteorology and Climatology of Aveiro University at their web page (CliM@UA, http://climetua.fis.ua.pt/fields/oceanoAtlantic/).

upwelling conditions. Therefore, the model is evaluated during one of the most dynamic and biologically productive seasons of the year.

Surface model currents are compared with a high frequency radar data, owned by the Spanish Merchant Navy, at three locations off Vigo (latitude 42°N and longitudes 9°W, 9.75°W and 10.5°W). Given the importance of atmospheric forcing for the ocean model to adequately reproduce the circulation, the surface wind provided by the WRF atmospheric model is compared with wind measurements at University of Aveiro weather station. Then, in order to assess model ability to reproduce coastal blooms, the onset and evolution of a strong upwelling/coastal bloom event (13th to 26th of July) is shown, comparing modeled sea surface temperature and chlorophyll concentration fields in the model with satellite observations (OSISAF-EUMETSAT Ocean & Sea Ice Satellite Application Facility and IFREMER optimised interpolation of MODIS, SeaWiFS and MERIS observations, respectively). To better evaluate the model skill for surface temperature and chlorophyll along the four months, and at different locations within the domain, time series comparing model results and satellite data are presented for two latitudes (42°N and 38°N) in three locations for each latitude, corresponding to middle shelf, off the shelf break and open-sea (same longitudes as used for currents comparison at 42°N). Finally, the model skill in the whole domain is further explored by plotting model bias of SST and chlorophyll which allow to evaluate whether the model is over- or underestimating the observations.

Due to the lack of reliable observational data other than satellite chlorophyll and SST for the time period under study, we do not further explore model skill assessment methods (Allen et al., 2007; Jolliff et al., 2009). For the same reason, neither concentration of nitrate or the vertical structure of the variables was analysed in the current study.

4.4.1 Surface wind and currents

The surface wind measured at Aveiro University weather station (the location is indicated in Figure 4.2 as x, near the Vouga river mouth) is displayed in Figure 4.3 a. The wind field, upwelling favourable, is typical of the summer season for Western Iberian region, with predominance of northerly winds (Wooster et al., 1976). The most intense event is observed between 13 and 28 of July, with wind intensity higher than 5 m s^{-1} during most of the days. Figure 4.3 b shows the ocean model forcing wind, generated by the WRF atmospheric model, interpolated at the same location. In general, the modeled wind is more intense than the observed one and the wind inversion after the relaxation is also more prominent.

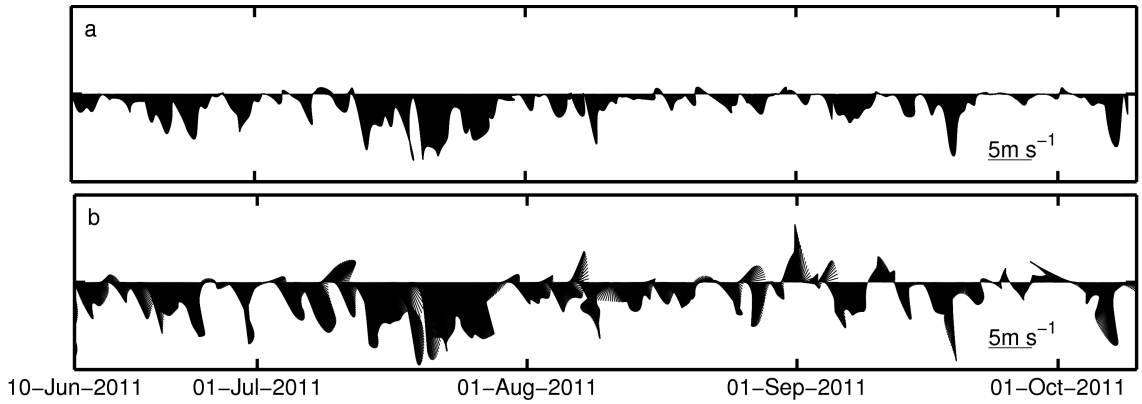

Figure 4.3: Wind measured by the Aveiro University automatic weather station (a) and ocean model forcing wind at the same location (b). The site is indicated in Figure 4.2 as x close to the Vouga river mouth.

The comparison of modeled and observed surface currents at the latitude 42°N is shown in Figure 4.4 (the three comparison sites are indicated in Figure 4.2). The data shown has been filtered with a low-pass filter with sub-diurnal cutoff frequency. In the shelf (Figure 4.4 a,b), the model reproduces correctly the intensity and direction of the current field, which is dominated by an equatorward flow in response to the upwelling favourable wind forcing, with presence of typical velocities of 0.2 m s^{-1} , and maximum values of about 0.35 m s^{-1} associated to the peak of wind forcing by day 22nd of July. In the vicinity of the shelf break (Figure 4.4 c,d), the southward tendency is also present in the observations and model results, but the model presents in general higher intensities. In the open-ocean (Figure 4.4 e,f) the mesoscale variability is very high and the model cannot reproduce the observed eddy activity.

4.4.2 Coastal bloom event, 13th to 26th July 2011

The general trend on chlorophyll concentration simulated along the considered period was that expected for a typical summer situation in the Iberian upwelling region. Successive coastal blooms appeared associated with upwelling pulses, and were more persistent in the northwest coast around Galicia and in the proximity of Cape Roca. In several occasions the bloom occupied the coast from North to South.

We selected the period 13th to 26th July, characterised by strong northerly wind, upwelling favourable, that led to the onset and evolution of a conspicuous coastal bloom, to evaluate model performance reproducing this kind of blooms. Surface temperature and chlorophyll in the model were compared with satellite observations (Figures 4.5 and

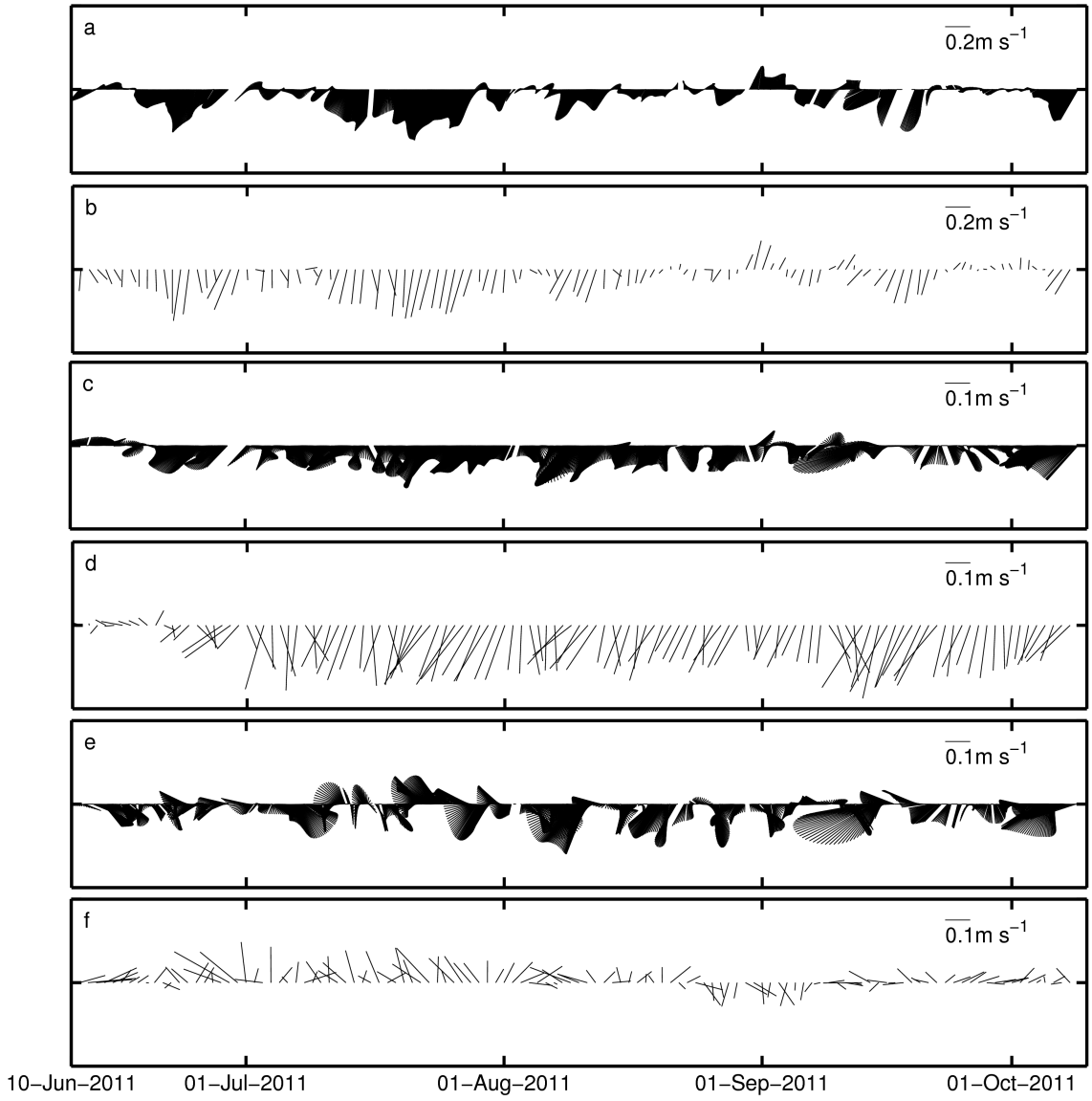

Figure 4.4: Observed and modeled surface currents at three locations along the latitude 42°N at the longitudes 9°W (a and b), 9.75°W (c and d) and 10.5°W (e and f). These locations are shown in Figure 4.2 as triangles.

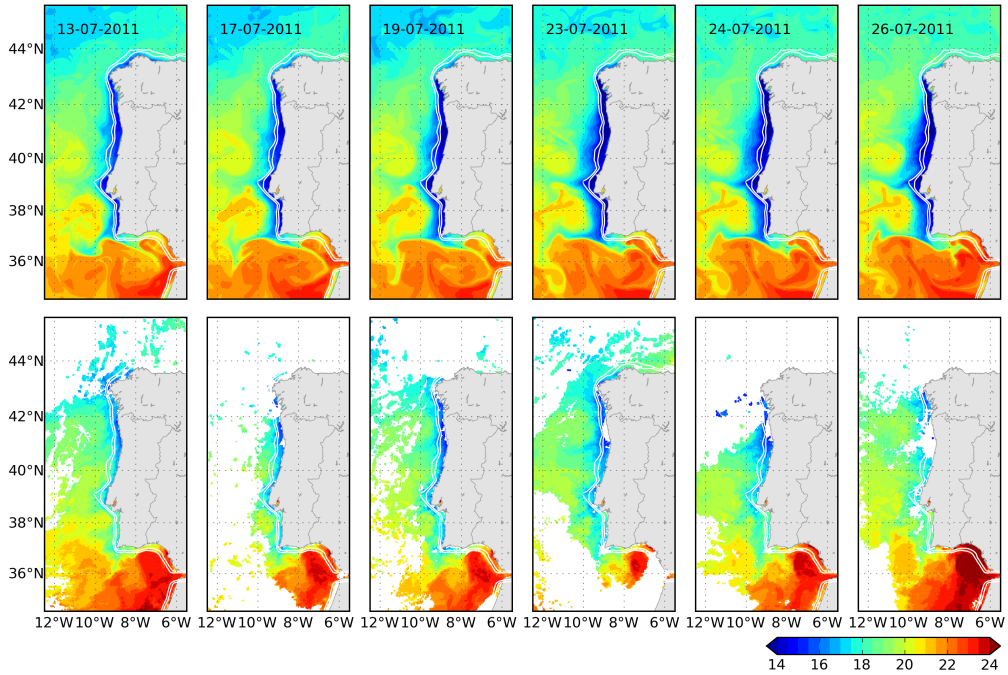

Figure 4.5: Sea surface temperature from model (upper panel) and from satellite observations provided by OSISAF (lower panel, processed by Meteo-France/CMS-Lannion in the framework of the OSISAF project). Snapshots between 13th and 26th July 2011 are depicted, illustrating one episode of upwelling intensification and coastal bloom (next Figure).

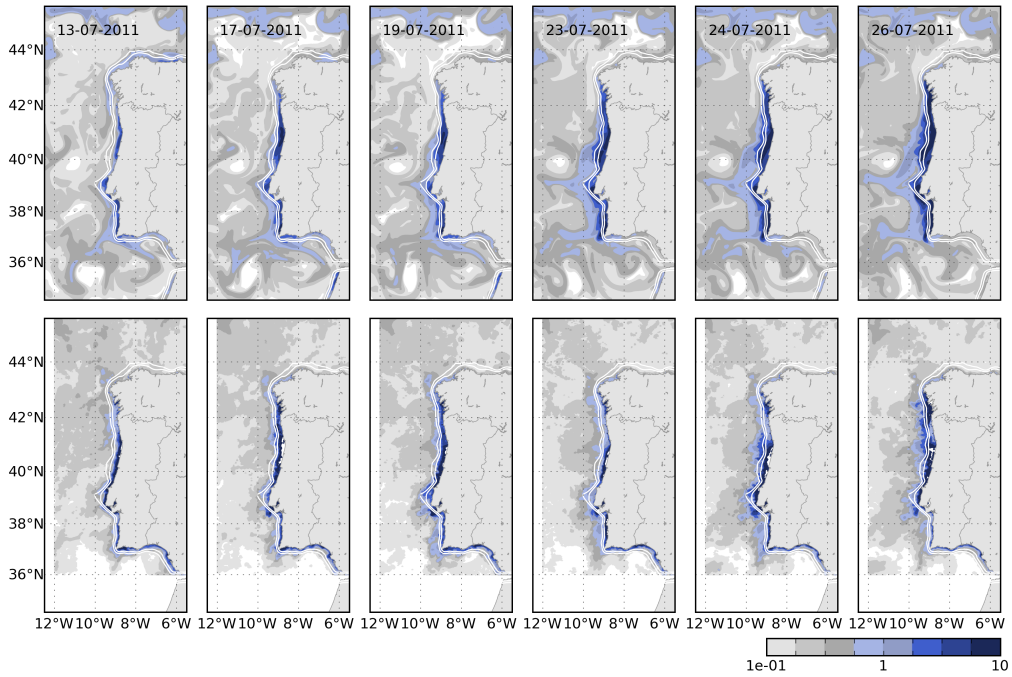

Figure 4.6: Same as previous Figure but showing the chlorophyll coastal bloom. Chlorophyll observations are provided by IFREMER and obtained from OC5 optimised interpolation of MODIS, SeaWiFS and MERIS observations.

4.6). Surface temperature shows a distinctive band of cold, upwelled water near the coast which was narrower and more restricted to the North coast in the satellite images than in the model. Two filaments with origin in Cape Roca and Cape S. Vicente appeared in the model, and some evidence of their presence was also observable in the satellite (e.g. days 23rd and 24th). As for the phytoplankton bloom, the increase in chlorophyll concentration along the coast (up to about 6 mg m^{-3}) appeared at about the same time in the model and in the satellite, around 13th of July. The trend was particularly well reproduced in the region between 40°N and 42°N, where the concentration reached 10 mg m^{-3} , whereas in the southwest coast (37°N to 39°N), the concentration in the model was higher than in observations (highest values around 6 and 2 mg m^{-3}, respectively). In contrast, the model was not able to reproduce the high inner shelf chlorophyll concentration along the South coast of Portugal and the Gulf of Cadiz (36°N to 37°N). The bloom situation continued on the next days, spreading offshore with increasing chlorophyll concentration. By day 23th , the bloom seemed to decrease on satellite observations, and then it intensified again (24th to 26th). This decrease was not observed in the model and the bloom continued extending offshore and along the coast. As a consequence, at the end of July, the bloom was more intense and spread farther offshore in the model than in the satellite observations. This is probably related with a slower relaxation of the upwelling winds in the model than in the real ocean.

4.4.3 SST and chlorophyll time series

The model skill for sea surface temperature and chlorophyll was investigated comparing time series between the model and the satellite at six points within the domain (Figure 4.7 and 4.8). The comparison sites are indicated in Figure 4.2 and represent different zones: middle shelf; offshore vicinity of shelf brake; and offshore zone, for two latitudes, in the northern and southern part of the domain (42°N and 38°N).

At both latitudes, the modeled shelf surface temperature was lower than temperature from satellite during most part of the analysed period, with typical bias higher than 1 °C (Figure 4.7 a and Figure 4.8 a). At the offshore sites the model had a better skill reproducing both the low and high (event scale) variability of the surface temperature (Figure 4.7 c,e and Figure 4.8 c,e). The relatively colder waters near the coast may be associated with several factors including over-mixing and inability of the model to re-stratify after strong wind events, deficient parametrisation of air-sea heat fluxes and wind-stress. However, the mixing parametrisations we have used are the ones that are standard and recommended in the majority of ROMS applications. The K-Profile Parameterization,

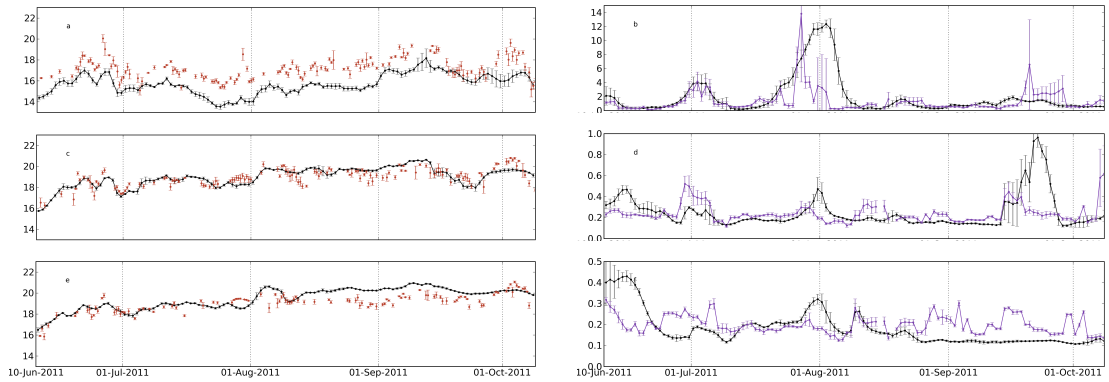

Figure 4.7: Observed and modeled (in black) sea surface temperature (a, c and e) and chlorophyll (b, d and f) at latitude 42°N and longitudes 9°W, 9.75°W and 10.5°W (locations indicated as triangles in Figure 4.2). The satellite observations are distributed by OSISAF and by IFREMER. Note the different vertical scales for chlorophyll. Each data point is the average of the data inside a circle of radius 7 km. Error bars are the corresponding standard deviations.

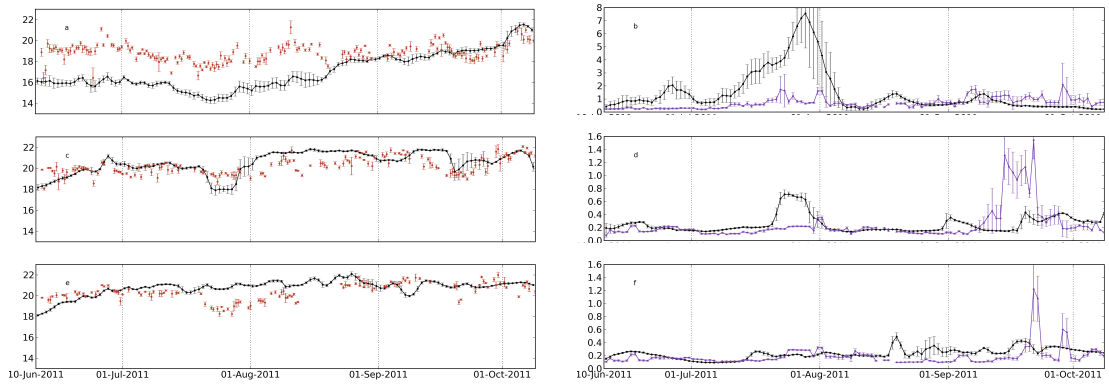

Figure 4.8: Same as Figure 4.7 but for the latitude 38°N.

KPP model, described in detail in Large et al. (1994), is fully tested for most of the mesoscale applications. It can be argued that near the coast other mixing schemes could perform better, but they usually require additional local information. On the other hand, the colder bias near the coast have been reported in several upwelling systems studies, and attributed to the lack of resolution of the wind stress field near the coast, in which the wind curl is not properly resolved (e.g. Capet et al., 2004; Otero and Ruiz-Villarreal, 2008). A recent comparison across different upwelling systems (Dufois et al., 2012a) shows that the bias is common to all upwelling systems and that in part there is a warm tendency of SST data bases.

The surface chlorophyll comparisons shows that the relatively simple biological model is able to reproduce many of the observed features, mainly in terms of variability. At 42°N the model simulated the main episodes of chlorophyll concentration variability,

namely the shelf blooms by the end of July and beginning of August (Figure 4.7 b). Chlorophyll concentration in both peaks was similar in the model and in satellite observations. The model peak in August lasted longer, most probably as a consequence of the model difficulty to represent the relaxation of the upwelling (Figure 4.3). A third bloom appeared in early autumn (end of September) that was not captured by the model in the shelf (Figure 4.7 b), but it was captured next to the shelf brake (Figure 4.7 d). In general, chlorophyll concentration in the model was of the same order as satellite values, except for the most offshore location (10.5°W) at the end of the period, when model values tended to be systematically lower (Figure 4.7 f).

For the latitude 38°N (Figure 4.8) the model also shows some sensitivity to the event at the end of July, but giving much higher chlorophyll concentrations than the observed ones. The model simulated blooms in the shelf (Figure 4.8 b) and near the shelf brake (Figure 4.8 d) that were considerably higher than in the satellite observations (or even non-existent in the satellite). This behaviour is believed to be a consequence of the stronger modeled upwelling in the southern coast, which is reflected in lower temperatures with a bias of near 2 °C at the shelf until middle of August (Figure 4.8 a). It is worth noting that the southern shelf is considerably narrower than the northern shelf (Figure 4.2), which may play a role in this difference due to the lower numerical discretization of the shelf in this region, and hence higher sensitivity to wind forcing accuracy. Conversely, the chlorophyll peaks observed offshore in early autumn were not properly captured in the model (Figure 4.8 d,f). Still, the model shows evidences of being able to reproduce the slowly varying base concentration, around 0.2 mg m^{-3}.

4.4.4 SST and chlorophyll model bias

The model bias (MB) indicates whether the model is overestimating or underestimating the observations, being the model results as better as MB is closest to zero. For each grid point, it was calculated as:

$$MB = \frac{\sum_{t=1}^{n_t}(M_t - D_t)}{\sum_{t=1}^{n_t} D_t} \tag{4.2}$$

where M_t and D_t are the modeled and observed values at time index t, respectively. Figure 4.9 shows the model bias of sea surface temperature and chlorophyll for the domain. There is a systematic negative bias of temperature over the western shelf, as expected, because of the higher intensity of modeled wind than measured (Figure 4.3), leading to higher upwelling and lower surface temperatures extending offshore, beyond the shelf break. The bias of chlorophyll was lowest in the inner shelf and the offshore region around

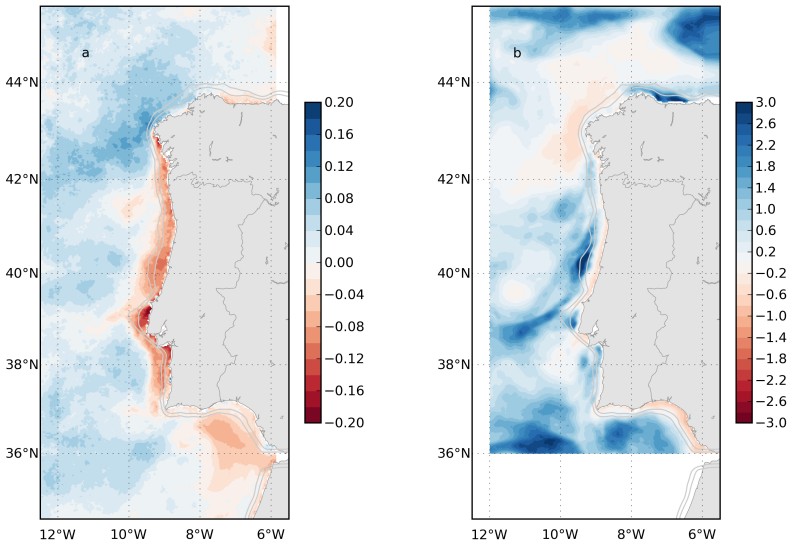

Figure 4.9: Model bias of sea surface temperature (a) and chlorophyll (b) for the period 10th June 2011 to 10th October 2011.

Galicia. Higher differences are found throughout the western outer shelf and in general near the model domain boundaries. In some regions, like the shelf off Asturias (northern coast) and the outer shelf and slope around 40.5°N, modeled chlorophyll concentration was three times higher than satellite values. The chlorophyll bias in the outer shelf is supposed to be related with the negative bias in temperature, i.e., higher upwelling. Near the boundaries, the differences reflect the usage of climatological boundary conditions biogeochemical variables, which vary very slowly and are very often in disagreement with reality.

4.5 Discussion

A ROMS based operational hydrodynamic system was implemented covering the Portuguese and Galician coast. The ocean model has high horizontal and vertical resolution (about 3 km and 60 σ-levels) and is running since November 2008. It uses monthly climatological lateral boundaries provided by a climatological run of a larger scale model with about 10 km of horizontal resolution (see Figure 4.1). The surface is forced with realistic momentum, temperature and salinity fluxes modeled by a local implementation of the atmospheric model WRF. The main rivers of the region are included in the model as monthly climatological means. Also included is the Peliz et al. (2007a) Gibraltar inflow/

outflow parametrisation.

The operational system is totally automatic and runs systematically daily analysis and three days forecasts. This implementations relies on the OOFε (Operational Ocean Forecast Python Engine) described in Marta-Almeida et al. (2011b).

More recently, on 10th June 2011, a 4-component nitrogen based biogeochemical model was initiated operational as a module of the ocean model. The rivers are considered a source of nitrates and chlorophyll with input concentrations constant along the year.

The modeled ocean and biological state variables of the first four months of the coupled hydrodynamic and biogeochemical model were compared with observations for validation. The observations consisted in radar measured surface currents, wind from a weather station and satellite sea surface temperature and chlorophyll.

The model reproduced adequately the wind-forced circulation over the shelf, typical of the western Iberia summer season. Namely the surface currents, the broad spatial and temporal variability of the upwelling circulation and consequent sea surface temperature. However, the consistent temperature deficit, reaching 2 ℃ is an indication of overestimated upwelling. This arises from the difficulty of the atmospheric model to properly resolve the wind field near the coast. Such overestimation leads to artificial surplus of nutrients within the euphotic layer, and consequent overestimation of the intensity and duration of the phytoplankton bloom. It is worthy to note that the model has no relaxation of sea surface temperature, a numerical resource frequently used in long term simulations, to assure convergence to the correct seasonal pattern.

In the northern shelf the model was able to simulate the main blooms observed by the satellite along the upwelling season, and gave similar chlorophyll concentrations, although showing differences in the duration of the most intense coastal bloom. On the other hand, model results in the southern shelf tended to overestimate observed blooms. The main differences between model and satellite have hydrodynamic origin, namely the more intense upwelling and slower wind relaxation in the model. Nevertheless, in general, the base concentration and variability of surface chlorophyll is reasonably reproduced by the NPZD model. It is important to note that satellite observations can neither be taken as the “real value” in the ocean, since they have associated errors.

A more thorough validation of the model would require further comparisons of model data with high quality in situ measurements (buoys and sampling stations), which are not easily available. Comparisons for a longer time period are also needed. Though, work is

underway to cope with the limitations of the current validation.

By providing information about the model skill, the comparison with observations gives clues about possible steps to improve the operational system. Among the future developments, the most important for the coastal and shelf regions, is to have a better representation of the wind field. The local WRF solutions should be improved, namely through optimisation of modelling parametrisations and data assimilation. Ensemble forecasts and assimilation of observations are currently in phase of test and implementation. The rivers have great impact on the shelf dynamics and the use of climatological monthly discharges is certainly an important limitation of the model. Another important limitation in the rivers is the use of constant concentration of nutrients (although the total amount of nutrients varies with river flux). Attempts to estimate at least seasonal patterns should be addressed. This can be done with ensemble Kalman filter optimisation techniques, for instance. The complexity of the biogeochemical model can also be increased to include more variables, that may improve model results. Currently test are underway adding a second subgroup of nitrates (ammonia) and subdividing the detritus in small and large size.

Because of the use of climatological lateral boundaries, the model lacks the ability to reproduce the eddy mesoscale features away from the continental shelf. Some operational eddy-resolving global models with data assimilation are available (like HYCOM, http://www.hycom.org, and MERCATOR http://www.mercator-ocean.fr) and our regional model can be offline nested in the nowcasts and forecasts of such models (e.g. Barth et al., 2008). Also modifying boundary information for the biogeochemical variables, by using data from a global of large-scale parent model, may improve the model results offshore. The results obtained so far with the operational oceanic and biogeochemical implementation are satisfactory and encourage the continuation of the work. The limitations detected incentive improvement efforts, which are currently being studied and tested. In the mean time, results of the oceanic and biogeochemical models are already available online at the web page of the operational system, http://neptuno.fis.ua.pt/oof[2]. Also available are some satellite observations, for comparison. The full model input/output data sets are free to be accessed by any end user through OPenDAP, at the same web address.

[2]This homepage is no longer available. Currently the results of the ocean operational system are provided in collaboration with the Group of Meteorology and Climatology of Aveiro University at their web page (CliM@UA, http://climetua.fis.ua.pt/fields/oceanoAtlantic/).

Chapter 5

Oxygen in the Iberian margin: a modelling study

Rosa Reboreda, Carmen G. Castro, Xosé A. Álvarez-Salgado, Rita Nolasco, Nuno G. F. Cordeiro, Henrique Queiroga, Jesus Dubert

5.1 Abstract

Highly productive eastern boundary coastal upwelling areas provide interesting environments to study the physical-biological interactions that govern O_2 dynamics. The Iberian Upwelling is located in the northern limit of the eastern North Atlantic upwelling region, along the Iberian margin off Portugal and Spain. It presents a marked seasonality in the hydrodynamics and it is under the influence of water masses of different origin. Here, we describe the seasonal variability and spatial patterns of O_2 in this system taking advantage of the 3D Regional Ocean Modeling System (ROMS). The model was satisfactorily validated and allowed a sound 3D description of the O_2 dynamics of the coast and adjacent ocean, showing a strong seasonality in the O_2 concentration of the upper water column. This seasonality is mainly caused by the deepening and shoaling of the seasonal mixed layer from winter to summer. O_2 concentration is high during winter and reaches maximum values in spring due to the seasonal phytoplankton bloom. Minimum O_2 values are obtained in summer and autumn. Additionally, the regional circulation of Eastern North Atlantic Central Water noticeably influences the O_2 distribution. Over the shelf and slope, more variability is introduced by the intense hydrodynamics of the upwelling season (spring/summer), the slope poleward flow (autumn/winter) and continental runoff.

5.2 Introduction

The distribution and variability of dissolved oxygen (O_2) in the ocean is controlled by physical and biological factors and the complex interactions among them. These include the large scale and regional circulation, vertical mixing, air-sea exchange, oxygen release by primary production and oxygen consumption by respiration/mineralization. Highly productive eastern boundary coastal upwelling areas have received special attention to study oxygen trends and variability (e.g. the California Current System: Bograd et al., 2008) (review of oxygen trends in these and other oceanic regions in Keeling et al., 2010). The production and processing of considerable amounts of phytogenic organic matter in these areas coupled to the dynamics of the system is intimately related to the pronounced oxygen gradient between the equatorward-flowing surface layer and the compensating poleward-flowing subsurface layer, which provides interesting conditions to study the physical-biological interactions that govern oxygen dynamics (Bianucci and Denman, 2012).

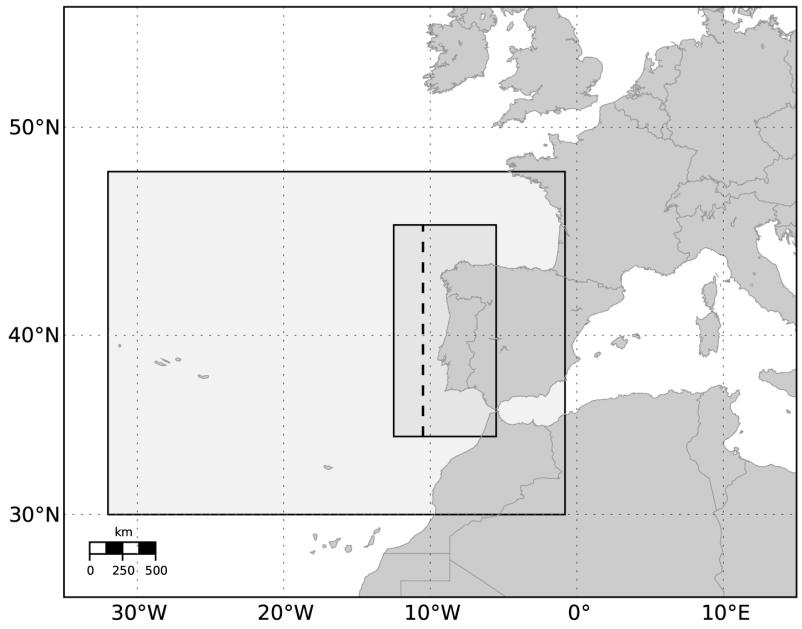

Figure 5.1: Region of study and nested model grids. Dashed line indicates the position of the meridional section at 10.5° W.

The Iberian Upwelling System (IUS) is located in the northern limit of the eastern North Atlantic upwelling region (Wooster et al., 1976; Barton et al., 1998) (Fig. 5.1). It is characterized by a spring-summer upwelling season from April-May to September-

October, when northerly winds off western Iberia prevail, forcing an offshore Ekman transport and the upwelling of cold and nutrient rich water in the surface along the coast (Fraga, 1981; Relvas et al., 2007). This season is characterized by a high biological production (Álvarez-Salgado et al., 2002). During the rest of the year, the wind direction changes and a predominant surface poleward flow, the Iberian Poleward Current (IPC), is observable over the shelf edge and the slope, characterized by relatively warm and saline water (Haynes and Barton, 1990; Relvas et al., 2007). The region has the particularity of being well oxygenated due to the presence of Eastern North Atlantic Central Water (ENACW) in the main thermocline (Castro et al., 2000), consisting of a water branch of subpolar origin (ENACWp) and a water branch of subtropical origin (ENACWt) (Fiuza, 1984; Rios et al., 1992). The IPC transports northwards relatively low oxygen/low nutrient ENACWt along the slope and outer shelf (Perez et al., 1993; Álvarez-Salgado et al., 2003). In contrast, recently ventilated ENACWp is sometimes observed to slowly move southward from its subduction area north of 46° N due to density differences (Pollard and Pu, 1985). At sea surface a weak southward flow known as the Portugal Current (PC) is often thought to exist in the northwestern part of the region (Perez et al., 2001; Peliz et al., 2005), which may influence the O_2 distribution conveying oxygen rich water (Perez et al., 2001). Although, such southward flow seems to be quite variable and reversible east of 13° W, with periods of dominant northward flow (Maze et al., 1997). Deeper in the water column, the presence of Mediterranean Water (MW) is characterized by a conspicuous salinity maximum and O_2 minimum spreading northwards close to the continental slope (Perez et al., 1993; Fiuza et al., 1998).

Given the described seasonal hydrodynamics and the influence of water masses of different origin, coupled physical-biogeochemical ocean modelling arises as a useful tool to study the spatial and temporal patterns of variability along the Atlantic Iberian margin. This approach can help to understand the complex interactions between the physical and biogeochemical mechanisms controlling oxygen variability (Deutsch et al., 2006; Bianucci and Denman, 2012). Furthermore, although numerical models of future global change scenarios predict a significant O_2 decline (Keeling et al., 2010), the current confidence in these projections is limited (Gruber, 2011). Therefore, an appropriate understanding of the present situation is a mandatory first step to move forward into exploring future trends in the biogeochemical dynamics of any ecosystem.

This is the first study devoted to describe the seasonal and spatial variability of O_2 concentration in the Atlantic Iberian margin, taking advantage of an ocean model and some available observations. For that, we use a high-resolution configuration of the Regional Ocean Modeling System (ROMS) coupled to a NPZD + O2 (Nitrate-Phytoplankton-

Zooplankton-Detritus + Oxygen) biogeochemical model to simulate the three-dimensional (3D) seasonal oxygen dynamics in the western Iberian margin (Fig. 5.1). ROMS has been widely used to model the hydrodynamics of the region (e.g. Peliz et al., 2007a; Otero et al., 2008; Nolasco et al., 2013), which gives a good base to explore O_2 distributions using the biogeochemical model of ROMS. In the following sections we describe the model configuration and data used for validation of the model, we present the validation of model results and we do a characterization of the seasonal O_2 distribution in the western Iberian shelf and adjacent ocean.

5.3 Model setup, data and methods

5.3.1 Hydrodynamic model

The seasonal dynamics of the IUS was simulated with the oceanic model Regional Ocean Modeling System (ROMS) (Shchepetkin and McWilliams, 2005; Penven et al., 2006; Haidvogel et al., 2008). ROMS is a 3D ocean circulation model with free-surface terrain-following coordinates which can be configured in high resolution to resolve coastal areas and regional seas at the mesoscale. We implemented a high-resolution configuration for the western Iberian margin using two offline nested domains, as described in Nolasco et al. (2013). Similar configurations of the model have been used in the region (Peliz et al., 2007a; Oliveira et al., 2009; Peliz et al., 2009). The large domain has 1/10° ($\sim$9 km) horizontal resolution and 30 vertical s-levels, in order to resolve the large-scale circulation features, such as the Azores Current. The high-resolution nested domain, our target region of study, includes the coastal and adjacent oceanic region from the Strait of Gibraltar to northwest Iberia (Galicia) (34° N - 46° N; $\sim 1200 \times 600$ km) (Fig. 5.1) and has horizontal resolution of 1/27° ($\sim$3 km) and 60 vertical s-levels ($188 \times 389 \times 60$ grid) in order to properly resolve the Mediterranean undercurrent (MU).

The large domain was initialized with temperature and salinity climatologies from Conkright et al. (2002), which also provided the open boundary conditions. The surface was forced with monthly climatological wind stress and fluxes of heat and freshwater from the Comprehensive Ocean-Atmosphere dataset (COADS; da Silva et al., 1994). Initial velocities were zero and monthly geostrophic velocities (referenced to 1200 m) and Ekman velocities were calculated from the climatologies and applied along the lateral boundaries. The Mediterranean outflow was introduced as a nudging condition as described in Peliz et al. (2007a). This configuration was run for 15 years, and it was validated by a comparison of mean eddy kinetic energy maps with AVISO altimetry data, with a methodology

similar to that described by Peliz et al. (2007a).

The high-resolution nested domain (Fig. 5.1) was thus initialized and the boundary conditions provided by the large domain described above. The exchange of Atlantic and Mediterranean waters at the Strait of Gibraltar was explicitly represented in the high resolution domain by the imposition of vertical profiles of temperature, salinity and zonal velocity at the strait, similarly to Peliz et al. (2007a). The process of entrainment of ENACW with the MU was also parameterized by increasing the viscosity and diffusivity coefficients. The surface forcing was the same used in the large domain, i.e. the COADS climatology. The nested domain was run for 6 years, having reached a stable equilibrium solution in the 3rd year, until the Mediterranean water was in equilibrium and adjusted along the western and northern Iberian margin. The month of January of the 7th year run was chosen to initialize the biogeochemical model described in section 5.3.2, which ran for 9 years.

In addition to the climatological simulation described above, a realistic simulation of the period May 2001 - April 2002 was performed using the same two-nested domains configuration. The surface forcing for that period was extracted from NCEP 2 reanalysis for air-sea fluxes (Kanamitsu et al., 2002) provided by the NOAA (http://www.esrl.noaa.gov/psd/) and QuickSCAT surface wind reanalysis (2001–2008) at $0.5° \times 0.5°$ spatial resolution provided by CERSAT (http://www.ifremer.fr/cersat). The year 2001 was initialized from 1st January for the nested domain, using initial conditions from the climatological run (9th year) for the physical and biogeochemical variables. The physical boundary conditions were provided by a realistic simulation of 2001–2002 for the large domain, whereas the biogeochemical boundary conditions were climatological, as will be described in the next section.

The freshwater continental runoff from the main rivers of the region was included with monthly climatological discharge values (Río-Barja and Rodríguez-Lestegás, 1992) or, when available, realistic discharges for 2001–2002 provided by Instituto Nacional da Água (INAG) (http://www.inag.pt) (available for the three main rivers: Minho, Douro, and Tagus).

5.3.2 Biogeochemical model

Biogeochemical simulations were performed with a $NChlPZD+O_2$ model (Nitrate-Phytoplankton-Zooplankton-Detritus + Oxygen) coupled to ROMS. The $NChlPZD$ model was a simple 4-components nitrogen based biogeochemical model based in that developed by

Fasham et al. (1990) computing the mentioned state variables in mmol N m^{-3}. O_2 concentration (expressed in mmol O_2 m^{-3}) was computed in the model so that it was influenced by other biogeochemical variables, but O_2 did not have an effect on them, as will be detailed below. The 3D time evolution of the concentration of any biogeochemical variable (B_i) is influenced by diffusion, horizontal advection, vertical mixing and the biogeochemical processes that act as sink or source for the variable:

$$\frac{\partial B_i}{\partial t} = \nabla \cdot K \nabla B_i - u \cdot \nabla_h B_i - (w + w_{sink}) \frac{\partial B_i}{\partial z} + SMS(B_i) \tag{5.1}$$

where K is the eddy kinematic diffusivity tensor, u is the horizontal velocity, w and w_{sink} are the vertical velocity and the vertical sinking rate of the biogeochemical variable, respectively, with the exception of zooplankton, nitrate, and O_2 to which no sinking rate was attributed. The biogeochemical processes included in the source minus sink (SMS) term are specific for each variable (Fig. 2.2), and the parameters used to represent them are listed in Table 2.2. Since O_2 is the focus of our study, we next describe in more detail the sinks ands sources considered for this variable in the model. A detailed description of the sink and sources for the other biogeochemical variables can be found in Koné et al. (2005).

Oxygen is produced by photosynthesis during phytoplankton growth, so its production rate can be calculated from nitrate uptake using a Redfieldian $r_{O_2:NO_3}$ stoichiometric ratio. Zooplankton metabolism consumes O_2, and this is estimated from the excretion of nutrients to the environment. Bacterial mineralization of detritus to nutrients also consumes O_2. Since the model only has one nutrient compartment, nitrate, the mineralization process was simplified to a direct oxidation from detritus to nitrate and the O_2 consumed was computed using again the $r_{O_2:NO_3}$ ratio. The sediment compartment was not included in the model, so the detritus reaching the seafloor was simply incorporated to the bottom layer of the model in the water column, where it mineralized to nitrate at the specified mineralization rate. This representation of detritus mineralization near the bottom was in agreement with the findings of Arístegui et al. (2009), showing that in the Iberian shelf most organic matter reaching the bottom during the upwelling period was oxidized in the nepheloid layer and not in the sediment. Gas exchange with the atmosphere at the ocean surface was introduced in the top cells of the model. Thus, the O_2 SMS term takes the form:

$$\begin{aligned} SMS(O_2) = \mu(PAR,T) \cdot \mu(NO_3) \cdot Phyt \cdot r_{O_2:NO_3} - t_{Z_{metab}}\, Zoo \cdot r_{O_2:N_{metab}} \\ - t_{D_{remin}}\, Det \cdot r_{O_2:NO_3} + Q_{ge}\, (O_2 sat - O_2) \end{aligned} \tag{5.2}$$

where the first term in the right hand side of the equation accounts for O_2 production by

photosynthesis (phytoplankton growth). Phytoplankton growth rate (μ) is limited by light (photosynthetically available radiation: PAR), temperature (T) and nutrients (NO_3) using the equations $\mu(PAR,T)$ and $\mu(NO_3)$ described in Koné et al. (2005), with $\mu(PAR,T)$ modified as in Gruber et al. (2006) to include a variable chlorophyll:C ratio (θ).

The second term in Equation 5.2 accounts for O_2 consumption by zooplankton respiration (basal metabolism), estimated from the excretion of nutrients to the environment, with $t_{Z_{metab}}$ the zooplankton specific excretion rate (Table 2.2). The third term of the equation formulates detritus mineralization as an O_2 sink, with $t_{D_{remin}}$ the detrital mineralization to nitrate rate (Table 2.2). The stoichiometric ratios for photosynthesis/mineralization ($r_{O_2:NO_3}$) and zooplankton respiration ($r_{O_2:N_{metab}}$) convert Nitrogen concentration to O_2 concentration (Table 2.2).

The last term in Equation 5.2 represents the exchange of O_2 with the atmosphere at the sea surface. This flux can be either to the ocean (source) or from the ocean to the atmosphere (sink), depending on whether the surface layer is under-saturated or over-saturated in O_2. It is calculated after the biogeochemical reactions were calculated. The gas exchange rate of O_2 is calculated as:

$$Q_{ge} = \frac{K_v}{\Delta z} \tag{5.3}$$

where Δz is the height of the top cell and K_v is the gas transfer coefficient calculated as:

$$K_v = 0.31 \cdot u^2 \cdot \sqrt{\frac{660}{Sc}} \tag{5.4}$$

with u the wind speed and Sc the Schmidt number calculated after Wanninkhof (1992). The saturation concentration of oxygen (O_2sat) is calculated in a separated subroutine.

Initial and boundary conditions for O_2 and nitrate were supplied from climatological data of the World Ocean Atlas (WOA) 2009 (Garcia et al., 2010a,b). Seasonal (for depths down to 500 m) and annual (depths below 500 m) climatologies were used. Initial and boundary chlorophyll-a concentrations were attributed from SeaWiFS seasonal climatology. Seasonal vertical profiles were created from these surface concentrations using the algorithm of Morel and Berthon (1989). Phytoplankton and zooplankton initial and boundary data where derived from chlorophyll-a ($Phyt = 0.5 \cdot Chl$; $Zoo = 0.2 \cdot Chl$) (Gruber et al., 2006). Initial and boundary values of detritus concentrations were introduced as constant (0.02 mmol N m^{-3}). Boundary conditions for all the biogeochemical variables were supplied seasonally (15th February for Winter, 15th May for Spring, 15th August for Summer, and 15th November for Autumn).

Constant river inputs of nitrate and chlorophyll were used along the year (see table 2 in Marta-Almeida et al. (2012)). Also, a constant river input of oxygen was used

(125 mmol O_2 m^{-3}), based on data from Ferreira et al. (2003).

The biogeochemical model, which runs as a module integrated in the ocean model, was run for 9 years. This configuration converges in 1-2 years as observed by the time evolution of the biogeochemical variables. Therefore, we let 3 years of spinup.

5.4 Data series and methods

Model results presented are seasonal averages over 6 years (4th to 9th climatological years). Seasonal averages correspond to winter (January, February, and March), spring (April, May, and June), summer (July, August, and September), and autumn (October, November and December).

Apparent oxygen utilization (AOU) (mmol O_2 m^{-3}) was calculated from model outputs as:

$$AOU = O_2sat - O_2 \tag{5.5}$$

where O_2 is the dissolved oxygen concentration output from the model and O_2sat is the saturation concentration of oxygen calculated as a function of in situ model temperature and salinity (Weiss, 1970) (*oxsat* Matlab® routine from the *Ocean toolbox* by the Scripps Institution of Oceanography). Climatological seasonal means of O_2 concentration and AOU for comparison with model results were provided by the WOA 2009 dataset at one-degree resolution (Garcia et al., 2010a). The climatological data set does not contain O_2 values on the shelf. Oxygen data from the shelf for model comparisons were obtained from a series of surveys carried out in the northwestern Iberian region by the Spanish "Consejo Superior de Investigaciones Científicas" (CSIC): (1) The cruises GALICIA VII (February–March 1984) (Fraga et al., 1985) and GALICIA IX (September 1986) (Fraga et al., 1987) were selected among a series of surveys carried out during the 80's, which constitute a comprehensive hydrographic dataset around the region, made available through a series of public reports; (2) Two stations off the NW Iberian coast sampled weekly between 15th May 2001 and 24th April 2002 in the framework of the DYBAGA (Dinámica y Biogeoquímica Anual en la costa GAllega) project (location in Fig. 5.6). They represent a shelf location ($\sim$150 m depth) (Stn. 3) and a slope location ($\sim$1500 m depth) (Stn. 5). More details about the analysis and interpretation of the biogeochemical data collected at these two stations can be found in Álvarez-Salgado et al. (2006) and Castro et al. (2006). DYBAGA time series of O_2, temperature and salinity at the two stations were compared to the corresponding modelled time series for these variables for a specific simulation of the period May 2001–April 2002. Model values shown are averages over 3 days and 9 grid

points around the geographic positions of the stations (a square of ∼0.1° x 0.1°).

A quantitative analysis of model skill in representing O_2 concentration at the surface was performed by calculating the percentage model bias ($Pbias$), i.e., the sum of model error normalized by the data:

$$Pbias = \frac{\sum(M_t - D_t)}{\sum D_t} \cdot 100 \tag{5.6}$$

were M_t and D_t are the modelled and observed values at time index t. M_t is the mean of the last 6 years of model run and D_t the climatological mean.

5.5 Results and Discussion

The ability of the coupled hydrodynamic–biogeochemical model to reproduce the 3D seasonal and event variability of O_2 in the Iberian shelf and adjacent oceanic region (NE Atlantic) was explored. A first assessment is presented by comparing seasonal means of O_2 at the sea surface with WOA climatological data (section 5.5.1). Next, O_2 model results in the water column are evaluated along a meridional section at 10.5° W. Additionally, the remineralized component of O_2 in this section, i.e. the AOU computed from model results, is compared with climatological AOU (section 5.5.2).

Finally, model results on the shelf are assessed by comparing the model to surveyed data in the northwestern (Galician) shelf, and the shelf–ocean interaction was explored using three cross-shelf model sections (section 5.5.3).

5.5.1 Sea surface seasonal mean of O_2 and surface model bias

The seasonal trend of sea surface dissolved O_2 was well reproduced by the model (Fig. 5.2). The highest O_2 concentrations were obtained in spring, especially in the northwest oceanic region ($>$265 mmol O_2 m^{-3}), coinciding with the northeast Atlantic spring phytoplankton bloom. Winter O_2 concentrations were also high in the region, with values above 250 mmol O_2 m^{-3}. This is an expected consequence of ventilation of the water column during winter mixing, as the upper mixed layer depth increases from 20 m in late summer–early autumn to 150 m between 40° N and 43° N (Álvarez-Salgado et al., 2003), and to more than 300 m North of 43° N, in late winter (February–March) (Arhan et al., 1994; Perez et al., 2005). The lowest O_2 concentrations at the sea surface were obtained in summer and autumn, corresponding to periods of intense thermal stratification and thus low oxygen solubility. The characteristic North to South latitudinal gradient was well captured by the model, with

remarkable similarities in spring (Fig. 5.2). Average values of dissolved O_2 concentration compared well with WOA climatological data for the four seasons.

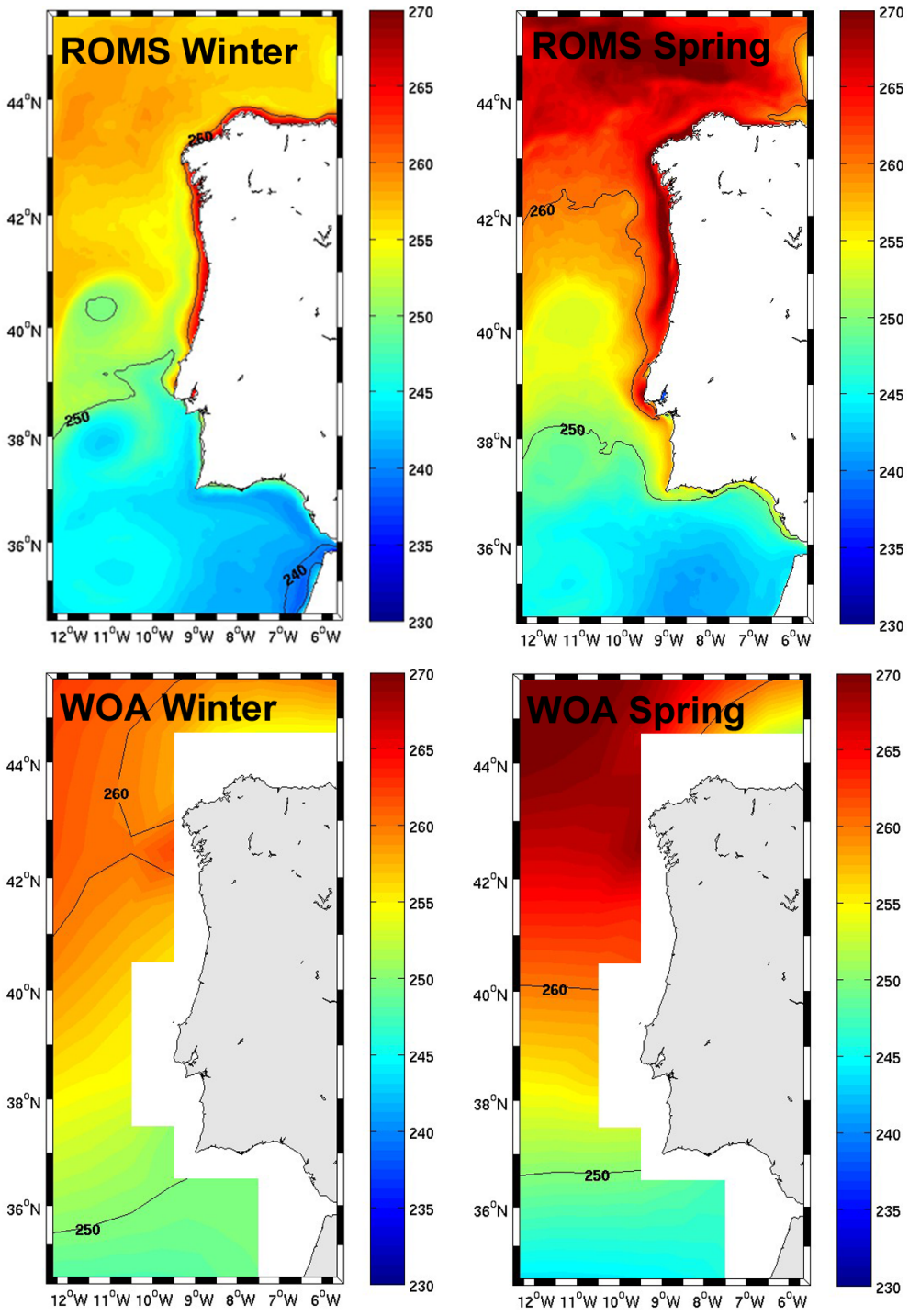

Figure 5.2: Seasonal mean of sea surface dissolved oxygen (mmol O_2 m^{-3}) from model results (ROMS) and from climatological data (WOA 2009).

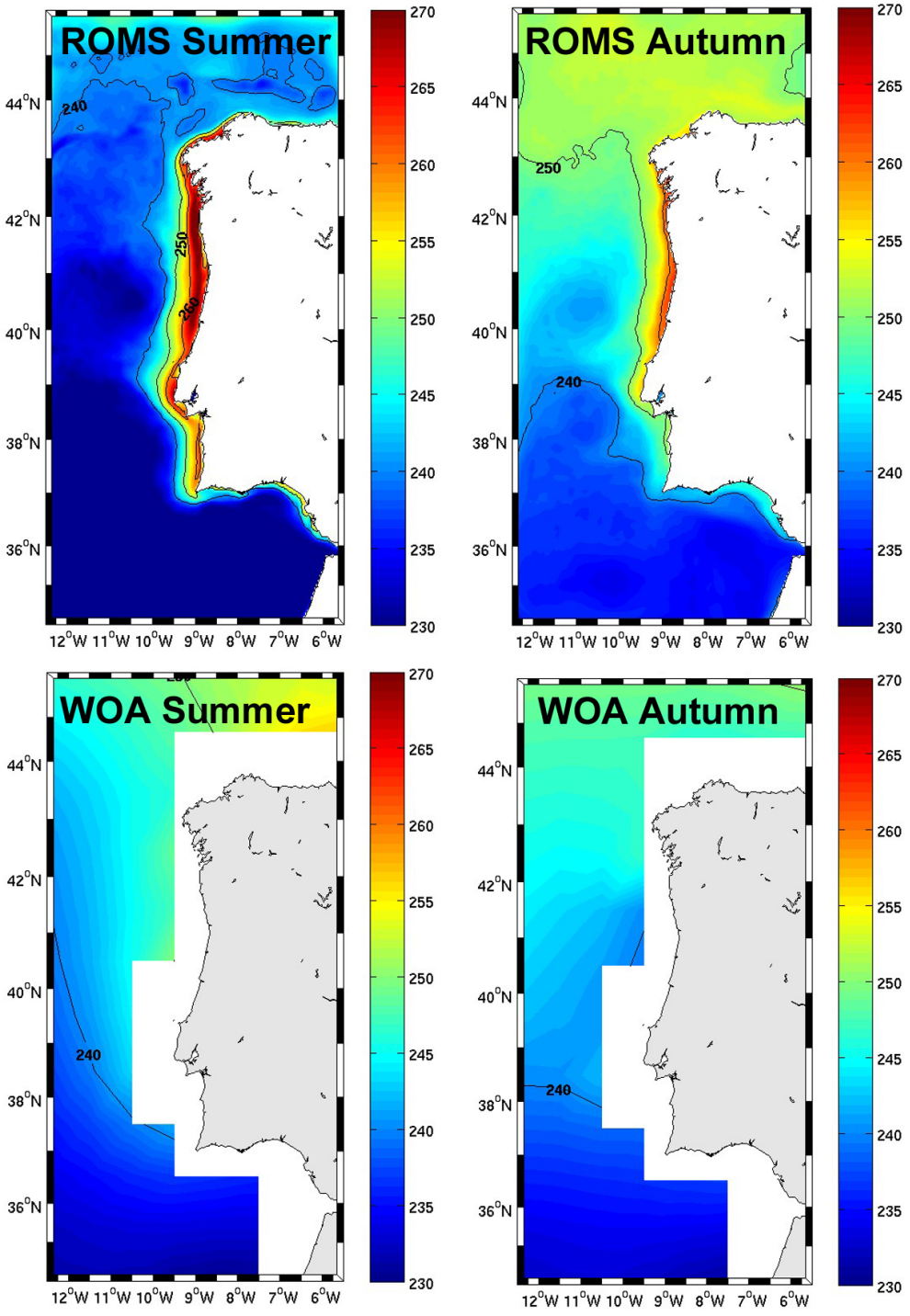

Figure 5.2: Continued.

Figure 5.3 shows the $Pbias$ of the model at the sea surface for the four seasons. This analysis gives a measure of whether the model is systematically underestimating or overestimating the climatological data. The $Pbias$ observed can be rated as very good, roughly between $\pm 2.5\%$ in most of the domain for all periods. As a general trend, the model slightly underestimated data in winter, spring and a bit more in summer, while it tended to slightly overestimate data in autumn.

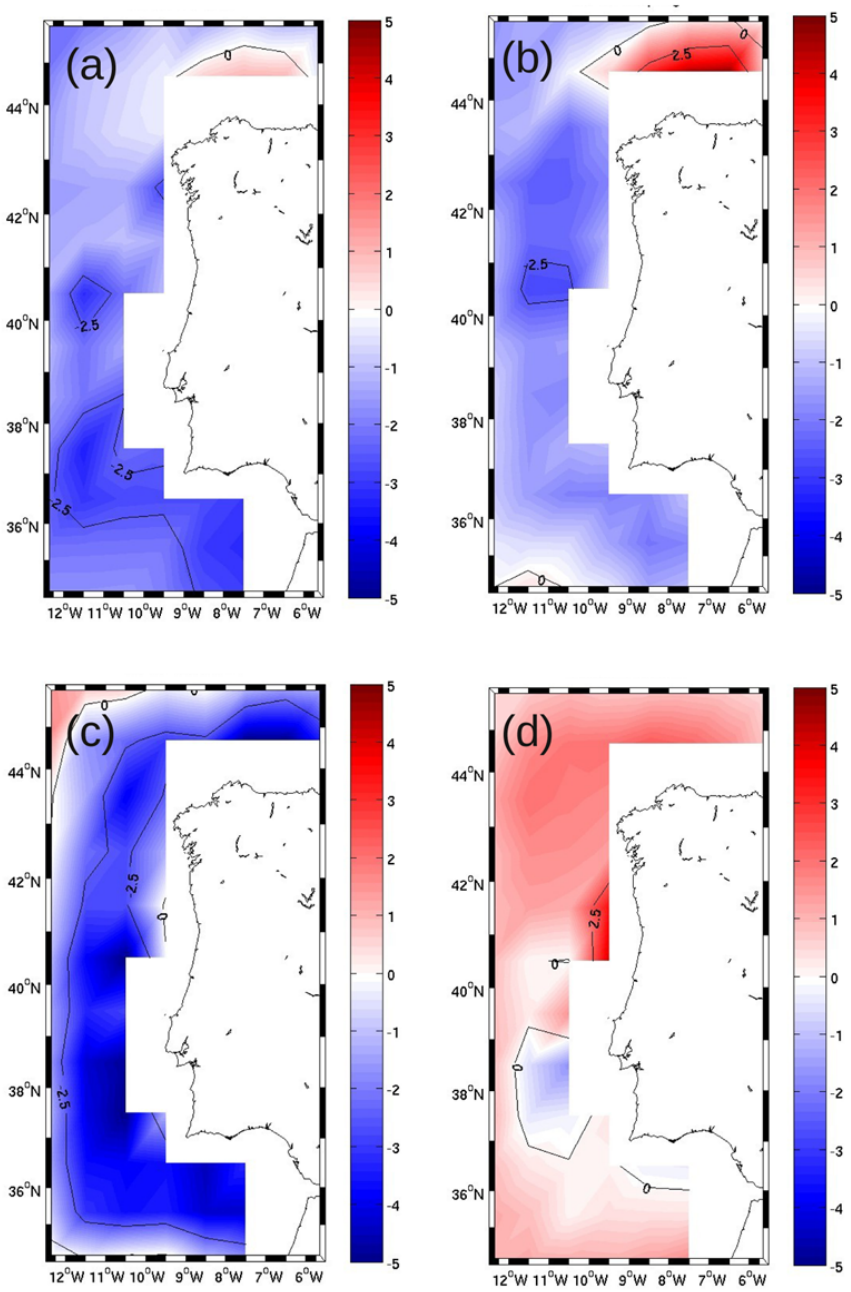

Figure 5.3: $Pbias$ (%) of seasonal mean of dissolved oxygen from ROMS model results vs. climatological data (WOA 2009): (a) winter; (b) spring; (c) summer; (d) autumn.

5.5.2 Seasonal mean of O_2 and AOU along a meridional section

The North-to-South section at longitude 10.5° W (Fig. 5.1) shows that the model vertical distribution of O_2 in the oceanic region is comparable to seasonal climatological data (Fig. 5.4). The general North-to-South vertical distribution of O_2 consists of: 1) an upper layer ($\sim$0-400 m) with a marked seasonal variation and a northward increase in O_2 concentration; 2) an O_2 minimum ($<$200 mmol O_2 m^{-3}) centred at about 1000 m depth, with wider vertical extension to the South; 3) a deep layer ($>$1500 m) showing almost nule seasonal variations and increasing O_2 concentration with depth. Between $\sim$2000 and 2500 m depth a tongue of high O_2 concentration ($>$250 mmol O_2 m^{-3}) of northern origin, with slightly seasonal variation, was present. The seasonal variability and latitudinal gradient in the uppermost layer ($\sim$0-100 m) were the same described in the previous section, corresponding to the surface seasonal varying mixed layer, highly influenced by ocean–atmospheric interactions and biological activity (Mann and Lazier, 2006). Below this layer, the O_2 distribution was related to the water masses present in the region, an extensive thermohaline description of which can be found in Fiuza et al. (1998), Fraga et al. (1982) and Rios et al. (1992). Between $\sim$100-400 m, the latitudinal and seasonal differences in O_2 were related to the presence and variability of ENACW. The increase in O_2 concentration to the North was related to ENACWp (S $<$35.6), subducted into the North Atlantic ($>$43° N), conveying high O_2 concentration southwards due to its recent contact with atmosphere during winter mixing (Perez et al., 1993, 2005). In the near surface of the southern part ENACWt (S $>$35.7) carried water with relatively low O_2 concentration to the North (Perez et al., 1993, 2001). The vertical O_2 minimum at $\sim$1000 m was in average slightly above the salinity maximum of MW (Fig. 5.4). A similar position of the O_2 minimum was observed by Perez et al. (1993) from 40° N to 47° N and Castro et al. (1998) in a section across 42° N. O_2 minima development is the result of the imbalance between physical ventilation and microbial consumption processes (Keeling et al., 2010; Gruber, 2011). Some studies have suggested that the position of the O_2 minimum between the ENACWp, slowly moving southward, and the MW flowing northward in the MU, corresponds to a level of slow motion between these two water masses, where longer residence times enhance the effect of mineralisation (Perez et al., 1993; Castro et al., 1998). Our results also pointed out to a prevailing position of the O_2 minimum in the transition between ENACW and MW (i.e., above the salinity maximum). However this was not clearly associated to a minimum in the meridional velocity profile (data not shown). In fact, there was a prevalence of northward movement of both water masses. Thus, the position of the minimum maybe emphasized at the low motion level when an opposing advance of ENACW and MW occurs, as suggested in the literature, however this

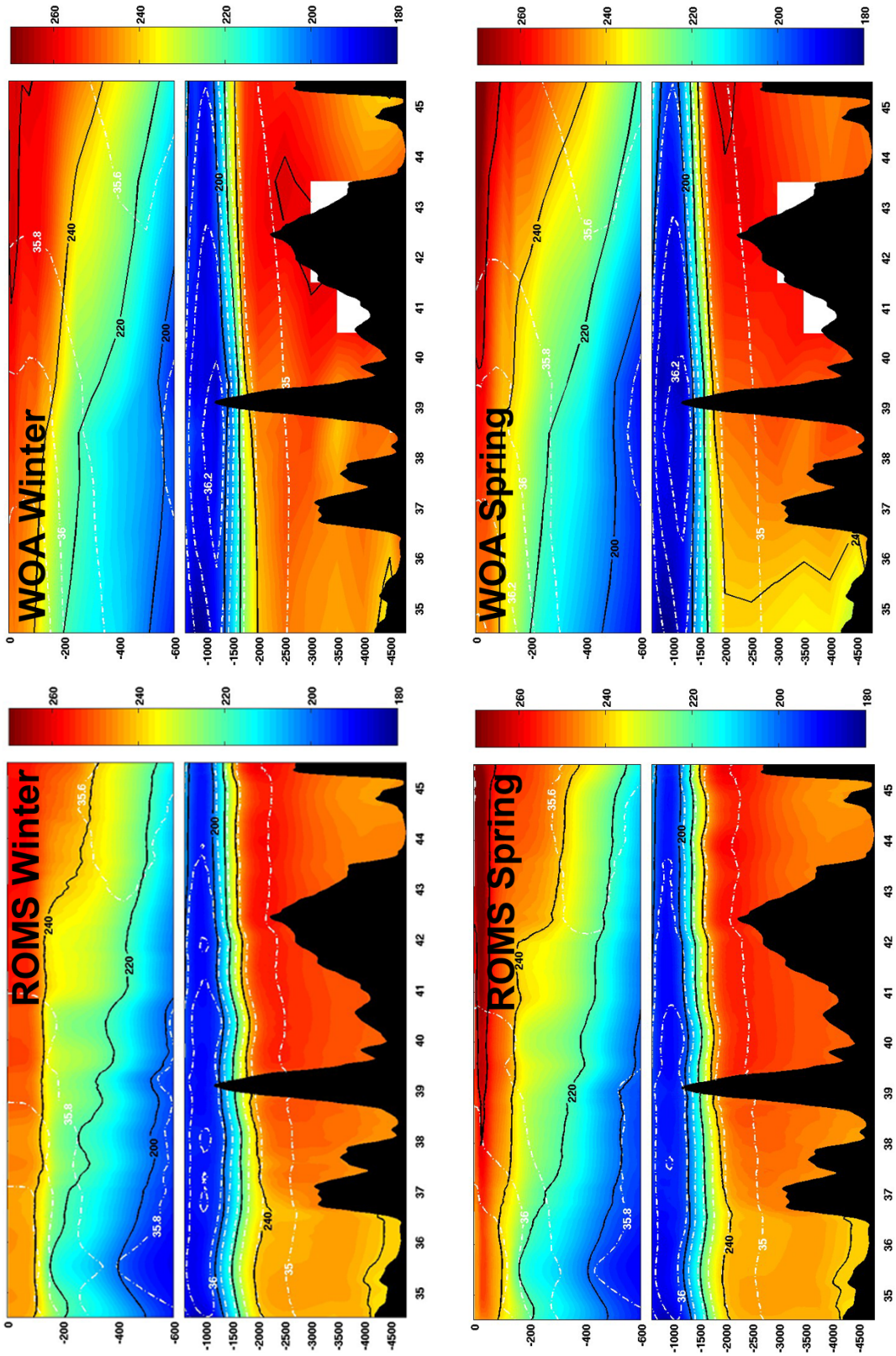

Figure 5.4: Seasonal mean of dissolved oxygen (mmol O_2 m^{-3}) in the water column along a meridional section at 10.5° W from model results (ROMS) and from climatological data (WOA 2009) (solid line). Also shown salinity (psu) (white dashed line).

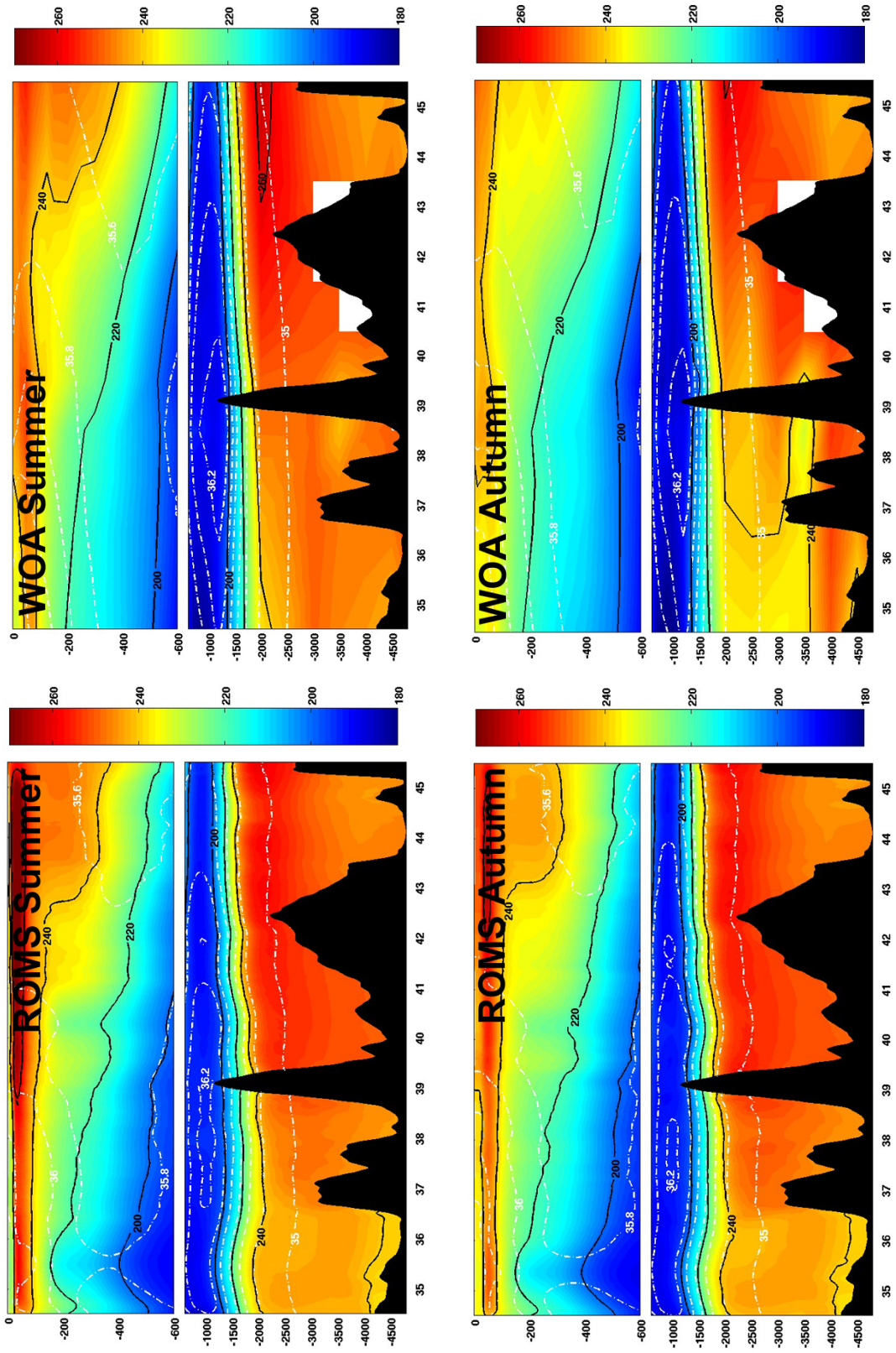

Figure 5.4: Continued.

did not seem to be the prevailing situation. Still, the position of the minimum appeared to be result of a combination of slow water movement (there was a general trend for diminishing velocity with depth in the water column, continuing below the O_2 minimum) and remineralization rates. We identified the position of the O_2 minimum for the entire model domain and found that for most part of the region it was situated at an average depth between 800 m and 1000 m (maximum depth 1600 m) , except for a region in the southern part of the domain, where it was shallower. The uplift of the O_2 minimum in this region, which can be appreciated in Figure 5.4 together with the uplift of the isohalines, was a consequence of the cyclonic circulation in the Gulf of Cadiz known as the beta-plume (Peliz et al., 2007a). The cyclonic circulation seemed to cause a higher variability in the vertical O_2 minimum along the year. The average depth of the O_2 minimum in the domain (excluding shelf values) was 870 $\pm$ 36 m. Over the shelf, O_2 minimum was associated to the bottom. Mean annual values of O_2 concentration at the minimum were between 190 and 200 mmol O_2 m^{-3} for most of the model domain, with slightly lower values to the South. Minimum O_2 concentration within the shelf did not fall below 200 mmol O_2 m^{-3}. Below 1500 m, the O_2 concentration increased again with the presence of North Atlantic Deep Water (NADW). Within this water mass, the tongue of high O_2 concentration from the North matches the tongue of Labrador Sea Water (LSW) observed in the region (Castro et al., 1998; Fiuza et al., 1998).

The ability of the model to reproduce the impact of aerobic remineralization on the vertical distribution of dissolved O_2 in the region was evaluated comparing seasonal AOU calculated from model results and climatological AOU data, for the vertical section at 10.5° W (Figs. 5.1 and 5.5). The AOU from the model reproduced well the climatological observations for the four seasons. As described for O_2, AOU showed seasonal variability in the surface layer ($<$200 m), where biological activity is high, whereas it stayed rather stable in deeper layers. Negative values of AOU (O_2 concentration higher than O_2 saturation concentration) were found in the surface all the year round, except in winter, when low surface water temperatures give high O_2 saturation concentrations and the photosynthetic activity of phytoplankton is quite reduced (Álvarez-Salgado et al., 2003). AOU increased with depth (from 0 to $\sim$100 mmol O_2 m^{-3}), reflecting aerobic remineralization of sinking organic matter and the presence of deep older water masses. The tongue of high O_2 concentration described before and attributed to LSW showed lower AOU ($<$80 mmol O_2 m^{-3}) than the surrounding waters.

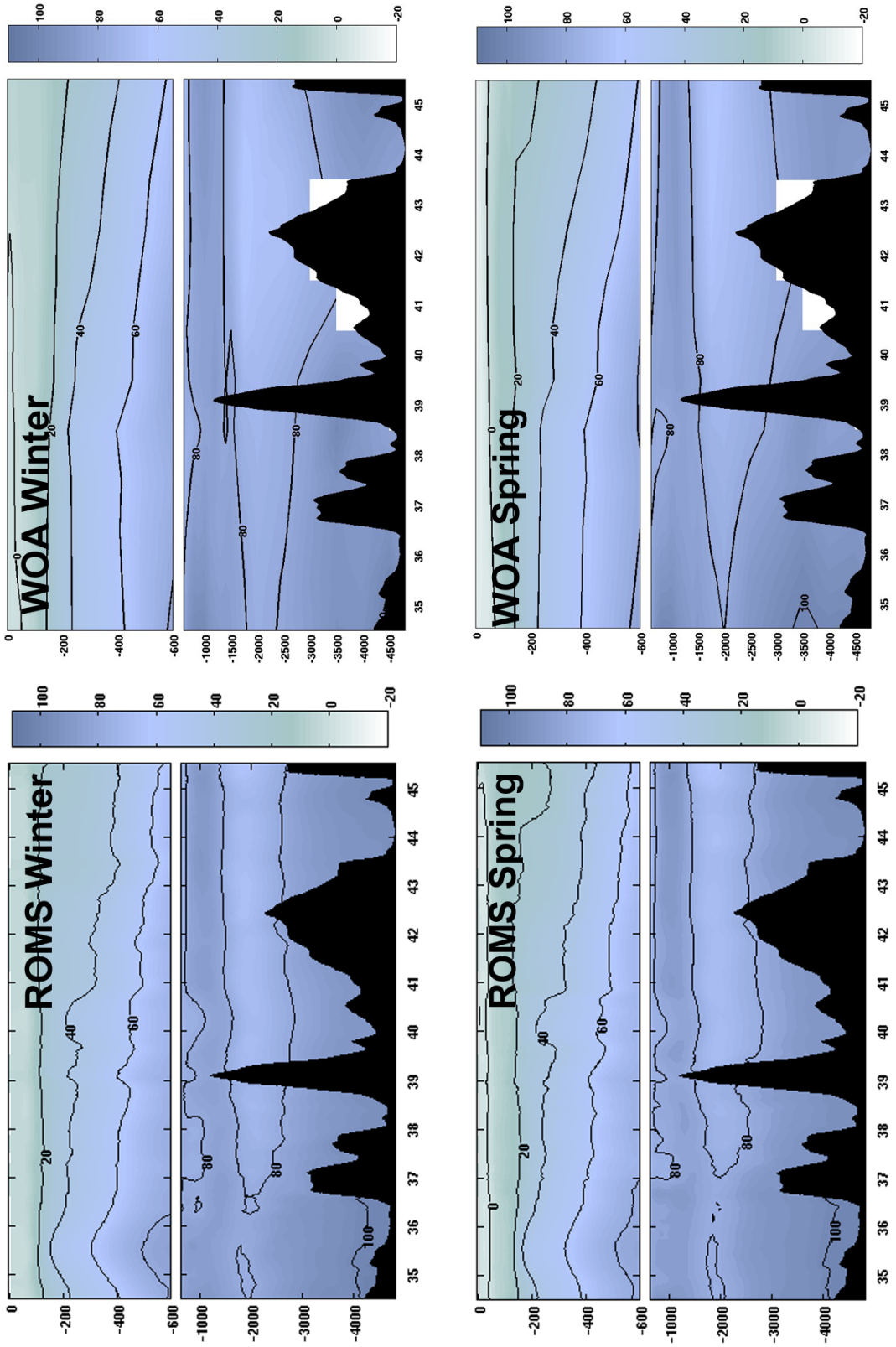

Figure 5.5: Seasonal mean of apparent oxygen utilization (AOU) (mmol O_2 m^{-3}) in the water column along a meridional section at 10.5° W calculated from model results (ROMS) and from climatological data (WOA 2009).

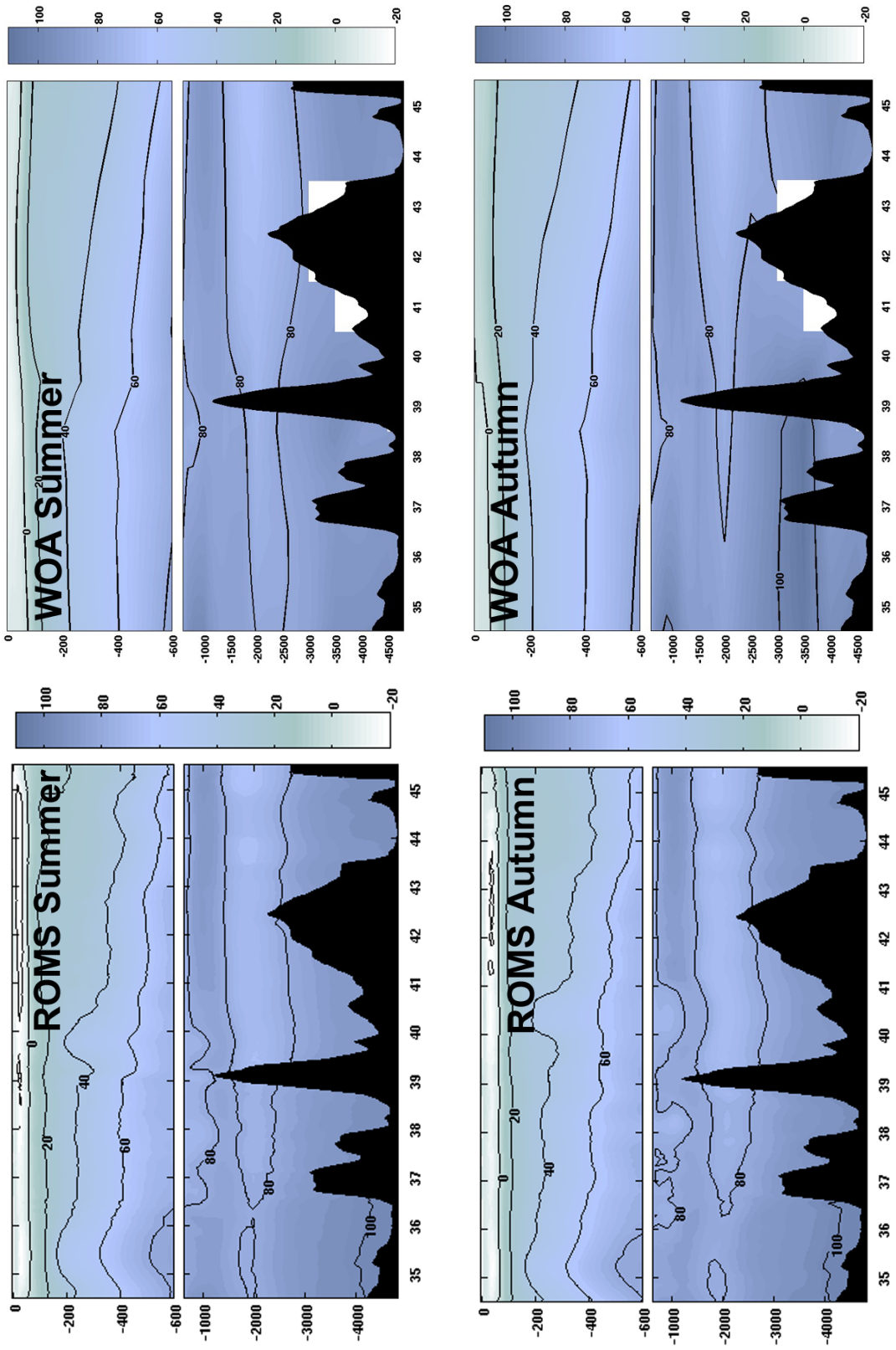

Figure 5.5: Continued.

5.5.3 Characterization of O_2 distribution over the shelf

5.5.3.1 Model comparison with observed data in the Galician shelf

We based our evaluation of the model results for the shelf on comparisons with data referred in section 5.4 (Fig. 5.6) and observations referred in the literature.

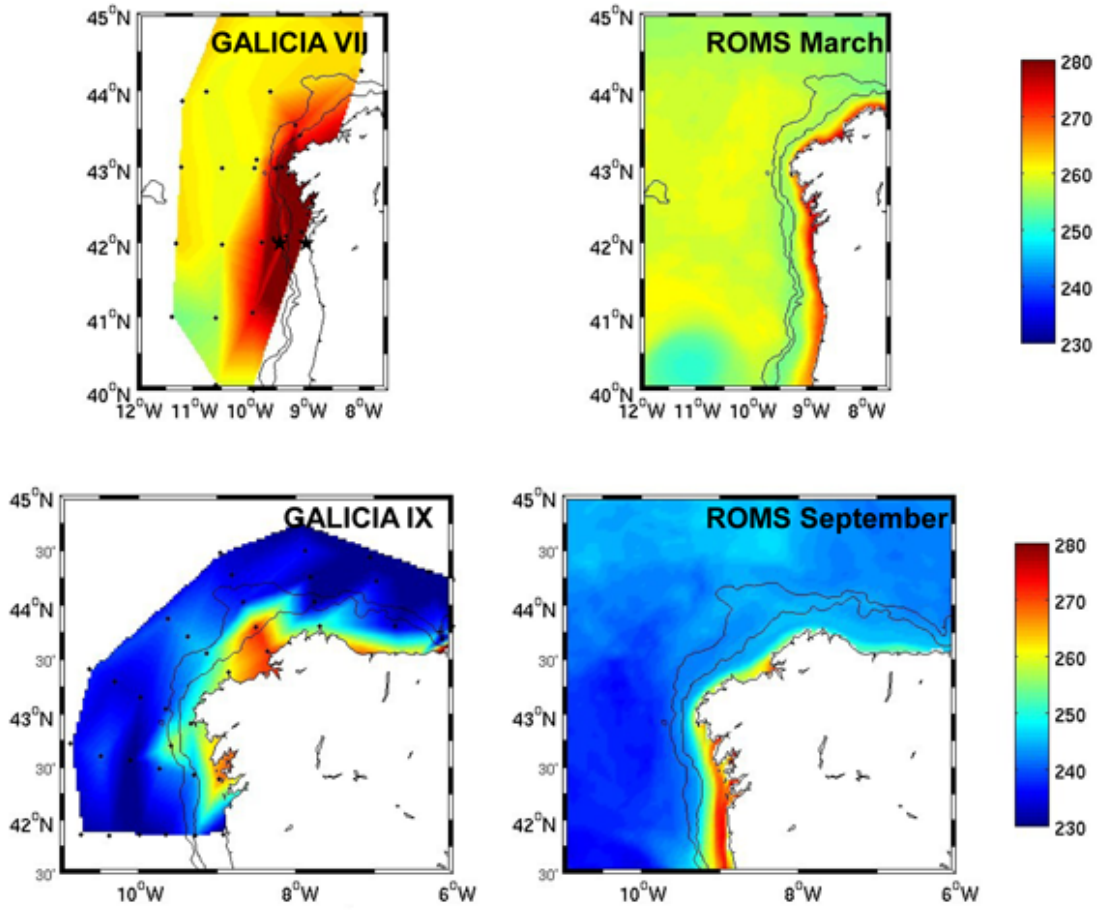

Figure 5.6: Sea surface dissolved O_2 (mmol O_2 m^{-3}) in the Galician shelf during the cruises GALICIA VII (February-March 1984) and GALICIA IX (September 1986) (sampling stations shown) and the corresponding ROMS climatological mean for March and September. Stars indicate the position of the two weekly sampling stations for the period May 2001–April 2002. Isobaths of 200 m and 1000 m are represented.

Spatial and seasonal distributions of surface dissolved O_2 obtained during the CICLOS cruises along the western (37° N–41.8° N) and southern (7.5° W–9° W) Portuguese shelf (August/November 1985; January/March 1986) were reported in Moita (2001). These data showed a seasonal trend from the highest O_2 concentrations in spring (∼9 mg/L) and the lowest in autumn (∼8 mg/L) (corresponding to ∼280 and 250 mmol O_2 m^{-3}, re-

spectively), which compares fairly well with model values (Fig. 5.2). Model results show the highest shelf O_2 concentrations in summer, instead of spring, presumably related to the upwelling-associated phytoplankton blooms. High values of dissolved O_2 were also found by Moita (2001) in summer (August), associated with upwelling centres. Thus, the disagreement in the timing of the highest concentration between the model and CICLOS data might be explained by the fact that the model simulation is climatological, i.e. it gives a spatial and time long-term average over the period, while data represent a synoptic situation, so that a particular upwelling event is likely to be weaker (or stronger) than the average situation over the upwelling season. The model trend to higher O_2 concentrations in the Northern shelf than in the Southern shelf was also observed by Moita (2001) in January and August.

Figure 5.6 shows comparisons between surface dissolved O_2 in the Galician shelf for the cruises GALICIA VII (February-March 1984) and GALICIA IX (September 1986) and the corresponding climatological model averages for March and September. The two cruises represent two contrasting situations regarding surface O_2 concentration, with GALICIA VII showing a typical late winter situation with high O_2 concentration and GALICIA IX showing a typical autumn situation with low O_2 concentration. Model values were high near the coast in March ($>$260 mmol O_2 m^{-3}), and this was also observed in the GALICIA VII data, although higher O_2 values were observed ($>$270 mmol O_2 m^{-3}) extending further offshore. This could be a consequence of slightly upwelling-favourable conditions during the cruise (Álvarez-Salgado et al., 2003). Model shelf values in September were comparable to the observations made in the cruise GALICIA IX, except for some high O_2 values observed in the northwestern Galician shelf. These high values may be attributable to high chlorophyll concentrations ($>$1 mg m^{-3}) found in the region at the time of the cruise (Álvarez-Salgado et al., 1997).

Figures 5.7 and 5.8 present a 1-year time series of observed and modelled O_2, temperature and salinity at the two stations, described in section 5.4 (see position in Fig. 5.6), off the NW Iberian coast (note different depth scales). At both the middle shelf (Stn. 3) and off the shelf edge (Stn. 5) the model was able to reproduce the seasonal and short term variability of the thermohaline properties and O_2 concentration in the water column, with very similar values to observed ones. Seven hydrographic periods were described by Nieto-Cid et al. (2004) and Álvarez-Salgado et al. (2006) for the sampling period May 2001–April 2002 at Stn. 3, based on offshore Ekman transport, continental runoff and water column stratification. Similar hydrographic situations were described by Castro et al. (2006) for Stn. 5, though with lower temporal variability, as expected for an offshore location. Here, we summarize their description of these periods and comment

on the ability of the model to reproduce them and the observed O_2 concentration:

1) Upwelling season (15th May–25th September): Regardless of upwelling favourable northerly winds, thermal stratification of the upper water column prevailed at Stn. 5, with model temperatures very similar to those observed (Fig. 5.7b and e). Throughout this period O_2 concentration in the seasonal thermocline remained high (240–260 mmol O_2 m^{-3}) with model values slightly higher than observations (Fig. 5.7a and d). This high O_2 concentration was related to a subsurface chlorophyll maximum (not shown). A subsurface salinity maximum was observed beneath the seasonal thermocline and identified as a core of poleward flowing ENACWt by Castro et al. (2006), which was not detected in the model until the end of September (Fig. 5.7c and f). Over the shelf (Stn. 3), the hydrographic situation along this period was characterized by upwelling episodes with short intervals of wind relaxation and marked thermal stratification until late August (Fig. 5.8b and e). These episodes were more clearly separated in the model due to its higher temporal resolution. Oxygen concentration within the seasonal thermocline was high following upwelling episodes ($>$260 mmol O_2 m^{-3}) in both observed and modelled values (Fig. 5.8a and d), and was related to phytoplankton blooms as in Stn. 5. Colder underlying ENACW showed values between 220-240 mmol O_2 m^{-3}, with model values $\sim$10 mmol O_2 m^{-3} higher. This seemed to be related with the differences identified in thermohaline properties between the model and observations, with colder and less salty deeper ENACW in the model suggesting a higher proportion of ENACWp (O_2 rich) in the water mass than observed. The presence of such ENACW in the shelf was a consequence of the referred lack in the model of the subsurface core of poleward flowing ENACWt in the vicinities of the slope (Stn. 5) (lower O_2 concentration). Between the 28th August and 18th September there was a strong upwelling event with subsequent uplift of cold and salty ENACW water (Fig 5.8b, c, e, and f), which also brought relatively low O_2 concentration water closer to the surface (Fig. 5.8a and d).

2) Downwelling (25th September–30th October): At the end of September there was a shift in the wind regime to the characteristic southwesterlies of this period, which caused a downwelling episode at Stn. 3 (Fig. 5.8b, and e), whereas at Stn. 5 the water column remained stratified (Fig. 5.7b and e). Castro et al. (2006) attributed this stratification to intense continental runoff from the adjacent Rías Baixas, given the low salinity lens observed on the surface (Fig. 5.7c). The contribution of the Minho river estuary, located a few km to the south, was also likely. The model reproduced the same low salinity lens, though with somewhat higher salinity values (Fig. 5.7f). The use in the model of monthly climatological discharges for the Verdugo river ($\sim$40 m^3 s^{-1} for October), flowing into the adjacent Ría de Vigo (and for the other main rivers flowing into the Rías Baixas),

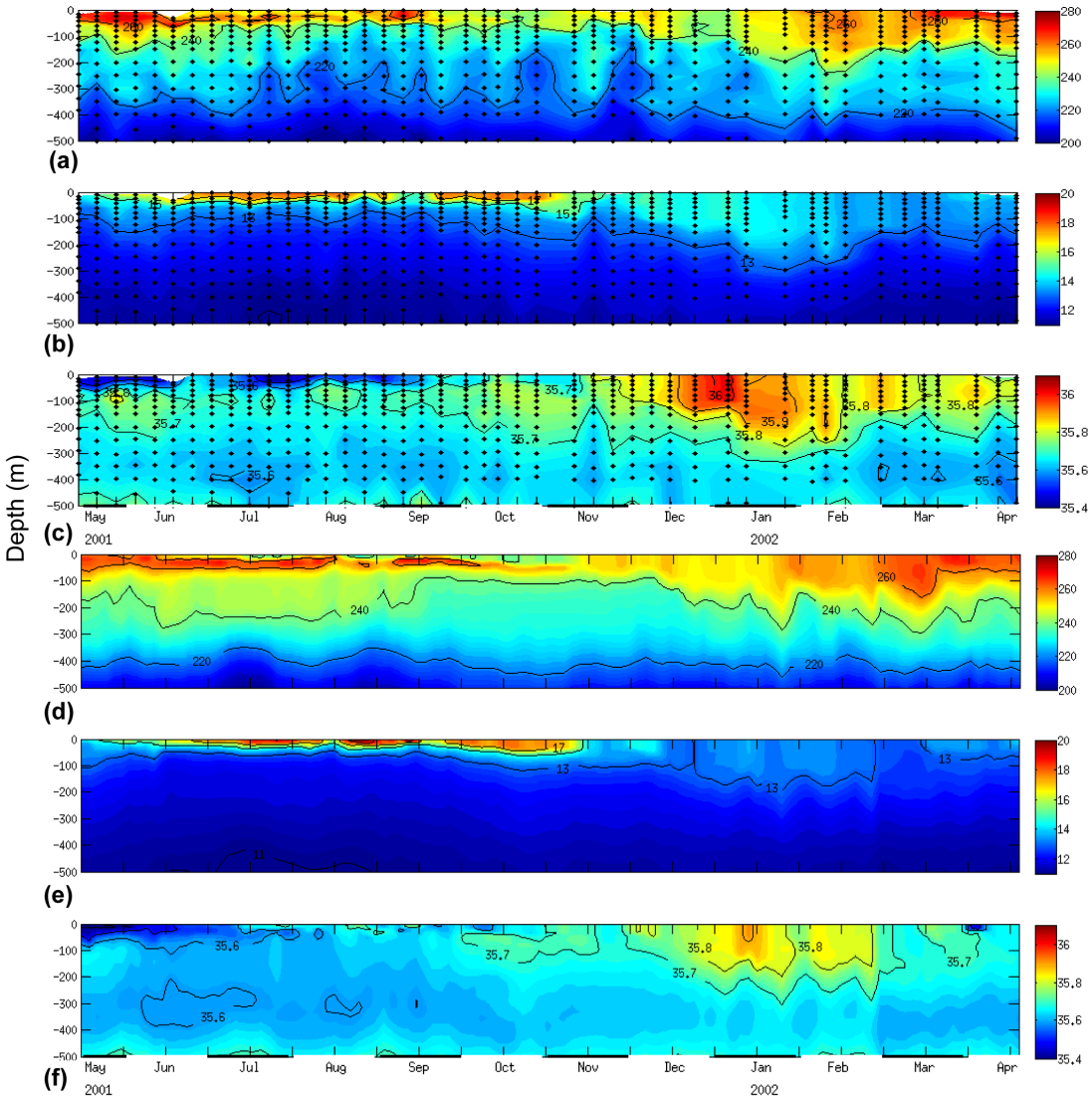

Figure 5.7: Time evolution of observed and modelled dissolved O_2 (mmol O_2 m^{-3}) (a, d), temperature (°C) (b, e) and salinity (psu) (c, f) in the water column at station 5 (42° N, 9.5° W) (slope) for the sampling period May 2001–April 2002.

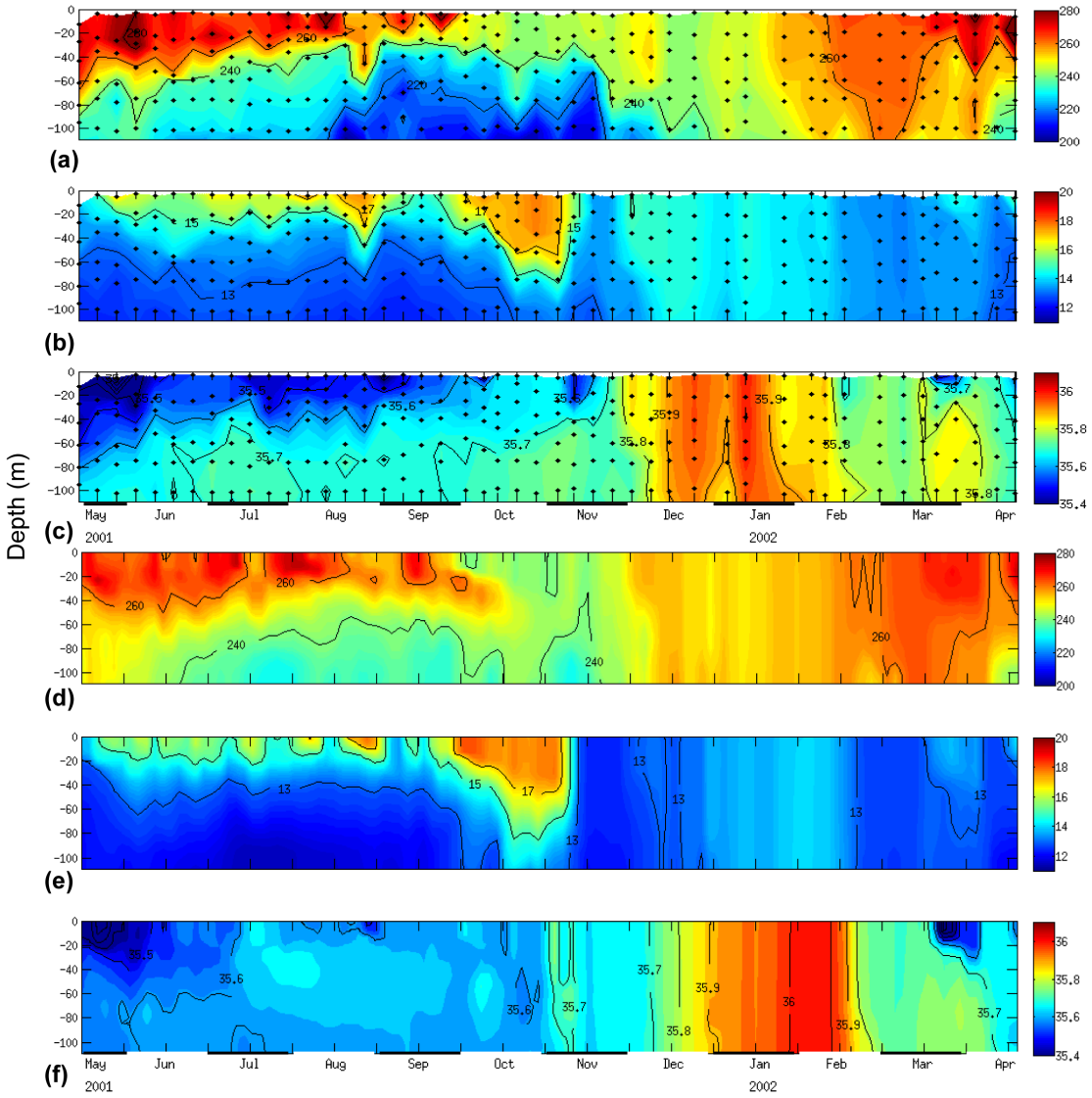

Figure 5.8: Time evolution of observed and modelled dissolved O_2 (mmol O_2 m^{-3}) (a, d), temperature (°C) (b, e) and salinity (psu) (c, f) in the water column at station 3 (42° N, 9.16° W) (shelf) for the sampling period May 2001–April 2002.

introduced a modelled continental runoff lower than the estimated daily runoff referred in Nieto-Cid et al. (2004) for this month, which reached an intense peak of $\sim$300 m^3 s^{-1}. The southwesterlies transported warm ($>$17°C) and salty oceanic water to the vicinities of the shelf (Fig. 5.7b and c), which was reproduced by the model (Fig. 5.7e and f). There was an influx of this warm and relatively low O_2 concentration ($<$240 mmol O_2 m^{-3}) oceanic water into the shelf (Fig. 5.8a, b, d, and e).

3) Transient autumn upwelling period (6th–20th November): The anomalously strong northerly winds of November favoured vertical homogenization of the water column by inducing an upwelling situation at both Stn. 3 and 5 (Figs. 5.7 and 5.8). The low salinity lens observed at Stn. 3 (Fig. 5.8c) was not evident in the model (Fig. 5.8f), presumably due to the mentioned use of monthly climatological discharges to the adjacent Ría de Vigo, which could not reproduce the peak of intense runoff showed in Nieto-Cid et al. (2004) and Álvarez-Salgado et al. (2006) in late October. Most probably the low salinity lens followed the typical evolution described by Otero et al. (2008), being confined to the shelf during the downwelling event, and expanding offshore under the upwelling conditions. This out-of-season upwelling event promoted O_2-poor but inorganic nitrogen-rich bottom-shelf ENACW to the surface layer (Álvarez-Salgado et al., 2006) leading to a phytoplankton bloom (not shown) and the concomitant increase in O_2 concentration ($>$240 mmol O_2 m^{-3}) (Fig. 5.8a and d) (Fig. 5.7a and d).

4) Arrival of the IPC to the shelf (27th November–13th February): The reversal in wind direction to southwesterlies brought the presence of warm and saline ENACWt conveyed by the IPC to the continental slope (Stn. 5) (Fig. 5.7b and c), and the shelf (Stn. 3) (Fig. 5.8b and c). At Stn. 5, ENACWt in the model was slightly colder and less saline than observations and, accordingly, showed higher O_2 concentration (Fig. 5.7). Note the coincidence of the salinity maximum of ENACWt and the O_2 minimum (Fig. 5.7a and c). Surface model results indicated that this ENACWt came frequently from an eastward recirculation of the IPC associated with an anticyclonic eddy (at the end of January, for instance, Fig. 5.9). A similar eddy conveying ENACWt was observed in the same area (between 41.5° N and 42° N) by Fiuza et al. (1998) in May 1993. ENACWt values of temperature and salinity over the shelf were similar in the model and in observations, except for slightly higher salinities in the model in February (Fig. 5.8b, c, e, and f). Oxygen values were 10 mmol O_2 m^{-3} higher in the model than in observations all along this period (Fig. 5.8a and d). From the model we could identify that the ENACWt present in the shelf at this latitude (42° N) was conveyed northwards either by the IPC circulating over the slope and entering the shelf or often by a branch of IPC circulating entirely within the shelf, as that detected at the beginning of February (salinity maximum, delayed in

the model relative to observations) (Fig. 5.8c and f). The surface model results illustrated clearly the downstream O_2 enrichment of the IPC by mixing with shelf waters, as observed by Perez et al. (2001) (Fig. 5.9).

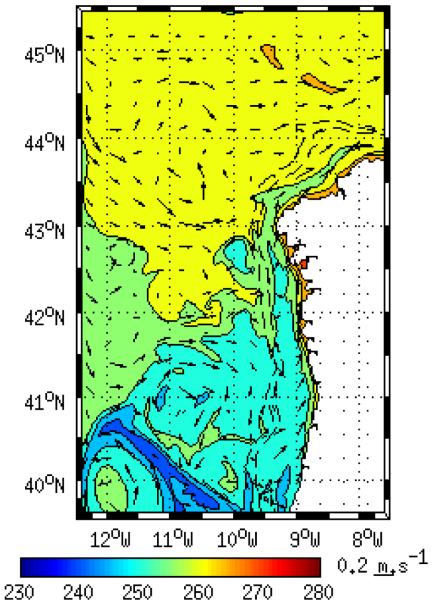

Figure 5.9: Snapshot of the northwestern part of the domain on the 30th January 2002 under strong influence of the IPC: modelled sea surface dissolved O_2 (mmol O_2 m^{-3}) and surface velocities field (arrows) (m s^{-1}).

5) Winter mixing (20th February–26th March): There was an increase in O_2 concentration enhanced by winter mixing of the water column at both stations ($\sim$200 m at Stn. 5 and reaching the bottom depth over the shelf, at Stn. 3, which enhanced the entry of O_2 from the atmosphere. Modelled O_2 concentration in the shelf was very similar to observations (Fig. 5.8a and d).

6) Spring stratification (2nd–24th April): Spring stratification developed under upwelling favourable winds at the end of the study period (Fig. 5.7b and e) (Fig. 5.8b and e) . There was a clear uplift of the isotherms at Stn. 5 in the model which was not so evident in observations. These upwelling conditions, together with the incipient spring thermal stratification, induced a phytoplankton bloom (not shown) with a subsequent increase in O_2 concentration produced by photosynthesis in both the model and observations (Fig. 5.7a and d) (Fig. 5.8a and d).

5.5.3.2 Shelf–ocean interaction

The seasonal variability of dissolved O_2 in the Iberian shelf and the shelf-ocean interactions have been studied along three cross-shelf sections at 42° N, 40° N and 38° N from model results. These three locations were chosen because they represent three different zones of the Atlantic Iberian shelf with contrasting characteristics: (1) The northern shelf from Cape Finisterre to the River Minho ($\sim$43° N–41.5° N), off the Galician coast, being medium width and presenting an irregular coastline due to the presence of the Rías Baixas, four large coastal embayments ($>$30 km length, $>$2.5 km^3 volume); (2) The wide shelf between the river Minho and Cape Roca ($\sim$41.5° N–39° N); and (3) The Southern narrow shelf between Cape Roca and Cape São Vicente ($\sim$37° N–39° N). Both areas (2) and (3) show a regular coastline with meridional orientation. These differences along the Iberian shelf and their effect on biogeochemical cycles dynamics, namely on in situ oxidation of organic mater vs. offshore export have been studied by Álvarez-Salgado et al. (1997) based on several surveys along the Northwest Iberian region.

Figure 5.10 shows model seasonal averages of O_2 along the three cross-shelf sections. As a general seasonal trend, O_2 concentration decreased in shelf waters during summer and autumn, except in the upper water column affected by the subsurface chlorophyll maximum (not shown). This subsurface O_2 maximum was located at about 50 m depth offshore and raised to the surface near the coast, showing lower O_2 concentration toward the south. The summer/autumn seasonal decrease has been attributed to the intensification of remineralization during summer and autumn (Álvarez-Salgado et al., 1993, 1997; Castro et al., 2006). An increase in O_2 concentration was detected during winter, and it continued increasing throughout spring. Winter mixing favours high O_2 concentrations on the shelf by deepening of the mixed layer depths. Remnants of winter mixed layer can still be present during spring (Fiuza et al., 1998). Also, the spring phytoplankton bloom provides O_2 to surface layers through photosynthesis. Oxygen concentration on the shelf tended to decrease from North to South, which is an expected consequence of the hydrography of the region, where the southern shelf is more influenced by the presence of ENACWt, typically carrying lower O_2 concentration (Álvarez-Salgado et al., 1997).

Seasonal anomalies of model O_2 and nitrate concentration (relative to annual means) are shown in Fig. 5.11. The previously described seasonal trend in O_2 concentration over the shelf is also evident here (Fig. 5.11, upper panel). Oxygen anomalies over the shelf tended to be positive in winter and spring and negative in summer and autumn (excluding the upper mixed layer, which was more affected by saturation equilibrium with the atmosphere and phytoplankton blooms). Oxygen and nitrate anomalies were opposite,

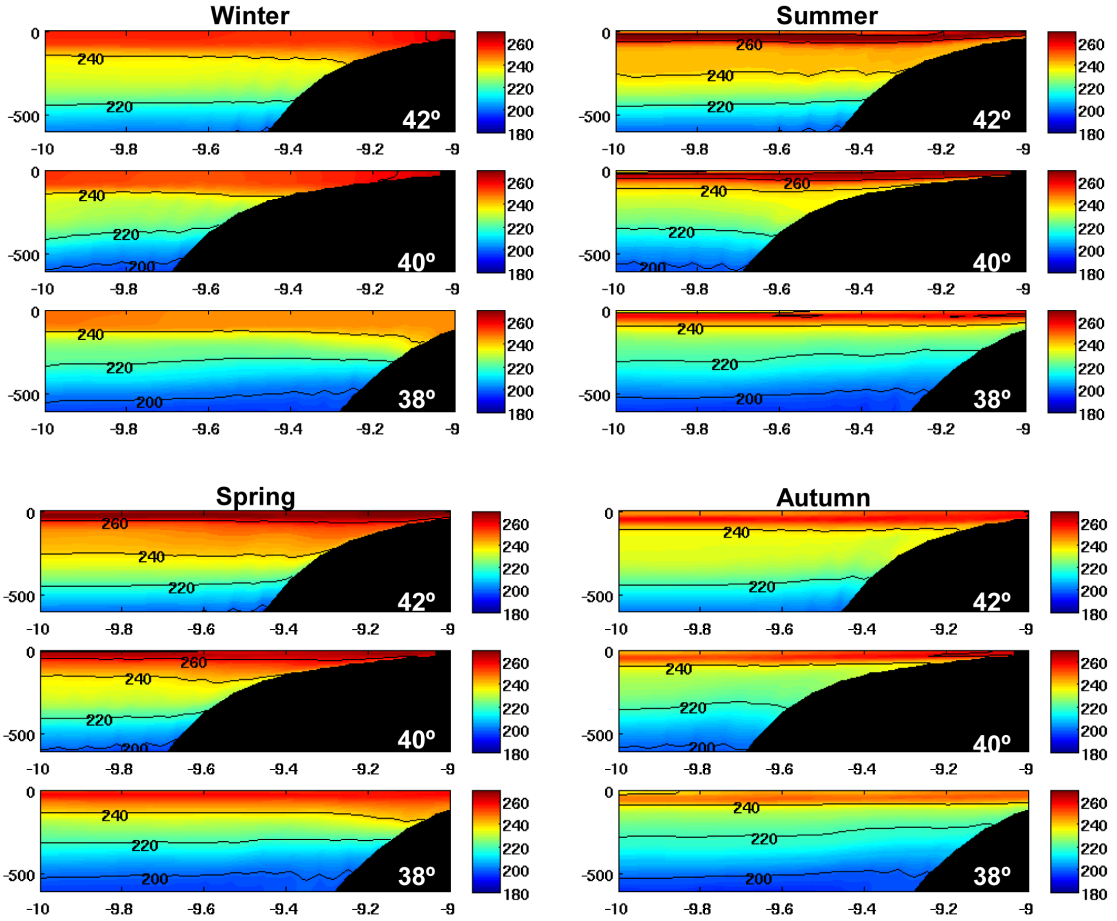

Figure 5.10: Seasonal mean of ROMS dissolved O_2 (mmol O_2 m^{-3}) along three cross-shelf sections in the Iberian Atlantic margin at 42° N, 40° N and 38° N.

an indication of organic matter degradation and subsequent nitrification to nitrate. A strong negative O_2 anomaly (positive nitrate anomaly) was noticeable in autumn, with maximum values in the near bottom water of the outer shelf. This points out to high recycling of organic matter at this position, i.e., mineralization of sinking particulate organic matter (detritus) out of the photic layer (Álvarez-Salgado et al., 1997). The onset of downwelling favourable conditions occurs in autumn, after the summer upwelling season, accompanied by the autumn plankton bloom, influencing the shelf biogeochemistry (Álvarez-Salgado et al., 2003). Downwelling is enhanced by the shift in the winds regime (from northeasterlies to southwesterlies) and by the presence of the IPC flow over the shelf edge and the slope. The presence of the IPC over the slope in autumn was described for Fig. 5.8 in the previous section. Model results support the hypothesis that the presence of the IPC limits the offshore export of particulate organic matter and thus enhances mineralization of organic matter over the shelf through recycling near the bottom shelf and on top of

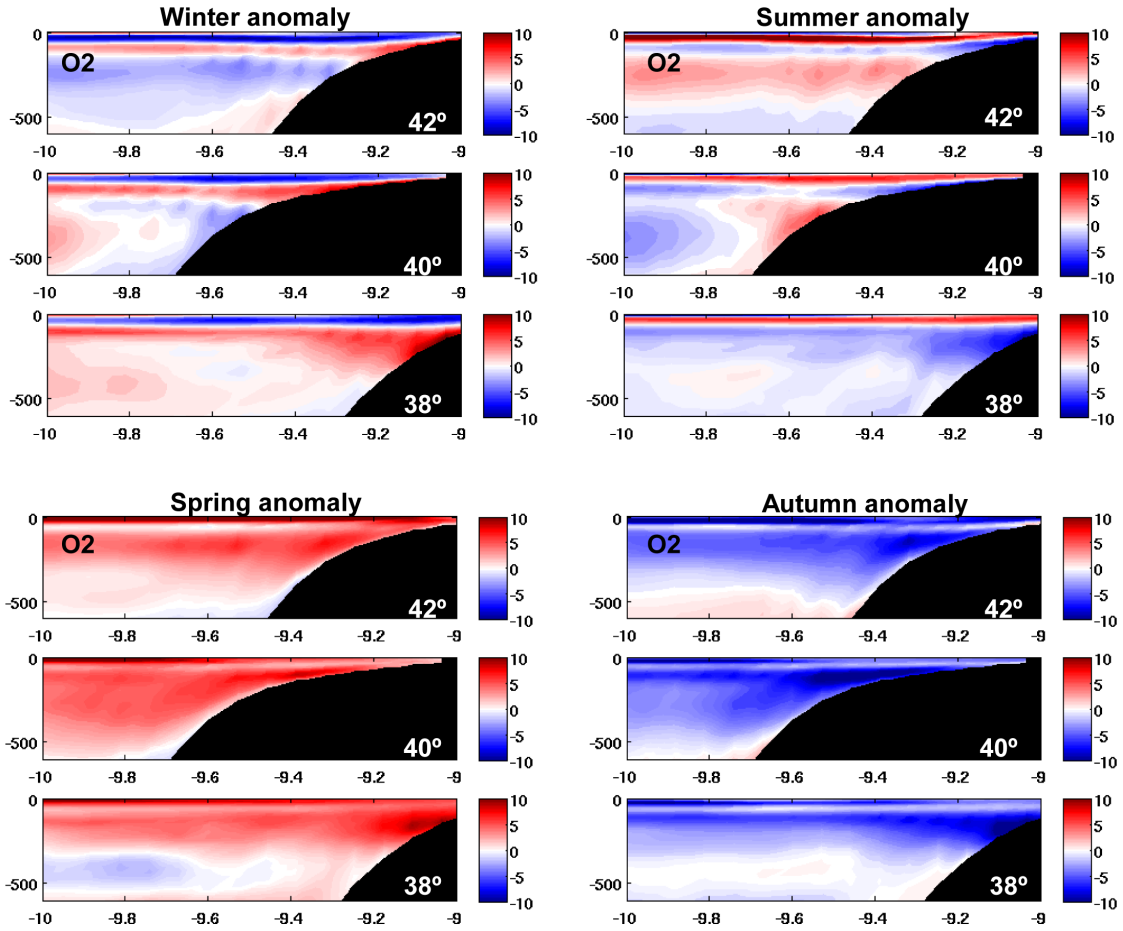

Figure 5.11: Seasonal ROMS O_2 anomalies (mmol O_2 m^{-3}) (upper panel) and nitrate anomalies (mmol N m^{-3}) (lower panel) [anomaly = seasonal mean $-$ annual mean] along three cross-shelf sections in the Iberian Atlantic margin at 42° N, 40° N and 38° N.

the sediments (Álvarez-Salgado et al., 1997, 2003). This effect was more intense in the cross-shelf section at 40° N, where the shelf is wider, as noted by Álvarez-Salgado et al. (1997) (Fig. 5.11). In summer, the upwelling conditions favour a prevailing southward circulation over the shelf and slope (upwelling jet) and an offshore Ekman transport promoting organic matter export from the shelf. Also in summer, the negative O_2 anomaly (positive nitrate anomaly) near the bottom shelf indicates mineralization of sinking organic matter from the surface coastal plankton bloom (Fig. 5.11). This intensified mineralization extends offshore, as a consequence of the enhanced export of organic matter to the adjacent ocean mediated by filaments (Álvarez-Salgado et al., 2007; Cravo et al., 2010). In addition, there are noticeable differences in positive O_2 anomalies (negative nitrate anomalies) of the shelf-slope from North to South; the anomalies tended to be reduced to the South, suggesting less offshore export of organic matter in the northern sections,

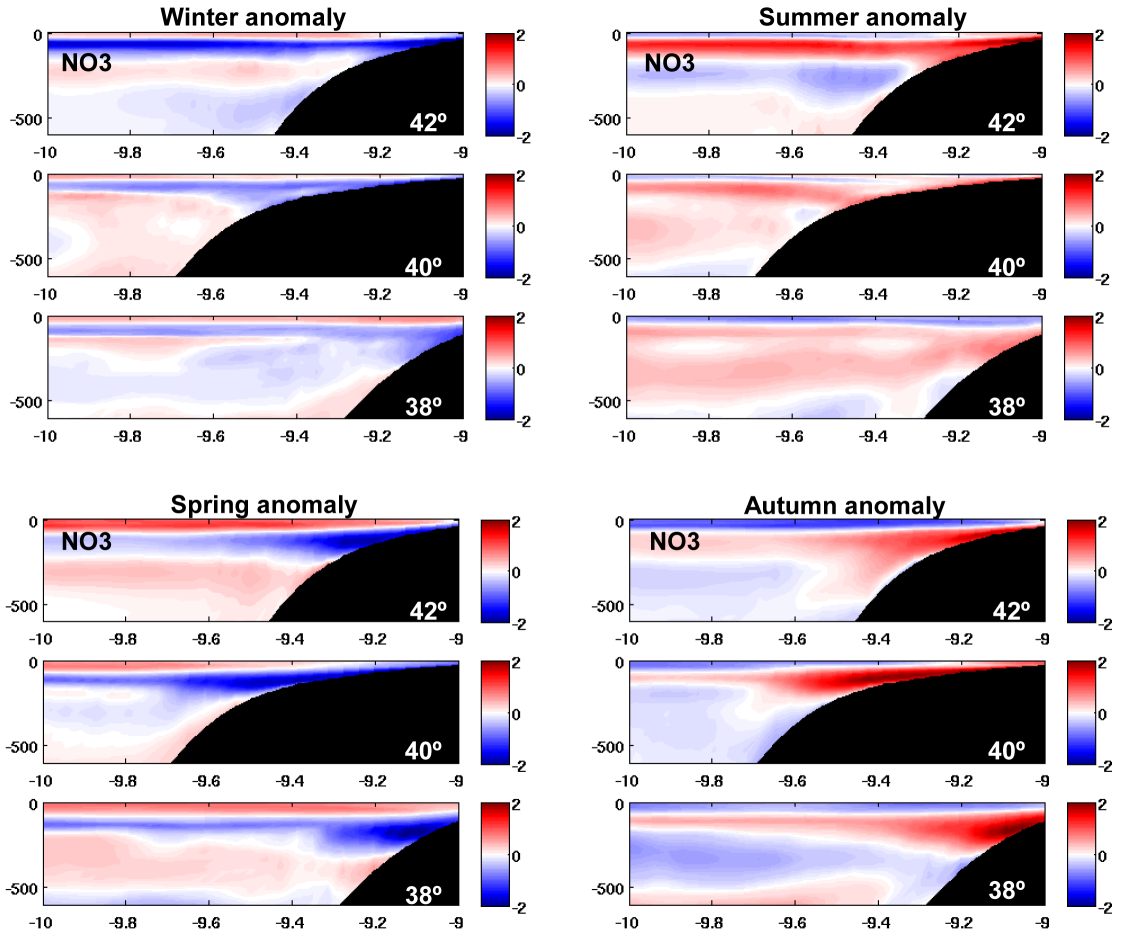

Figure 5.11: Continued.

i.e., where the shelf is wider (Fig. 5.11). In this sense, a more efficient recycling would be expected where the shelf is wider (Álvarez-Salgado et al., 1997). The winter situation is opposite to the summer situation, as low primary production along the season keeps positive O_2 anomalies (negative nitrate anomalies) near the bottom shelf, indicating lower mineralization rates (Fig. 5.11). The negative O_2 anomaly (positive nitrate anomaly) near the surface indicates the absence of the O_2 produced (the presence of the nitrate not consumed) by photosynthesis.

5.6 Summary and conclusions

Reliable predictions of the evolution of ocean oxygen content in future global change scenarios should be based on the ability of models to reasonably reproduce the actual conditions (Gruber, 2011). The model used in this work has been quite satisfactorily

validated and allowed a sound 3D description of the variability and spatial distribution of O_2 along western Iberian coast and adjacent ocean. The Atlantic Iberian margin shows a strong seasonality in the O_2 concentration of the upper water column. In the adjacent ocean, seasonality is mainly controlled by solar radiation and heat exchange with the atmosphere, which drives the deepening and shoaling of the seasonal mixed layer from winter to summer. Ventilation of the water column in winter ($\sim$February–March) provides a massive influx of atmospheric O_2 to the water column up to 150 m to the south of 43° N and more than 300 m to the north of that latitude. O_2 continues increasing during spring due to the seasonal phytoplankton bloom, reaching maximum values by that time. Minimum O_2 values are obtained in summer and autumn, periods of strong thermal stratification and O_2 consumption by remineralization. Still, a subsurface O_2 maximum at about 50 m, associated to the subsurface chlorophyll maximum, remains along the season. Additionally, the regional circulation of central waters influences the O_2 distribution, mainly by the interplay between the southward displacement of oxygen-rich ENACWp and the northward transport of oxygen-poor ENACWt by the IPC. Deeper in the water column, at $\sim$800-1000 m, there is a conspicuous O_2 minimum nearly coincident with the salinity maximum of the MW. The described seasonal pattern generally applies to the shelf region, but here more variability is introduced by the intense hydrodynamics of the upwelling season (spring/summer), the poleward flow of ENACWt over the slope and shelf in autumn/winter and continental runoff. These influence also primary production and remineralization patterns and, thus, O_2 concentration. During upwelling episodes cold and nitrate rich ENACW from 150-250 m depth in the adjacent ocean raises to the photic layer of the shelf carrying lower O_2 concentrations than the remnant coastal waters. However, its nitrate content rapidly induces phytoplankton blooms that raise the O_2 concentration. The shift to prevailing downwelling conditions in autumn/winter with the arrival of the IPC to the shelf and slope brings lower O_2 concentration, although ENACWt transported by the IPC over the slope becomes more O_2 rich as it displaces poleward because of mixing with the surrounding oxygen richer shelf surface waters. The presence of the IPC over the slope limits the off-shelf export of organic matter, causing intense remineralisation near the bottom shelf, decreasing O_2 concentration there. Evident latitudinal gradients exist related to the regional circulation and the differences in shelf extension and topography.

Chapter 6

Modelling the seasonal and interannual variability (2001-2010) of chlorophyll-a in the Iberian margin

Rosa Reboreda, Nuno G. F. Cordeiro, Rita Nolasco, Carmen G. Castro, Xosé A. Álvarez-Salgado, Henrique Queiroga, Jesus Dubert

6.1 Abstract

A modeling study of the seasonal and interannual variability of chlorophyll-a has been carried out for the period 2001-2010 along the Iberian shelf and adjacent ocean. A high resolution regional configuration of the three-dimensional Regional Ocean Modeling System (ROMS) has been used, coupled to a N_2PZD_2-type biogeochemical model. Chlorophyll-a concentration ([Chl]) model outputs were compared to regional objective analysis of remotely sensed [Chl] data for the same period, in order to evaluate the model ability to reproduce the seasonal pattern and the interannual variability in the region. The spatio-temporal variability of modeled and satellite derived [Chl] was analyzed applying an individual Empirical Orthogonal Function (EOF) analysis to monthly time series, which resulted in three main modes of sea surface [Chl] variability explaining more than 90% of modeled variability and more than 85% of remotely sensed variability. The first EOF accounted for the spring phytoplankton bloom (March-April). The second EOF was related to the spring-summer coastal upwelling season (April-September). The third EOF showed a recurrent [Chl] minimum in winter coinciding with the maximum vertical mixing (February)

for the northern part of the region. The influence of the hydrographic conditions on [Chl] variability was explored through a cross-correlation analysis of the three EOFs and an assortment of physical descriptors given by the model: Namely the mixing/stratification cycles, the occurrence of coastal upwelling and the influence of continental runoff.

6.2 Introduction

The coastal ocean supports 80-90% of the global new production due to the enhanced land-ocean-atmosphere interaction that occur in these regions (Chen et al., 2003). Nutrient rich continental and atmospheric inputs, and the hydrodynamics resulting from the interaction of the coastal currents with bathymetry, coastal morphology and the atmospheric-ocean interaction strongly influence the primary production through a tight physical-biogeochemical coupling. The high spatio-temporal variability in some of these factors, which are also influenced by the large scale ocean and atmosphere circulation (Chávez et al., 1999; Behrenfeld et al., 2006; Perez et al., 2000; Cianca et al., 2012), result in remarkable event, seasonal and interannual variability in chlorophyll (proxy of phytoplankton biomass and primary production).

The seasonal pattern of chlorophyll in the Iberian margin, located in the northern limit of the eastern North Atlantic upwelling off NW Africa (Fig. 6.1), is characterized by high concentrations from May to September, when northeasterly winds prevail along the N-S oriented Western Iberian coast , inducing the upwelling of cold and nutrient rich Eastern North Atlantic Central Water (ENACW) in intermittent pulses (Fraga, 1981; Peliz et al., 2002; Relvas et al., 2007). By the end of summer (September-October), there is a shift in the wind regime to downwelling favorable southwesterlies, together with the onset of the relatively warm and saline Iberian Poleward Current (IPC) over the slope (Haynes and Barton, 1990; Peliz et al., 2005; Relvas et al., 2007). This change of regime is usually associated to a phytoplankton autumn bloom in the coast (Castro et al., 1997; Álvarez-Salgado et al., 2003; Silva et al., 2009), followed by a decrease in chlorophyll concentration ([Chl]) in winter. [Chl] during this season can sometimes be relatively high due to episodic uwpelling events and the presence of the Western Iberia Buoyant Plume (WIBP), a low-salinity water lens originated by accumulated river runoff (Peliz et al., 2002), which supplies stratification conditions suitable for phytoplakton growth (Ribeiro et al., 2005). This succession of seasonal production stages is commonly found in the literature (e.g. Bode et al., 1996; Casas et al., 1997; Nogueira et al., 1997). From interannual observations (1984-1992) in the N-NW Iberian shelf, Bode et al. (1996) obtained that average [Chl] during bloom stages (upwelling/spring/autumn blooms) were double of the

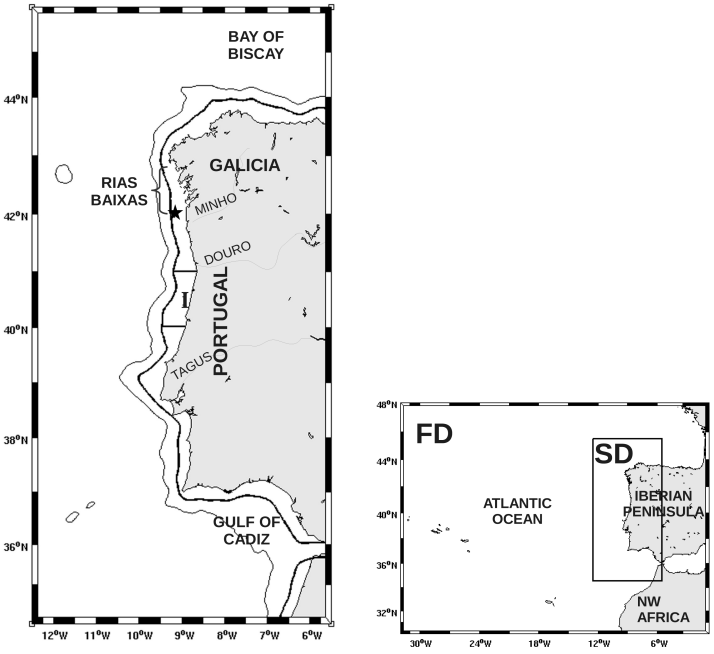

Figure 6.1: Region of study and nested model domains. Target domain (left), with indication of the parent domain used to provide lateral boundaries (right). FD stands for First Domain and SD stands for Second Domain. Model isobaths of 200 m (black line) and 1000 m (gray line) are depicted (real depth smoothed). Box I indicates the shelf region used for time series comparisons in section 6.4.1. The star shows the location of the shelf station used to compare water column observations with model outputs.

concentrations in periods of thermal stratification (summer), which in turn were about twice the concentrations during winter. A remarkable feature in the seasonal distribution of [Chl] in western Iberia is the offshore spring phytoplankton bloom that occurs over the Northeast Atlantic (Longhurst, 1998).

Superimposed to this seasonal variability, noticeable interannual differences have been reported, for example in the timing (month) of maximum offshore and shelf primary production (Joint et al., 2002), in new production associated to upwelling (Álvarez-Salgado et al., 2002), or in the onset and cessation of the downwelling period (Álvarez-Salgado et al., 2003). Also, long-term trends in primary production have been detected (Bode et al., 2009, 2011) similarly to what was referred by Chávez et al. (2011) for the global ocean. Therefore, the interannual and seasonal variability in physical forcings leads to changes in biological production or, as described in Silva et al. (2009), shifts in the phytoplankton community structure. Other sources of variability, independent of physical forcing may occur as a result of complex, non-linear interactions in the ecosystem (Williams and Follows, 2003). Understanding the physical-biogeochemical interactions that may underly the variability in [Chl] would help to elucidate the ecosystem variability, intimately related

to the rich marine biodiversity and fishing resources of the region (Tenore et al., 1995; Figueiras et al., 2002; Santos et al., 2005).

Inherent difficulties exist to obtain high quality long-term observations, specially for a large region, and including both biogeochemical and physical variables. Ocean numerical models can help to overcome this gap, by complementing observations and allowing to explore the physical-biogeochemical interactions through coupled hydrodynamic-biogeochemical models (Machu et al., 2005; Gruber et al., 2006; Echevin et al., 2008). In this study a high resolution regional configuration of the Regional Ocean Modeling System (ROMS) coupled to a NPZD-type (Nutrients-Phytoplankton-Zooplankton-Detritus) biogeochemical model has been implemented to the Iberian margin for the period 2001-2010. The modeling approach with ROMS has contributed to the understanding of the ocean dynamics and hydrography in Western Iberia (e.g. Peliz et al., 2007a, 2009, Nolasco et al., in revision), including some ecosystem applications (Oliveira et al., 2009). Using the same ROMS model configuration presented here, Cordeiro Pires et al. (in preparation) have studied the interannual variability of western Iberia hydrodynamics for the decade 2001-2010. Here, we couple a biogeochemical model to reproduce the interannual variability in [Chl] over the same period. Model outputs are compared to satellite and some in situ observations to evaluate the model performance. Next, we aim to find the main modes of variability of [Chl] performing and Empirical Orthogonal Function (EOF) analysis and correlate this variability with the hydrographyc conditions.

6.3 Methods

6.3.1 Model setup

6.3.1.1 Hydrodynamic model

The interannual simulation of the period 2001-2010 was run for a high resolution regional configuration of the Regional Ocean Modeling System (ROMS) (Shchepetkin and McWilliams, 2005; Haidvogel et al., 2008; Penven et al., 2006) for the Iberian margin, using a two-domain approach, as shown in Figure 6.1. A large-scale or first domain (FD) was run independently (offline) in order to provide initial and boundary conditions to our second domain (SD). ROMS is a three dimensional (3D) ocean circulation model with free-surface, vertical terrain-following coordinates (sigma-coordinates), and horizontal orthogonal curvilinear coordinates, designed to resolve regional problems, such as coastal areas and regional seas at the mesoscale. Our first domain (FD) included the northeast

Atlantic region between 30° N - 48° N and 0.8° E - 32° W, and had 1/10°(∼9 km) horizontal resolution and 30 vertical s-levels, in order to resolve the large-scale circulation features. The high-resolution nested domain, or second domain (SD), included the western Iberian region from the Gulf of Cádiz to northwest Iberia (Galicia) (34.5° N - 45.5° N and 5.5° W - 12.5° W; ∼1200 x 600 km) (Fig. 6.1) and had horizontal resolution of 1/27°(∼3 km) and 60 vertical s-levels in order to properly resolve the Mediterranean undercurrent, which circulation is known to influence the surface transport of chemical and biological properties (Serra et al., 2010). A more detailed description of this regional configuration of ROMS can be found in Nolasco et al. (2013), applied for a climatological study of the regional hydrodynamics. The same configuration has been used for an interannual approach in Cordeiro Pires et al. (in preparation).

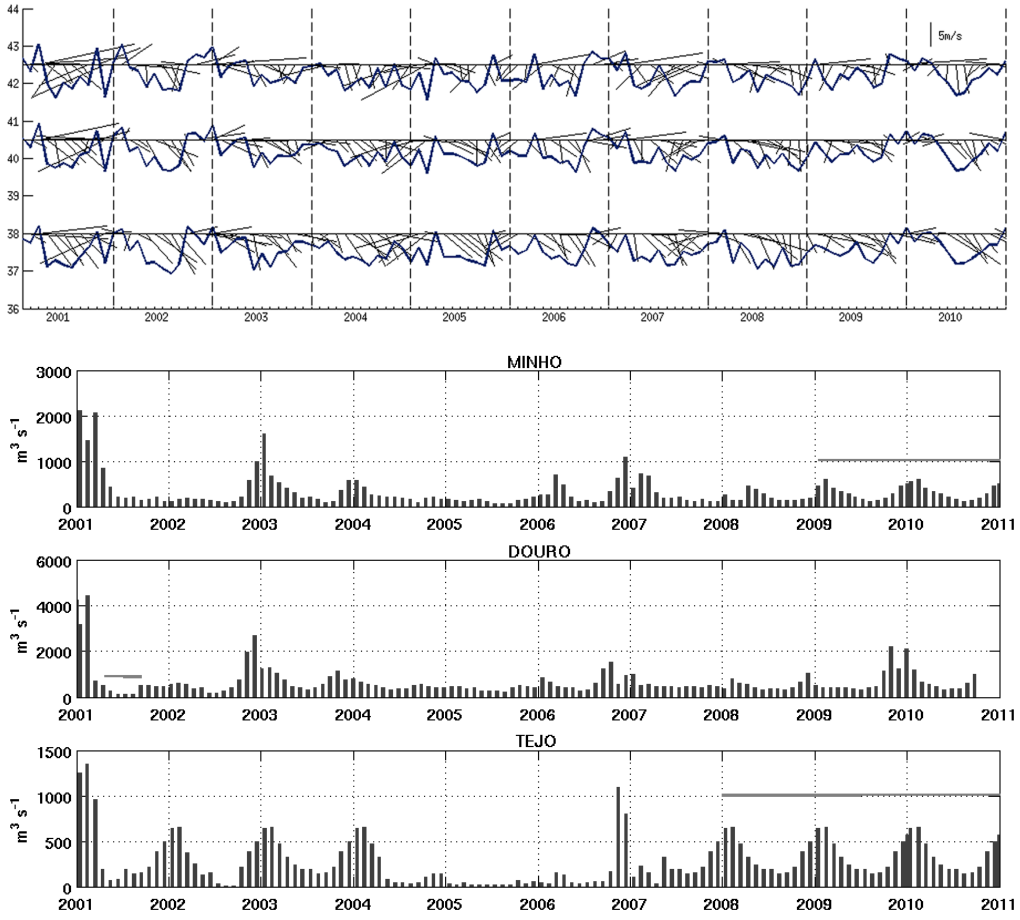

Figure 6.2: Local forcings in the Iberian shelf (2001-2010). Upper panel: Monthly time series of QuikSCAT (2001-2008) and ASCAT (2009-2010) wind velocity and direction (black sticks) and meridional component (solid line) at three locations along the Iberian shelf (9.5° W): 38° N, 40.5° N and 42.5° N; Lower panel: Monthly continental runoff from the main rivers: Douro, Minho, and Tagus (m^3 s^{-1}; note different scales). The lines over the bars indicate climatological values, otherwise values are averaged from real daily discharges.

A climatological run of the 5th year of the FD was used as the initial state to run a realistic simulation of the hydrodynamic model for the period 2001-2010 for this outer domain. The surface forcing was extracted from NCEP 2 reanalysis for air-sea fluxes (2001-2010), provided by the NOAA (http://www.esrl.noaa.gov/psd/) and QuikSCAT surface wind reanalysis (2001–2008) at 0.5° × 0.5° spatial resolution provided by CERSAT (http://www.ifremer.fr/cersat). For 2009 and 2010, ASCAT surface wind reanalysis (0.25° × 0.25° spatial resolution) was used, also provided by CERSAT, since QuikSCAT mission stopped towards the end of 2009 (Fig. 6.2 upper panel). For the SD, the year 2001 was initialized from 1st January using initial conditions from a previous climatological run of the coupled hydrodynamic-biogeochemical model (9th year) for this domain (Reboreda et al., in revision). The boundary conditions were provided by the simulation of 2001–2010 for the FD, and the same surface forcing was applied. The exchange of Atlantic and Mediterranean waters at the Strait of Gibraltar was explicitly represented in the SD by the imposition of vertical profiles of temperature, salinity and zonal velocity at 5 grid points at the Strait, similarly to Peliz et al. (2007a).

The freshwater continental runoff from the main rivers of the region was included with realistic discharge values for 2001-2010 provided by Instituto Nacional da Água (INAG; http//inag.pt) when available (Fig. 6.2 lower panel). When no realistic discharges were available, climatological values were obtained from INAG for the Portuguese rivers, and from Río-Barja and Rodríguez-Lestegás (1992) for the Galician rivers.

6.3.1.2 Biogeochemical model

A biogeochemical model was run coupled to the hydrodynamic model to simulate the base trophic levels and biogeochemical components of the system. The $N_2ChlPZD_2$ model consists of a nitrogen based model, computing 7 state variables: two nutrient compartments, nitrate (NO_3) and ammonium (NH_4), phytoplankton ($Phyt$), zooplankton (Zoo), and two detritus compartents, fast-sinking large detritus ($LDet$) and slow-sinking small detritus ($SDet$), all expressed in mmol N m^{-3} (Fig. 2.3). Additionally, chlorophyll-a (mg m^{-3}) is derived from phytoplankton concentration using a variable chlorophyll:carbon ratio, θ (mg chlorophyll-a (mg C)$^{-1}$) and a constant C:N Redfield ratio of 6.625 (mmol C (mmol N)$^{-1}$). The variable θ describes the proportion of photosynthetically fixed carbon that is used for chlorophyll-a biosynthesis considering the model of Geider et al. (1997). Its implementation in the ROMS biogeochemical model is described in Gruber et al. (2006) (online additional material).

The 3D time evolution of any of the biogeochemical variables (B_i) is calculated

considering its diffusion, horizontal advection, vertical mixing and the biogeochemical processes that act as sink or source for the variable:

$$\frac{\partial B_i}{\partial t} = \nabla \cdot K \nabla B_i - u \cdot \nabla_h B_i - (w + w_{sink}) \frac{\partial B_i}{\partial z} + SMS(B_i) \tag{6.1}$$

Where K is the eddy kinematic diffusivity tensor, u is the horizontal velocity, w and w_{sink} are the vertical velocity and the vertical sinking rate of the biogeochemical variable (all particulated variables, except zooplankon), respectively. The biogeochemical processes included in the source minus sink (SMS) term are specific for each variable.

The following set of SMS equations for each of the biogeochemical variables was used, which is next described:

$$SMS(NO_3) = -\mu(PAR, T) \cdot \mu(NO_3) \cdot Phyt + t_{NH4_{nitr}}\ NH_4 \tag{6.2}$$

$$\begin{aligned} SMS(NH_4) = &-\mu(PAR, T) \cdot \mu(NH_4) \cdot Phyt - t_{NH4_{nitr}}\ NH_4 + t_{Z_{metab}}\ Zoo \\ &+ t_{SD_{remin}}\ SDet + t_{LD_{remin}}\ LDet \end{aligned} \tag{6.3}$$

$$\begin{aligned} SMS(Phyt) = &\mu(PAR, T) \cdot \mu(NO_3, NH_4) \cdot Phyt - m_{PD}\ Phyt \\ &- g_{max}\ Zoo\ \frac{Phyt}{K_P + Phyt} \end{aligned} \tag{6.4}$$

$$SMS(Zoo) = \beta\ g_{max}\ Zoo\ \frac{Phyt}{K_P + Phyt} - m_{ZD}\ Zoo - t_{Z_{metab}}\ Zoo \tag{6.5}$$

$$\begin{aligned} SMS(SDet) = &m_{PD}\ Phyt + m_{ZD}\ Zoo + (1 - \beta)\ g_{max}\ Zoo\ \frac{Phyt}{K_P + Phyt} \\ &- t_{SD_{remin}}\ SDet - S_{agg}\ SDet \cdot (Phyt + SDet) \end{aligned} \tag{6.6}$$

$$SMS(LDet) = -t_{LD_{remin}}\ LDet + Sagg \cdot (Phyt + SDet)^2 \tag{6.7}$$

$$SMS(\theta) = \mu(PAR, T) \cdot \mu(NO_3, NH_4) \cdot \left(\frac{\mu(T) \cdot \mu(NO_3, NH_4) \cdot \theta_{max}}{\sqrt{\mu(T)^2 + (\alpha\ PAR\ \theta)^2}} - \theta \right) \tag{6.8}$$

The biogeochemical processes included in the SMS terms are similar to those described for the ROMS $NPZD$ model in Koné et al. (2005), except for including nitrogen limitation of phytoplankton growth by two nutrients, nitrate and ammonium, and including two pools of detritus, large detritus and small detritus. The introduction of a small detritus pool mimicks DON and fine, slow sinking particles, as in Gruber et al. (2006). Phytoplankton growth rates (Eq. 6.4) are controlled by nitrate and ammonium concentration, light (photosynthetically available radiation: PAR), and temperature (T). The light dependent, temperature limited growth rate, $\mu(PAR, T)$, is calculated as in equation 10 of Gruber et al. (2006). The exponential decrease of PAR with depth is calculated as in equation

2 of Koné et al. (2005). Taking into account that ammonium is taken up preferencially over nitrate, phytoplankton growth rates $\mu(NO_3)$ and $\mu(NH_4)$ are formulated using a Michaelis-Menten equation where NH_4 is preferred to NO_3 for phytoplankton uptake, as in equation 12 of Gruber et al. (2006), with K_{NO_3} and K_{NH_4} the half-saturation constants for nitrate and ammonium uptake, respectively. Phytoplankton dies at a constant linear rate (m_{PD}) been automatically incorporated to the small detritus pool (Eq. 6.6), a formulation similar to the model of Gruber et al. (2006) and references therein. Zooplankton growth (Eq. 6.5) relies on its grazing on phytoplankton, which rate depends on prey (phytoplankton) concentration, through a Michaelis-Menten function and on zooplankton assimilation efficiency (β). The fraction of organic nitrogen that is consumed by zooplankton but not assimilated ($(1-\beta)\ g_{max}\ Zoo\ \frac{Phyt}{K_P+Phyt}$), i.e., egestion as fecal pellets, is incorporated to the small detritus pool (Eq. 6.6). A constant excretion rate ($t_{Z_{metab}}$) is attributed to zooplankton, providing a source of nutrients to the ammonium pool (Eq. 6.3). Zooplankton incorporates to the small detritus pool at a constant linear mortality rate (m_{ZD}) (Eq. 6.6). Large detritus (fast sinking) particles are formed by coagulation of phytoplankton with small detritus (slow sinking) particles (Eq. 6.7). The particle coagulation is formulated assuming that the probability of particles making contact and coagulating is proportional to the concentration of particles ($S_{agg} \cdot (Phyt + SDet)^2$), with S_{agg} the specific aggregation rate, as in Gruber et al. (2006). Mineralization of large and small detritus is formulated as transformation into ammonium at constant ammonification rates, $t_{LD_{remin}}$ and $t_{SD_{remin}}$, respectively (Eq. 6.3). Detritus reaching the seafloor was incorporated to the bottom layer of the water column in the model, where it continued mineralization. Nitrification, i.e. the conversion of ammonium to nitrate, is represented using a constant nitrification rate $t_{NH4_{nitr}}$, the process being limited to the night period ($PAR = 0$) to account for photoinhibition of the nitrifying bacteria (Eq. 6.2). The SMS equation for θ (Eq. 6.8) was formulated as in equation 8 of Gruber et al. (2006). Model parameters values for the sink/source terms selected to represent our region of study with this model are listed in Table 2.3. These parameters aimed at representing the eutrophic coastal ecosystem and the offshore spring bloom, both dominated by diatoms. This necessarily implied reducing the ability of the model to represent correctly the oligotrophic offshore environment, dominated by nanophytoplankton, as only one phytoplankton functional group was included.

The NO_3, $Phyt$ (and chlorophyll-a), and Zoo for the model initial conditions (January 2001) were obtained from the 9th year of a climatological simulation of a simpler $NChlPZD$ biogeochemical model (Reboreda et al., in revision). Boundary conditions for NO_3 and chlorophyll-a were supplied by the climatological data sets of the World Ocean Atlas 2009 (Garcia et al., 2010b) and SeaWiFS, respectively. For NO_3, seasonal (for depths down to 500 m) and annual (depths below 500 m) climatologies were used.

For chlorophyll-a, the seasonal climatology of surface concentrations from SeaWiFs data was used. Seasonal vertical profiles were created from these surface concentrations using the algorithm of Morel and Berthon (1989). The boundary values of $Phyt$ and Zoo were derived from chlorophyll-a ($Phyt = 0.5 \cdot Chl$; $Zoo = 0.2 \cdot Chl$), as in Gruber et al. (2006). Boundary conditions were supplied seasonally. NH_4, $SDet$, and $LDet$ initial and boundary conditions were not available from climatological data sets, so they were introduced as constant analytical values: 0.1 mmol N m^{-3} (NH_4) and 0.02 mmol N m^{-3} (both detritus sizes). The riverine inputs of NO_3 and chlorophyll-a were used constant along the year, with the values indicated in Marta-Almeida et al. (2012).

6.3.2 Data series for model evaluation

Model sea surface temperature (SST) and [Chl] outputs were evaluated by comparison with satellite products for the period 2001-2010. Daily SST was compared with data retrieved from the Advanced Very High Resolution Radiometer (AVHRR) of the National Oceanic and Atmospheric Administration (NOAA). The data were extracted from the EUMETSAT Ocean & Sea Ice Satellite Application Facility (OSI-SAF) (www.osi-saf.org) and were made available by CERSAT (IFREMER, France). The product has an approximate horizontal resolution of 2 km. Daily surface [Chl] was compared with CERSAT-IFREMER ocean color derived (OC5 algorithm) [Chl] obtained from merging the following three sensors: Sea-viewing Wide Field of View Sensor (SeaWiFS) on the Orbview platform (January 01, 1998-December 31, 2004), Moderate Resolution Imaging Spectroradiometer (MODIS) on the Aqua platform (October 01, 2002 to present), and the MEdium Resolution Imaging Spectrometer Instrument (MERIS) on the ENVISAT platform (October 01, 2002-April 08 2012) (ftp://ftp.ifremer.fr/ifremer/cersat/products/gridded/ocean-color/atlantic/EUR-L4-CHL-ATL-v01/). The optimal interpolation merging method, which provides cloudless daily fields of [Chl], was described and validated in Saulquin et al. (2011). The product is provided at 1.1 km horizontal resolution.

The model evaluation was complemented with comparisons of model outputs in the water column with in situ observations obtained at a 1-year intensively sampled shelf station off the Galician coast (NW Iberian margin, Fig. 6.1), sampled weekly between 15th May 2001 and 24th April 2002 within the frame of the DYBAGA project (Spanish "Consejo Superior de Investigaciones Científicas" -CSIC). The succession of hydrographic periods detected for this station have been described in detail in Nieto-Cid et al. (2004), Álvarez-Salgado et al. (2006), and Herrera et al. (2008), and from a modeling approach in Reboreda et al. (in revision). The corresponding succession of microbial plankton has

been described in Espinoza-González et al. (2012).

Additionally, a mixed layer depth (MLD) monthly climatology (2002-2010) constructed from ARGO floats profiles (Holte et al., 2010) was used to evaluate the MLD derived from model outputs. They calculated the MLD using a hybrid algorithm between the classical threshold method and the shape of the profile for either potential density, potential temperature, or salinity profiles (Holte and Talley, 2009). We used the MLD calculated with the temperature algorithm for a better comparability with modeled MLD calculated from modeled temperature profiles. Our method for calculating the MLD considered a 0.2 ℃ temperature threshold relative to a surface reference level of 10 m, in order to avoid the effect of surface diurnal heating (de Boyer Montégut et al., 2004), establishing a maximum MLD of 450 m. Given that some of the years in the Holte et al. (2010) dataset had few values within the area of the model domain, and/or they were unevenly distributed, we selected only the years having more than 200 MLD values and presenting an homogeneous distribution within the model domain (2005-2008). Then, an spatial MLD mean was calculated for each of these years.

6.3.3 Statistical analysis

6.3.3.1 Model error statistics

Model error relative to satellite observations of surface [Chl] were calculated applying four reliability indices commonly used for ocean-ecosystem models validation (Allen et al., 2007; Stow et al., 2009; Warner et al., 2005). They were calculated in a daily basis comparison of both time series. The indices are briefly described next, with an explanation of the type of information they provide about the model performance:

Bias gives an indication of whether the model is systematically overestimating or underestimating the observations, being the model result as better as the bias is closest to zero. It gives a measure of the accuracy of the model.

$$Bias = \frac{\sum_{n=1}^{n}(M_n - D_n)}{\sum_{n=1}^{n} D_n} \tag{6.9}$$

Where M is the model estimation, D the data, and n is the nth comparison of total grid points.

Rms is the *root mean squared error* of n model-data comparisons (total grid points).

$$rms = \sqrt{\frac{\sum_{n=1}^{n}(M_n - D_n)^2}{n}} \tag{6.10}$$

It contributes to evaluate model precision. The closer the rms to zero the better the fit between the model and observations.

Skew gives the degree of asymmetry of the error distribution.

$$Skew = \frac{N}{(N-1)(N-2)} \sum_{n=1}^{n} \left(\frac{(M_n - D_n) - (\overline{M_n - D_n})}{\sigma_D} \right)^3 \tag{6.11}$$

where N is the total number of model-data matches, and σ_D the standard deviation of the data. Positive skewness indicates that model tends to make more overestimations, whereas negative skewness indicates that model tends to make more underestimations.

Skill is a quantitative agreement between the model and observations where M_n is compared with a time mean $\overline{D}$.

$$Skill = 1 - \frac{\sum |M_n - D_n|^2}{\sum (|M_n - \overline{D}| + |D_n - \overline{D}|)^2} \tag{6.12}$$

Perfect agreement between model results and observations would yield a skill of one, and complete disagreement would correspond to zero model skill.

6.3.3.2 Empirical Orthogonal function analysis

The spatio-temporal variability of modeled and satellite derived [Chl] was analyzed applying an individual Empirical Orthogonal Function (EOF) analysis to monthly time series. The EOF analysis consists of a representation of the data in terms of a reduced set of orthogonal functions or modes (Glover et al., 2011). The outputs consist of spatial fields and their associated relative variance (eigenvalues) and temporal weightings (eigenvectors), allowing to study the temporal and spatial variability of data (Shutler et al., 2011). For that, we created an $N \times M$ data matrix X, consisting of N time data and M grid points, i.e., a 10 year record of monthly averages ($N = 120$) of [Chl] on a grid of $M = 320 \times 162$ points. This grid was smaller than the actual model grid (390×189 points) because half degree was removed from each boundary of the model domain to avoid using points near the boundaries, where climatological [Chl] values (SeaWiFS) were applied when running the model. The M grid of satellite data had the same number of points used for the model ($M = 320 \times 162$), as an interpolation of the original grid to the model grid was performed and the same boundary points were removed. The EOF eigenvectors and eigenvalues were obtained via singular value decomposition (SVD) of X (Preisendorfer, 1988) as $X = BL^{1/2}F^T$, where L is the diagonal matrix of the eigenvalues giving information on the percentage variance explained in each EOF, F is the right matrix of eigenvectors (the

spatial field), and B is the left matrix of eigenvectors which is used to obtain the temporal mode (temporal mode $= B \times L$). Three EOFs were retained for analysis.

The contribution of one EOF at any time in a particular point is obtained by multiplying the value at that location times the value of the temporal coefficient at a given time.

6.3.3.3 Cross-correlation analysis

The possible physical forcings underlying the three [Chl] EOFs with the largest eigenvalues were explored by performing an individual cross-correlation analysis between each of the modeled EOFs time series and the corresponding time series of the physical forcing to be tested. All correlations presented have a 95% confidence interval. The cross-correlation analysis was selected because it would allow to find not only the degree of correspondence between the two time series, but also the possible time lags between them. Thus, a significant correlation may imply a causality between the physical forcing and the biological response, although bearing in mind that it does not proof it, as a co-causal relationship may also exist (Glover et al., 2011).

The spatial pattern of correlations between the [Chl] and the hydrographic forcings was further explored by plotting maps of the correlation coefficients between each of the three spatial EOFs and the physical forcing and time lag which showed the maximum correlation in the cross-correlation analysis.

6.4 Results and discussion

The interannual [Chl] variability obtained from model results for the period 2001-2010 was evaluated comparing time series of modeled [Chl] with satellite observations at the sea surface (section 6.4.1). A general evaluation was performed comparing domain averaged time series, and for a more specific evaluation of the model performance in the shelf, time series averaged over a selected shelf region (Fig. 6.1) were compared. The same approach was applied to assess modeled SST, i.e., the ability of the model to reproduce the interannual variability in the hydrography.

In order to identify the main modes of [Chl] variability for the studied period, and the percentage of variability explained, an EOF analysis of modeled and satellite [Chl] time series (domain averaged) was carried out (section 6.4.2). After having identified

these modes, and described the similar variability found in model outputs and satellite observations, we tried to correlate the main modes of [Chl] variability with an assortment of physical forcings using model data. This tried to elucidate some mechanisms of physical-biogeochemical coupling that may underlay the ecosystem functioning and variability.

The [Chl] variability in the water column was also explored, firstly comparing model outputs to weekly observations at a shelf station along one year (May 2001-April 2002), and then extending the [Chl] variability over the 10 years for that location using model results (section 6.4.4).

6.4.1 Model evaluation: temporal series of [Chl] and SST

Chlorophyll time series at the sea surface averaged over the study region showed a conspicouos [Chl] peak detected every year, corresponding to the North Atlantic spring bloom (March-April) (Fig. 6.3a). The model reproduced the spring bloom captured by the satellite observations, although it occurred earlier and with [Chl] values generally higher than observed, even though this difference was highly variable from year to year (0.5-2 mg m^{-3}). The best correspondence occurred for year 2009, when both peaks (modeled and observed) were nearly coincident. The model also reproduced satisfactorily the seasonal evolution of the domain averaged SST (Fig. 6.3c), showing the characteristic succession of winter minima and summer maxima, with values similar to observations. Over the shelf, the model was able to reproduce the high [Chl] variability with concentration values close to observations (Fig. 6.3b). From April to September recurrent [Chl] maxima over the shelf, associated to the upwelling of cold and nutrient rich subsurface waters, were captured by the model (Figs. 6.3b and d). Exceptionally, years 2009 and 2010 were not well reproduced by the model in terms of [Chl], with model values being systematically lower than observations. On the other hand, modeled SST during the upwelling season seemed to improve for these two years, as temperature minima were more close to satellite observation than in previous years, when SST reached noticeably lower minima in the model (Fig. 6.3d). We have evidences that these changes in 2009 and 2010 were related to the shift from QuikSCAT to ASCAT wind products for the surface model forcing. The use of ASCAT seemed to improve the model results related to the upwelling reducing its intensity, probably due to the higher spatial resolution of wind stress compared to QuikSCAT, which tends to overestimate alongshore winds due to its limitations representing the coastal wind drop-off (Albert et al., 2010). Accordingly, a possible reduction in the modeled upwelling intensity would lead to a reduction the modeled [Chl] in the shelf.

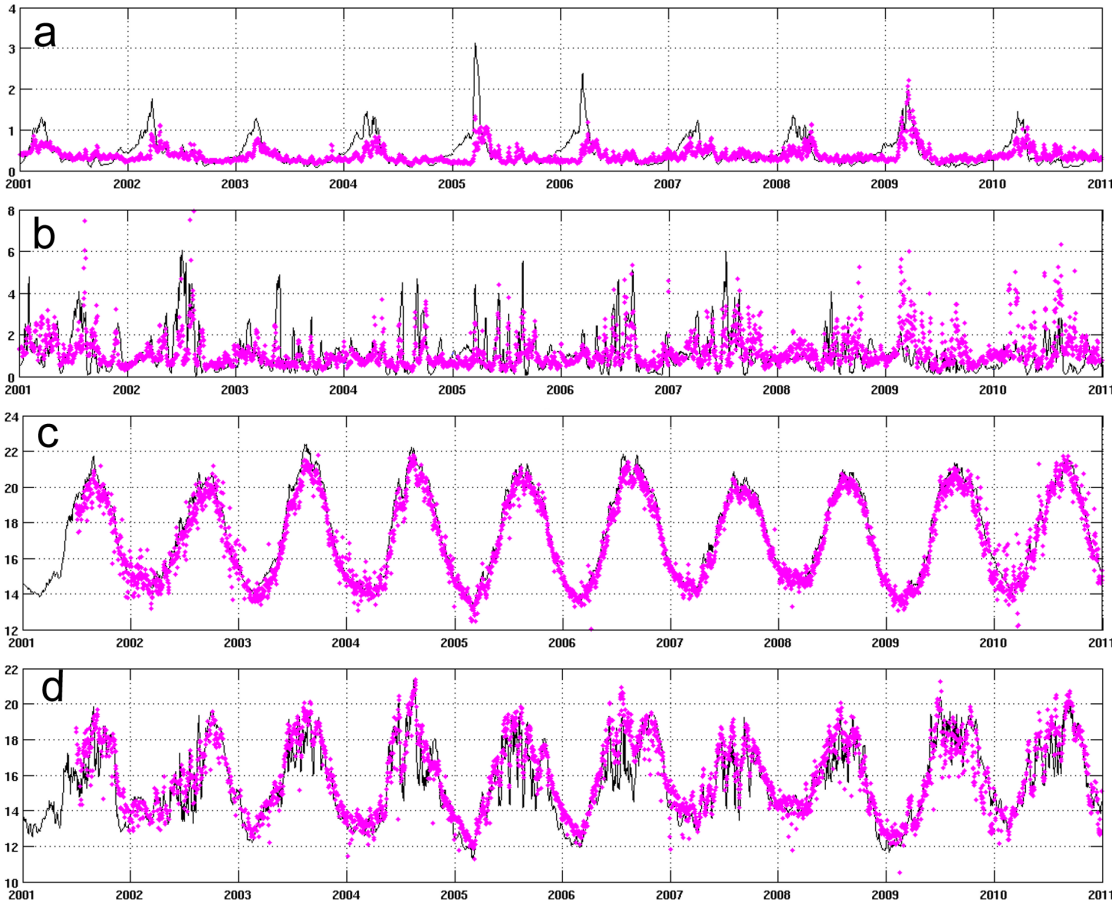

Figure 6.3: Time series of daily surface [Chl] (mg m^{-3}) and SST from model outputs (solid line) and satellite observations (dots): a) domain averaged [Chl]; b) central shelf (box I Fig.6.1) averaged [Chl]; c) domain averaged SST; d) central shelf (box I Fig.6.1) averaged SST.

Table 6.1 presents statistics that quantify the model ability to reproduce the observed (satellite derived) [Chl] interannual variability for the period 2001-2010. All the indices showed a considerable variability among years, which indicated that model-satellite differences were not constant, and varied for particular years. Still, general trends for model-satellite comparisons could be distinguished. Regardless of the mentioned overestimation in modeled [Chl] during the spring bloom (Fig. 6.3a), the model bias and skew indicated that the model tended to slightly underestimate surface [Chl] for most part of the year (negative values in Table 6.1). Underestimation was particularly detected in the years 2009 and 2010, coinciding with the shifts already discussed for the shelf. However, it should be noted that the years 2009 and 2010 still had a good skill, because of the good model-satellite match on the spring bloom. On the other hand, the year 2005 stand out for the highest positive bias, skew and rms, as expected for the strong spring bloom simulated (Fig. 6.3a). Model skill pointed to 2009, 2004, and 2003 as the years of best model-satellite correspondence, whereas 2006, 2007, and 2005 as years of worst

correspondence.

	bias	rms	skew	skill
2001	-0.277	0.183	-0.046	0.716
2002	-0.08	0.207	0.031	0.64
2003	-0.191	0.15	-0.013	0.786
2004	0.003	0.164	0.039	0.805
2005	0.057	0.35	0.101	0.617
2006	-0.026	0.283	0.085	0.532
2007	-0.226	0.182	-0.035	0.574
2008	-0.143	0.203	-0.037	0.639
2009	-0.335	0.239	-0.061	0.853
2010	-0.365	0.231	-0.055	0.637

Table 6.1: Error statistics of model-satellite comparisons for domain averaged daily [Chl] time series.

It should be considered that some uncertainties are also associated to the satellite observations (Gregg and Casey, 2007). These can be originated by errors in the algorithm estimations of [Chl], as the overestimations reported in the coastal zone when using SeaWiFS data (Le Fouest et al., 2006). In the shelf region of the Iberian Peninsula, [Chl] overestimations have also been reported when using MERIS and MODIS data (case 1 waters) (Oliveira et al., 2007). On the other hand, underestimations were detected during the validation of the method used for merging SeaWiFS/MODIS/MERIS data (dataset used here) with in situ data in the west French coast (Saulquin et al., 2011).

6.4.2 Main modes of [Chl] variability: EOF analysis of model and satellite observations

An EOF analysis was carried out to split the modeled and remotely sensed [Chl] variability into statistical modes that would give an initial idea of the processes that contribute for that variability. Also, comparing the EOF analysis of model outputs and observations would let us evaluate to what extent was the model able to reproduce the observed variability. Three [Chl] EOFs were retained for analysis, which explained more than 90% of modeled variability and more than 85% of remotely sensed variability. For each EOF, the spatial variability (spatial field) and its associated time series of amplitude (temporal mode) are presented (Figs. 6.4,6.5,6.6). An EOF analysis of the model SST is presented in Cordeiro Pires et al. (in preparation).

The first mode of the EOF analysis of [Chl] explained 69.25% of [Chl] variability in the model and 46.32% of variability in the remotely sensed [Chl] (Fig. 6.4). The latter percentage was coincident with the first EOF mode found by Miles and He (2010)

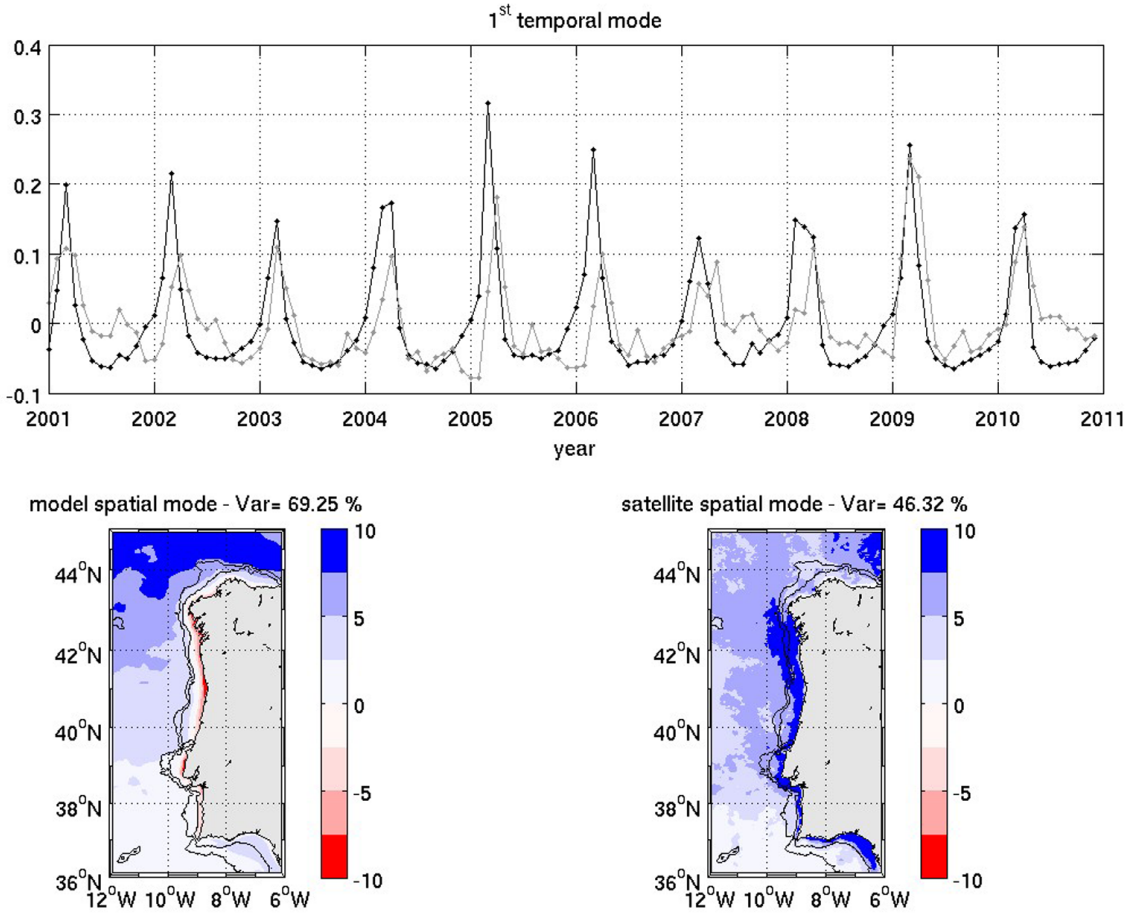

Figure 6.4: First mode of temporal (upper panel) and spatial (lower panel) variability from the EOF analysis of domain averaged surface [Chl] (monthly means): comparison between model outputs (black line in temporal mode, left panel in spatial field) and satellite observations (gray line in temporal mode, right panel in spatial field). Points represent months from January to December.

(46.35%) when analyzing satellite (MODIS) [Chl] data for the South Atlantic Bight over 2003-2008. The temporal evolution showed that this mode captures the seasonality of the spring bloom (March-April) in both model results and observations, which followed the seasonal solar heating cycle of the water column, reflected in the MLD seasonality (Fig. 6.7). The maximum model MLD generally occurred in February (winter mixing), which was confirmed by the MLD obtained from ARGO floats, and followed by the spring thermal stratification in March-April (Fig. 6.7), coinciding with the increase in [Chl] detected in the temporal mode of the EOF 1 (Fig. 6.4). The comparison of the MLD derived from model results and ARGO profiles showed that the mean winter mixing over the domain tended to be deeper in the observations than in the model, in particular for years of deepest MLD (Fig. 6.7). The EOF 1 (Fig. 6.4) confirmed the trend for the anticipation ($\sim$1 month) of the spring bloom in the model mentioned in section 6.4.1. The same

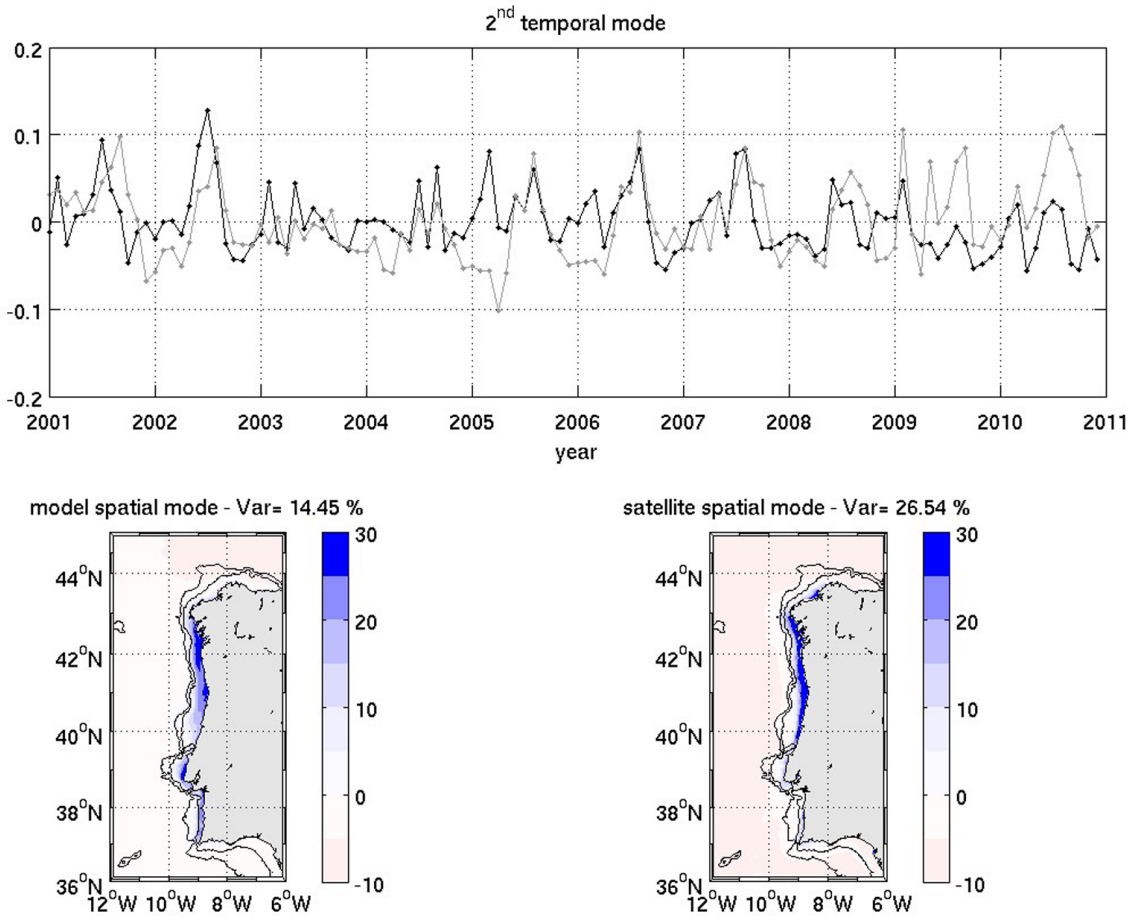

Figure 6.5: As for Fig. 6.4 but for the second mode of the EOF analysis.

anticipation was generally detected on the spring shoaling of the MLD in the model, with MLD values in March usually shallower in the model than observed, given that the shoaling started from a shallower winter mixing (Fig. 6.7). This pointed out to the shallower MLD in March as the possible reason for the bloom anticipation. The spatial field revealed that the variability explained by EOF 1 affected mainly the offshore region, with a noticeable latitudinal gradient in the model, whereas this gradient was less pronounced in satellite observations, where the variability affected also the shelf (Fig. 6.4). The temporal mode of the satellite EOF also revealed a smaller peak which occurred between August and November, i.e., late summer or autumn. The peak was not present in the temporal mode of the model EOF. The timing of the signal would suggest the increase in [Chl] associated with the autumn bloom (Castro et al., 1997; Álvarez-Salgado et al., 2003; Silva et al., 2009). However, this peak in the satellite temporal mode had frequently a negative or nearly zero value, which multiplied by the positive value of the spatial field would actually indicate a negligible effect increasing [Chl]. The difference in the percentages explained by the model and by the satellite observations in EOF 1 indicated that the seasonal variability

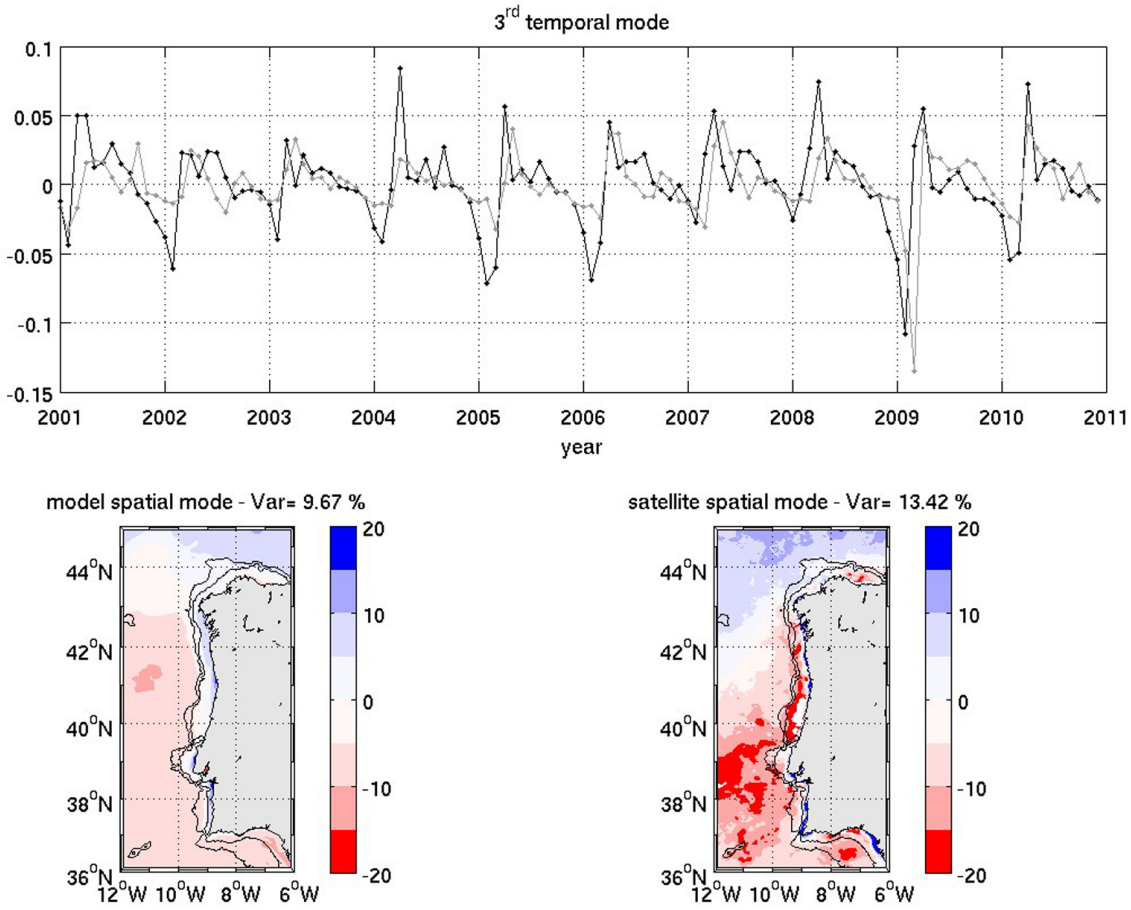

Figure 6.6: As for Fig. 6.4 but for the third mode of the EOF analysis.

associated to the spring bloom dominated the variability in model outputs, whereas, still being the most important, it was lower in satellite data, which variability is more distributed among the following EOFs.

The second EOF explained 14.45% of modeled vs. 26.54% of observed [Chl] variability (Fig. 6.5). The temporal and spatial fields indicated that this variability accounted for the increase in [Chl] during the spring-summer upwelling season (April-September) over the shelf, which is driven by the upwelling of subsurface cold and nutrient rich ENACW due to prevailing northerly winds along the Iberian margin (Fig 6.2, upper panel). The increase in [Chl] was higher in the model than in observations, and affected a higher extension of the shelf (Fig. 6.5). The temporal mode showed a variable intensity of the spring-summer upwelling signal from year to year, as expected from the known variable intensity and persistence of the northerly winds (e.g. Álvarez-Salgado et al., 2002). For example, years of strong and persistent northerly winds, such as 2001, 2002, and 2006 (Fig 6.2) were also years with a noticeable [Chl] signal of the temporal EOF 2 (Fig. 6.5), whereas years

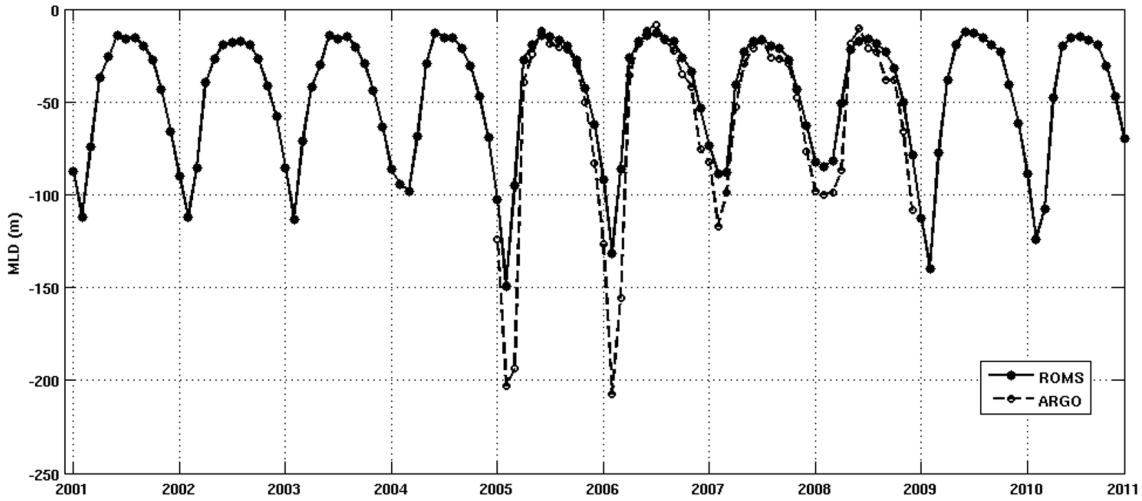

Figure 6.7: Monthly time series of ROMS domain averaged mixed layer depth (m) for the period 2001-2010 (solid line) and average mixed layer depth obtained from Argo floats data available for the same area (n>200 for every year) for the period 2005-2008 (dashed line) (Holte et al., 2010).

of more variable winds, such as 2003 and 2004 (Fig 6.2) presented an intermittent [Chl] signal of the temporal EOF 2 over the upwelling season (Fig. 6.5). An analysis of SST and wind patterns in western Iberia by Sánchez et al. (2007) showed that at the regional-scale most modes showed upwelling-downwelling patterns, with the strengthening and weakening of upwelling-favorable northerlies having a significant relationship with the North Atlantic Oscilation (NAO) phases (interplay between the Azores High-Iceland Low). The spatial field of EOF 2 also revealed a slight decrease of the offshore [Chl] in summer.

The third EOF mode explained 9.67% of modeled [Chl] variability and 13.42% of the observed variability (Fig. 6.6). The temporal and spatial analysis pointed out to a decrease (increase) in [Chl] in winter (spring) in the northern offshore region of the domain, both in model outputs and observations. A similar pattern also affected the shelf, in particular the innermost part. There was an opposite pattern in the offshore region south of $\sim$43° N, i.e., a progressive increase in [Chl] in winter and a subsequent decrease after February-March. This variability suggested it might be associated to the cycle of winter vertical mixing, which is maximum in February for the Iberian region as already mentioned (Fig. 6.7), and would tend to decrease [Chl] north of $\sim$43° N by a dilution/light limitation effect also known as a *phyto-convection* mechanism, proposed for several oceanic regions and also described for the NW Iberia oceanic region in Perez et al. (2005). The late winter (February-March) MLD in the Iberian margin reaches 150 m south of 43° N, and more than 300 m to the north (Arhan et al., 1994; Álvarez-Salgado et al., 2003), which is coincident with the latitudinal limit found in the spatial field of EOF 3.

South of that latitude, the deepening in MLD throughout winter to relatively shallow depths seemed to favor [Chl] increase, by providing new nutrients to the surface after the summer depletion. The negative peak of this winter signal in the model EOF 3 (February) tended to precede in 1 month the peak on the satellite EOF 3 (March) (Fig. 6.6, upper panel). Thus, in the model, the winter [Chl] minimum in the North (relative maximum in the South) tended to be coincident with the time of deepest MLD, whereas it was 1 month delayed in observations. It is likely that, as discussed for EOF 1, a shallower model MLD in March than observed caused an early increase in [Chl] in the North, and an early decrease in the South. After this, a positive peak in the model EOF 3 appeared in spring (April), generally also preceding in 1 month the corresponding peak of the satellite EOF (May). Again an opposite spatial pattern occurred, here corresponding to a [Chl] increase in the northern part of the region, and to a [Chl] decrease south of $\sim$43° N. The time and spatial sequence described suggested that the spring signal captured in EOF 3 corresponded to the second stage of the spring phytoplankton bloom detected in EOF 1. In this stage there was a 'displacement' of the bloom from South to North, with [Chl] progressively decreasing south of $\sim$43° N and progressively increasing to the north of that latitude. The described differences between the time evolution of [Chl] in the northernmost part of the region and the rest of the region supported the idea that the ocean off West Iberia could be divided in two distinct biogeographic provinces following the classification of Longhurst (1998): Most of the region would present characteristics of the Eastern North Atlantic Subtropical Gyre (NASTE), whereas the region to the north of $\sim$43° N would present characteristics of the North Atlantic Drift Province (NADP). Lévy et al. (2005) also described different production regimes in an oceanic region between 16-22° W along West Iberia, characterized by a changing effect of the winter MLD in [Chl] from North to South.

On the other hand, Peliz and Fiuza (1999) found the highest [Chl] for both the oceanic and the shelf region along western Iberia in winter, from an analysis of CZCS images. They argued that this apparently contradiction with what is generally accepted (spring [Chl] maximum) may be caused, among other reasons, by multiple scattering not been corrected by the algorithm employed. Although this is a likely reason for their high [Chl] over the shelf, the offshore maximum detected might not be so strange, at least south of 43° N, considering the February/March increase in [Chl] detected in this EOF analysis of model/satellite data. Oliveira et al. (2007) supported that, for the inner Iberian shelf, some satellite products tend to overestimate [Chl] in winter. If this would be the case with the satellite data used here, it would help to explain the negligible winter decrease in shelf [Chl] in satellite EOF 3, in contrast with the model EOF 3. Unfortunately, we do not have enough in situ [Chl] data to evaluate this. The coastal signal revealed by the model spatial EOF 3 may also be a signature of the convergence conditions typical of this

season, contributing for the downwelling of chlorophyll-a. On the other hand, [Chl] may also increase in winter due to sporadic upwelling events and the presence of the WIBP originated by accumulated river runoff (Peliz et al., 2002), which supplies stratification conditions suitable for phytoplakton growth (Ribeiro et al., 2005), although this did not seem to be detected by the EOF 3 of the model.

6.4.3 Cross-correlation analysis

The correlograms of the cross-correlation analyses between the temporal modes of each of the three [Chl] EOFs described and several hydrographic descriptors (model data for both time series) are presented in Figs. 6.8, 6.9 and 6.10.

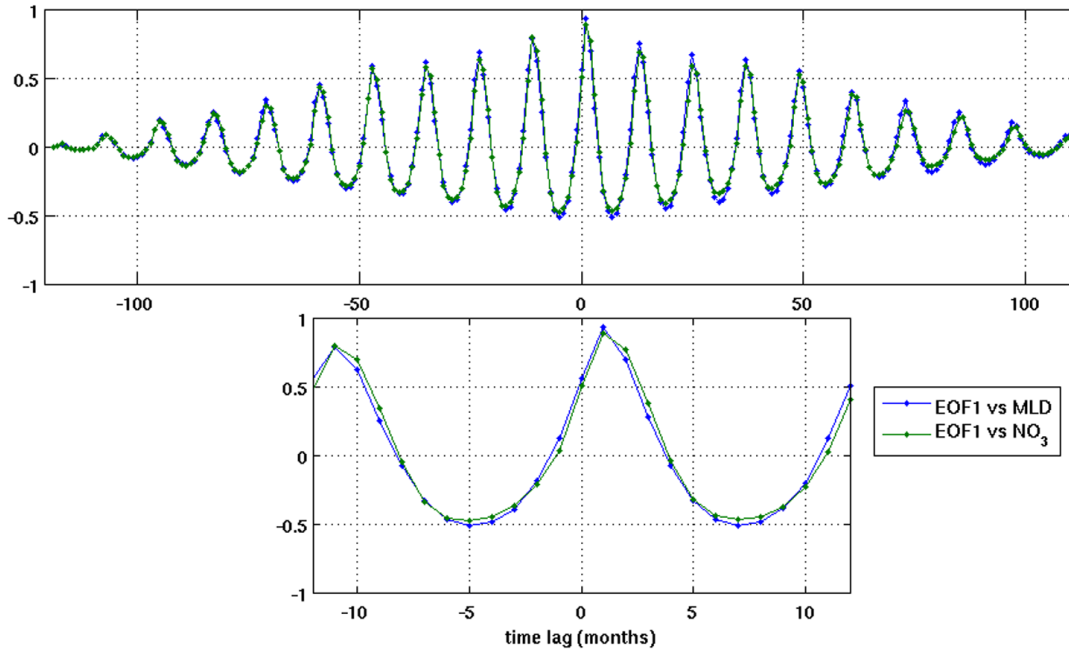

Figure 6.8: Cross-correlation between the *spring EOF* time series and the monthly mixed layer depth and the monthly NO_3. Upper panel: cross-correlation for the 10 years time series. Lower panel: zoom showing cross-correlation out to 12 months.

The first EOF mode, which we named the *spring EOF*, was tested against the monthly MLD, calculated from the temperature model outputs (section 6.3.2). For a correct interpretation of the correlations it should be noted that MLD time series for the cross-correlation analysis had positive values. The second EOF, named the *upwelling EOF*, was tested against the monthly meridional component of the wind over the shelf (9.5° W, 40.5° N), and against the monthly SST (subtracting the seasonal cycle) at the same shelf location, which we selected as representative of the coastal wind variability. Finally, we

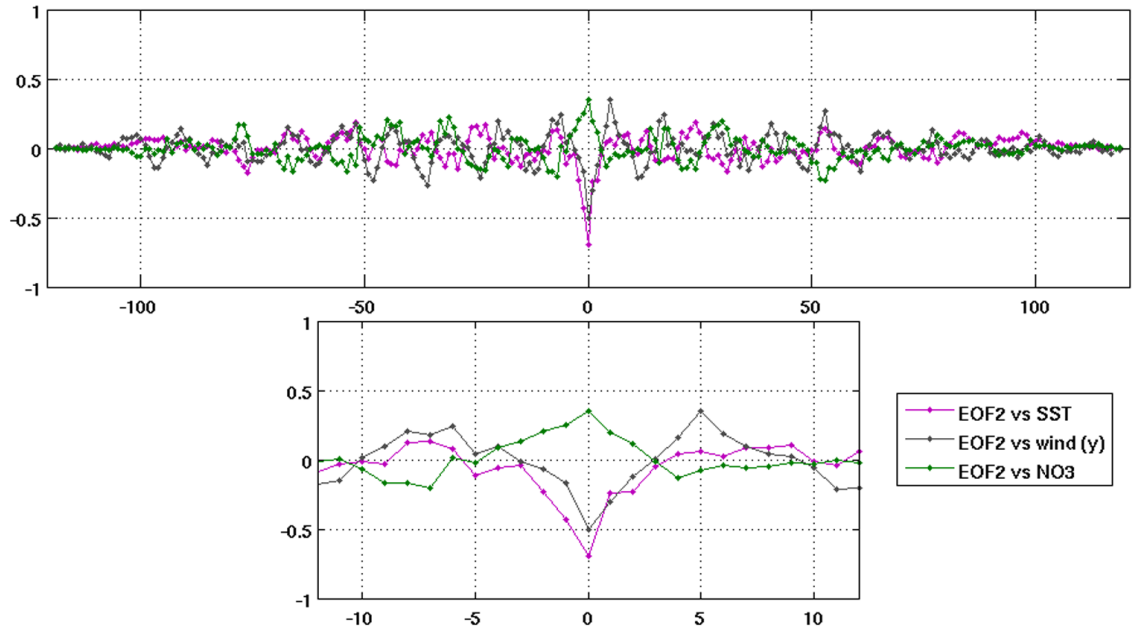

Figure 6.9: Cross-correlation between the *upwelling EOF* time series and: (1) the monthly SST at the shelf (40.5° N 9.5° W), after subtracting the seasonal cycle; (2) the monthly meridional component of the wind at the shelf (40.5° N 9.5° W); and (3) the monthly NO_3 after subtracting the seasonal cycle. Upper panel: cross-correlation for the 10 years time series. Lower panel: zoom showing cross-correlation out to 12 months.

performed a cross-correlation between the third EOF, to which we refer as the *winter EOF*, and the monthly MLD; and the monthly river Douro outflow (the most mighty river in the Atlantic Iberian margin). In order to complement the physical descriptors of hydrography, and try to relate them with the nutrients availability, for each of the three EOFs a cross-correlation with the monthly surface NO_3 was performed. The domain averaged surface NO_3 time series was used for comparison with the *spring EOF* and the *winter EOF*, whereas the time series of NO_3 over the shelf (9.5° W, 40.5° N) was compared to the *upwelling EOF*.

The cyclic correlation in the 10 years correlograms, particularly for the *spring EOF* (Fig. 6.8 upper panel), revealed the well defined seasonal nature of the EOF and the hydrographic descriptor studied, showing a correlation > 0.5 out to 4 years lag. A strong positive correlation was found between the *spring EOF* and NO_3 at time lag 1 month (Fig. 6.8). A similar correlation was detected between this EOF and the monthly MLD also at time lag 1 month, corroborating that the spring bloom in the model tended to occur one month after the maximum MLD, usually reached in February (Fig. 6.7). The coincidence of the NO_3 and MLD correlations indicated the co-occurrence of the maximum surface NO_3 concentration and the maximum MLD one month before the spring bloom. However,

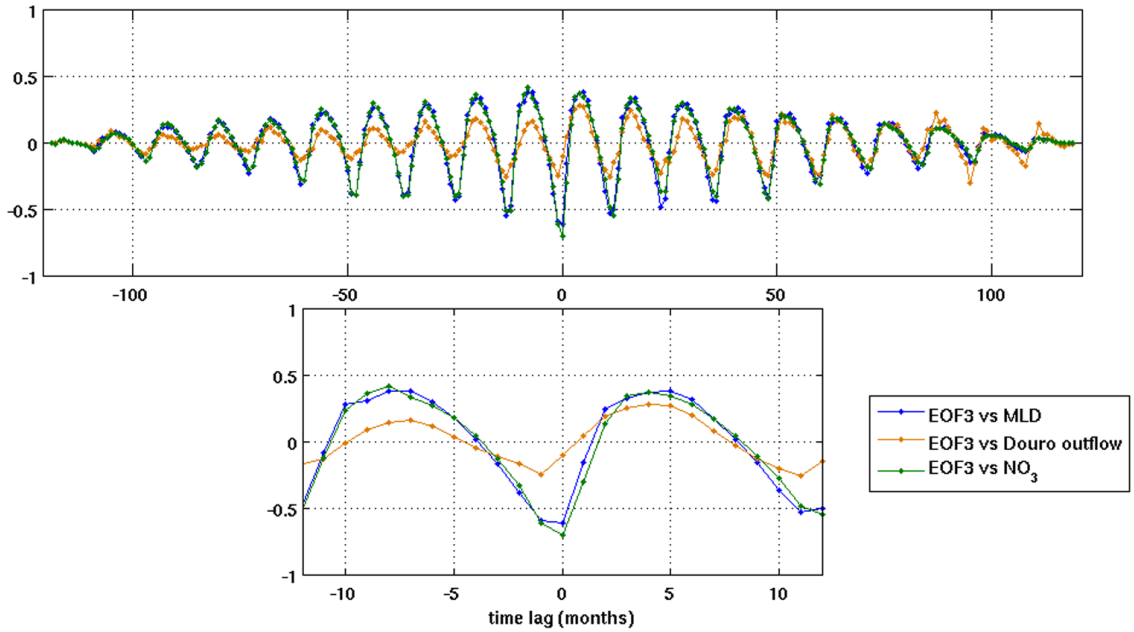

Figure 6.10: Cross-correlation between the *winter EOF* time series and: (1) the monthly mixed layer depth; (2) the monthly river Douro outflow; and the monthly NO_3. Upper panel: cross-correlation for the 10 years time series. Lower panel: zoom showing cross-correlation out to 12 months.

as previously discussed, it seemed that the shoaling of the MLD in the model from a less deep maximum vertical mixing reached shallower values in March than observed, resulting in stratification about 1 month earlier, the same anticipation detected in the spring bloom. Therefore, we expect the real lag to be more approximate to 2 months. Still, the correlation found suggested a relationship between the winter mixing and the the intensity of the subsequent spring bloom, as also proposed by Follows and Dutkiewicz (2001) and Waniek (2003) from model results. This idea was well exemplified for the years 2005, 2006, and 2009 when maxima in MLD were reached (Fig. 6.7), coinciding with the years of model [Chl] maxima in the spring bloom (Fig. 6.3a). However, for 2005 and 2006 the bloom observed from satellite data was not as intense as in the model, in spite of the deeper MLD observed from ARGO floats, which we think is related to the referred anticipation of the March stratification in the model. It is hypothesized that the better model-satellite [Chl] correspondence of 2009 was related to an earlier stratification than usual after the winter mixing (based on ARGO profiles, not shown). A positive correlation was also found, at 2 months and 0 time lag, between both the MLD and NO_3 and the *spring EOF*. Figure 6.11 (a) showed the quite equal distribution of this 1 month-lag correlation of the *spring EOF* and the MLD, although with the northern region presenting the highest correlations. The low correlation observed in the shelf region is

not significant, because there was a considerable reduction of the data points with MLD values in the shelf. This was a consequence of the imposition of a minimum of 10 m in the calculations of the MLD (section 6.3.2), which removed a considerable number of points from the shelf, limiting the point to point matches of the spatial comparison. To overcome this, a spatial mean of the monthly MLD was calculated for an area in the shelf (box I; Fig. 6.1) and a cross-correlation analysis with the *spring EOF* performed. We obtained a correlation of 0.9 at time lag 1 month, very similar to that obtained for the domain averaged MLD (Fig. 6.8), corroborating that in spite of what may be suggested by Fig. 6.11a the correlation occurred also for the shelf region.

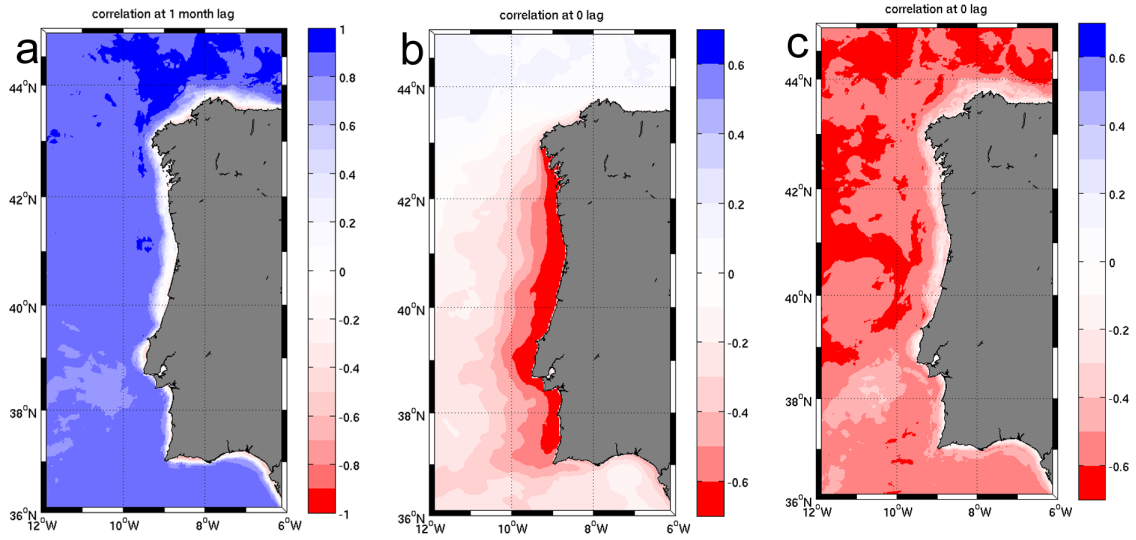

Figure 6.11: Map of correlation coefficients between: (a) *spring EOF* and MLD at 1 month lag; (b) *upwelling EOF* and SST at the shelf (40.5° N 9.5° W), after subtracting the seasonal variation, at 0 lag; (c) *winter EOF* and MLD at 0 lag.

Figure 6.9 shows the correlogram between the temporal mode of the *upwelling EOF* of [Chl] and several hydrographic descriptors. A maximum negative correlation (more than -0.6) was found with the SST over the shelf at 0 time lag (after subtracting the seasonal sinusoidal signal of the SST which accounted for more than 90% of the variability; Cordeiro Pires et al. in preparation), supporting the idea that the second source of variability of [Chl] in the Iberian margin was related with the periodic upwelling of cold and nutrient rich ENACW along the Iberian shelf. Note also the positive correlation with NO_3 at 0 lag. The spatial distribution of this correlation (Fig. 6.11 b) clearly supported the same conclusion. The correlation with the monthly meridional component of the wind (negative sign) over the shelf was similar to that of the SST, as expected given that the spring-summer upwelling period in western Iberia is known to be driven by prevailing northerly winds (Wooster et al., 1976; Fraga, 1981), increasing [Chl] in the shelf. Still, the correlation coefficient was not

as high as it would be expected, attributable to the fact that most of the wind variability is associated to event time scales (< 30 days), with the monthly cycle retaining a low intensity signal (Álvarez-Salgado et al., 2003).

The correlogram between the *winter EOF* and the monthly MLD revealed a negative correlation of -0.6 at time lag 0 (Fig. 6.10), indicating a co-occurrence of the winter deepening (spring shoaling) of the MLD and a decrease (increase) in [Chl], for the northern part of the domain. The opposite was true for the rest of the region, i.e., a co-occurrence of the winter deepening (spring shoaling) of the MLD and an increase (decrease) in [Chl], since as described in the previous section the EOF 3 captured opposite patterns of [Chl] to the north and south of $\sim$43° N. A similar negative correlation was found with NO_3 at 0 time lag, indicating the coincidence of the increasing NO_3 concentration and the decreasing [Chl] with the winter MLD deepening (opposite south of 43° N). A slightly lower correlation occurred also at time lag -1 month between the *winter EOF* and both the MLD and NO_3, which suggested that the NO_3 concentration was still high one month after the [Chl] minimum in February (winter mixing), whereas it was reduced by phytoplankton consumption as we moved to the South. The 0 time lag correlation between the *winter EOF* and the MLD was spatially distributed, but showing a higher correlation in some parts of the northern half of the domain (Fig. 6.11 c). As explained for the *spring EOF* a low correlation was found over the shelf, but it cannot be taken as representative. Trying otherwise to find an explanation for the shelf signal of the *winter EOF* in the model, overcoming the referred limitation of the data points with MLD values, a spatial mean of the monthly MLD for the shelf box I (Fig. 6.1) was calculated and a cross-correlation analysis with the *winter EOF* performed. We found a correlation coefficient of -0.6 at time lag 0, the same correlation found for the domain averaged monthly MLD (Fig. 6.10). Additional explanations for the shelf signal of the *winter EOF* in the model were explored, namely the cross-correlation with the monthly river Douro discharge (taken as representative of the variability in the continental runoff to the Iberian shelf for the studied period) was carried out (Fig. 6.10), however we did not find a correlation.

6.4.4 [Chl] variability in the water column

The 3D model results allowed to study the biological variability in the water column of the Iberian margin. We focus on the shelf, where short-term highly variable hydrographic conditions (e.g. upwelling, downwelling, continental runoff) overlap the seasonal atmospheric/oceanographic changes, and seem to influence the short-term changes in [Chl] (as seen in Fig. 6.3 b,d). In particular, a location in the NW Iberian shelf was selected for

comparisons with 1-year observations from a sampling station (section 6.3.2; see position in Fig. 6.1). This allowed for model evaluation in the water column, and subsequently describe the 10-years interannual [Chl] variability from model results at that location.

6.4.4.1 Comparison of ROMS outputs with 1-year in situ observations in the NW Iberian shelf

The ability of this ROMS configuration to reproduce the thermohaline properties at this location for the same observational dataset was already discussed, and found satisfactory, in Reboreda et al. (in revision). Therefore, for simplification, we omit here salinity comparisons and refer just to temperature for describing the hydrographic evolution.

Figure 6.12 presents the observed (a, b, c, d) and modeled (e, f, g, h) water column evolution of temperature, [Chl], NO_3 and NH_4 at a location in the NW Iberian shelf (Fig. 6.1) between May 2001-April 2002. The seasonal and short-term variability of hydrographic conditions, as represented by the temperature variability, was well captured by the model, which showed temperature values very similar to observations (Fig. 6.12 a, e).

The model was able to reproduce the recurrent upwelling episodes of the spring-summer period (May-September 2001), breaking the thermal stratification and bringing cold and nitrate rich subsurface ENACW to the surface (Fig. 6.12 a, e). The higher temporal resolution of the model (daily) allowed a clearer separation of these episodes. The model reproduced the increase in [Chl] immediately after these episodes and the subsequent decrease with the relaxation of the upwelling conditions, even though the [Chl] was higher in model results during most episodes (Fig. 6.12 b, f). The latter could be, in part, a consequence of the referred higher temporal resolution of model results, given the rapid changes that usually occur in [Chl] in this periods, as showed by the daily surface [Chl] in satellite time series (Fig. 6.3 b). Still, some higher [Chl] in the model could be attributable to the higher NH_4 simulated by the model (Fig. 6.12 d, h). It should be noted that the model lacked a dissolved organic nitrogen (DON) compartment, so the modeled NH_4 distribution was probably representing in part the DON distribution. On the other hand, the high NO_3 observed in the subsurface cold ENACW was well reproduced by the model (Fig. 6.12 c, g). At the end of September a strong downwelling event occurred, that was also appropriately reproduced by the model, as a consequence of the seasonal shift in the wind direction to southwesterlies, which brought warm ($>$17ºC) and nitrate poor ($<$1 mmol N m^{-3}) surface offshore water into the shelf (Fig. 6.12 a, c, e, g). It was associated to a pronounced decrease in [Chl] as shown by observations and model results, which

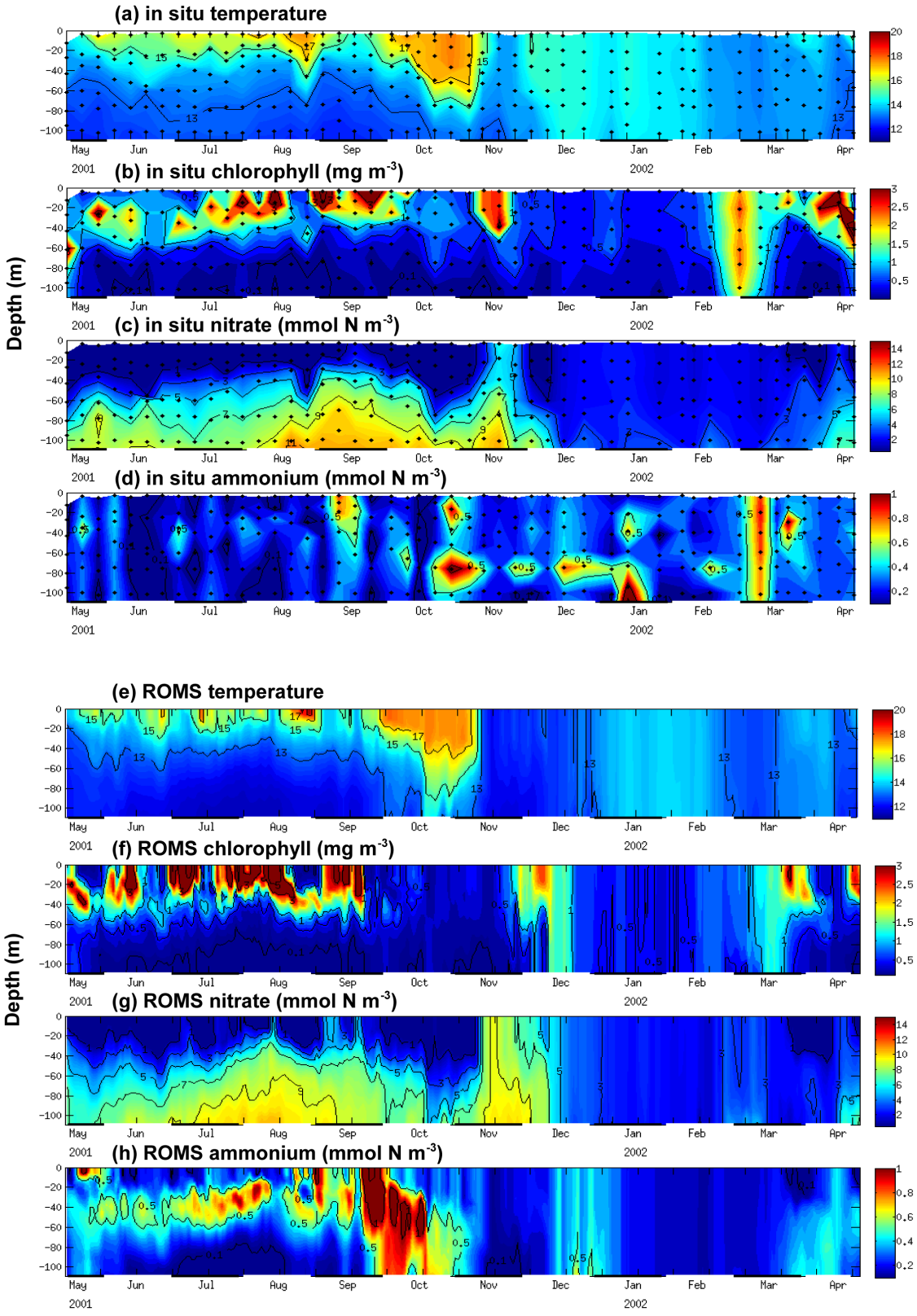

Figure 6.12: Hydrographic/biogeochemical data observed at a sampled station in NW Iberia (Fig. 6.1) between May 2001-April 2002 (a, b, c, d) compared with model outputs for the same period (e, f, g, h).

presented similar concentration values (Fig. 6.12 b, f) and an increase in NH_4 in the water column (Fig. 6.12 d, h), presumably due to downward advection of organic matter and its subsequent mineralization. The out-of-season strong upwelling event of November 2001, which introduced cold and highly nitrate rich subsurface ENACW into the sea surface, causing an unusual strong phytoplankton bloom for this epoch was also reproduced by the model, although the [Chl] maxima was delayed relative to observations (Fig. 6.12 a, b, c, e, f, g). After this event, the wind regime returned to the typical southwesterlies of this time of the year, coinciding with a warming of the water column due to the onset of the IPC over the Iberian slope, conveying warm and saline ENACW of subtropical origin (ENACWt). As pointed out in Reboreda et al. (in revision) the ENACWt simulated by the model was colder and less saline (not shown) than observed ENACWt in the beginning of winter. The dominant downwelling/IPC situation prevailed until February, characterized by low [Chl] ($\sim$0.5 mg m^{-3}) in both observations and model results (Fig. 6.12 b, f). During late February-March 2002 the model reproduced the winter mixing of the water column, driven by strong ocean-atmospheric interaction, decreasing the water temperature. Then, a first phytoplankton bloom occurred in the still homogeneous water column, before the spring thermal stratification, also reproduced by the model although with lower [Chl] and a delayed maximum. These kind of spring blooms in the absence of stratification have been reported as a possible consequence of deep penetration of light in relatively clear late-winter waters (Townsend et al., 1992). In late March, the model reproduced the haline stratification caused by a river plume (not shown), which seemed to coincide with a surface intensification of the bloom (Fig. 6.12 b, f). Finally, the thermal spring stratification developed in April, under upwelling favorable conditions, giving rise to a new phytoplankton bloom which seemed to be somehow weaker in the model.

6.4.4.2 Interannual variability : ROMS simulation of 10-years biogeochemical evolution in the NW Iberian shelf

ROMS outputs were used to reconstruct the water column [Chl] variability, together with other biogeochemical variables and thermohaline properties, at the shelf location just described (Fig. 6.1) for the 10 years period (2001-2010) (Fig. 6.13). Note that the detail of the variability is coarser here than for the description of 2001-2002, as a 30-day running mean was applied in order to compact the information for a much longer period and to make it easier to interpret. As expected, the spring-summer [Chl] (phytoplankton) blooms, driven by the upwelling pulses of cold and nitrate rich ENACW, were the main source of [Chl] variability throughout the years. Interannual differences in the upwelling intensity and persistence could be deduced from the temperature and [Chl] distribution, showing years

of clearly separated upwelling pulses, as 2005, and years of more persistent stratification, as 2003, when surface [Chl] was lower than usual (Fig. 6.13 a, b). Modeled [Chl] was also lower than usual in 2009 and 2010, but this has already been interpreted as a possible adjustment to the shift in the surface model forcing (section 6.4.1). Out-of-season strong upwelling events, such as that of November 2001, that can be captured with a 30-day running mean, did not seem to be frequent. The autumn shift to prevailing downwelling conditions was clearly detectable every year from the surface warming and the decrease in [Chl] (Fig. 6.13 a, b). This shift could be more abrupt, as in 2002 and 2006, or it could be more gradual, as in 2005. From that moment to the beginning of the next year (autumn-winter) the presence of the IPC over the slope was also reflected in the thermohaline properties of the shelf waters (more saline and warm; Fig. 6.13 b, c). This period was also characterized by a gradual increase in [Chl] until a phytoplankton bloom occurred, either coinciding with the maximum of vertical homogenization of the winter mixing (sharp temperature decrease), as in 2001 and 2003, or with the spring stratification, as in 2005 and 2006.

Trends in [Chl] and temperature, for the upper 10 m of the water column and the 10 m above the bottom, were studied at this shelf location for the period 2001-2010. Trends were calculated considering the annual anomalies and also the anomalies of the summer upwelling period (April-September) and the winter downwelling period (October-March) separately, and fitting them to a straight line. The slope of these regression analyses are presented in Table 6.2. There was a significant positive trend in temperature, considering the annual anomalies, both in the upper water column and in the bottom, however the trend was not significant when considering the upwelling/downwelling periods separately, except the bottom temperature for the upwelling period. A slightly negative trend was found in the upper water column [Chl], but it was not significant. Notice that the significant trends found for temperature should be taken with caution, because of the short period tested (10 years) and the change in the surface forcing used for model simulations of the last two years, with the implications already discussed.

	[Chl] (mg m^{-3} year^{-1})		**Temperature (ºC year^{-1})**	
	Upper 10 m	Bottom 10 m	Upper 10 m	Bottom 10 m
Upwelling season	-0.07	0.001	0.14	0.1*
Winter season	-0.02	0.0002	0.1	0.04
Annual	-0.04	0.001	0.09*	0.08*

Table 6.2: Trends in [Chl] and temperature for the upper 10 m of the water column and the 10 m above the bottom at the shelf station in Fig 6.1. Analysis based on annual, upwelling season (April-September), and downwelling season (October-March) anomalies fitting to a straight line. *$p < 0.05$

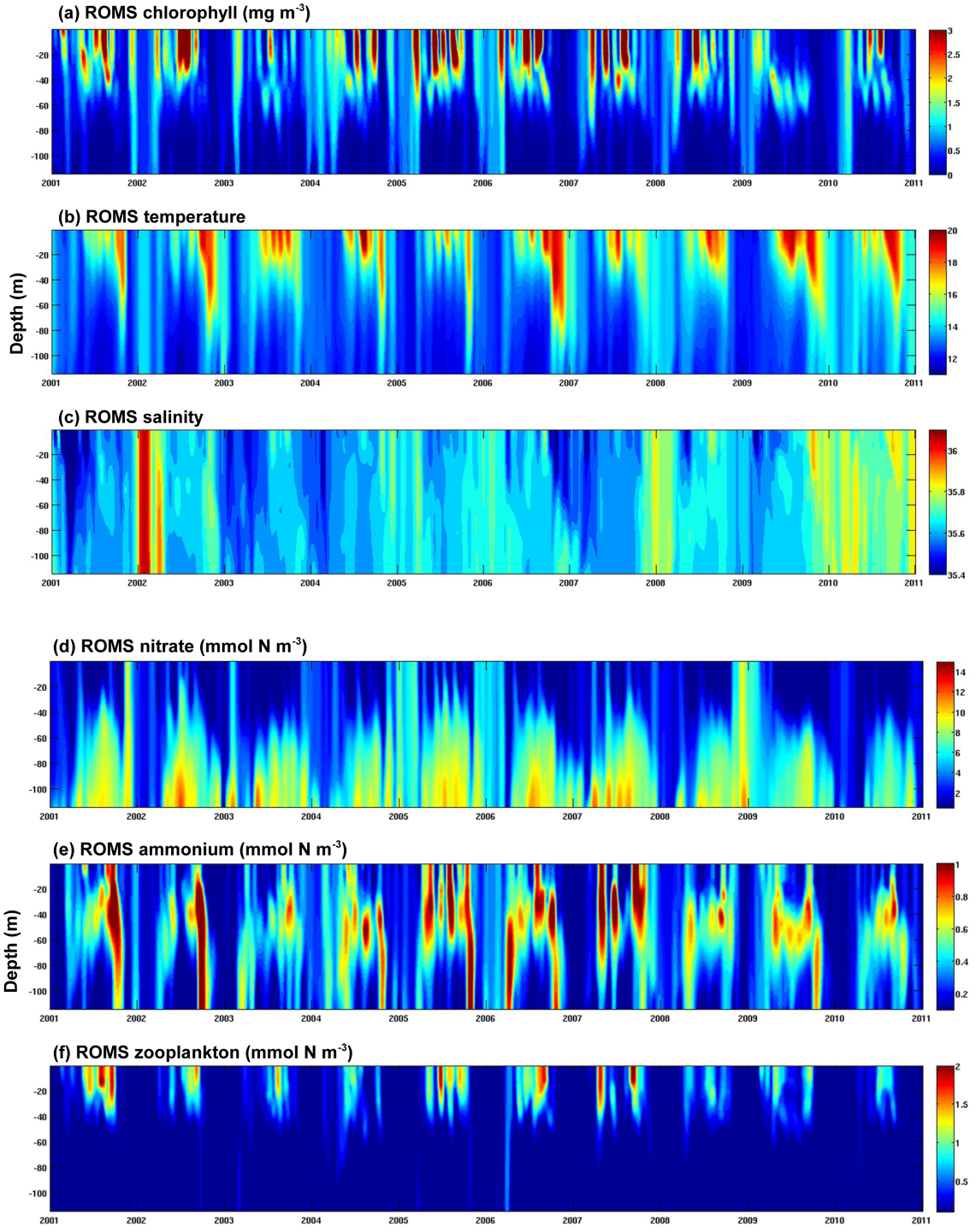

Figure 6.13: Interannual (2001-2010) model results (30-days running mean) for hydrography (temperature and salinity) and biogeochemistry (chlorophyll, zooplankton, nitrate and ammonium) at the same location of the DYBAGA station (Fig. 6.1).

6.5 Summary and conclusions

The capability of the ROMS configuration, coupled to a simple biogeochemical model, to reproduce the [Chl] variability in the study region has been satisfactorily tested. The model was able to reproduce the observed (satellite derived) seasonal variability on [Chl] at the sea surface in the Iberian margin for the decade 2001-2010, as well as the observed (sampling station) vertical short-term variability of [Chl], NO_3 and thermohaline properties on the shelf along 1-year cycle. It thus provides a useful tool, presenting potentialities for further research and as an operational product for the marine community. The model presented however some limitations that should be taken into account for future applications, namely the anticipation of the spring phytoplankton bloom in about 1 month, also presenting somewhat higher [Chl] than observed during the bloom, and slightly lower concentrations than observed along the rest of the year.

Three main modes of sea surface [Chl] variability were found for the western Iberia oceanic and shelf regions, both from EOF analysis of model results and satellite observations, which represented the seasonal variability in the region (monthly time scale). The first one, which we named the *spring EOF* because of the evident spring (March-April) signal in the temporal mode, explained 69.25% of [Chl] variability in the model and 46.32% of variability in the remotely sensed [Chl]. The second source of variability (EOF 2) explained 14.45% of modeled vs. 26.54% of observed [Chl] variability, and was found to be related to the spring-summer increase in [Chl] over the shelf during the upwelling season (*upwelling EOF*). The EOF 3 explained 9.67% of modeled [Chl] variability and 13.42% of the observed variability, and we named it the *winter EOF* because the strongest signal in the temporal mode was a minimum in winter (February), although it also presented a positive signal in spring (March-April). The cross-correlation analyses showed that the MLD had a strong positive correlation with the *spring EOF* at time lag 1 month, and a negative correlation with the *winter EOF* at 0 time lag. This revealed a possible double (and opposite) effect of the MLD on the seasonal evolution of [Chl] in the western Iberia. On one hand the deepening of the MLD during the winter mixing seemed to be related with the intensity of [Chl] increase (spring bloom) in the subsequent months, particularly in the northern part of the region, where the winter MLD gets deeper (up to 300 m). On the other hand, there seemed to be a synchronization of the winter MLD deepening (spring shoaling) and [Chl] decrease (increase) north of $\sim$43° N. South of that latitude the deepening of winter MLD coincided with a [Chl] increase, reaching a maximum in late winter/early spring (February-March), after which the [Chl] decreased as the MLD started shoaling (March-April) and the surface nutrients were used. At the same time, the bloom in the North was progressively intensified as the deep winter MLD disappeared by the

spring stratification, giving the impression of a South-to-North displacement of the bloom. Thus, the proposed opposite influence of the MLD on [Chl] would present both a time and a spatial dependence, supporting the existence of two production regimes off western Iberia, to the north and south of $\sim$43° N, with differing time evolution of [Chl]. Additionally, the summer upwelling production regime characterized the Iberian shelf, which for the 10 years time-span analyzed here was the second source of [Chl] variability.

The vertical [Chl] variability on the shelf showed the effect of this seasonal variability as well, with a noticeable spring-summer upwelling [Chl] increase and a decrease coinciding with the maximum winter mixing. However, the short-term variability in the shelf seemed to play a more relevant role, as expected, which needs do be further explored in future studies, taking advantage of the modeling possibilities demonstrated here.

Chapter 7

Overall conclusions and outlook

This section provides a general overview of the results, after particular conclusions for each chapter/paper have been presented. Some shortcomings detected in the model are commented. Finally, some future perspectives for the research are proposed.

A high resolution (3 km) 3D configuration of the Regional Ocean Modeling System (ROMS) has been satisfactorily coupled to three NPZD-type (Nutrient-Phytoplankton-Zooplankton-Detritus) biogeochemical modules for the Atlantic Iberian margin. The model domain included the coastal and adjacent oceanic region from the Gulf of Cádiz to north-west Iberia (Galicia) (34.5° N to 45.5° N and 5.5° W to 12.5° W, i.e., $\sim$1200$\times$600 km). Model results were validated by comparisons with remotely sensed data, in situ observational data, and values from the literature. This modeling approach allowed to have an integrated view of the time and space variability of the planktonic production and some biogeochemical properties of the system, limited so far for the difficulties of long time and space oceanographic samplings. Besides, one of the biogeochemical modules was implemented to a pre-existing operational oceanographic system, providing on-line information of chlorophyll concentration in the region (Chapter 4).

Over the oceanic part of the domain the seasonal changes in the phytoplankton biomass were parallel to the seasonal changes in the mixed layer depth (MLD), that determined the availability of nutrients and light for phytoplankton growth in what seemed to follow a classical Sverdrup's mechanism (Sverdrup, 1953) for temperate waters. Thus, from the first climatological approach (Chapter 3), the modeled seasonal evolution of chlorophyll concentration ([Chl]) showed that the spring phytoplankton bloom seemed to coincide with a steep shoaling of the MLD over the domain, as a consequence of confining the phytoplankton to a well-lit zone in which daily photosynthesis exceeds daily respiration. On the other hand, the statistical analysis performed for the interannual simulation of the

decade 2001-2010 (Chapter 6) revealed an opposite correlation of the monthly evolution of [Chl] and MLD to the north and south of about 43° N throughout winter-spring. There was a synchronization of the winter MLD deepening (spring shoaling) and [Chl] decrease (increase) north of ∼43° N, where the winter MLD gets down to 300 m. South of that latitude the deepening of winter MLD (down to 150 m) coincided with a [Chl] increase, reaching a maximum in late winter/early spring (February-March), after which the [Chl] decreased as the MLD started shoaling (March-April) and the surface nutrients were used. This supported the existence of two production regimes off western Iberia with differing time evolution of [Chl], and characterized by a changing effect of the winter MLD in [Chl] from North to South. Where the winter mixing is deeper (to the north) phytoplankton biomass would tend to decrease by a dilution/light-limitation effet, whereas the deepening in winter MLD to relatively shallow depths (to the south) seemed to favor phytoplankton biomass increase, by providing new nutrients to the surface after the summer depletion. Over the shelf, the short-term vertical analysis of the annual cycle for 2001-2002 showed the occurrence of an early spring phytoplankton bloom in the absence of water column stratification, both in model results and in situ observations, under upwelling favorable conditions, indicating that other event-scale mechanisms may influence the development of the bloom. The spring phytoplankton bloom was shown to be the main source of [Chl] variability along the annual cycle over the domain.

Similarly, the strong seasonality in the O_2 concentration of the upper water column (Chapter 5) is mainly controlled by the deepening and shoaling of the seasonal MLD from winter to summer. Ventilation of the water column in late winter (February-March) provides a massive influx of atmospheric O_2 to the water column. O_2 continues increasing throughout spring due to the seasonal phytoplankton bloom, reaching maximum values by that time. Minimum O_2 values are obtained in summer and autumn, periods of strong thermal stratification and O_2 consumption by remineralization. Still, a subsurface O_2 maximum at about 50 m, associated to a subsurface chlorophyll maximum, remains along the season. Bellow this upper layer, the O_2 distribution was related to the water masses present in the region. At ∼800-1000 m the conspicuous O_2 minimum was nearly coincident with the salinity maximum of the Mediterranean water.

The seasonal pattern found offshore for the phytoplankton biomass and O_2 generally applies to the shelf region, but here more variability is introduced by the intense hydrodynamics of the upwelling season (spring/summer), the poleward flow of ENACWt over the slope and shelf in autumn/winter and continental runoff. The phytoplankton spring bloom is followed by a coastal [Chl] maximum in summer associated to the dominant upwelling conditions, driven by northerly winds. This [Chl] increase througout the upwelling

season explained 14% of modeled (26% of remotely sensed) variability, representing the second source of [Chl] variability (Chapter 6). It was positively correlated to the nitrate concentration and negatively correlated to the SST, as it was a consequence of cold and nitrate rich ENACW rising to the photic layer along the shelf, inducing phytoplankton growth. Also, upwelled ENACW carries lower O_2 concentrations than the remnant coastal waters, although its nitrate content rapidly induces phytoplankton blooms that raise the O_2 concentration over the shelf.

Overlapped to the seasonal and interannual changes in atmospheric forcings (light intensity, wind stress, fluxes of heat) the regional oceanography influenced the spatio-temporal patterns of the oxygen concentration and plankton ecosystem. The regional circulation of central waters influences the O_2 distribution mainly by the interplay between the southward displacement of oxygen-rich ENACWp and the northward transport of oxygen-poor ENACWt by the IPC. Over the western shelf, the general north-to-south decrease in phytoplankton and zooplankton biomass during the summer upwelling period was shown to be parallel to a general decrease in the nitrate concentration and an increase in temperature and salinity of the upwelled water. This difference in nitrate availability was a consequence of the transition from the influence of ENACWp in the north to the influence of ENACWt in the south, supporting that in the Iberian western shelf there was a trend for better conditions for primary and secondary production in the north than in the south. This factor seemed to be independent of other morphological and bathymetic differences along the shelf, which influence on the phytoplankton production needs otherwise to be further explored.

Differences in the shelf width from north to south were also related to differences in the offshore export of organic matter, which was highest in the southern narrower shelf. Where the shelf was wider, there was a trend for detritus accumulation and intense mineralization overt the shelf bottom. This was reflected in negative oxygen anomalies and positive nitrate anomalies in the shelf bottom, an indication of organic matter degradation, particularly in summer and autumn. The hypothesis that the onset of the IPC over the slope in autumn limits the offshore export of organic matter enhancing in situ mineralization (Álvarez-Salgado et al., 1997, 2003) was supported by the model.

Despite the reasonably good agreement between the model results and satellite derived or in situ observations, during the validation some shortcomings were detected. Both in the climatological and interannual approach (Chapters 3 and 6) a trend for an anticipation (1 month) of the offshore spring phytoplankton bloom was detected (chlorophyll peak in March instead of April). This was found do coincide with an anticipation of the spring shoaling of the MLD in the model, with MLD values in March usually shallower in

the model than observed, given that in the model the shoaling started from a shallower winter mixing. This pointed out to the shallower MLD in March as the possible reason for the bloom anticipation. The modeled [Chl] during the bloom presented somewhat higher values than observed, although for the rest of the year there was a trend for slightly lower values. There was an apparent overestimation of modeled [Chl] in summer over the inner NW-shelf when using climatological winds (Chapter 3), which was attributed to an intensified upwelling in the model (typical SST bias of -1 to -2 ℃) due to the lack of wind stress drop-off near the coast. An overestimation of [Chl] was also detected in August 2011 over the SW-shelf when using the atmospheric model WRF as the surface forcing for the operational implementation (Chapter 4).

Some limitations of the model are known and further efforts are necessary to overcome this limitations to improve the model capabilities for future applications:

- Lateral boundaries for the biogeochemical variables need to be improved. The use of seasonal climatological information at the lateral boundaries (4 values/year) for the second domain (SD) is certainly a limitation for the model to properly reproduce the biogeochemical variability, particularly in the offshore region near the boundaries. More efforts to satisfactorily implement a biogeochemical model in the first domain (FD) are needed, so that it could give higher resolution information for the biogeochemical variables to the SD. Otherwise, an offline nesting to an eddy-resolving global model providing information for biogeochemical variables could be tried (e.g. NEMO http://www.nemo-ocean.eu).

- The use of constant nitrate concentration values for the rivers (although the total amount of nitrate varies with river flux) does not properly represent the nutrient input to the shelf from the continental runoff. Attempts to estimate at least seasonal patterns should be addressed. Also, the availability of realistic discharges of the main rivers is important to properly reproduce the shelf dynamics.

- Efforts to implement more complex biogeochemical models, including more plankton functional groups and nutrients (phosphate, silicate) or dissolved organic matter (e.g. PISCES, Aumont et al., 2003) would be advantageous for research applications.

The advance in the biogeochemical modeling of the the Iberian margin will also depend on the availability of enough in situ observational data for model validation. There is an evident need for more systematic sampling of biogeochemical information in the

region. The biogeochemical research will also benefit from synergies using field work and models.

After this first approach to the biogeochemical modeling of the western Iberia, which allowed to make a general characterization of the system and explore some physical-geochemical-biological couplings, it is proposed that the future research should focus on process-oriented studies and hypothesis testing. This would allow to address some research questions that need further clarification, such as:

- The influence of the continental runoff on the formation of phtyoplankton blooms over the shelf, particularly in winter.
- The biogeochemical consequences of the IPC flowing over the slope in autumn-winter, namely on the cross-shelf organic matter export and in situ mineralization.
- The surface offshore organic matter export through filaments during the summer upwelling.
- The effect of morphological and bathymetric differences, as well as wind stress variability, along the shelf.
- Response of the ecosystem to perturbations.

Appendix A

Biogeochemical model additional material

A.1 Derivation of the equation for the Phytoplankton Chlorophyll to Carbon ratio

The derivation of the equation for the phytoplankton chlorophyll-a to carbon ratio (θ) presented here is the same described in the supplementary material of Gruber et al. (2006). It is based in the considerations of the model of Geider et al. (1997). The source-sink term for phytoplankton, $SMS(Phyt)$, in the main text (Eq. 3.3),

$$SMS(Phyt) = \mu(PAR,T) \cdot \mu(N) \cdot Phyt - m_{PD}\ Phyt - g_{max}\ Zoo\ \frac{Phyt}{K_P + Phyt} \quad \text{(A.1)}$$

is converted into an equation for cellular chlorophyll-a with units of mg Chl-a m^{-3} by multiplying the growth term (first term on the right hand side) with a conversion factor

$$a = \frac{\mu(PAR,T) \cdot \mu(N) \cdot \theta_{max} \cdot r_{C:NPhyt} \cdot 12mg\ C(mmolC)^{-1}}{\alpha\ PAR\ \theta} \quad \text{(A.2)}$$

derived from the equation 4 in Geider et al. (1997) that estimates the proportion fo photosynthetically fixed carbon that is used in chlorophyll-a biosynthesis. The stoichiometric carbon to nitrogen ratio of phytoplankton, $r_{C:NPhyt}$, is assumed to be constant at 106:16. The remaining terms in equation A.1 are converted into chlorophyll-a units by multiplying each term by the present chlorophyll-a to nitrogen ratio in phytoplankton, Chl/P.

$$SMS(Chl) = \mu(PAR,T) \cdot \mu(N) \cdot Phyt \cdot a - m_{PD}\ Phyt\ \frac{Chl}{P} - g_{max}\ Zoo\ \frac{Phyt}{K_P + Phyt}\ \frac{Chl}{P} \quad \text{(A.3)}$$

The equation for the chlorophyll-a to carbon ratio (mg Chl (mg C)$^{-1}$) takes the form:

$$\theta = \frac{Chl}{Phyt \cdot r_{C:NPhyt} \cdot 12mg\ C(mmolC)^{-1}}. \tag{A.4}$$

Using the chain rule, the partial differencial equation for θ is obtained:

$$\frac{\partial \theta}{\partial t} = \frac{Phyt\ \frac{\partial Chl}{\partial t} - Chl\ \frac{\partial Phyt}{\partial t}}{Phyt^2 \cdot r_{C:NPhyt} \cdot 12mg\ C(mmolC)^{-1}}, \tag{A.5}$$

which governs the time and space distribution of this non-conservative scalar. The resulting source-sink term is

$$SMS(\theta) = \mu(PAR,T) \cdot \mu(N) \cdot \left(\frac{\mu(T) \cdot \mu(N) \cdot \theta_{max}}{\sqrt{\mu(T)^2 + (\alpha\ PAR\ \theta)^2}} - \theta \right) \tag{A.6}$$

as given in equation 3.6 in the main text.

A.2 Selection of parameter values

A.2.1 Trial runs/tuning

Most parameter values used in the $NChlPZD$, $NChlPZD + O_2$ and $N_2ChlPZD_2$ modules were those provided by default in the ROMS code. As a first approach, the sensitivity of the models to the different parameters was explored, and those parameters found to have a higher effect on model results were tuned in order to find an appropriate value to reproduce observed results in the study region. A literature review was conducted to find contrasted values for these parameters in other biogeochemical ocean modeling studies around the world. When tuned/literature values could not improve the results obtained with the default values, the latter were selected.

A.2.2 Optimization experience

For the $N_2ChlPZD_2$ model an attempt to make a more systematic selection of the parameter values was made. A data-assimilation framework was designed in collaboration with Dr. Diego Santaren (ETH, Zürich). Assimilated observations consisted of fortnightly profiles of chlorophyll and nitrate obtained during the DYBAGA project (May 2001-April2002, IIM-CSIC) at two observation sites in the NW Iberian margin (location in Fig. 5.6, Chapter 5). The optimization of the 1D configuration at the observational stations could improve the seasonal variability of the surface chlorophyll simulated by the 3D configuration within

the whole domain. However, this enhancement lead at the same time to an increased bias in the simulated annual means over the domain. For that reason, it was decided not to use the parameter values for the simulations with the $N_2ChlPZD_2$ model. Improvements observed in the local chlorophyll vertical profiles were otherwise promising for a local configuration of the model. Here, a brief exposition of the results is made.

Three types of optimizations were carried out using observations from: (**A**) A coastal station (150 m); (**B**) An oceanic station (1500 m); (**C**) Both stations at the same time.

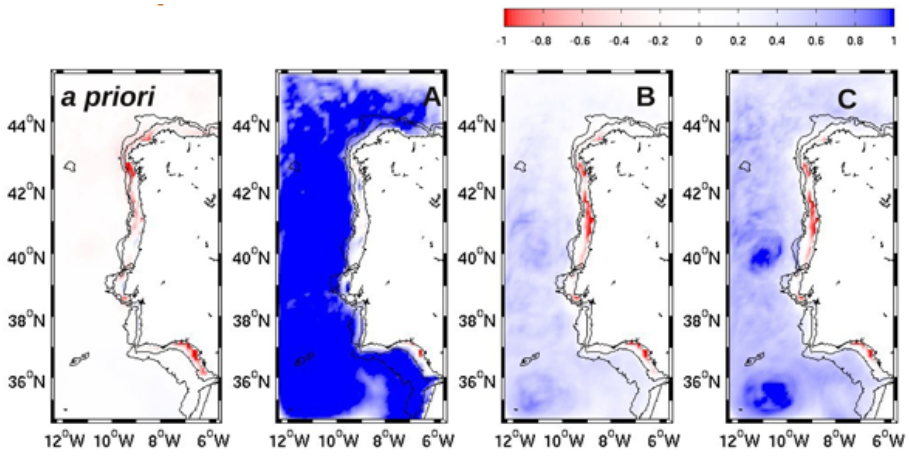

Figure A.1: Chlorophyll bias of annual mean (model vs SeaWiFS climatology) for the different optimization tests.

Chlorophyll profiles at the 2 stations were improved with the three optimizations (3D configuration), whereas nitrate profiles were already similar to observations prior to optimization. Annual biases were however introduced by all optimizations with respect to the prior simulation of surface chlorophyll concentrations (Fig. A.1).

The results of the optimization were presented in the form of a poster at the European Geophysical Union (EGU) Annual Conference 2012 (22th-27th April) in Vienna: *Reboreda R., Santaren D., Castro C. G., Álvarez-Salgado X. A., Nolasco R., Queiroga H., Dubert J. Solving the equation for the Iberian upwelling biogeochemical dynamics: an optimization experience*.

A.3 Spin-up of the biogeochemical variables

The time evolution of the volume averaged concentrations of the biogeochemical variables over the western Iberian model domain for 8 climatological years are presented (Fig. A.2). This time evolution shows the short time needed to reach a fairly stable annual cycle for the biogeochemical variables, given that the biogeochemical run started from an already stable hydrodynamic simulation. The year to year variations that were detected could only be attributable to the internal variability of the model, since the surface forcings used were climatological (i.e., without interannual variability). Model results presented for the climatological simulations (chapter 3 and chapter 5) were averaged over 6 climatological years in order to smooth this internal variability.

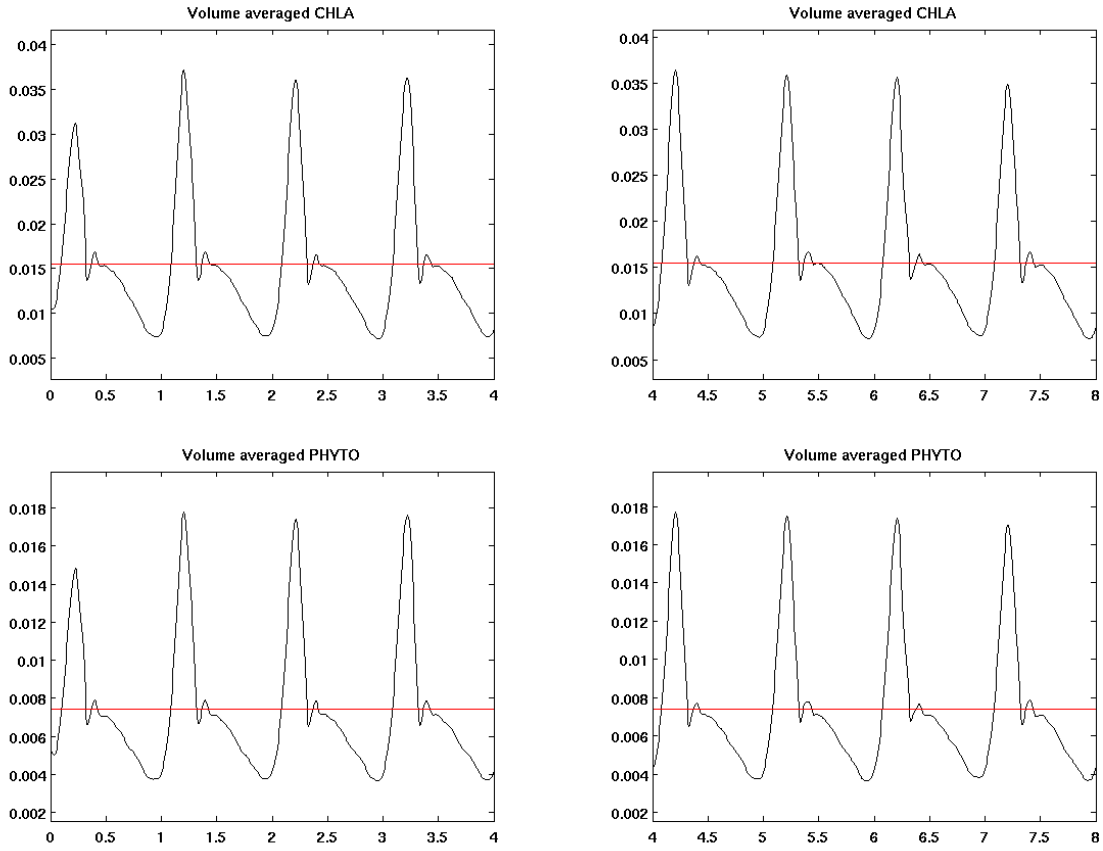

Figure A.2: Time evolution of the volume averaged concentrations of $Chla$ (mg m^{-3}) and $Phyt$ (mmol N m^{-3}) throughout 8 climatological years.

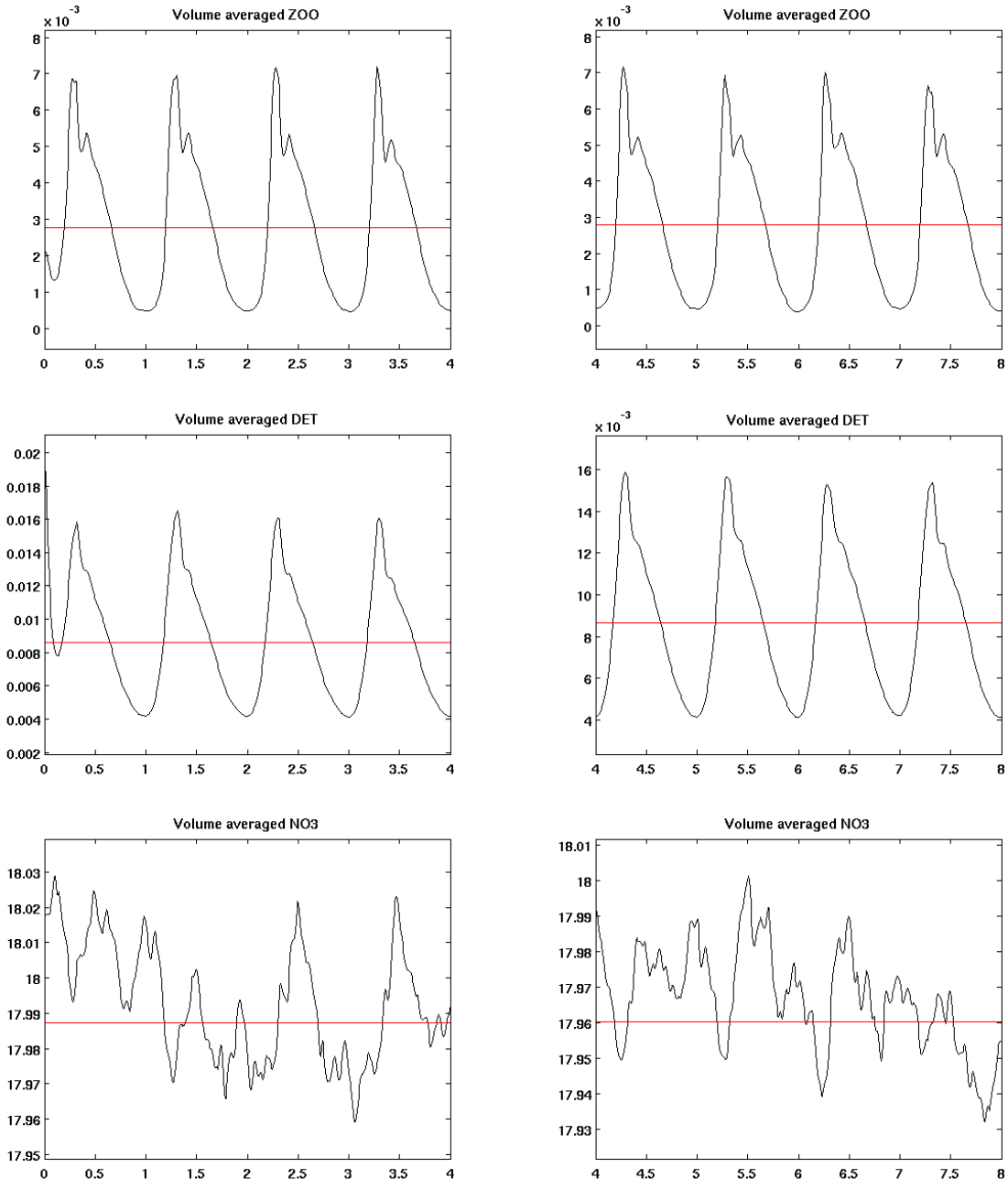

Figure A.2: Continued. Time evolution of the volume averaged concentrations of Zoo and Det (mmol N m^{-3}) and O_2 (mmol m^{-3}) throughout 8 climatological years.

Appendix B

Hydrodynamical model additional material

In this appendix, some figures from Nolasco et al. (2013) are presented, in order to support the validation of the hydrodynamical model that was outlined in section 3.5.1. This validation corresponds to the climatological configuration of the model described in section 2.1.2.

The mean seasonal hydrography and circulation of the Western Iberian Margin (WIM) are studied by means of a high-resolution configuration of the Regional Ocean Modeling System (ROMS). A comparison of 5-year model averages for January and July with climatological datasets shows a general good agreement in the reproduction of the mean water mass properties and hydrographic distribution. We find that there is a prevailing tendency for slope poleward flow at about 80-100 km offshore at all latitudes from the surface to 1500 m with strong vertical coupling. This northward flow, which is mainly along-slope and amounts up to 8-10 cm s-1, encounters several mean-flow recirculation regions on its way, and evidences of a secondary offshore pathway of poleward flow. Transports at different zonal sections further confirm the poleward flow tendency, with two peaks of poleward transport in summer (3-10 Sv) and winter (2-7 Sv). The transport time series emphasize the seasonal character of the alongshore circulation, and the interannual internal variability of the circulation, since the forcing fields are climatological (Nolasco et al., 2013).

B.1 Seasonal sea surface temperature and salinity

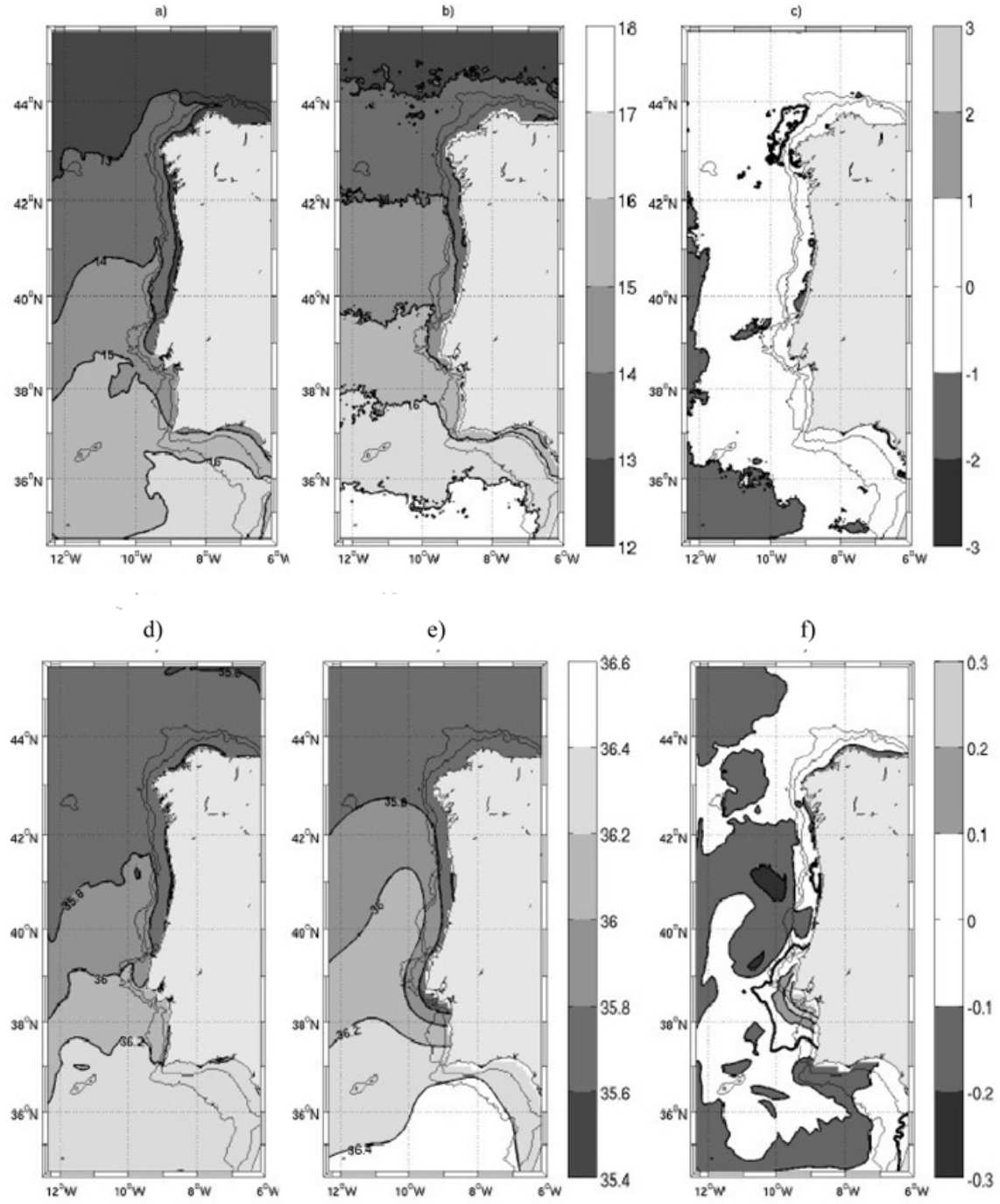

Figure B.1: Sea Surface Temperature (SST) in ℃ (a-c) and Sea Surface Salinity (SSS) (d-f) for January. (a, d) 5-year mean of ROMS output; (b, e) 7-year mean of AVHRR at 02h and GHER-NEA climatology (Troupin et al., 2010), respectively; (c, f) Difference between (a) and (b) and between (d) and (e), respectively. Thick contours outline null difference. From Nolasco et al. (2013).

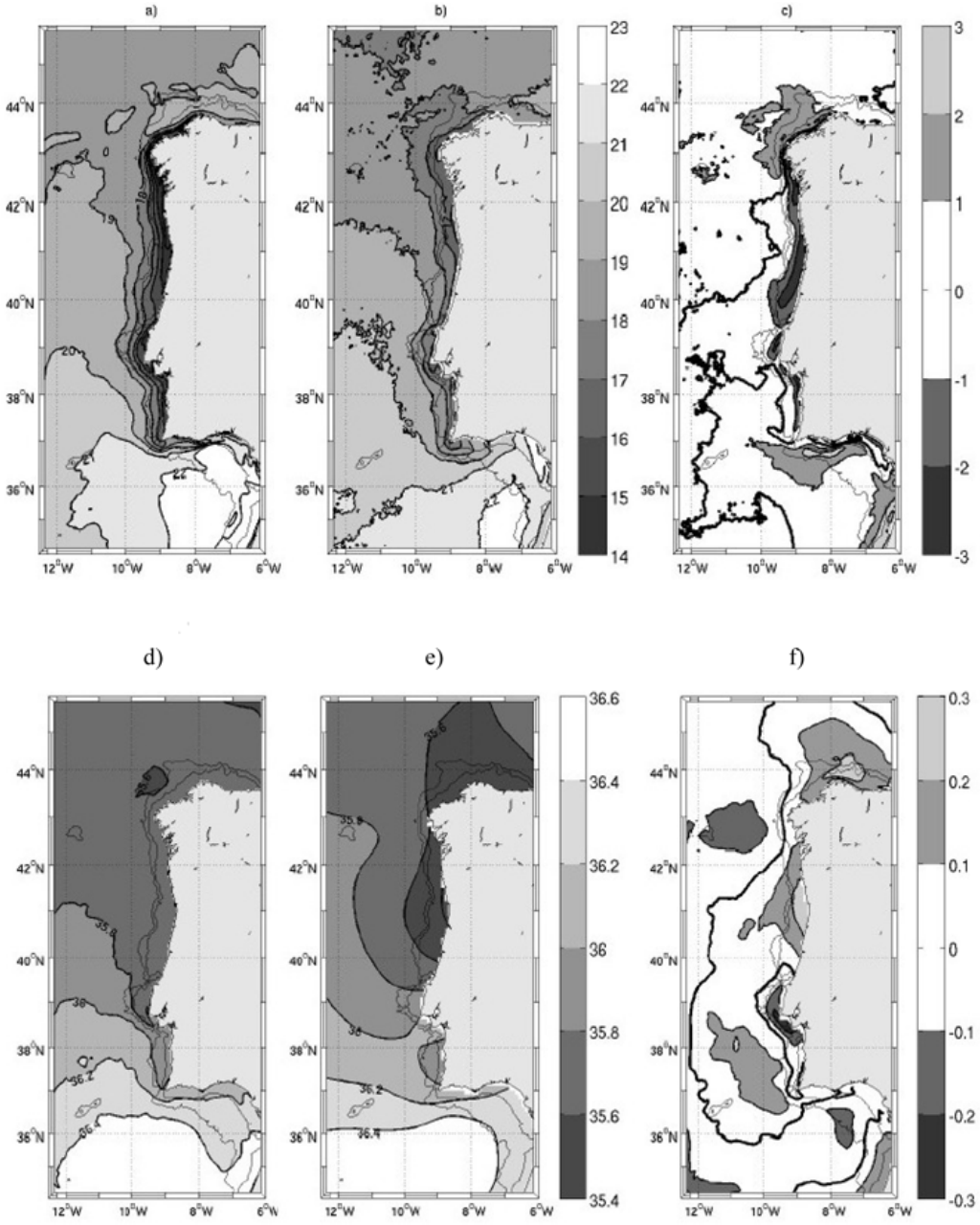

Figure B.2: Same as figure B.1 but for July.

B.2 Water masses

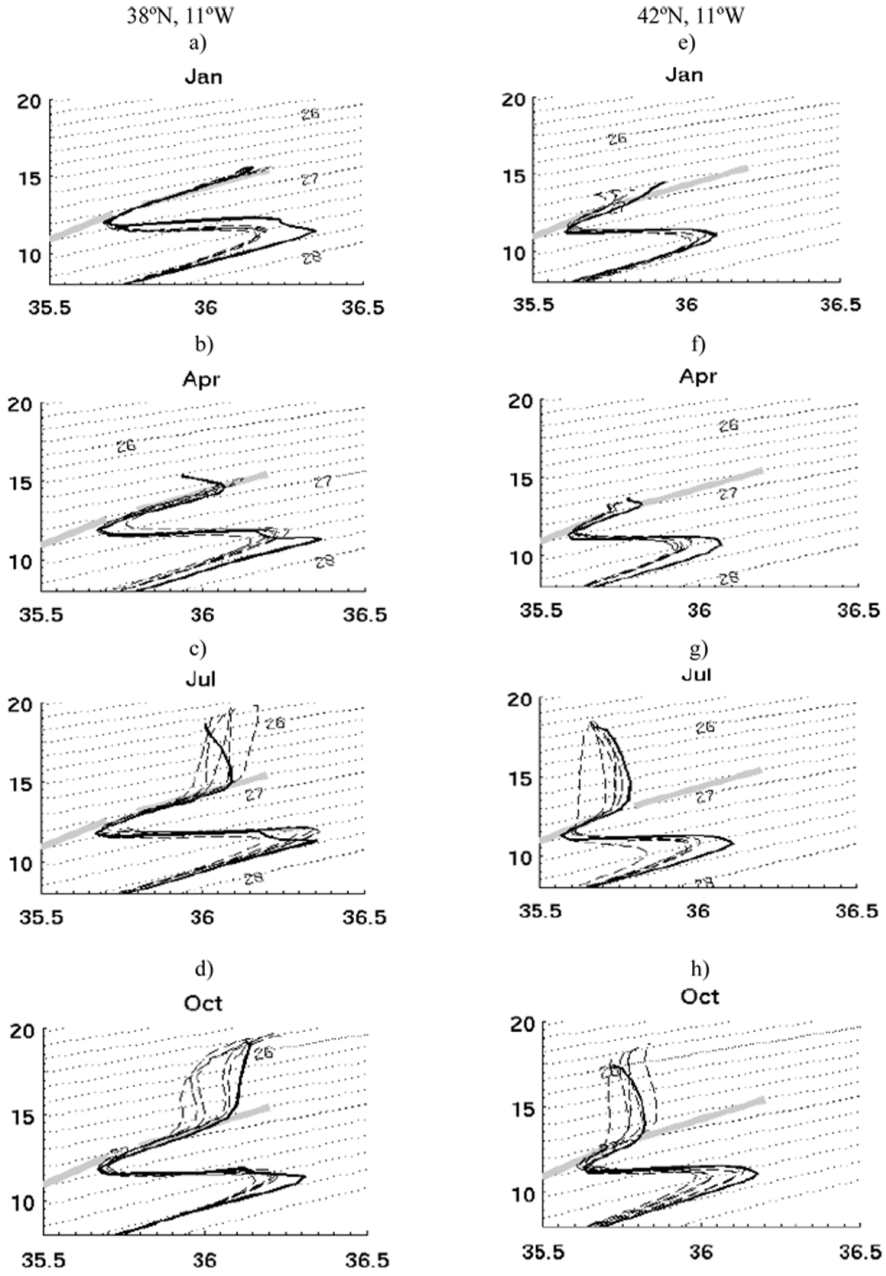

Figure B.3: $\theta - S$ diagrams of 5-year monthly means of ROMS output (dashed lines) and GHERNEA climatology (solid line; Troupin et al., 2010) for January (a, e), April (b, f), July (c, g) and October (d, h) for two regions: one centered at 38° N, 10° W (a-d), the other centered at 42° N, 10° W (e-h). Potential density anomaly (σ_θ) is superimposed in dotted lines every 0.2 kg m^{-3}; the shaded line corresponds to the standard definitions of ENACWst and ENACWsp, defined as $\theta = 10 + 8.462 \cdot (S - 35.4)$ for the subpolar branch ($34.8 < S < 35.7$) and $\theta = 13.13 + 5.653 \cdot (S - 35.8)$ for the subtropical branch ($35.8 < S < 36.2$), as defined by Fiuza (1984). From Nolasco et al. (2013).

B.3 Seasonal surface circulation

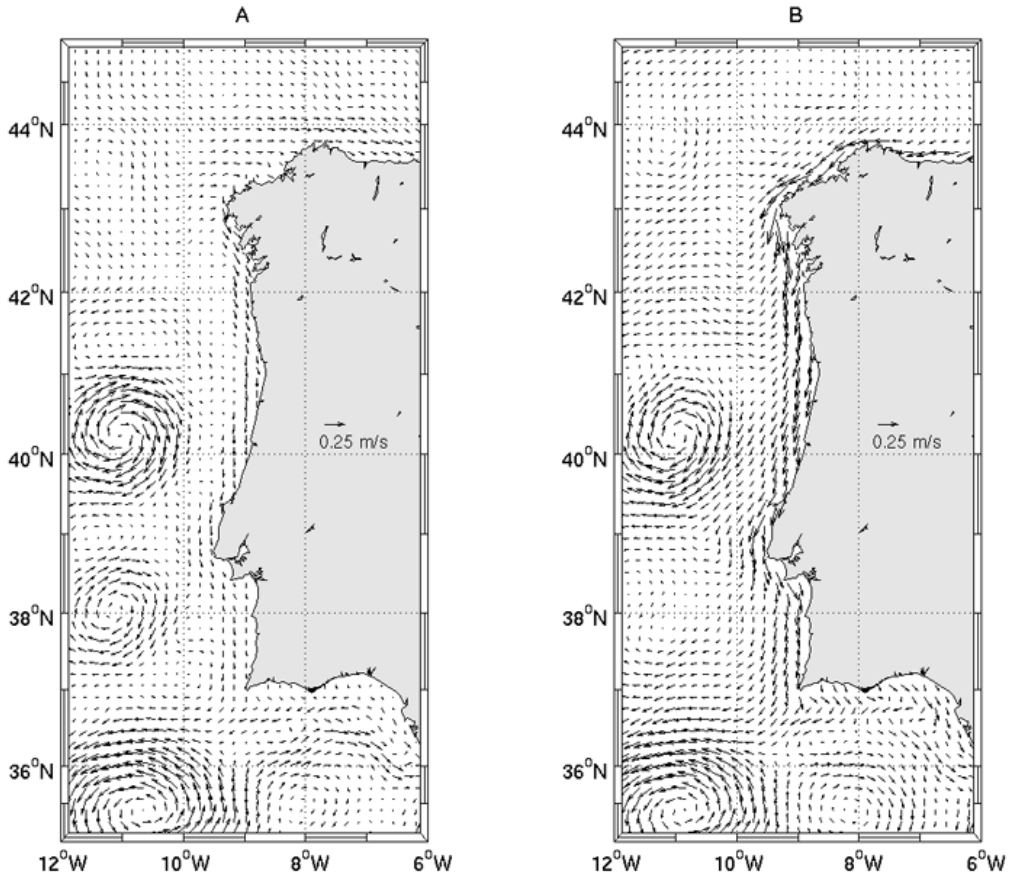

Figure B.4: Modeled seasonal mean velocity fields at the sea surface: downwelling season (October-March) (A) and upwelling season (April-September) (B).

B.4 Shelf-Slope meridional transport

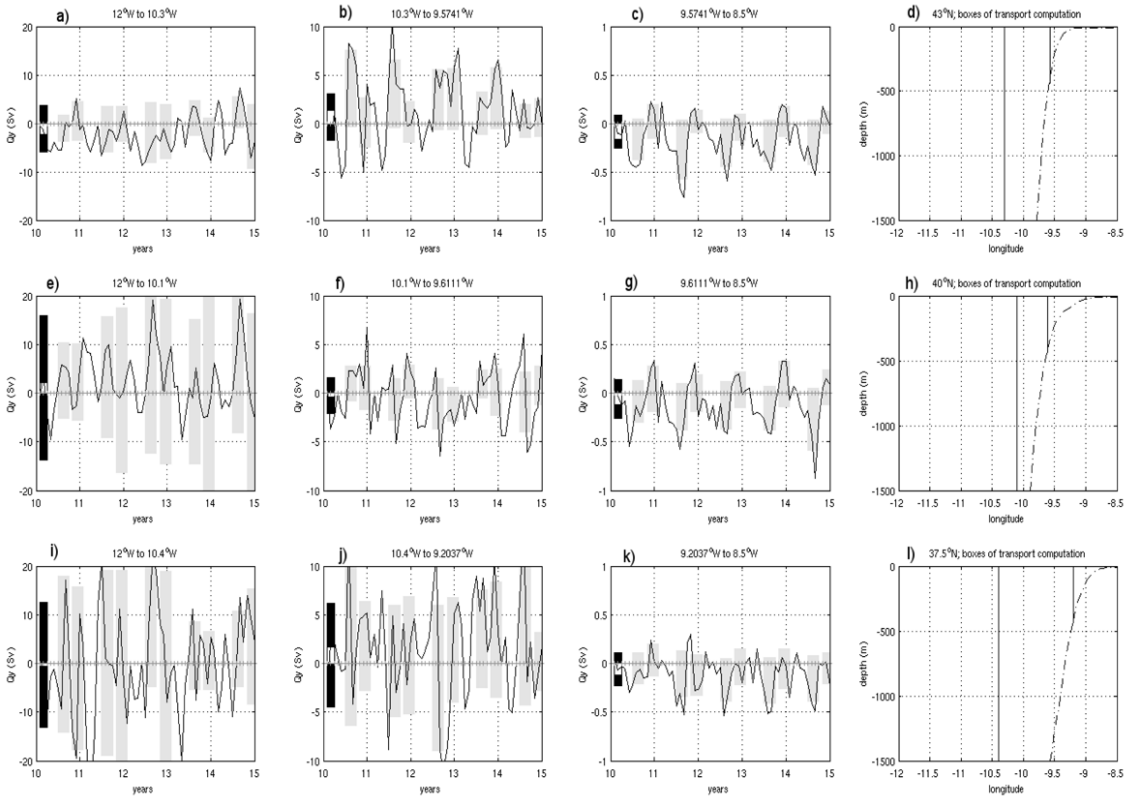

Figure B.5: Time series of meridional transport monthly means along: (a-d) 43° N; (e-h) 40° N; and (i-l) 37.5° N. Each column corresponds to a sub-section represented in the rightmost column (d, h, l). From left to right: (a, e, i) offshore; (b, f, j) lower slope and adjacent upper layers; (c, g, k) shelf/upper slope (down to 400 m). Seasonal averages (July, August, September - JAS - and November, December, January - NDJ) are plotted in shades of gray for northward and southward transports. To the left of each plot, total northward and southward averages are in black bars and the net average is in white bars. From Nolasco et al. (2013).

References

Albert, A., Echevin, V., Levy, M., Aumont, O., 2010. Impact of nearshore wind stress curl on coastal circulation and primary productivity in the Peru upwelling system. Journal of Geophysical Research-Oceans 115, C12033, doi:10.1029/2010jc006569.

Alldredge, A. L., Gotschalk, C. C., 1989. Direct observations of the mass floculation of diatom blooms: characteristics, settling velocities, and formation of diatom aggregates. Deep-Sea Research I 36, 159–171.

Allen, J. I., Holt, J. T., Blackford, J., Proctor, R., 2007. Error quantification of a high-resolution coupled hydrodynamic-ecosystem coastal-ocean model: Part 2. Chlorophyll-a, nutrients and SPM. Journal of Marine Systems 68, 381–404.

Álvarez, I., Lorenzo, M. N., de Castro, M., 2012a. Analysis of chlorophyll-a concentration along the Galician coast: seasonal variability and trends. ICES Journal of Marine Science: Journal du Conseil 69 (5), 728–738.

Álvarez, I., Prego, R., de Castro, M., Varela, M., 2012b. Galicia upwelling revisited: out-of-season events in the rias (1967-2009). Ciencias Marinas 38 (1B), 143–159.

Álvarez-Salgado, X. A., Aristegui, J., Barton, E. D., Hansell, D. A., 2007. Contribution of upwelling filaments to offshore carbon export in the subtropical Northeast Atlantic Ocean. Limnology and Oceanography 52 (3), 1287–1292.

Álvarez-Salgado, X. A., Beloso, S., Joint, I., Nogueira, E., Chou, L., Perez, F. F., Groom, S., Cabanas, J. M., Rees, A. P., Elskens, M., 2002. New production of the NW Iberian shelf during the upwelling season over the period 1982-1999. Deep-Sea Research Part I-Oceanographic Research Papers 49 (10), 1725–1739.

Álvarez-Salgado, X. A., Borges, A., Figueiras, F. G., Chou, L., 2010. Iberian Margin: The Rias. In: Liu, K., Atkinson, L., Quinones, R., Talaue-McManus, L. (Eds.), Carbon and Nutrient Fluxes in Continental Margins. Global Change - The IGBP series. Springer-Verlag, Berlin Heidelberg, pp. 102–119.

Álvarez-Salgado, X. A., Castro, C. G., Perez, F. F., Fraga, F., 1997. Nutrient mineralization patterns in shelf waters of the western Iberian upwelling. Continental Shelf Research 17 (10), 1247–1270.

Álvarez-Salgado, X. A., Doval, M. D., Borges, A. V., Joint, I., Frankignoulle, M., Woodward, E. M. S., Figueiras, F. G., 2001. Off-shelf fluxes of labile materials by an upwelling filament in the NW Iberian Upwelling System. Progress in Oceanography 51 (2-4), 321–337.

Álvarez-Salgado, X. A., Figueiras, F. G., Perez, F. F., Groom, S., Nogueira, E., Borges, A., Chou, L., Castro, C. G., Moncoiffe, G., Rios, A. F., Miller, A. E. J., Frankignoulle, M., Savidge, G., Wollast, R., 2003. The Portugal coastal counter current off NW Spain: new insights on its biogeochemical variability. Progress in Oceanography 56 (2), 281–321.

Álvarez-Salgado, X. A., Nieto-Cid, M., Gago, J., Brea, S., Castro, C. G., Doval, M. D., Perez, F. F., 2006. Stoichiometry of the degradation of dissolved and particulate biogenic organic matter in the NW Iberian upwelling. Journal of Geophysical Research-Oceans 111, C07017, doi:10.1029/2004jc002473.

Álvarez-Salgado, X. A., Roson, G., Perez, F. F., Pazos, Y., 1993. Hydrographic variability off the Rias Baixas (NW Spain) during the upwelling season. Journal of Geophysical Research-Oceans 98 (C8), 14447–14455.

Amante, C., Eakins, W., 2009. Etopo1 1 arc-minute global relief model: Procedures, data sources and analysis. NOAA technical memorandum NESDIS NGDC-24.

Arhan, M., de Verdière, A. C., Memery, L., 1994. The eastern boundary of the subtropical North-Atlantic. Journal of Physical Oceanography 24 (6), 1295–1316.

Arístegui, J., Álvarez-Salgado, X. A., Barton, E. D., Figueiras, F. G., Hernández-León, S., Roy, C., Santos, A. M. P., 2006. The global coastal ocean. Vol. 14 of The Sea. Harvard Univ. Press, Cambridge, Cambridge, Ch. Oceanography and fisheries of the Canary Current/Iberian region of the Eastern North Atlantic, pp. 877–931.

Arístegui, J., Barton, E. D., Álvarez-Salgado, X. A., Santos, A. M. P., Figueiras, F. G., Kifani, S., Hernández-León, S., Mason, E., Machú, E., Demarcq, H., 2009. Sub-regional ecosystem variability in the Canary Current upwelling. Progress in Oceanography 83, 33–48.

Aumont, O., Maier-Reimer, E., Blain, S., Monfray, P., 2003. An ecosystem model of the global ocean including Fe, Si, P colimitations. Global Biogeochemical Cycles 17 (2), doi: 10.1029/2001GB001745.

Barciela, R. M., Garcia, E., Fernandez, E., 1999. Modelling primary production in a coastal embayment affected by upwelling using dynamic ecosystem models and artificial neural networks. Ecological Modelling 120 (2-3), 199–211.

Barth, A., Alvera-Azcárate, A., Weisberg, R. H., 2008. Benefit of nesting a regional model into a large-scale ocean model instead of climatology: Application to the West Florida Shelf. Cont Shelf Res 28, 561–573.

Barton, E. D., Aristegui, J., Tett, P., Canton, M., Garcia-Braun, J., Hernandez-Leon, S., Nykjaer, L., Almeida, C., Almunia, J., Ballesteros, S., Basterretxea, G., Escanez, J., Garcia-Weill, L., Hernandez-Guerra, A., Lopez-Laatzen, F., Molina, R., Montero, M. F., Navarro-Perez, E., Rodriguez, J. M., van Lenning, K., Velez, H., Wild, K., 1998. The transition zone of the Canary Current upwelling region. Progress in Oceanography 41 (4), 455–504.

Behrenfeld, M. J., O'Malley, R. T., Siegel, D. A., McClain, C. R., Sarmiento, J. L., Feldman, G. C., Milligan, A. J., Falkowski, P. G., Letelier, R. M., Boss, E. S., 2006. Climate-driven trends in contemporary ocean productivity. Nature 444 (7120), 752–5.

Berx, B., Dickey-Collas, M., Skogen, M. D., Roeck, Y. H. D., Klein, H., Barciela, R., Forster, R. M., Dombrowsky, E., Huret, M., Payne, M., Sagarminaga, Y., Schrum, C., 2011. Does operational oceanography address the needs of fisheries and applied environmental scientists? Oceanography 24, 166–171.

Bianucci, L., Denman, K. L., 2012. Carbon and oxygen cycles: Sensitivity to changes in environmental forcing in a coastal upwelling system. Journal of Geophysical Research-Biogeosciences 117 (G1), doi: 10.1029/2011JG001849.

Bode, A., Alvarez-Ossorio, M. T., Cabanas, J. M., Miranda, A., Varela, M., 2009. Recent trends in plankton and upwelling intensity off Galicia (NW Spain). Progress in Oceanography 83 (1-4), 342–350.

Bode, A., Anadon, R., Moran, X. A. G., Nogueira, E., Teira, E., Varela, M., 2011. Decadal variability in chlorophyll and primary production off NW Spain. Climate Research 48, 293–305.

Bode, A., Casas, B., Fernandez, E., Maranon, E., Serret, P., Varela, M., 1996. Phytoplankton biomass and production in shelf waters off NW Spain: Spatial and seasonal variability in relation to upwelling. Hydrobiologia 341 (3), 225–234.

Bograd, S. J., Castro, C. G., Di Lorenzo, E., Palacios, D. M., Bailey, H., Gilly, W., Chavez, F. P., 2008. Oxygen declines and the shoaling of the hypoxic boundary in the California Current. Geophysical Research Letters 35 (12), doi: 10.1029/2008GL034185.

Borja, A., 2005. The European water framework directive: A challenge for nearshore, coastal and continental shelf research. Cont Shelf Res 25, 1768–1783.

Borja, A., Elliott, M., Carstensen, J., Heiskanen, A.-S., van de Bund, W., 2010. Marine management–Towards an integrated implementation of the European Marine Strategy Framework and the Water Framework Directives. Mar Pollut Bull 60, 2175–2186.

Brachet, G., 2004. From initial ideas to a European plan: GMES as an exemplar of European space strategy. Space Policy 20, 7–15.

Capet, X., Marchesiello, P. P., McWilliams, J. C., 2004. Upwelling response to coastal wind profiles. Geophys Res Lett 31, L13311, doi: 10.1029/2004GL020123.

Casas, B., Varela, M., Canle, M., Gonzalez, N., Bode, A., 1997. Seasonal variations of nutrients, seston and phytoplankton, and upwelling intensity off La Coruna (NW Spain). Estuarine Coastal and Shelf Science 44 (6), 767–778.

Castro, C. G., Alvarez-Salgado, X. A., Figueiras, F. G., Perez, F. F., Fraga, F., 1997. Transient hydrographic and chemical conditions affecting microplankton populations in the coastal transition zone of the Iberian upwelling system (NW Spain) in September 1986. Journal of Marine Research 55 (2), 321–352.

Castro, C. G., Nieto-Cid, M., Alvarez-Salgado, X. A., Perez, F. F., 2006. Local remineralization patterns in the mesopelagic zone of the Eastern North Atlantic, off the NW Iberian Peninsula. Deep-Sea Research Part I-Oceanographic Research Papers 53 (12), 1925–1940.

Castro, C. G., Perez, F. F., Alvarez-Salgado, X. A., Fraga, F., 2000. Coupling between the thermohaline, chemical and biological fields during two contrasting upwelling events off the NW Iberian Peninsula. Continental Shelf Research 20 (2), 189–210.

Castro, C. G., Perez, F. F., Holley, S. E., Rios, A. F., 1998. Chemical characterisation and modelling of water masses in the Northeast Atlantic. Progress in Oceanography 41 (3), 249–279.

Chávez, F. P., Messie, M., Pennington, J. T., 2011. Marine primary production in relation to climate variability and change. Annual Review of Marine Science 3 (3), 227–260.

Chávez, F. P., Strutton, P. G., Friederich, G. E., Feely, R. A., Feldman, G. C., Foley, D. G., McPhaden, M. J., 1999. Biological and chemical response of the Equatorial Pacific Ocean to the 1997-98 El Niño. Science 286 (5447), 2126–2131.

Chen, C. A., Liu, K. K., Macdonald, R., 2003. Continental Margin Exchanges. In: Fasham, M. J. R. (Ed.), Ocean Biogeochemistry. Springer-Verlag, pp. 53–95.

Cianca, A., Godoy, J. M., Martin, J. M., Perez-Marrero, J., Rueda, M. J., Llinas, O., Neuer, S., 2012. Interannual variability of chlorophyll and the influence of low-frequency climate modes in the North Atlantic subtropical gyre. Global Biogeochemical Cycles 26, GB2002, doi:10.1029/2010gb004022.

Conkright, M., Locarnini, R. A., Garcia, H. E., O'Brien, T. D., Boyer, T. P., Stephens, C., Antonov, J., 2002. World ocean atlas 2001: Objective analyses, data statistics, and figures. Tech. rep., National Oceanographic Data Center Report.

Cordeiro Pires, A., Nolasco, R., Cordeiro, N. G. F., Dubert, J., in preparation. Interannual variability of the upper ocean circulation in the Western Iberian Margin for 2001-2011: a modeling approach.

Cornillon, P., Adams, J., Blumenthal, M. B., Chassignet, E., Davis, E., Hankin, S., Kinter, J., Mendelssohn, R., Potemra, J. T., Srinivasan, A., Sirott, J., 2009. NVODS and the Development of OPeNDAP. Oceanography 22, 116–127.

Cravo, A., Relvas, P., Cardeira, S., Rita, F., Madureira, M., Sánchez, R., 2010. An upwelling filament off southwest Iberia: Effect on the chlorophyll a and nutrient export. Continental Shelf Research 30 (15), 1601–1613.

Cunha, M. E., 2002. Physical control of biological processes in a coastal upwelling system. PhD Thesis, Universidade de Lisboa, Portugal.

da Silva, A., Young, A., Levitus, S., 1994. Atlas of surface marine data 1994, volume 1: Algorithms and procedures.

de Boyer Montégut, C., Madec, G., Fischer, A. S., Lazar, A., Iudicone, D., 2004. Mixed layer depth over the global ocean: An examination of profile data and a profile-based climatology. Journal of Geophysical Research 109, C12003, doi:10.1029/2004JC002378.

Deutsch, C., Emerson, S., Thompson, L., 2006. Physical-biological interactions in North Pacific oxygen variability. Journal of Geophysical Research-Oceans 111 (C9).

Doney, S. C., 1999. Major challenges confronting marine biogeochemical modeling. Global Biogeochemical Cycles 13 (3), 705–714.

Doney, S. C., Lima, I., Lindsay, K., Moore, K., Dutkiewicz, S., Friedrichs, M. A. M., Matear, R., 2001. Marine biogeochemical modelling: Recent advances and future challenges. Oceanography 14 (4), 93–107.

Dufois, F., Penven, P., Whittle, C. P., Veitch, J., 2012a. On the warm near shore bias in Pathfinder monthly SST products over Eastern Boundary Upwelling Systems. Ocean Model 47, 113–118.

Dufois, F., Penven, P., Whittle, J., Veitch, J., 2012b. On the warm nearshore bias in Pathfinder monthly SST products over Eastern Boundary Upwelling Systems. Ocean Modelling 47, 113–118.

Dugdale, R. C., Goering, J. J., 1967. Uptake of new and regenerated forms of nitrogen in primary productivity. Limnology and Oceanography 12 (2), 196–206.

Echevin, V., Aumont, O., Ledesma, J., Flores, G., 2008. The seasonal cycle of surface chlorophyll in the peruvian upwelling system: A modelling study. Progress in Oceanography 79 (2-4), 167–176.

Eppley, R. W., 1972. Temperature and phytoplankton growth in sea. Fishery Bulletin 70 (4), 1063–1085.

Espinoza-González, O., Figueiras, F. G., Crespo, B. G., Teixeira, I. G., Castro, C. G., 2012. Autotrophic and heterotrophic microbial plankton biomass in the NW Iberian upwelling: seasonal assessment of metabolic balance. Aquatic Microbial Ecology 67, 77–89.

Fasham, M. J. R., Ducklow, H. W., Mckelvie, S. M., 1990. A nitrogen-based model of plankton dynamics in the oceanic mixed layer. Journal of Marine Research 48 (3), 591–639.

Ferreira, A. P., 2007. Sensibilidade às parametrizações físicas do WRF nas previsões à superficie em Portugal Continental. Relatorio de estagio-MOF. Universidade de Aveiro.

Ferreira, J., Simas, T., Schifferegger, K., Lencart e Silva, J., 2003. Identification of sensitive areas and vulnerable zones in transitional and coastal Portuguese systems. application of the United States national estuarine eutrophication assessment to the Minho, Lima, Douro, Ria de Aveiro, Mondego, Tagus, Sado, Mira, Ria Formosa and Guadiana systems. technical report. Tech. rep.

Figueiras, F. G., Labarta, U., Reiriz, M. J. F., 2002. Coastal upwelling, primary production and mussel growth in the Rias Baixas of Galicia. Hydrobiologia 484 (1-3), 121–131.

Fiuza, A. F. G., 1984. Hidrologia e dinámica das águas costeiras de Portugal. phd thesis. Ph.D. thesis, Universidade de Lisboa, Portugal.

Fiuza, A. F. G., Demacedo, M. E., Guerreiro, M. R., 1982. Climatological space and time-variation of the Portuguese coastal upwelling. Oceanologica Acta 5 (1), 31–40.

Fiuza, A. F. G., Hamann, M., Ambar, I., del Rio, G. D., Gonzalez, N., Cabanas, J. M., 1998. Water masses and their circulation off western Iberia during May 1993. Deep-Sea Research Part I-Oceanographic Research Papers 45 (7), 1127–1160.

Follows, M., Dutkiewicz, S., 2001. Meteorological modulation of the North Atlantic spring bloom. Deep Sea Research Part II: Topical Studies in Oceanography 49, 321 – 344.

Fraga, F., 1981. Upwelling off the Galician coast, Northwest Spain. In: Richards, S. A. (Ed.), Coastal upwelling series. Vol. 1. AGU, Washington DC, pp. 176–182.

Fraga, F., Figueiras, F. G., Prego, R., Perez, F. F., Rios, A. F., 1987. Campaña Galicia IX oceánica. Tech. rep.

Fraga, F., Mouriño, C., Manríquez, M., 1982. Las masas de agua en la costa de Galicia: junio-octubre. Tech. rep.

Fraga, F., Mouriño, C., Pérez, F. F., Rios, A. F., Marrasé, C., 1985. Campaña Galicia VII. Tech. rep.

Garcia, H., Locarnini, R. A., Boyer, T., Antonov, J., Baranova, O., Zweng, M., Johnson, D., 2010a. World ocean atlas 2009, volume 3: Dissolved Oxygen, Apparent Oxygen Utilization, and Oxygen Saturation.

Garcia, H. E., Locarnini, R. A., Boyer, T., Antonov, J., Zweng, M., Baranova, O., Johnson, D., 2010b. World Ocean Atlas 2009, volume 4: Nutrients (phosphate, nitrate, silicate).

Garcia, H. E., Locarnini, R. A., Boyer, T. P., Antonov, J. I., 2006. World Ocean Atlas 2005, Volume 4: Nutrients (phosphate, nitrate, silicate). NOAA Atlas NESDIS 64, Washington, D.C.

García Lafuente, J., Ruiz, J., 2007. The Gulf of Cádiz pelagic ecosystem: A review . Progress in Oceanography 74, 228 – 251.

Geider, R. J., MacIntyre, H. L., Kana, T. M., 1997. Dynamic model of phytoplankton growth and acclimatation: responses of the balanced growth rate and the chlorophyll a:carbon ratio to light, nutrient-limitation and temperature. Marine Ecology Progress Series 148, 187–200.

Glover, D. M., Jenkins, W. J., Doney, S., 2011. Modeling Methods for Marine Science. Cambridge University Press, Cambridge, UK.

Gregg, W. W., Casey, N. W., 2007. Sampling biases in MODIS and SeaWIFS ocean chlorophyll data. Remote Sensing of the Environment 111, 25–35.

Gruber, N., 2011. Warming up, turning sour, losing breath: ocean biogeochemistry under global change. Philosophical Transactions of the Royal Society a-Mathematical Physical and Engineering Sciences 369 (1943), 1980–1996.

Gruber, N., Frenzel, H., Doney, S. C., Marchesiello, P., McWilliams, J. C., Moisan, J. R., Oram, J. J., Plattner, G. K., Stolzenbach, K. D., 2006. Eddy-resolving simulation of plankton ecosystem dynamics in the California Current System. Deep-Sea Research Part I-Oceanographic Research Papers 53 (9), 1483–1516.

Haidvogel, D., Beckmann, A., 1999. Numerical ocean circulation modeling. Vol. 2 of Series on Environmental Science and Management. Imperial College Press, London.

Haidvogel, D. B., Arango, H., Budgell, W. P., Cornuelle, B. D., Curchitser, E., Di Lorenzo, E., Fennel, K., Geyer, W. R., Hermann, A. J., Lanerolle, L., Levin, J., McWilliams, J. C., Miller, A. J., Moore, A. M., Powell, T. M., Shchepetkin, A. F., Sherwood, C. R., Signell, R. P., Warner, J. C., Wilkin, J., 2008. Ocean forecasting in terrain-following coordinates: Formulation and skill assessment of the regional ocean modeling system. Journal of Computational Physics 227 (7), 3595–3624.

Haynes, R., Barton, E. D., 1990. A poleward flow along the Atlantic coast of the Iberian Peninsula. Journal of Geophysical Research-Oceans 95 (C7), 11425–11441.

Herrera, J. L., Rosón, G., Varela, R. A., Piedracoba, S., 2008. Variability of the western Galician upwelling system (NW Spain) during an intensively sampled annual cycle. An EOF analysis approach. Journal of Marine Systems 72 (1Ã**?**â**?**â4), 200–217.

Holte, J., Gilson, J., Talley, L., Roemmich, D., 2010. Argo Mixed Layers. Scripps Institution of Oceanography/UCSD. http://mixedlayer.ucsd.edu.

Holte, J., Talley, L., 2009. A new algorithm for finding mixed layer depths with applications to Argo data and Subantarctic Mode Water formation. Journal of Atmospheric and Oceanic Technology 26, 1920–1939.

Jackson, G. A., 2001. Effect of coagulation on a model planktonic food web. Deep Sea Research Part I: Oceanographic Research Papers 48 (1), 95 – 123.

Joint, I., Groom, S. B., Wollast, R., Chou, L., Tilstone, G. H., Figueiras, F. G., Loijens, M., Smyth, T. J., 2002. The response of phytoplankton production to periodic upwelling and relaxation events at the Iberian shelf break: estimates by the c-14 method and by satellite remote sensing. Journal of Marine Systems 32 (1-3), 219–238.

Jolliff, J. K., Kindle, J. C., Shulman, I., Penta, B., Friedrichs, M. A. M., Helber, R., Arnone, R. A., 2009. Summary diagrams for coupled hydrodynamic-ecosystem model skill assessment. Journal of Marine Systems 76, 64–82.

Kanamitsu, M., Ebisuzaki, W., Woollen, J., Yang, S. K., Hnilo, J. J., Fiorino, M., Potter, G. L., 2002. Ncep-Doe Amip-Ii Reanalysis (R-2). Bulletin of the American Meteorological Society 83 (11), 1631–1643.

Keeling, R. F., Kortzinger, A., Gruber, N., 2010. Ocean deoxygenation in a warming World. Annual Review of Marine Science 2, 199–229.

Koné, V., Machu, E., Penven, P., Andersen, V., Garcon, V., Fréon, P., Demarcq, H., 2005. Modeling the primary and secondary productions of the southern Benguela upwelling system: A comparative study through two biogeochemical models. Global Biogeochemical Cycles 19 (4), GB4021, doi:10.1029/2004GB002427.

Large, W. G., Mcwilliams, J. C., Doney, S. C., 1994. Oceanic vertical mixing - a review and a model with a nonlocal boundary-la yer parameterization. Reviews of Geophysics 32 (4), 363–403.

Lazzari, P., Teruzzi, A., Salon, S., Campagna, S., Calonaci, C., Colella, S., Tonani, M., Crise, A., 2010. Pre-operational short-term forecasts for Mediterranean Sea biogeochemistry. Ocean Science 6, 25–39.

Le Fouest, V., Zakardjian, B., Saucier, F., Cizmeli, S. C., 2006. Application of seawifs- and avhrr-derived data for mesoscale and regional validation of a 3-d high-resolution physical-biological model of the gulf of st. lawrence (canada). Journal of Marine Systems 60, 30 – 50.

Levitus, S., Boyer, T., 1994. World ocean atlas 1994, volume 4: Temperature.

Levitus, S., Burgett, R., Boyer, T., 1994. World ocean atlas 1994 volume 3: Salinity.

Lévy, M., Lehahn, Y., André, J. M., Mémery, L., Loisel, H., Heifetz, E., 2005. Production regimes in the northeast Atlantic: A study based on Sea-viewing Wide Field-of-view Sensor (SeaWiFS) chlorophyll and ocean general ciruculation model mixed layer depth. Journal of Geophysical Research 110, C07S10, doi:10.1029/2004jc002771.

Longhurst, A. R., 1998. Ecological Geography of the Sea. Academic Press.

Lopes, J. F., Cardoso, A. C., Moita, M. T., Rocha, A. C., Ferreira, J. A., 2009. Modelling the temperature and the phytoplankton distributions at the Aveiro near coastal zone, Portugal. Ecological Modelling 220 (7), 940–961.

Lorbacher, K., Dommenget, D., Niiler, P. P., Köhl, A., 2006. Ocean mixed layer depth: A subsurface proxy of ocean-atmosphere variability. Journal of Geophysical Research 111 (C7), C07010.

Machu, E., Biastoch, A., Oschlies, A., Kawamiya, M., Lutjeharms, J. R. E., Garcon, V., 2005. Phytoplankton distribution in the agulhas system from a coupled physical-biological model. Deep-Sea Research Part I-Oceanographic Research Papers 52 (7), 1300–1318.

Mann, K. H., Lazier, J. R. N., 2006. Dynamics of marine ecosystems. Wiley-Blackwell, Oxford.

Marchesiello, P., Debreu, L., Couvelard, X., 2009. Spurious diapycnal mixing in terrain-following coordinate models: The problem and a solution. Ocean Modelling 26 (3-4), 156 – 169.

Marchesiello, P., McWilliams, J. C., Shchepetkin, A., 2001. Open boundary conditions for long-term integration of regional oceanic models. Ocean Modelling 3 (1), 1–20.

Marta-Almeida, M., Dubert, J., Peliz, A., dos Santos, A., Queiroga, H., 2008. A modelling study of norway lobster (nephrops norvegicus) larval dispersal in southern portugal: predictions of larval wastage and self-recruitment in the algarve stock. Canadian Journal of Fisheries and Aquatic Sciences 65 (10), 2253–2268.

Marta-Almeida, M., Dubert, J., Peliz, A., Queiroga, H., 2006. Influence of vertical migration pattern on retention of crab larvae in a seasonal upwelling system. Marine Ecology-Progress Series 307, 1–19.

Marta-Almeida, M., Pereira, J., Cirano, M., 2011a. Development of a pilot Brazilian operational ocean forecast system, REMO-OOF. Journal of Operational Oceanography 4, 3–15.

Marta-Almeida, M., Reboreda, R., Rocha, C., Dubert, J., Nolasco, R., Cordeiro, N., Luna, T., Rocha, A., Lencart e Silva, J. D., Queiroga, H., Peliz, A., Ruiz-Villarreal, M., 2012. Towards operational modeling and forecasting of the iberian shelves ecosystem. PLoS ONE 7 (5), e37343.

Marta-Almeida, M., Ruiz-Villareal, M., Otero, P., Cobas, M., Peliz, A., Nolasco, R., Cirano, M., Pereira, J., 2011b. OOFε: A Phyton engine for automating regional and coastal ocean forecasts. Environmetal Modelling & Software 26, 680–682.

Maze, J. P., Arhan, M., Mercier, H., 1997. Volume budget of the eastern boundary layer off the Iberian Peninsula. Deep-Sea Research Part I-Oceanographic Research Papers 44 (9-10), 1543–1574.

Miles, T. N., He, R., 2010. Temporal and spatial variability of Chl-a and SST on the South Atlantic Bight: Revisiting with cloud-free reconstructions of MODIS satellite imagery. Continental Shelf Research 30 (18), 1951 – 1962.

Moisan, J. R., Hofmann, E. E., 1996. Modeling nutrient and plankton processes in the california coastal transition zone .1. a time- and depth-dependent model. Journal of Geophysical Research-Oceans 101 (C10), 22647–22676.

Moita, M. T., 2001. Estrutura, variabilidade e dinámica do fitoplâncton na costa de Portugal continental. PhD Thesis, Faculdade de Ciências da Universidade de Lisboa, Portugal. URL `http://www.inrb.pt/fotos/editor2/Tese_Teresa_Moita.pdf`

Morel, A., Berthon, J. F., 1989. Surface pigments, algal biomass profiles, and potential production of the euphotic layer: Relationships reinvestigated in view of remote-sensing application. Limnology and Oceanography 34, 1545–1562.

Neumann, T., 2000. Towards a 3D-ecosystem model of the Baltic Sea. J Mar Syst 25, 405–419.

Nieto-Cid, M., Alvarez-Salgado, X. A., Brea, S., Perez, F. F., 2004. Cycling of dissolved and particulate carbohydrates in a coastal upwelling system (NW Iberian Peninsula). Marine Ecology-Progress Series 283, 39–54.

NOAA, 2003. The GFS atmospheric model. Tech. rep., Environmental Modelling Center, NOAA-NCEP, Washington D. C., USA.

Nogueira, E., Pérez, F., Ríos, A., 1997. Seasonal patterns and long-term trends in an estuarine upwelling ecosystem (Ría de Vigo, NW Spain) . Estuarine, Coastal and Shelf Science 44 (3), 285 – 300.

Nolasco, R., Cordeiro Pires, A., Cordeiro, N. G. F., Le Cann, B., Dubert, J., 2013. A high-resolution modeling study of the Western Iberian Margin mean and seasonal upper ocean circulation. Ocean Dynamics. Published online. DOI:10.1007/s10236-013-0647-8.

Oliveira, P., Moita, T., Catarino, R., da Silva, A. J., 2007. Wintertime SST and Chla off NW Iberian shelf from satellite and insitu data. In: Joint 2007 EUMETSAT Meteorological Satellite Conference and the 15th Satellite Meteorology & Oceanography Conference of the American Meteorological Society. Amsterdam, The Netherlands.

Oliveira, P. B., Nolasco, R., Dubert, J., Moita, T., Peliz, A., 2009. Surface temperature, chlorophyll and advection patterns during a summer upwelling event off central Portugal. Continental Shelf Research 29 (5-6), 759–774.

Oliveira, P. B., Peliz, A. R., Fiuza, A. F. G., 1994. Space and time variability of satellite-derived sea surface temperatures and phytoplankton pigment concentrations in the eastern North Atlantic. In: Second International Conference on Air-Sea Interaction and on Meteorology and Oceanography of the Coastal Zone. pp. 300–301 311.

Ospina-Alvarez, N., Prego, R., Álvarez, I., deCastro, M., Álvarez-Ossorio, M., Pazos, Y., Campos, M., Bernárdez, P., Garcia-Soto, C., Gómez-Gesteira, M., Varela, M., 2010. Oceanographical patterns during a summer upwelling-downwelling event in the Northern Galician Rias: Comparison with the whole Ria system (NW of Iberian Peninsula). Continental Shelf Research 30 (12), 1362 – 1372.

Otero, P., García-García, M. R.-V. L., Marta-Almeida, M., Cobas, M., González-Nuevo, G., Cabanas, J. M., 2011. Walking on the sea side: Modeling and observational efforts of the Iberian Margin Ocean Observatory (RAIA). In: OCEANS 2011. OCEANS-IEEE, Santander.

Otero, P., Ruíz-Villareal, M., Peliz, A., Cabanas, J. M., 2010. Climatology and reconstruction of runoff time series in northwest iberia: influence in the shelf buoyancy budget off Ría de Vigo. Scientia Marina 74, 247–266.

Otero, P., Ruiz-Villarreal, M., 2008. Wind forcing of the coastal circulation off north and northwest Iberia: Comparison of atmospheric models. J Geophys Res 113, C10019.

Otero, P., Ruiz-Villarreal, M., Peliz, A., 2008. Variability of river plumes off Northwest Iberia in response to wind events. Journal of Marine Systems 72 (1-4), 238–255.

Otero, P., Ruiz-Villarreal, M., Peliz, A., 2009. River plume fronts off nw iberia from satellite observations and model data. Ices Journal of Marine Science 66 (9), 1853–1864.

Parker, R. A., 1993. Dynamic models for ammonium inhibition of nitrate uptake by phytoplankton. Ecological Modelling 66, 113–120.

Peliz, A., Dubert, J., Haidvogel, D. B., Le Cann, B., 2003. Generation and unstable evolution of a density-driven Eastern Poleward Current: The Iberian Poleward Current. Journal of Geophysical Research-Oceans 108 (C8), 3268, doi:10.1029/2002JC001443.

Peliz, A., Dubert, J., Marchesiello, P., Teles-Machado, A., 2007a. Surface circulation in the Gulf of Cadiz: Model and mean flow structure. Journal of Geophysical Research-Oceans 112, C11015, doi:10.1029/2007jc004159.

Peliz, A., Dubert, J., Santos, A. M. P., Oliveira, P. B., Le Cann, B., 2005. Winter upper ocean circulation in the Western Iberian Basin - fronts, eddies and poleward flows: an overview. Deep-Sea Research Part I-Oceanographic Research Papers 52 (4), 621–646.

Peliz, A., Marchesiello, P., Dubert, J., Marta-Almeida, M., Roy, C., Queiroga, H., 2007b. A study of crab larvae dispersal on the western iberian shelf: Physical processes. Journal of Marine Systems 68 (1-2), 215–236.

Peliz, A., Marchesiello, P., Santos, A. M. P., Dubert, J., Teles-Machado, A., Marta-Almeida, M., Le Cann, B., 2009. Surface circulation in the Gulf of Cadiz: 2. Inflow-outflow coupling and the Gulf of Cadiz slope current. Journal of Geophysical Research-Oceans 114 (C3), doi:10.1029/2008JC004771.

Peliz, A., Rosa, T. L., Santos, A. M. P., Pissarra, J. L., 2002. Fronts, jets, and counter-flows in the Western Iberian upwelling system. Journal of Marine Systems 35 (1-2), 61–77.

Peliz, A. J., Fiuza, A. F. G., 1999. Temporal and spatial variability of CZCS-derived phytoplankton pigment concentrations off the western Iberian Peninsula. International Journal of Remote Sensing 20 (7), 1363–1403.

Penas, E., Varela, M., 1986. Submodelo de la producción primaria en la plataforma de Galicia. Bol. Inst. Esp. Oceanogr. 3 (1), 111–130.

Penven, P., Debreu, L., Marchesiello, P., McWilliams, J. C., 2006. Evaluation and application of the ROMS 1-way embedding procedure to the central California upwelling system. Ocean Modelling 12 (1-2), 157–187.

Perez, F. F., Castro, C. G., Alvarez-Salgado, X. A., Rios, A. F., 2001. Coupling between the Iberian basin - scale circulation and the Portugal boundary current system: a chemical study. Deep-Sea Research Part I-Oceanographic Research Papers 48 (6), 1519–1533.

Perez, F. F., Castro, C. N. G., Rios, A. F., Fraga, F., 2005. Chemical properties of the deep winter mixed layer in the Northeast Atlantic (40-47 degrees N). Journal of Marine Systems 54 (1-4), 115–125.

Perez, F. F., Mourino, C., Fraga, F., Rios, A. F., 1993. Displacement of water masses and remineralization rates off the Iberian Peninsula by nutrient anomalies. Journal of Marine Research 51 (4), 869–892.

Perez, F. F., Pollard, R. T., Read, J. F., Valencia, V., Cabanas, J. M., Rios, A. F., 2000. Climatological coupling of the thermohaline decadal changes in Central Water of the Eastern North Atlantic. Scientia Marina 64 (3), 347–353.

Pinardi, N., Woods, J. (Eds.), 2002. Ocean forecasting: conceptual basis and applications. Springer-Verlag, London.

Pollard, R. T., Pu, S., 1985. Structure and circulation of the upper Atlantic ocean Northeast of the Azores. Progress in Oceanography 14 (1-4), 443–462.

Powell, T. M., Lewis, C. V. W., Curchitser, E. N., Haidvogel, D. B., Hermann, A. J., Dobbins, E. L., 2006. Results from a three-dimensional, nested biological-physical model of the California Current System and comparisons with statistics from satellite imagery. Journal of Geophysical Research-Oceans 111 (C7).

Prego, R., Barciela, M. D., Varela, M., 1999. Nutrient dynamics in the galician coastal area (northwestern iberian peninsula): Do the rias bajas receive moire nutrient salts than the rias altas? Continental Shelf Research 19 (3), 317–334.

Preisendorfer, R. W., 1988. Principal Component Analyses in Meteorology and Oceanography. Elsevier.

Queiroga, H., Cruz, T., dos Santos, A., Dubert, J., Gonzalez-Gordillo, J. I., Paula, J., Peliz, A., Santos, A. M. P., 2007. Oceanographic and behavioural processes affecting invertebrate larval dispersal and supply in the western Iberia upwelling ecosystem. Progress in Oceanography 74 (2-3), 174–191.

Queiroga, H., Silva, C., Sorbe, J. C., Morgado, F., 2005. Composition and distribution of zooplankton across an upwelling front on the northern portuguese coast during summer. Hydrobiologia 545, 195–207.

Reboreda, R., Castro, C. G., Álvarez-Salgado, X. A., Nolasco, R., Cordeiro, N. G. F., Queiroga, H., Dubert, J., in revision. Oxygen in the iberian margin: a modelling study. Progress in Oceanography.

Relvas, P., Barton, E. D., Dubert, J., Oliveira, P. B., Peliz, A., da Silva, J. C. B., Santos, A. M. P., 2007. Physical oceanography of the western Iberia ecosystem: Latest views and challenges. Progress in Oceanography 74 (2-3), 149–173.

Ribeiro, A. C., Peliz, A., Santos, A. M. P., 2005. A study of the response of chlorophyll-a biomass to a winter upwelling event off western Iberia using SeaWiFS and in situ data. Journal of Marine Systems 53 (1-4), 87–107.

Río-Barja, F., Rodríguez-Lestegás, F., 1992. Os ríos galegos. Morfoloxía e réxime. Consello da Cultura Galega, Santiago de Compostela.

Rios, A. F., Perez, F. F., Fraga, F., 1992. Water masses in the upper and middle North-Atlantic ocean East of the Azores. Deep-Sea Research Part a-Oceanographic Research Papers 39 (3-4A), 645–658.

Rodrigues, M., Oliveira, A., Queiroga, H., Fortunato, A. B., Zhang, Y. J., 2009. Three-dimensional modeling of the lower trophic levels in the ria de aveiro (portugal). Ecological Modelling 220 (9-10), 1274–1290.

Ruiz-Villarreal, M., González-Pola, C., Otero, P., Días del Río, G., Lavín, A., Cabanas, J. M., 2006. Circulation in the Galicia-Southern Bay of Biscay: Reanalysis of the circulation influencing the Prestige oil spill. In: European Operational Oceanography: present and future. EuroGOOS, pp. 342–348.

Sánchez, R. F., Relvas, P., Delgado, M., 2007. Coupled ocean wind and sea surface temperature patterns off the western Iberian Peninsula. Journal of Marine Systems 68, 103 – 127.

Santos, A. M. P., Chicharo, A., Dos Santos, A., Moita, T., Oliveira, P. B., Peliz, A., Re, P., 2007. Physical-biological interactions in the life history of small pelagic fish in the western iberia upwelling ecosystem. Progress in Oceanography 74 (2-3), 192–209.

Santos, A. M. P., Kazmin, A. S., Peliz, A., 2005. Decadal changes in the Canary Upwelling System as revealed by satellite observations: Their impact on productivity. Journal of Marine Research 63 (2), 359–379.

Sarmiento, J. L., Gruber, N., 2006. Ocean Biogeochemical Dynamics. Princeton University Press.

Saulquin, B., Gohin, F., Garrello, R., 2011. Regional objective analysis of merging high-resolution MERIS, MODIS/Aqua, and SeaWIFS chlorophyll-a data from 1998 to 2008 on the European Atlantic Shelf. IEEE Transactions on Geoscience and Remote Sensing 49 (1), 143–154.

Serra, N., Ambar, I., Boutov, D., 2010. Surface expression of Mediterranean Water dipoles and their contribution to the shelf/slope-open ocean exchange. Ocean Science 6(1), 191–209.

Shchepetkin, A. F., McWilliams, J. C., 2005. The regional oceanic modeling system (ROMS): a split-explicit, free-surface, topography-following-coordinate oceanic model. Ocean Modelling 9 (4), 347–404.

Shutler, J. D., Smyth, T. J., Saux-Picart, S., Wakelin, S. L., Hyder, P., Orekhov, P., Grant, M. G., Tilstone, G. H., Allen, J. I., 2011. Evaluating the ability of a hydrodynamic ecosystem model to capture inter- and intra-annual spatial characteristics of chlorophyll-a in the north east Atlantic. Journal of Marine Systems 88, 169–182.

Sibuet, J. C., Monti, S., Loubrieu, B., Maze, J. P., Srivastava, S., 2004. Carte bathymétrique de l'Atlantique nord-est et du Golfe de Gascogne: implications cinématiques. Bulletin de la Société Géologique de France 175 (5), 429–442.

Siddorn, J. R., Allen, J. I., Blackford, J. C., Gilbert, F. J., Holt, J. T., Holt, M. W., Osborne, J. P., Proctor, R., Mills, D. K., 2007. Modelling the hydrodynamics and ecosystem of the North-West European continental shelf for operational oceanography. J Mar Syst 65, 417–429.

Signell, R. P., Carniel, S., Chiggiato, J., Janekovic, I., Pullen, J., Sherwood, C. R., 2008. Collaboration tools and techniques for large model datasets. J Mar Syst 69, 154–161.

Silva, A., Palma, S., Oliveira, P. B., Moita, M. T., 2009. Calcidiscus quadriperforatus and calcidiscus leptoporus as oceanographic tracers in lisbon bay (portugal). Estuarine, Coastal and Shelf Science 81 (3), 333–344.

Silva, P. A., Ramos, M., Marta-Almeida, M., Dubert, J., 2007. Water Exchange Mechanisms Between Ria de Aveiro and the Atlantic Ocean. J Coastal Res 29, 1622–1626.

Skamarock, W. C., Klemp, J. B., Dudhia, J., Gill, D. O., Barker, D. M., Duda, M. G., Huang, X., Wang, W., Powers, J. G., 2008. A Description of the Advanced Research WRF Version 3. Tech. rep., MMMD-NCAR, Boulder, Colorado, USA.

Slagstad, D., Wassmann, P., 2001. Modelling the 3-D carbon flux across the Iberian margin during the upwelling season in 1998. Progress in Oceanography 51 (2-4), 467–497.

Smith, E., 1936. Photosynthesis in relation to light and carbon dioxide. In: Proceedings of the National Academy of Sciences. Vol. 22. pp. 504–511.

Sotillo, M. G., Fanjul, E. A., Castanedo, S., Abascal, A. J., Menendez, J., Emelianov, M., Olivella, R., García-Ladona, E., Ruiz-Villarreal, M., Conde, J., Gómez, M., Conde, P., Gutierrez, A. D., Medina, R., 2008. Towards an operational system for oil-spill forecast over Spanish waters: Initial developments and implementation test. Mar Pollut Bull 56, 686–703.

Sousa, F. M., Bricaud, A., 1992. Satellite-derived phytoplankton pigment structures in the Portuguese upwelling area. Journal of Geophysical Research-Oceans 97 (C7), 11343–11356.

Stolzenbach, K. D., Elimelech, M., 1994. The effect of particle density on collision between sinking particles: Implications for particle aggregation in the ocean. Deep-Sea Research I 41, 469–483.

Stow, C. A., Jolliff, J., McGillicuddy, D. J., Doney, S. C., Allen, J. I., Friedrichs, M. A. M., Rose, K. A., Wallheadg, P., 2009. Skill assessment for coupled biological/physical models of marine systems. Journal of Marine Systems 76 (1-2), 4–15.

Sverdrup, H. U., 1953. On conditions for the vernal blooming of phytoplankton. Journal du Conseil International pour l'Exploration de la Mer 18 (3), 287–295.

Tenore, K. R., Alonso-Noval, M., Alvarez-Ossorio, M., Atkinson, L. P., Cabanas, J. M., Cal, R. M., Campos, H. J., e. a., 1995. Fisheries and oceanographiy off Galicia, NW Spain (FOG): mesoscale spatial and temporal changes in physical processes and resultant patterns of biological productivity. Journal of Geophysical Research 100, 10943–10966.

Teruzzi, A., Salon, S., Bolzon, G., Lazzari, P., Campagna, S., Ficarelli, F., Solidoro, C., Crise, A., 2011. Operational forecasts of the biogeochemical state of Mediterranean Sea. Mercator ocean Newsletter 40.

Torres, R., Allen, J. I., Figueiras, F. G., 2006. Sequential data assimilation in an upwelling influenced estuary. Journal of Marine Systems 60 (3-4), 317–329.

Torres, R., Barton, E. D., Miller, P., Fanjul, E., 2003. Spatial patterns of wind and sea surface temperature in the Galician upwelling region. Journal of Geophysical Research 108 (C4), 3130.

Torres-López, S., Álvarez-Salgado, X., Varela, R., 2005. Offshore export versus in situ fractionated mineralization: a 1-D model of the fate of the primary production of the Rías Baixas (Galicia, NW Spain). Journal of Marine Systems 54, 175 – 193.

Townsend, D. W., Keller, M. D., Sieracki, M. E.and Ackleson, S. G., 1992. Spring phytoplankton blooms in the absence of vertical water column stratification. Letters to Nature 360, 59.

Troupin, C., Machín, F., Ouberdous, M., Sirjacobs, D., Barth, A., Beckers, J. M., 2010. High-resolution climatology of the northeast Atlantic using Data-Interpolating Variational Analysis (DIVA). J. Geophys. Res. 115 (C8), C08005.

Veitch, J., Penven, P., Shillington, F. A., 2010. Modeling equilibrium dynamics of the Benguela Current System. Journal of Physical Oceanography 40, 1942–1964.

Waniek, J. J., 2003. The role of physical forcing in initiation of spring blooms in the northeast Atlantic. Journal of Marine Systems 39, 57 – 82.

Wanninkhof, R., 1992. Relationship between wind-speed and gas-exchange over the ocean. Journal of Geophysical Research-Oceans 97 (C5), 7373–7382.

Warner, J. C., Geyer, W. R., Lerczak, J. A., 2005. Numerical model of an estuary: A comprehensive skill assessment. Journal of Geophysical Research-Oceans 110, C05001, doi:10.1029/2004jc002691.

Weiss, R. F., 1970. Solubility of Nitrogen, Oxygen and Argon in water and seawater. Deep-Sea Research 17 (4), 721–735.

Williams, R. G., Follows, M., 2003. Physical transport of nutrients and maintenance of biological production. In: Fasham, M. J. R. (Ed.), Ocean Biogeochemistry. Springer-Verlag, pp. 19–49.

Wooster, W. S., Bakun, A., Mclain, D. R., 1976. Seasonal upwelling cycle along Eastern boundary of North-Atlantic. Journal of Marine Research 34 (2), 131–141.

Zhang, X., Marta-Almeida, M., Hetland, R. D., 2012. A high-resolution pre-operational forecast model of circulation on the Texas-Louisiana continental shelf and slope. Journal of Operational Oceanography 5, 19–34.